Bulletin 51
(Part 1 of 3 Parts)

THE SHOCK AND VIBRATION BULLETIN

Part 1
Keynote Address, Invited Papers
Damping and Isolation, Fluid-Structure Interaction

MAY 1981

A Publication of
THE SHOCK AND VIBRATION
INFORMATION CENTER
Naval Research Laboratory, Washington, D.C.

Office of
The Under Secretary of Defense
for Research and Engineering

SYMPOSIUM MANAGEMENT

THE SHOCK AND VIBRATION INFORMATION CENTER

Henry C. Pusey, Director
Rudolph H. Volin
J. Gordan Showalter
Carol Healey
Elizabeth A. McLaughlin

Bulletin Production

Publications Branch, Technical Information Division,
Naval Research Laboratory

Bulletin 51
(Part 1 of 3 Parts)

THE SHOCK AND VIBRATION BULLETIN

MAY 1981

A Publication of
THE SHOCK AND VIBRATION
INFORMATION CENTER
Naval Research Laboratory, Washington, D.C.

The 51st Symposium on Shock and Vibration was held at the Holiday Inn at the Embarcadero, San Diego, CA on October 21-23, 1980. The Naval Ocean Systems Center, San Diego CA was the Host.

Office of
The Under Secretary of Defense
for Research and Engineering

CONTENTS

PAPERS APPEARING IN PART 1

PAPERS APPEARING IN PART 2

Environmental Testing

Shock Testing

Vehicle Systems

TITLES AND AUTHORS OF PAPERS PRESENTED IN THE SHORT DISCUSSION TOPICS SESSION

NOTE: These papers were only presented at the Symposium. They are not published in the Bulletin and are only listed here as a convenience.

SESSION CHAIRMEN AND COCHAIRMEN
51st Shock and Vibration Symposium
October 21-23, 1980, San Diego, CA

Date	Session Title	Chairmen	Cochairmen
Tuesday, 21 Oct. A.M.	Opening Classified Session	Mr. J. R. Sullivan, Naval Sea Systems Command Washington, DC	Mr. Henry C. Pusey, Shock and Vibration Information Center, Naval Research Laboratory, Washington, DC
Tuesday, 21 Oct. P.M.	Opening Plenary Session	Dr. Richard Swim, Superintendent, Marine Technology Division, Naval Research Laboratory, Washington, DC	Mr. James E. Colvard, Deputy Chief of Naval Material, Naval Material Command, Washington, DC
Tuesday, 21 Oct. P.M.	Submarine Shock	Dr. Michael Pakstys, General Dynamics/Electric Boat Division, Groton, CT	Mr. William Forehand, Naval Sea Systems Command, Washington, DC
Tuesday, 21 Oct. P.M.	Ship Dynamics	Mr. Mike Hattamer, Puget Sound Naval Ship Yard, Bremerton, WA	Dr. Richard A. Skop, Naval Research Laboratory, Washington, DC
Wednesday, 22 Oct. A.M.	Environmental Testing	Mr. James W. Daniel, U.S. Army Missile R&D Command, Redstone Arsenal, AL	Mr. E. Ken Stewart, U.S. Army Armament R&D Command, Dover, NJ
Wednesday, 22 Oct. A.M.	Specifications and Reliability	Mr. Robert Hancock, Vought Corporation Systems Division, Dallas, TX	Mrs. Phyllis Bolds, Air Force Wright Aeronautical Laboratories, Wright-Patterson AFB, OH
Wednesday, 22 Oct. P.M.	Damping and Isolation	Mr. E. V. Thomas, David W. Taylor Naval Ship Research and Development Center, Annapolis, MD	Mr. Ahid Nashif, Anatrol Corporation, Cincinnati, OH
Wednesday, 22 Oct. P.M.	Dynamic Analysis	Dr. George Morosow, Martin Marietta Corporation, Denver, CO	Mr. Jess Jones, NASA Marshall Space Flight Center, Huntsville, AL
Wednesday, 22 Oct. A.M.	Classified Session	Mr. Handley Ward, Naval Sea Systems Command, Washington, DC	Mr. Richard Chalmers, Naval Ocean Systems Center, San Diego, CA
Thursday, 23 Oct. A.M.	Shock Testing	Mr. John Favour, Boeing Company, Seattle, WA	Mr. Kenneth Cornelius, David W. Taylor Naval Ship R&D Center, Bethesda, MD
Thursday, 23 Oct. A.M.	Shock Analysis	Dr. Hansen Huang, Naval Research Laboratory, Washington, DC	Mr. Charles Moening, The Aerospace Corporation, El Segundo, CA
Thursday, 23 Oct. P.M.	Analysis	Dr. Ben Wada, Jet Propulsion Laboratory, CA	Mr. Paul Dunn, Aerospace Corporation, Los Angeles, CA
Thursday, 23 Oct. P.M.	Short Discussion Topics I	Mr. Sumner Leadbetter, NASA Langley Research Center, Hampton, VA	Dr. Gordan Showalter, Shock and Vibration Information Center, Naval Research Laboratory, Washington, DC
Thursday, 23 Oct. P.M.	Short Discussion Topics II	Mr. Michael Condouris, U.S. Army Electronics R&D Command, Monmouth, NJ	Mr. Rudolph H. Volin, Shock and Vibration Information Center, Naval Research Laboratory, Washington, DC

KEYNOTE ADDRESS

Mr. James E. Colvard
Naval Material Command
Washington, D.C.

I am pleased to speak to the 51st annual Shock and Vibration Symposium. I spent some time thinking about what would be appropriate remarks to make to a group like this, particularly a group that has been meeting for so long. And when I considered the nature of this symposium, I concluded that there were so many more expert people here than I in this subject area that I ought to be careful to stick to things that I understand. This so severely limited me that I almost asked to be excused from the assignment.

But then I thought a while and concluded that scientists and engineers by their very nature are rational, realistic, linear thinkers and they view the world as rational, realistic and amenable to linear solutions of problems. As a manager in Washington, I deal in a non-linear-probabilistic, irrational world. Therefore, if I talk about that, you'll be just as snowed and just as confused as I am when I listen to your esoteric, in-depth presentations on the subtle nuances of a physical world of shock and vibration. So I asked myself what do these two worlds have in common. Why is the linear world, the rational world of the scientist and engineer relevant to the irrational, non-linear world of war, politics, system acquisition, or the process of taking technology to the battle zone to accomplish political objectives? I concluded that in the modern day processes of war, the tools of war are so driven by and dependent on science and technology that it is impossible to separate the scientist and the warrior and the institutional processes by which we acquire those weapons of war. Since they are so intricate and complex and it is impossible to separate the scientist, the warrior and the politician, it is proper that we try to understand each others worlds.

It is exceptionally important that symposia such as this that communicate across service lines the knowledge of something so fundamental to war as shock and vibration be periodically held. Whether or not we've needed 51 of them in the last number of years I don't know. Maybe we've needed 151. Maybe we needed only one, but they are a part of the process of tying the complex system together. A lot of useful information is produced by technically sophisticated people in the very important science of shock and vibration. The sharing of this information is critical, otherwise we are repeating past mistakes or replicating past successes. It is unnecessary to do this. The center that Mr. Pusey runs at NRL for the dissemination of information produces cross-talk between services, even between nations, that use this organization that is representative of what you are all about. So if it takes San Diego and good weather to bring you together, then that is what we ought to do.

Speaking of complexity and sophistication, we in this country have long felt that we offset the numerical superiority of our potential enemies with the advanced, sophisticated technology that we were using in developing our weapons. The technological edge was our hedge against numbers. That is no longer as true as it was in the past. No one can precisely determine the relative positions of potential adversaries in the technology arena, but it is becoming more and more obvious that we no longer have the clear technological lead we've depended on in the past.

There is a challenge for all of us as scientists, and in spite of my remarks about being a politician working in a non-linear world, I started out in this business as a physicist at the Naval Weapons Center in China Lake, California. So, while I am not a brilliant, practicing scientist as many of you are, I do understand the point of view of the scientist. You as scientists have a tremendous challenge for the future, a challenge of dealing with a potential adversary that is now as technically sophisticated as we are. The standards of technical and professional excellence that you as scientists establish and maintain through your professional interaction both as practicing scientists in your day-to-day business and your interaction through symposia such as this must be of the highest caliber.

Over the past 15 to 20 years, we have perhaps lost sight of the need for professional excellence. We have succumbed to the manager's world. We as scientists have made the process its own purpose. The length of time it takes us to acquire weapons, the complexity of the weapons we acquire, the lack of understanding that not only does nature love simplicity, so does the warrior who has to use our weapons. Thus, we have drifted into the thought that acquisition is an end in itself rather than clearly understanding that the ultimate objective is the waging of a war and that we must bend science to that objective. That perhaps has been lost to a high degree in the last 20 years.

We've also entered an era in which we have a wholly-owned defense industry. Historically, we used to convert from peacetime production of automobiles and washing machines into wartime production—airplanes, tanks and guns. And then when the wars were over, go back about our peacetime business. That is no longer true. We now have

major industries that have one customer, the Department of Defense, who depend on our business and whose futures depend on continuing to produce the tools of war whether they be good or bad, or whether we need them or not. Nothing is wrong with this. In fact, the time of future war may be so short that we don't have the luxuries of converting a peacetime operation to a wartime operation. And in the past wars, we have tended to win them not only by technological superiority, but we could out-produce them. Our industrial base was a great source of our strength. That industrial base continues to be a great source of our strength, but the character of it has changed, and we have to understand that. The nature of our business has changed, and we as scientists in the government have an obligation now greater than ever to maintain a clear understanding and control of our technical destiny. We must see that the single customer defense industry produces what we truly need. We must not only avoid the technological surprise, we must provide to the Department of Defense the technological options that will allow us to meet the sophisticated threat.

We must maintain the understanding of that process in a Democratic society that must in fact use all of its institutions. It must depend on industry for its capacity, but we must never lose the internal capability in people such as you who continue to refine our understanding of the elements of war, however mundane or esoteric they may be. Nothing could be more fundamental to the element of war than shock and vibration. It is you who continue to refine that knowledge, continue to strive for excellence that will be the key to our national future. But just as you continue to maintain your technical excellence and refine our understanding of physical phenomenon and the tools of war, you must also strive to understand the legitimacy of a very slow, frustrating democratic process which we go about to bring this understanding of the technical world into reality of the weapons we need to provide for our common defense. Along with the other services, I am convinced that the Navy is critical to our future as an international power. I, personally, am very dedicated to it. I think you serve in this kind of a function for some of the same kind of motivations. So, I applaud your past performance and I commend you to your future task. Continue the excellence of your contribution, the continuity of your cause. Maintain the standards of professional excellence that have characterized your symposia in the past and extend it into the future. I appreciate being invited here today to participate in your 51st symposium on shock and vibration. I wish you success.

INVITED PAPERS

AN APPROACH TO THE LIMITATION AND CONTROL OF SHIPBOARD VIBRATION

Edward F. Noonan
NKF Engineering Associates, Inc., Vienna, Va.

INTRODUCTION AND BACKGROUND

Vibration aboard ship has been a problem since the introduction of mechanical propulsion systems. Prior to 1940 however, the understanding of the problems encountered was extremely limited, and with few exceptions, the solutions to such problems were obtained, if indeed they were, by trial and error approaches. In the commercial area structural resonances, balancing of rotating equipment and low frequency isolation systems were understood and utilized while torsional vibration of reciprocating drive systems were being studied. Hull vibration could be related to dynamic or hydrodynamic unbalance and propeller blade frequencies could be related to hydrodynamic flow and the proximimity of hull and appendages to the propeller disc. The average commercial ship had a single screw, less than 15,000 SHP, low RPM's and significant structural damping provided by riveted construction in many cases. Larger powered ships were usually passenger ships which had the advantage of multiple screws which permitted the propellers to operate in more open water conditions which was condusive to more even flow into the propeller disc area. Thus the seriousness of the problem was not really noted until the large shipbuilding program precipitated by the second world war.

The basic vibration instrument in use, prior to World War II was the Geiger, a seismic, mechanical unit, which was primarily useful in the study of torsional vibration in propulsion systems but which could also be rigged as a seismograph in the study of hull vibration. Hydrodynamic theory related to propeller forces had not been developed to a point of practical application and computers were identified as slide rules or desk calculators. Vibration specifications, if any, might say, "a good dynamic balance is required", or "the ship should be free of excessive vibration." Thus we could readily recognize that shipbuilding was considered an art, at that time.

In 1940 the Navy was not much further along. Most of our ships had been built in World War I or earlier. Battleships generally had reciprocating steam engines and multiple screws of modest powers, destroyers and cruisers were higher speed ships but again were multiple-screw ships of modest powers and with more careful study of the lines to obtain a good flow condition to the propeller, conducted at the Washington Navy Yard Experimental Model Basin, acceptable vibration characteristics could be obtained. At the New York Navy Yard, which had previously built submarine diesels, considerable contributions were made in the area of torsional vibrations. In passing, we should acknowledge the contributions of McGoldrick at the Experimental Model Basin, and Dashefsky at the New York Navy Yard.

World War II marked a series of rapid changes. The Navy opened the new Model basin facility at Carderock, Md., now known as the David Taylor Naval Research and Development Center, put the North Carolina class battleships and Midway class carriers to sea, both of which started with serious hull vibration and/or longitudinal vibration of the propulsion systems. Torsional vibration problems wreaked havoc in the reduction gears of destroyers and crankshafts, and couplings of diesel drives, periscope vibrations limited the submerged speed of submarines and many propeller shafts were lost to corrosion fatigue, while environmental vibration precipitated serious problems in maintaining basic electronic equipment operational. With the demand for all types of ships, the Navy was forced to obtain engines, from reciprocating steam and diesel to steam turbine, from whatever sources were available and tried to match them with propellers and shafts in all types of vessels, wooden as well as steel. With this situation, we encountered a myriad of vibration problems and vibration engineering in the Navy became a continuous road-trip of problem solving.

It was shortly thereafter, that Admiral Mills returned from a trip to England with the story of the vulnerability of the British ships to underwater explosions. Shock resistance was identified as a vital consideration in combatant ship design, cast iron was eliminated, wherever possible and, shock mountings were attached to all sensitive equipment. Shock and vibration research groups were developed in the various Naval Laboratories, most of which are still working in these vital areas but with budgets which fluctuate with the defense effort and frequently seriously limit the required progress, particularly in the vibration area.

During the latter war years, 1944 thru 1946 I served in the Naval Engineering Division of the U.S. Coast Guard and continued efforts in solving a number of serious vibration problems which had plagued the service since the early war years, and attempted to eliminate problems in new designs. In 1946 I returned to the Navy, Bu. Ships, in charge of Vibration Research and together with Russ Oliver, who acted in a similar capacity on the Shock Desk, participated in the development of the required R&D effort aimed at the consolidation of the gains made during the war and in planning for the future. At this point, accelerated by the introduction of the atomic bomb into our arsenal, the Shock and Vibration Symposium was formed, under the direction of Dr. Klein of NRL. The year was 1947.

The history of the Shock and Vibration Symposium has been well documented since its inception in 1947. Thru the years, starting with the shock tests carried out in the Pacific and heavily supported by atomic energy funds, the most

exciting and main thrust of research has been in the shock area. For this, the 51st meeting of the Shock & Vibration Symposium, I would like to bring you up to date on where we stand in the area of Shipboard Vibration, and leave some food for thought on how we might proceed from here on what remains to be the most serious shipboard vibration problem, that of the "Limitation and Control of Shipboard Vibration".

EARLY POST WORLD WAR II EFFORTS

Shortly after World War II steps were introduced to consolidate our technological gains in an effort to reduce the emergency calls whenever something aboard ship vibrated and to provide the basis for the prevention of a repetition of previous mistakes. These efforts were designed to provide practical fleet assistance while more fundamental studies were carried out in the laboratory. Some were necessarily applicable to problems of limited scope and generally related to specific designs. Others represented more general application and provided significant contributions to the advancement of the subject of ship vibration. Particularly in the latter case, ship vibration research in the U.S. was, almost exclusively, sponsored by the Navy. A few of the more significant accomplishments are noted, as follows:

1 — The DD692 Class Destroyers were a constant problem, were many in number, and required frequent investigations. Detailed studies were carried out on the Charles R. Ware. Based on these studies and the limited studies conducted on a number of sisterships, a letter report, outlining corrective action was issued by Bu ships in 1949. A formal report on the subject was published by DTMB in 1950 [1].

2 — The incidence of propeller shaft failures during and immediately after World War II necessitated both theoretical studies, a number of full scale investigations and metallurgical investigations. Most of the failures were experienced on commercial ship types but obviously was of importance to the Navy. A number of studies were carried out on commercial ship types, some of which were in Navy service: The theoretical study of Jasper and Rupp [2] was published in 1952. The studies sponsored by SNAME formed the basis for shaft design modifications [3], 1961. A summary technical report on the subject was published by SNAME in 1966 [4].

3 — U.S. Navy Training Film, "Shipboard Vibrations", No. MN-9180-A-D, was distributed in 1952. This four-reel film, issued in the early nineteen fifties, was developed for designers, builders and operators and provided an overview of the total ship vibration problem, as it was understood at that time, from fundamentals to the practical solution of some of the more common local problems encountered aboard ship

4 — MIL-STD-167 (Ships) 1954 "Mechanical Vibrations of Shipboard Equipment." This standard has been updated several times, most recently in 1974, and includes:

Type I — Environmental
Type II — Internally Excited
Type III — Torsional Vibration
Type IV — Longitudinal Vibration
Type V — Lateral Vibration

In this document the most significant gains have been achieved in these specific, although limited problem areas.

Type I — Under Environmental Vibration, qualification testing of shipboard equipment has been firmly established, and the need is currently under consideration by the International Organization for Standardization for possible use on commercial vessels. This specification has been very effective in the development of equipment and weapon systems which must function in the active vibration environment existing aboard ship. Most problems still encountered in this area stem from the omission or improper use of the specification. A background paper on the development and use of this specification was given at the 23rd S&V Symposium [5].

Type II — Internally Excited Vibration has greatly improved the performance of rotating machinery by eliminating the phrase "A good dynamic balance is required" and substituting an allowable residual unbalance, along with acceptable vibration tolerances of the machine. This specification was developed from detailed studies and experimentation to determine practical standards. The application of these standards has contributed to the improvement of the achievable quality of equipment so that commercially available equipment now exceeds the performance originally obtained at premium prices by the Navy. Tightening the specifications was therefore possible and is reflected in the current version of MIL-STD-167.

Type III — The Torsional Vibration requirements were originally generated from investigations carried out by the S.A.E. War Engineering Board Torsional Vibration Committee and crankshaft fatigue studies conducted by the Material Laboratory of the New York Naval Shipyard. This specification is widely used, in both commercial and Naval applications and has contributed much to the control of problems in

this area. As is always the case however, new designs are frequently encountered which require special considerations and strongly suggest the need for amendments to the present requirements.

Type IV — The Longitudinal Vibration requirements, originally established to insure the problem was not overlooked in the design phase, simply prohibited the presence of critical frequencies in the operating speed range. Designs were generated however, such as the propulsion system of the first nuclear powered submarine, the U.S.S. Nautilus, which did have an acceptable critical in the operating speed range. Based on this case and other studies, it was necessary to update this specification and identify what the detailed requirements should be. These changes were introduced in 1969. At this time, primarily based on recent data on commercial ship installation, in which the revised criteria had been invoked, further modifications are anticipated.

Type V — The Lateral Vibration requirements relate to propulsion shafting. It requires that detailed analyses be carried out to insure no criticals exist within the operating speed range. At this point in time we know further clarification is required to determine the critical frequencies we are concerned with, the allowable response and acceptable methods of analyses. Thus, although we have omitted the occurrence of some potentially serious problems, we can recognize the necessity of further amplification of the specification to cover new designs.

5 — "A Guide for the Selection and Application of Resilient Mountings to Shipboard Equipment" [6] was also published in 1954 to minimize the misapplication of resilient mountings. At that point in time, the rush to improve the shock resistance of sensitive equipment frequently resulted in serious vibration problems.

6 — In 1955 Russo of the Maritime Administration, and McGoldrick of DTMB published the results of their studies on the S.S. Gopher Mariner [7]. These full scale studies identified weaknesses in calculations then available for the prediction of hull response and contributed significantly to the development of future programs. A number of related papers of note were also published by McGoldrick [8], [9], Leibowitz and Kennard [10], while a book on the subject of Ship Hull Vibration was published by Todd [11].

7 — In the development of the Polaris Missile we encountered a direct challenge for the application of the available technology to the development of the delicate structure of an ICBM in a submarine environment which included shock and vibration to the same degree as other submarine equipment. Results of this development program were published in 1958 [12]. This case introduced the notion that flexibility must be maintained to treat special cases in a special manner, and not be too rigid in following old specifications.

8 — Following the development of the shock mitigation system for the Polaris submarines and the recognition that the present day nuclear-powered submarines, as true submersibles, generate a significantly different vibration environment than their predecessors, a study on submarine vibration environment was presented at the 31st Shock and Vibration Symposium in 1962, at Phoenix, Arizona [13]. The purpose of this study was to review the major submarine advances and their influences on the vibration environment.

9 — It has been established that vibration and noise aboard ship will generally cause physical annoyance to the crew before it adversely affects the ship structure, machinery or other equipment. Thus vibration and noise guidelines are based primarily on human reactions. In this area Buchmann developed a "Criteria for Human Reaction to Environmental Vibration in Naval Ships" in 1962 [14].

10 — The First International Ship Structures Congress met in Glasgow, Scotland, in 1961. A technical committee on Ship Vibration was established for the Second Congress in 1964 at which the ongoing research work in the U.S.A. was presented [15]. This effort primarily covered work sponsored by the Navy and by the Society of Naval Architects and Marine Engineers. It is only fair to say that the principal effort of the Navy was, at that time, still trouble shooting and the research effort was fragmentary in nature and extremely limited. The effort sponsored by S.N.A.M.E. at that time was extremely small and was largely concerned with how to measure and evaluate shipboard vibration. It did however, result in the development of the first instrumentation package for the Maritime Administration in 1965.

THE FIRST CONFERENCE ON SHIP VIBRATION

By 1965 it became evident that the need existed for developing methods of improving design procedures which would permit the development of ships, machinery systems and weapon systems, which are free from damaging vibration. To do this it was considered necessary to close the large technical gap which existed between the designed and the vibration research investigator.

The First Conference on Ship Vibration was jointly sponsored by the Acoustics and Vibration Laboratory of the David Taylor Model Basin and the Davidson Laboratory of the Stevens Institute of Technology in January, 1965. The Conference was held at Stevens, Hoboken, N.J. The theme of the Conference was primarily a review of the "State-of-the Art," with the end objective of establishing an approach to the design problem. The Proceedings of the First Conference on Ship Vibration was published by DTMB, in Aug. 1965 [16].

The program for this Conference was divided into two subjects, each occupying a full day. The first day was devoted to "Vibratory Forces and Moments from Hydrodynamic Theory and Model Experiments." The second day was devoted to the "Vibratory Response Characteristics of Ships." Based on the available data, experience obtained in trouble shooting over the previous twenty-five years and an understanding of the needs of the shipbuilder, an effort was made to develop an approach, useful in the preliminary design phase, which would permit a reasonable prediction of the anticipated vibration characteristics of the hull and main machinery system. A more refined analysis would of course be required as part of the detailed development of the hull and machinery plant.

The program division of the First Conference on Ship Vibration into Hydrodynamics and Vibratory Response reflects the technical division which existed, and generally continues to exist in the treatment of shipboard vibration problems. The Hydrodynamicists represent the field of Naval Architecture while the analysis and treatment of the problem of ship vibration is generally assumed by the Marine Engineer. This division reflects the assumption that vibration problems are the unfortunate result of structural or mechanical resonances and the correction or cure to be the responsibility of the engineer. It was then, and generally is true today, that the Naval Architect established the exciting forces and the Engineer attempted to design the mechanical system to live with these forces. Thus, the basic approach outlined in this presentation follows the traditional procedure of applying the propeller forces predicted, to the preliminary design analysis. Details of this approach will be given in the "Design of Naval Surface Ships," in preparation by NKF for NAVSEA.

THE PRELIMINARY DESIGN APPROACH

Since any mechanical system, subjected to periodic forces, may exhibit unsatisfactory vibration characteristics during normal operation, a dynamic analysis is highly recommended as an aid in preventing dangerous or damaging vibration, while the system is still in the design stage. A large ship includes many such systems, the response of which in turn provides the inputs to many sub-systems. Therefore, any attempt to control or minimize the effect of large vibratory forces on the performance of such a large and complex system, such as a naval ship, requires particular attention to the problem of vibration, while the ship is still in the design stage.

A rational design approach to the evaluation of the vibration characteristics of a ship would include the following elements:

1. A set of design objectives or specifications.
2. An analytical procedure which includes
   (a) A suitable math model of the mass-elastic system under consideration
   (b) Input or forcing functions determined by theoretical analyses, model testing or a combination of both
   (c) Appropriate damping coefficients
   (d) Empirical factors to bridge missing functions, to efficiently simplify the analyses or to compensate for weaknesses in, or missing aspects of the theory.
3. Full scale test and evaluation program to
   (a) Confirm the adequacy of the results, and
   (b) Obtain technical data to permit continued development of the procedure and improvement of empirical factors.

In the application of this approach, the total ship system may be conveniently divided into the following parts:

Part I — *Vibration of Hull Girder*—The most fundamental requirement pertains to the response of the hull girder. The adequacy of the design, principally the stern configuration and the propeller design, which control the forces generated, and the response of the hull girder to these forces are reflected in the vibration characteristics of the hull. These characteristics provide the base from which the response of major substructures, local structures and supporting systems for equipment may be judged.

Part II — *Vibration of Major Substructures*—The response of major substructures reflect the dynamic behavior of those structural components when subjected to the motions of the basic hull girder at the points of attachment to the hull girder. As a minimum, the vibration amplitudes and frequencies will correspond to those of the hull girder at the point of attachment. Some amplitude magnification may generally be expected as a result of flexibility and/or resonances present in these substructures. Examples of major substructures will include deck-houses, uptakes, masts, machinery platforms, decks, bulkheads, etc.

Part III — *Vibration of Local Structural Elements*—The vibration of panels, plates or minor structural members are evaluated in terms of the vibration of the main structural members to which they are attached. The reference

could, therefore, be the main hull girder at that point or a major substructure.

Part IV — *Vibration of Shipboard Equipment*—Equipment should be designed to meet the environmental requirements established for shipboard use. Balancing and vibration tolerances for rotating machines should meet the requirements of MIL-STD-167 [5]. Installation details, including the choice of mountings, if used, should be checked to see that the equipment vibration, as installed, does not exceed that for which the equipment is designed, and in the case of self-excited equipment, the supporting structure should be such as to prevent the generation of excessive vibration or noise from a habitability point of view.

Part V — *Vibration of Main Propulsion Systems*—Main engines, shafts and propellers are designed for structural adequacy under the conditions stipulated in the procurement specifications. Vibration characteristics of the propulsion system must be controlled to avoid the presence of damaging vibration within the system and with the generation of severe vibration of the hull. Potential problems include dynamic unbalance of components, lateral, torsional and longitudinal vibration of the propulsion system, which can be controlled by the application of the requirements of MIL-STD-167 [5], and the generation of hull structural resonances when stimulated by propeller forces or shaft and engine frequencies.

During the preliminary design phase, the Vibration of the Hull Girder, Part I, and the Vibration of the Main Propulsion System, Part V, directly effect each other. Therefore, the principal purpose of the study is to determine the anticipated vibratory characteristics of the hull girder and the main propulsion machinery system of the proposed design and to provide a detailed evaluation of the influence of the various parameters which affect these characteristics. The scope of the study should include an estimate of propeller exciting forces, an estimate of the principal hull criticals of vertical, athwartship and torsional modes of vibration and a prediction of the response and the importance of the various modes of vibration, relative to the acceptance criteria or design specifications. A detailed evaluation of the lateral, torsional and longitudinal vibration characteristics of the propulsion system should also be provided, together with suitable recommendations for the optimization of the hull and machinery system parameters to minimize the estimated vibratory response.

Since many of the calculations performed in the preliminary design phase, may be based on assumptions and estimates, detailed design studies will be required in the detailed design phase, to confirm the earlier predictions, to provide a basis for the test and evaluation studies and to permit continued improvement of design procedures. Also during the detailed design phase, when the necessary information is available, the Vibration of Major Substructure, Part II, and the Vibration of Local Structural Elements, Part III, can be more effectively evaluated.

EXPERIENCE WITH THE APPROACH

Shortly after the First Conference on Ship Vibration of 1965, NKF had the opportunity to carry-out a preliminary Hull and Machinery Vibration Analysis for the Fast Deployment Logistic Ship Project (FDL) designed by Litton, in which the approach outlined was employed. This work was done in 1966, and although the ship was never built, the study did demonstrate the practicality of the approach [17].

A second study was conducted for the U.S. Coast Guard on the New Design Polar Icebreaker, in 1967 [18]. This study indicated the feasibility of improving the flow characteristics at the propeller and resulted in the conduct of a second study aimed at the optimization of the bossing configuration [19]. Again, no opportunity to evaluate the predictions was possible since the design was changed to significantly higher power and the studies were not repeated. Details of the procedures employed were presented to the New York Metropolitan Section of The Society of Naval Architects and Marine Engineers, Feb. 17, 1970, and published in Marine Technology of S.N.A.M.E., January 1971 [20].

About thie time (1970), a number of significant actions took place which greatly influenced the course of events, relative to the development of a suitable design procedure directed toward the limitation and control of shipboard vibration.

1 — NAVSEA issued the construction contract for the SPRUANCE Class Destroyer (DD963), which included specific design objectives of specifications, relative to shipboard vibration. (1970).

2 — El Paso Natural Gas Co. signed a contract for the first 125,000 CM LNG Carrier with Chantiers De France-Dunkerque. The ship was to have a single screw, delivering 45,000 SHP, 25% greater than any single-screw ship previously built. Hull vibration was considered a possible major problem area. (1970). Specific vibration design criteria was established for these ships in February 1971.

3 — Pressure Forces, generated by the propeller and augmented by cavitation, were determined to be potentially the most serious exciting forces [2] and [22]. (1971)

4 — The International Standards Organization, Shock and Vibration Committee, under its Sub-Committee 2, established a Working Group dealing with Ship Vibration, ISO/TC108/SC2/WG2. (1971)

5 — Preliminary Vibration Design Analyses were carried out for the DD963 [23] and the El Paso LNG Carrier [24], during the initial design phases of these ships and evaluated against the specific design criteria. (1971)

6 — A Ship Vibration Research Program was developed by S.N.A.M.E. Panel HS-7 "Vibrations" in 1971, and approved by the Hull Structure Committee of S.N.A.M.E. in 1972.

During the period 1971 thru 1975, NKF actively served as Consultants to the technical staff and designers of Litton Systems, Inc., and El Paso Natural Gas, Inc., and directed their technical programs in the areas of Vibration and Air-Borne Noise during the detailed design development of the DD963 and the 125,000 CM LNG Carrier. In the case of the DD963, model studies and hull design features influencing vibration and noise were carried out by DTNSRDC and Hydronautics, Inc. In the case of the F-D designed LNG Carrier, a development program, jointly sponsored by France-Dunkerque and El Paso, was undertaken at the Netherlands Ship Model Basin and the vibration characteristics of three competitive designs were evaluated. The three stern configurations are shown in Figures 1, 2 and 3 and represent the three models tested at NSMB:

Model 4141 — Modified Hogner — Figure 1
Model 4147 — Conventional — Figure 2
Model 4148 — Open Transom — Figure 3

Based on model performance and wake components as shown in Figures 4, 5 and 6, the open transom design was selected as the hull form which would produce minimum exciting forces. This form was used for the F-D design.

At this point in time, only rough estimates could be made of the hull-pressure forces. However, in both cases, extra precautions were taken to minimize the influence of cavitation on ship performance. In the case of the DD-963, underwater noise had to be kept to a minimum and in the case of the LNG Carrier, structural vibration associated with the high power was the major concern.

Throughout the development phase of both ships, considerable attention was given to design details to insure adequate response characteristics of machinery systems and local structures. Both ships were tested in 1975 with the DD-963 Vibration Trials Report being published in April 1975 [25], while the El Paso PAUL KAYSER Vibration Trials Report was published in November 1975 [26]. Results of these trials were most gratifying in that the vibration target levels were readily achieved. Results of these trials were included in a paper dealing with "An Assessment of Current Shipboard Vibration Technology" [27], prepared for the 1975 Ship Structures Symposium.

Following the 1975 Ship Structures Symposium plans were set in motion to hold a second ship vibration symposium, sponsored jointly by the interagency Ship Structure Committee and the Hull Structure Committee of the Society of Naval Architects and Marine Engineers. The Ship Vibration Symposium '78 was held in Arlington, Virginia, Oct. 16-17, 1978, and brought together international representatives of the maritime Community, including ship operators, builders, designers, researchers and governmental and classification bodies, who discussed all aspects of ship vibration, noise and hull/machinery compatability problems. The eighteen technical papers presented at the Ship Vibration Symposium '78 were published by S.N.A.M.E. in Publication SY-8. Discussions to the papers are included in a second publication SY-8A, while a report on the Symposium [28] represents a post-mortem which summarizes the key conclusions and outlines recommendations for future research work.

In a more recent study on the "Limitation on the Maximum Power of Single Screw Ships" [29], we find vibration to be a major factor in limiting the maximum power to approximately 65,000 SHP. Based on the major problem areas identified and the anomolies referred to in the limited studies conducted to date, the research requirements necessary to obtain the higher single-screw power requirements necessitate the confirmation of the present technology by full-scale studies and evaluation. Because of the interrelation of the many factors which are included in the development of a reliable design procedure, these required studies include:

1 — Development of a suitable full-scale test method of evaluating the true forces and moments generated in a given design.

2 — Development of methods for correlating the measured forces and moments with analytical procedures and model basin measurement programs.

3 — Development of design procedures in which the application of known vibratory forces to the Math Model of the systems under study will provide reliable response predictions. Included in this development should be improved damping coefficients and empirical factors to simplify procedures or to compensate for weaknesses or missing aspects of the theory.

4 — The development of a program of study to be conducted on a suitable class of ships, in which there are enough similarities and variations (such as the 125,000 CM LNG Carriers) to permit the verification of the design procedures on an adequate statistical basis.

As a follow-on to this study and the most recent Ship Vibration Symposium the Advisory Committee for Ship Vibration Related Projects has prepared a draft of "A Proposed Five-Year Ship Vibration Research Program," culminating in a "Design Guide for Shipboard Vibration Control." This effort has been carried out under the aegis of the Ship Research Committee of the Maritime Transportation Research Board of the National Research Council. The implementation of the program, as ultimately approved, should bring us closer to a rational Ship Vibration Design Procedure and should include lessons learned in recent shipbuilding programs carried out in the U.S., Europe, and Japan.

During the same decade (1970-1980) we have been actively consolidating our gains in this important field of the Limitation and Control of Shipboard Vibration by developing strong interaction between the pertinent technical agencies in the U.S. and their counterparts in the rest of the world, thru the International Standards Organization. In the U.S. the principle participants include NAVSEA, the David Taylor Naval Ship Research and Development Center, the Society of Naval Architects and Marine Engineers, thru their Research Panels, the American Bureau of Shipping, the Maritime

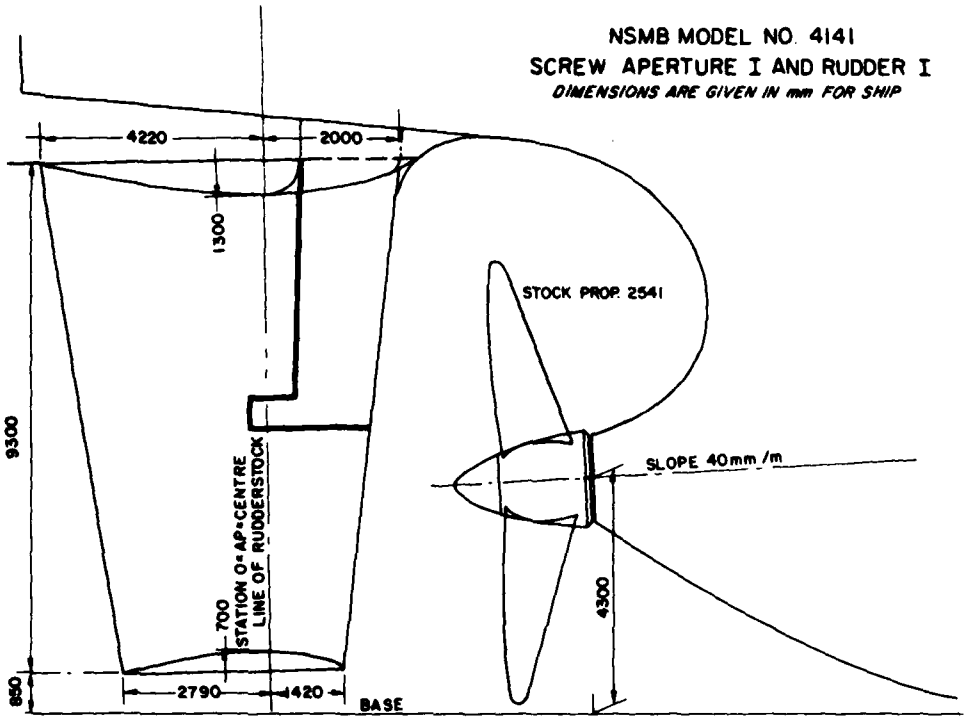

Figure 1 – Stern Configuration of Model 4141, Modified Hogner Design

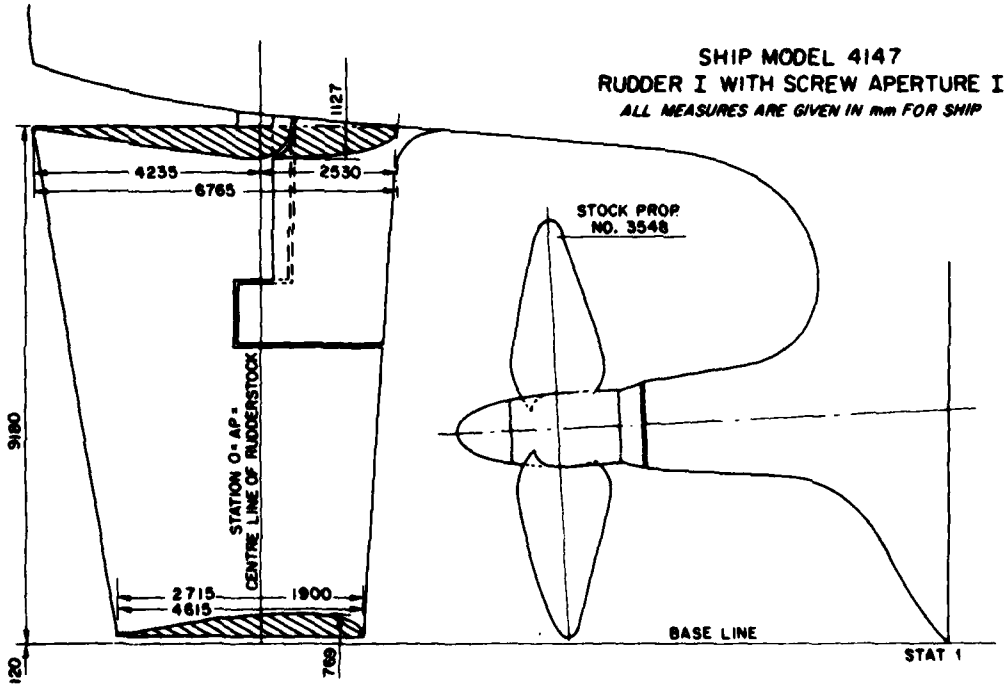

Figure 2 – Stern Configuration of Model 4147, Conventional Design

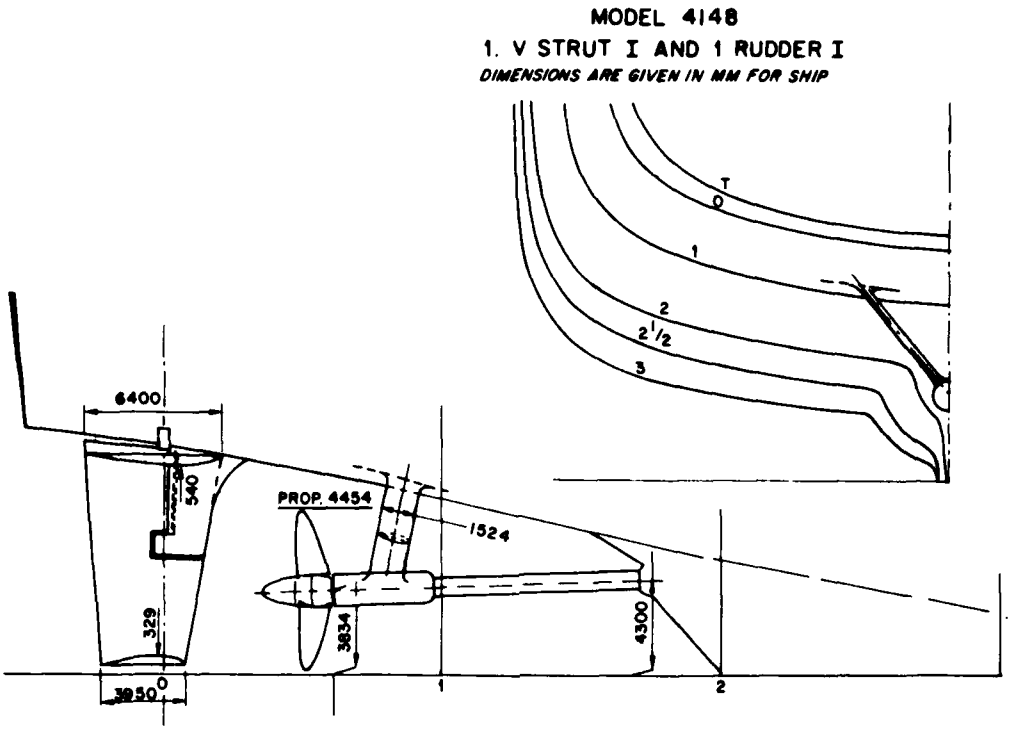

Figure 3 — Stern Configuration of Model 4148, Open Transom Design

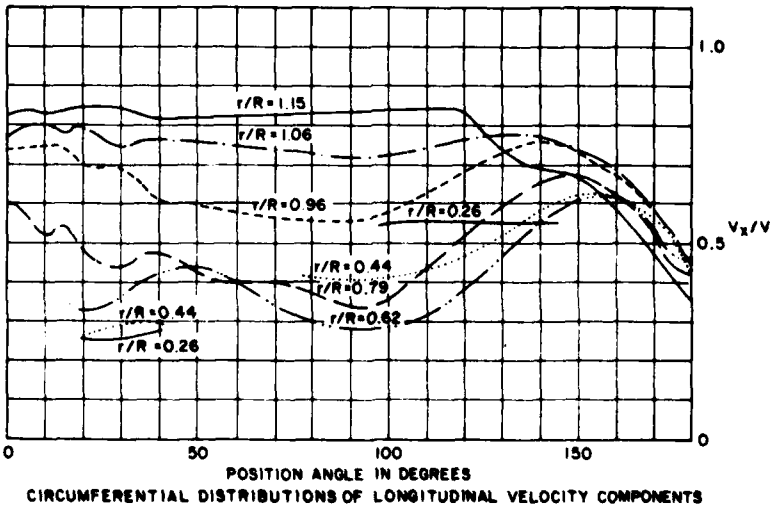

Figure 4 — Wake Components of Model 4141, Modified Hogner Design

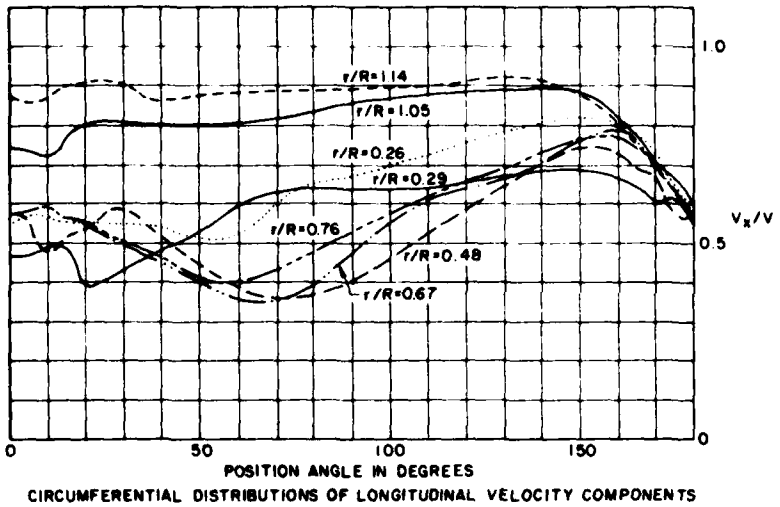

Figure 5 — Wake Components of Model 4147, Conventional Design

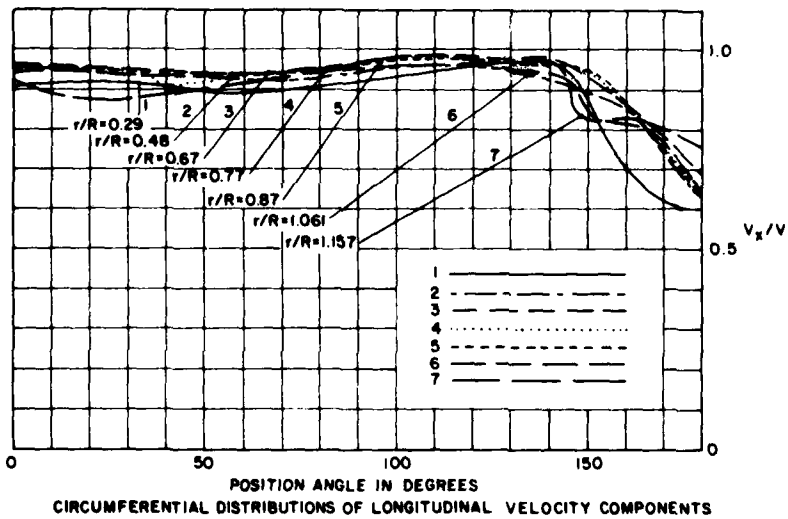

Figure 6 — Wake Components of Model 4148, Open Transom Design

Administration, Office of Ship Construction, and technical representatives of American Shipbuilders, Manufacturers and Naval Architectural Firms. Representatives of these organizations form Working Group S2-77 "Measurement and Evaluation of Ship Vibration," under the aegis of the American National Standards Committee (S2) on Mechanical Shock and Vibration, and represent the position of the U.S. when deliberating with their counterparts in the I.S.O.

Thru this process we have seen the S.N.A.M.E. T & R Bulletin 2-10 (1967) [30], the Navy Code (1968) [31], and the S.N.A.M.E. "Code for Shipboard Vibration Measurements" (1975) [32] develop into the Draft Proposal 4867 "Code for the Measurement and Reporting of Shipboard Vibration Data" (1979) [33]. In like manner, the S.N.A.M.E. Code C-4, "Shipboard Local Structure and Machinery Vibration Measurements" (1976) [34] has led to ISO D.P. 4868, "Code for the Measurement and Reporting of Shipboard Local Vibration Data" (1979) [35].

The I.S.O. D.P. 6954, "Guidelines for the Overall Evaluation of Vibration Merchant Ships" (1979) [36] corresponds, in part, with the S.N.A.M.E. T & R Bulletin 2-25 "Ship Vibration and Noise Guidelines (1980) [37]. All three of the ISO Draft Proposals have been favorably voted upon and should be issued shortly as International Standards. In each step, the process has resulted in technical improvements by the application of the expertise and experience of the contributors. In addition, it is extremely important that in international trade, as well as in military circles of the NATO

Alliance, that where feasible, we all speak the same language technically. This can best be done by the adoption of ISO standards, when applicable.

CONCLUSIONS AND RECOMMENDATIONS

In the development and utilization of such standards, specifications, technical bulletins or guidelines we are taking the most direct approach to the solution of a most complex problem. In so doing we find we can bridge a number of traditional gaps which tend to inhibit technical progress:

- The technical gap which exists when two or more disciplines are involved.
- The natural gap between researchers and designers.
- The proprietary gap existing between shipbuilders, or Manufacturing Corporations.

The utilization of specific technical requirements in ship specifications which identifies vibration tolerances, for example, should automatically introduce a design "line-item" which insures that funding and technical effort are included in the development program. When supported by adequate experience, well documented studies and a rational design approach the ultimate end objective should be forthcoming much more rapidly than might otherwise be anticipated. It should be noted however, that the initial specification should be achievable within the current state-of-the-art but can be expected to be modified or updated as the development of technology permits.

Let us apply this concept to the particular case in hand, that of designing a commercial ship. Based on past experience, we knew what level of hull vibration would be acceptable, regardless of the power required to meet the shipper's delivery program. Because we were extending the frontiers in this case, we undertook to study alternate stern configurations, selected the most promising and conducted suitable trial studies. We did achieve our design objectives. Thus, for similar ship types, we have the basis for specifying allowable hull vibration. This is now being done on a regular basis in most new ship contracts.

Similarly, it should be possible to generate a specification, limiting selected propeller forces to practical and achievable values, based on the results of full scale studies. In so doing, hydrodynamic studies, directed toward the limitation of these forces, becomes a line item at the model basin, and may require the optimization of the initial configuration to achieve the specification requirements. Thus, the design requirement would not only result in improved ship performance but would also accelerate the development of more reliable prediction techniques. At the same time, the design requirement becomes a known input function to the preliminary design studies carried out by the vibration engineer. In turn, improved measurement procedures designed to evaluate the true forces existing in the ship, when correlated with full-scale trial results directly leads to improved estimates of damping and ultimately more accuracy in the design procedure.

Although this all sounds like an over-simplification, it should not be dismissed too lightly. Just remember, if you define what you want, you *may* get it. If you *omit* it because you can't define your requirements today, with the precision you would like to have, you are much less likely to achieve your objective. I would like to conclude, therefore, that progress can be accelerated thru specifications. However, they must be reasonable, practical and *alive*. That is, through their use, they can and should be improved.

In regard to specifications, I would like to add a word in the form of a recommendation. First, the supplier will normally prefer not to have a specification, since this becomes a burden on his construction program. No specification, no requirement, no responsibility. It therefore behooves us, in our program development work, to insure our specifications are reasonable, up-to-date, properly used, and not in conflict with others. Toward this end, I would strongly recommend that we take the following steps:

- Do not operate in a vacuum, do not generate a specification, if one already exists elsewhere.
- Periodically review the specifications to insure they are up-to-date. It is reasonable to expect that progress will result from the use of the specification.
- In the development of specifications or standards, utilize all available data, such as is available thru the I.S.O., I.T.T.C., I.S.S.C., A.N.S.I., etc.
- Utilize the specifications in the development of more extensive programs, such as discussed herein.

REFERENCES

1. Jasper, N.H., "Structural Vibration Problems of Ships—A Study of the DD692 Class of Destroyers," DTMB Report C-36 (Feb. 1950).
2. Jasper, N. H. and Rupp, L. A., Cdr. USN, "An Experimental and Theoretical Investigation of Propeller Shaft Failures," SNAME Transactions (1952).
3. Noonan, E. F., "Tailshaft Bending Stresses on S. S. Esso Jamestown," A.S.N.E. August 1961.
4. S.N.A.M.E. T & R Report R-2, "Summary Report of the Investigation of Tailshaft Failures," A. M. Nickerson, January 1966.
5. "Environmental Vibration Testing for Shipboard Equipment," E. F. Noonan, Bu Ships, Shock and Vibration Bulletin No. 23, June 1956.
6. Vane, Francis F., "A Guide for the Selection and Application of Resilient Mountings to Shipboard Equipment," DTMB Report No. 880, July 1954.
7. Russo, V. L. and McGoldrick, R. T., "Hull Vibration Investigation on S. S. Gopher Mariner," Society of Naval Architects and Marine Engineers (1955).

8. McGoldrick, R. T., "Comparison Between Theoretically and Experimentally Determined Natural Frequencies and Modes of Vibration of Ships," DTMB Report 906 (August 1954).

9. McGoldbrick, R. T., "Ship Vibration," DTMB Report 1451, December 1960.

10. Leibowitz, R. C. and Kennard, E. H., "Theory of Freely Vibrating Non-Uniform Beams, Including Methods of Solutions and Application to Ships," NSRDC Report 1317, May 1961.

11. Todd, F. H., "Ship Hull Vibration," Edward Arnold, Limited, London (1961).

12. "Shock and Vibration Environment on the Polaris Missile in SSGN," E. F. Noonan, Bu Ordnance and R. O. Belsheim, USNRL, Shock and Vibration Bulletin No. 26, Part I, September 1958, p. 106 (Confidential).

13. Noonan, E. F., Cummings & Hardy, "Environmental Vibration on Submarines," 31st Shock and Vibration Symposium, Phoenix, Arizona, October 1962 (Confidential).

14. Buchmann, E., "Criteria for Human Reaction to Environmental Vibration in Naval Ships," DTMB Report 1635, June 1962.

15. Noonan, E. G., "Shipboard Vibration Research in the U.S.A.," *Presented at the 2nd International Ship Structures* Congress, Delft, The Netherlands, July 1964. DTMB Report 1891, September 1964.

16. "Proceedings of the First Conference on Ship Vibration," Stevens Center, Stevens Institute of Technology, Hoboken, New Jersey, 25 and 26 January, 1965, DTMB Report No. 2002, August 1965.

17. "Hull and Machinery Vibration Analysis for Fast Deployment Logistic Ship Project (FDL)," for Litton Industries, Inc., NKF Project No. 6704, December 1966.

18. "Integrated Vibration Study for New Design Polar Icebreaker" for D.O.T., U.S.C.G., Washington, D.C. NKF Project No. 6811, November 1967.

19. "Bossing Design for the Wing Screws of the New Design Polar Icebreaker" for D.O.T., U.S.C.G., Washington, D.C. NKF Project No. 6819, August 1968.

20. Noonan, E. F., "Design Considerations for Shipboard Vibration," Marine Technology, January 1971.

21. Manen, F. D. von, "The Effect of Cavitation on the Interaction Between Propeller and Ship's Hull," presented at the I.V.T.A.M. Symposium on non-steady Flow of Water at High Speeds, Leningrad, 1971.

22. Huse, E., "Propeller-Hull Vortex Cavitation," Norwegian Ship Model Experiment Tank Publication No. 106, May 1971.

23. Noonan, E. F., "Preliminary Hull and Machinery Vibration Analyses for DD963 Class Destroyer Design," NKF Report No. R-7105-4 to Litton Systems, Inc., 26 Febary 1971.

24. Noonan, E. F., "Vibration Considerations on Project and Conventional Hulls for 120,000 CM LNG Ships," NKF Report No. 7107, 28 May 1971.

25. "U.S.S. Spruance, DD-963, Vibration Trials Report," for Ingalls Shipbuilding Division, Litton Systems, Inc., NKF Report No. 7404-2, April 1975.

26. "El Paso Paul Kayser, Vibration Trials Report," for Methane Tanker Service Co., Houston, Texas, NKF Report No. 7321-2, November 1975.

27. Noonan, E. F., "An Assessment of Current Shipboard Vibration Technology," Ship Structure Symposium '75, S.N.A.M.E. Publication SY-5.

28. "Report on Ship Vibration Symposium '78, Ship Structure Committee Report 292, September 1979.

29. Chang, Noonan, Scherer, Seebold and Wechsler, "Limitations on the Maximum Power of Single-Screw Ships," S.N.A.M.E. Transactions, Vol. 87, 1979.

30. S.N.A.M.E. T & R Bulletin No. 2-10, "Code for Shipboard Hull Vibration Measurements," (Revised 1967).

31. Hardy, V. D., "*Code for Hull Vibration Measurements* on Naval Ships," NSRDC Report 2781, July 1968.

32. "Code for Shipboard Vibration Measurement," S.N.A.M.E. Code C-1, January 1975.

33. I.S.O. D-P 4867, "Code for the Measurement and Reporting of Shipboard Vibration Data," September, 1979.

34. "Shipboard Local Structures and Machinery Vibration Measurements," S.N.A.M.E. Code C-4, 1976.

35. I.S.O. D-P 4868, "Code for the Measurement and Reporting of Shipboard Local Vibration Data," September 1979.

36. I.S.O. D-P 6954, "Guidelines for the Overall Evaluation of Vibration in Merchant Ships," September 1979.

37. "Ship Vibration and Noise Guidelines," S.N.A.M.E. T & R Bulletin 2-25, January 1980.

STATE-OF-THE ART ASSESSMENT OF MOBILITY MEASUREMENTS–A SUMMARY OF EUROPEAN RESULTS

D. J. Ewins
Imperial College
London, England

SUMMARY

Two parallel surveys have been conducted to assess the various techniques currently in use in the UK and in France for measuring structural mobility properties. A set of test structures were circulated amongst some 18 laboratories in the UK and 16 in France, all actively using measured mobility data, and their submitted results were subjected to detailed scrutiny and comparison. The different excitation methods available were all included and some attention was given to the major applications for mobility data of modal analysis and subsystems coupling. Composite graphs have been made of the submitted mobility measurements and consistency checks applied to the results of modal analysis. The survey highlighted difficulties in the transmission of mobility data and also showed the existence of a considerable degree of scatter in the different participants' definitive measurements of specific mobility parameters.

1. INTRODUCTION

1.1 Background

Mobility measurement techniques have become one of the standard tools used by vibration engineers as a means of describing accurately the dynamic behaviour of structures. Formerly, the procedures were known as "mechanical impedance measurements," but current practices and applications demand a more precise definition and the word "impedance" has now been replaced by "mobility."

In the early 1960's, newly-developed instrumentation for measuring mechanical impedance was becoming widely available and one of the research groups who were active in developing the transducers and general measurement techniques for mechanical impedance testing decided it would be interesting to conduct a survey to assess how consistently different people could measure specific structural impedance properties. This survey, which was conducted by the U.S. Naval Research Laboratory, became known as the "Round Robin"* Survey and its findings were published in a Shock and Vibration Bulletin in 1964 [1]. Many interesting and useful results emerged from the comparisons of different laboratories' measurements on a set of three structures which were circulated amongst some twenty organizations, all of whom were actively using impedance testing techniques as part of their structural vibration studies.

Since the time of that Round Robin project, there has been an enormous growth in the use of these (now) mobility measurement techniques, encouraged by the advent of new instrumentation and, more recently, by the availability of sophisticated computer-controlled measurement facilities, all of which serve to make the acquisition of mobility data much easier, much faster and potentially much more accurate than in the past. In addition to facilitating the measurement of mobility data, these computer-based systems also provide a valuable analytical capability, most commonly in the form of curve-fitting modal analysis.

1.2 Requirements for a New Survey

At the same time as there have been considerable developments in mobility measurement technology, there has also been a proliferation in the number of organizations who are making use of the techniques. Mobility measurements and their subsequent analysis are being undertaken in order to tackle a wide range of structural vibration problems, quite often by engineers who are relatively unfamiliar with structural vibration characteristics, although quite conversant with instrumentation and computer devices. It was felt that there may be many instances in which mobility data were being measured and used, but where the quality of those data was neither checked nor of a sufficiently high standard to justify the applications to which they were being put. This phenomenon, if indeed it existed, could arise from the facility with which individual mobility measurements can be "made" using modern equipment.

It was considered that the time was ripe to conduct another survey of mobility techniques, following the pattern of the Round Robin survey some fifteen years earlier, but devised to tax the current measurement state-of-the-art much more than was appropriate in 1960 and also to focus on the applications and analyses to which the measurements were usually directed. To this end, a new survey was proposed which would consist of circulating a number of specially-designed test structures around a group of laboratories, all of whom possessed working experience of mobility

*It is interesting to note the following definition of the phrase "Round Robin," (from Brewer's Dictionary of Phrase and Fable-1978): "A petition or protest signed in such a way that no name heads the list .... The device is French, and the term a corruption of *rond* (round) *ruban* (ribbon) .... and was first used by the officers of government to make known their grievances."

measurement techniques. These "participants" would be invited to measure a specified set of mobility properties on each of the test structures and to submit their results to a control coordinator who would then incorporate them in a comparison with everybody else's results. In addition to the mobility properties, some further information would also be requested in the form of the modal properties which could be extracted from individual mobility curves via modal analysis. However, at all times the primary objective was to assess the state-of-the-art of the mobility measurement techniques, and the extraction of modal properties or other applications were a secondary objective.

1.3 Outline Plan

The initial idea for this new survey arose from discussions between Imperial College and S. A. Metravib in France, and the proposal was to conduct parallel surveys in the U.K. and in France. Because of their considerable interest in the successful application of mobility measurements, the Navy and Aerospace branches of the respective Defense Ministries were approached for sponsorship of this survey, late in 1976. A preliminary enquiry was circulated amongst interested parties early in 1977 and following an enthusiastic and active response, plans were made and contracts placed for the two parallel surveys. The anticipated timetable called for the circulation of the structures to all the participants to take place during 1978 and for the results to be processed and presented towards the end of 1979. This timescale was relatively short and required that the structures be available to each participant for only a few working days, and it also required that the minimum amount of time be lost in transporting the structures from one laboratory to the next. The timescale also imposed a constraint on the number of participants that could be accommodated, and the initial target was for about twelve laboratories to test the structures. Another requirement which influenced the selection of participants was the wish to cover as many as possible of the various techniques and instrumentation facilities currently in use for mobility measurement—including sine testing, transient testing and the various kinds of random excitation which are now popular.

2. DETAILED PLANS FOR SURVEY

2.1 Test Structures

2.1.1 Frequency range. In order to encompass the frequency range which is normally covered by typical structural vibration investigations -2 Hz to 50 kHz—it was necessary to design a number of different structures, each one concentrating on one part of the frequency spectrum. It was considered that the maximum range of frequencies normally covered on a single test was approximately two decades and so three categories of structure were planned: I, for the range 2-200 Hz; II, for the range 30-3,000 Hz; III, for the frequency range 500-50,000 Hz. (In practice, 50,000 Hz is much higher than one would normally venture, but it is not a totally unrealistic ceiling to a frequency range for mobility testing.)

2.1.2 Structure design. It was expected that many of the participants would be used to testing relatively large structures, but the problems of transportation which would would arise if the survey test structures were large would be quite considerable and so it was considered necessary to use relatively small structures. While posing problems for those participants unfamiliar with testing techniques for small test pieces, such structures do have the advantage that they are more demanding in many respects than are the larger ones.

2.1.3 Materials. The majority of engineering structures whose mobility properties are required would be made of metal—either steel or aluminum—and so the majority of the test pieces were designed accordingly. However, it was recognized that there exist some particular problems when testing a non-metal structure and so a fourth testpiece (IV), made from GRP, was added to the set.

2.1.4 Damping. Another problem which had to be resolved at the outset concerned the desirability of including at least one structure with a significant amount of damping. This requirement is difficult to meet as one important constraint on the structures is that their dynamic properties must remain constant over a relatively long period of time, for a relatively wide range of temperatures and during quite a lot of vibration testing. It was felt that with typical high-damping devices, such as constrained layer components, it would be difficult to guarantee consistency of the dynamic properties. The structures to be used tended to have very light damping in order to avoid uncertainty as to its exact magnitude and, with one exception, had no deliberate damping added. In one structure (I) the joints were very tightly bolted, in another (II), the joints were welded and the non-metallic structure had no joints. The only structure to possess any artificial damping was the high frequency one, (III), which contained a special high-frequency damping treatment in two of the three planes.

2.1.5 Dynamic characteristics. It was proposed that the structures should be relatively difficult to test, and to this end they were, for the most part, asymmetrical and the required excitation and response directions did not pass through the geometric or mass centres. This last feature would result in the structures having responses at the excitation point in all directions (not just that of excitation); a characteristic which is known to give rise to experimental difficulties.

2.1.6 Final designs. Based on the above criteria, plus some calculations to ensure that natural frequencies would lie in the frequency range of interest, a basic design for each of the structures was drawn up and a prototype test-piece made of each. Following measurements on these prototypes, a number of detailed modifications were made and the final designs were agreed and submitted for manufacture. Four identical structures were made to each design, it being agreed that any parallel surveys should use structures which are as near as possible identical to each other. The first set (α) was destined for the UK survey, a second, β, set was for the French survey, a third set, γ, was available for another survey if required (and is currently in use in the USA), while the last set (δ) was to be kept as spares. The structures are shown in Figures 1-4 and, as can be seen from Figure 2, structure II comes in two parts, IIA and IIB, which can be connected together to form an assembled structure, with a view to assessing the feasibility of predicting assembly mobility properties from knowledge of those of the constituent parts.

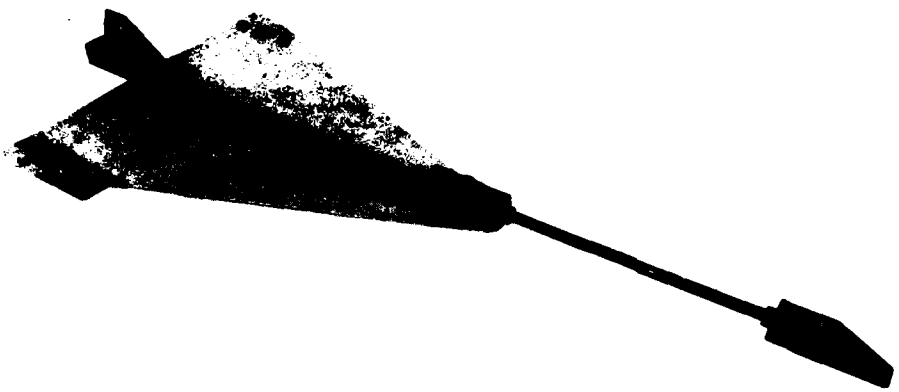

Figure 1 – Structure I

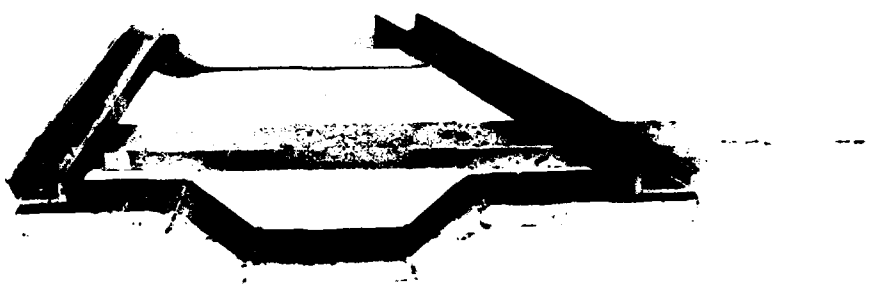

Figure 2 – Structure II

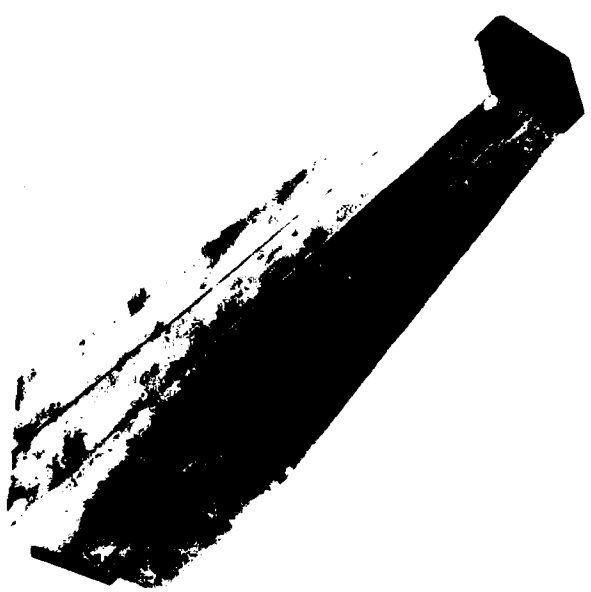

Figure 3 – Structure III

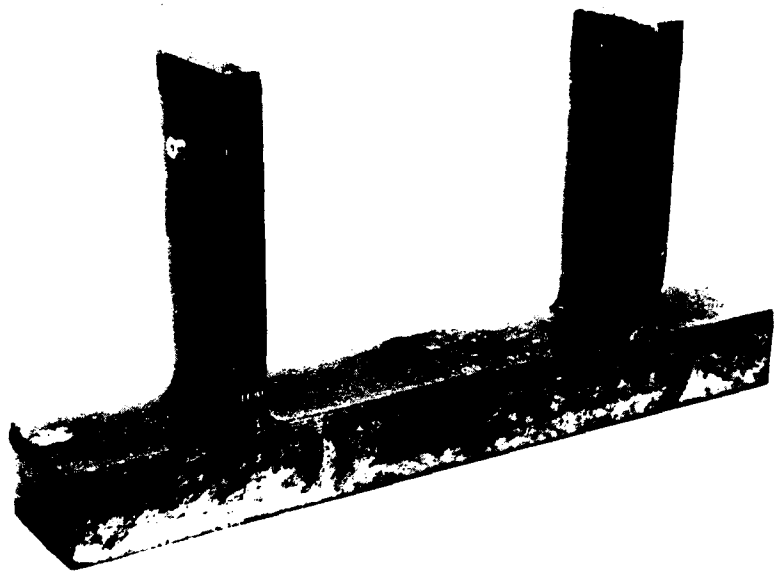

Figure 4 — Structure IV

2.1.7 Attachment adapters. It was realized that the many different laboratories which would test the structures would wish to connect their own various shakers and transducers and that some flexibility of attachment was required at the selected points for excitation and measurement. It was clearly impractical to allow each participant to modify the structure as his attachment conditions required, and so a set of interchangeable adapters was provided for structures I, IIA and IIB which could accommodate any thread or other connection device.

2.1.8 Control measurements. It was accepted that some control measurements would be necessary to establish the extent to which the test-piece properties changed throughout the course of the survey and so a series of repeat measurements was planned at approximately three-month intervals throughout the survey, at which times one mobility measurement on each structure was re-made, using the same transducers and instrumentation each time.

2.2. Data Requirements

2.2.1 Mobility measurements. The first objective of this exercise was to compare mobility data measured by different laboratories and so the *Primary data* to be submitted by each participant was to be their definitive measured curve for each of a number of specified point and transfer mobilities. In addition to these primary data, there was to be a request for *Secondary data*, which would be measured curves of the same mobility parameters, but perhaps using one or more alternative testing techniques, not necessarily what the individual participant regarded as his best method. The basic plan for the required mobility data was to select two points on each structure, i and j, and to specify the 2 x 2 mobility matrix between these two points as the required mobility parameters, i.e., Y_{ii}, Y_{ji}, Y_{ij}, Y_{ji} and Y_{jj}. In the initial plan, these measured mobility data would be required in graphical form, plotted to a standard format on a log-log scale covering two decades of frequency and 100 dB of mobility modulus. Some optional additional plots over 1 decade of frequency by 100 dB mobility were also included. It was decided at the outset that all the graphical data should be presented as mobility (rather than receptance or inertance) and that wherever possible, the results should be plotted on a standard size using blank graph sheets provided.

2.2.2 Modal analysis data. In view of the importance of the modal analysis application for mobility measurements, it was decided to include, (albeit in a secondary role) some assessment of the ability to extract modal properties from measured mobilities. To this end, there were two options— (i) by submission of data which could be processed through a single modal analysis procedure at Imperial College, and (ii) the analysis by participants using their own analysis routines, enabling them to submit the required modal properties directly. These two types of data submission were defined as *Digital Data* (for modal analysis) and *Modal Data* respectively.

It was clearly desirable to limit the quantity of data to be submitted to the minimum which would still provide the necessary degree of comparison and to this end it was decided to restrict the modal analysis aspects to a limited part of the frequency range on each structure. Thus, a limited frequency range, typically less than 1 decade, was selected from two decades used for the mobility measurement.

Modal properties were sought from all four mobility curves on each structure in order to permit a consistency check to be applied, made possible by the inter-relationship between any two point mobilities and the corresponding two transfer mobilities. This is discussed in more detail in Section 3.

2.2.3 Coupling data. Another application to which measured mobility data may be put is the process of analyzing a complex structure assembled from several components by defining the properties of each component separately and then connecting them by impedance coupling. (Although there are many techniques for performing the coupling process other than direct addition of the impedance matrices, they all rely on the same data to specify each subsystem.) An assessment of at least some aspects of this application is included in the survey in the form of two parts of Structure II. Accordingly, participants were invited to provide what they regarded as the mobility data for each component which would be required in order to predict corresponding mobility properties of the assembled Structure IIC, formed by joining IIA and IIB at the two points 1 and 2 already used as the locations for the primary mobility measurements. These *Coupling Data* were to be provided at a number of specified discrete frequencies (30(5)600 Hz). The data would be converted into an impedance matrix of the assembled structure and the results, in the form of mobilities of the assembled structure, would be compared with measurements made on the actual structure with IIA and IIB bolted together at the two points. Participants were not required to perform the coupling calculations, nor to undertake any measurements on the assembled structure, but simply to provide data adequate for such a coupling analysis.

2.3 Participation Conditions

2.3.1 Qualification. In order to make the results a valid assessment of the state-of-the-art of mobility measurement techniques, and also to limit the number of participants in order to maintain the target time-scale, it was decided that all the laboratories participating in the exercise should already be regularly involved in the measurement of mobility in the course of their engineering investigations.

2.3.2 Timing. In order to minimize the total time taken to conduct the survey, each participant was allowed access to the structures for only ten working days. The data to be submitted in the various categories described in Section 2.2 were not required immediately upon completion of the actual measurement phase, but participants were urged to submit their results not later than three months after completion of their measurements.

2.3.3 Instructions. Also in the interests of minimizing the demands on the participants, a detailed set of instructions was prepared which attempted to specify every detail of the testing requirements and the data required. Precise instructions were included to ensure that the required mobility parameters were clearly specified and some constraints on the levels of vibration to be encountered during measurement were also given. However, no instructions or guidance were offered concerning the method of suspension of the structures or of the choice of transducer or measurement technique, save that of requiring mobility measurements of the structures in a "freely-supported" condition.

3. METHODS FOR PROCESSING SUBMITTED DATA

3.1 Mobility Measurements

3.1.1 Original plan. The original proposal for providing a comparison of all the participants' measurements of the various mobility properties requested was to produce for each of the 19 different mobility parameters a single plot which showed the envelope encompassing all the individual measured curves. This format followed exactly that used in the previous Round Robin exercise, as illustrated in the Figures of Reference 1.

3.1.2 Revised plan. There was always some doubt as to the value of an envelope plot as described above in that it tends to highlight the extreme (and thus probably the worst) measurements, without giving any indication of the consensus or average properties of the collected results from many different measurements, and so alternative or modified versions of this form of presentation were sought right from the outset. In the event, the main advantage of the proposed envelope presentation—which was that it could be readily constructed from tracings of the individual curves as submitted—was lost because of the relatively small number of results which were submitted in exactly the right graphical format.

In the event, just 50% of the primary data were submitted in the required format, and as a result of this trend, an alternative plan was required for the presentation and comparison of the measured results. It was decided that all the primary data should be stored in digitised format on a main-frame computer which could then be used to make composite plots of the various measurements as required to compare particular features. For example, it would be possible to superimpose all the measured data for one particular mobility parameter, or to superimpose all the plots of one mobility obtained by random excitation, or to focus on the results obtained in a selected narrow frequency range.

3.1.3 Data handling and presentation. The software used to process the mobility data submitted to the CDC computer consisted of two main parts. The first was involved with the input of digital data in a range of different formats and with their standardization and storage in the most compact manner possible in the data bank. The second part of the software consisted of a series of routines which enabled data stored on the data bank to be summoned and plotted in any desired presentation.

3.2 Modal Properties

3.2.1 Analysis of digital data. One of the options for data submission was the provision of a small number of accurately measured points in the vicinity of each of a number of specified resonances. These digital data were to be subjected to a modal analysis process in order to extract the modal properties. It was proposed that the program POLAR, developed at Imperial College, be used for this task, and as part of

an overall assessment of that program, some comparative analyses were made using it and a French equivalent on a number of sets of test data. The program POLAR works by fitting a circle to measured values of receptance plotted on a Nyquist diagram—an approach which is valid for clearly-defined and relatively lightly-damped modes. These characteristics were exhibited by the test structures used in the survey. Each mobility curve analyzed by this program yielded a set of modal parameters—natural frequency (ω_r), damping loss factor (η_r), (based on a hysteretically-damped modal) and modal constant ($_rA_{ij}$)—for each mode of vibration in the frequency range covered, as described in the following equation :

$$Y_{ij}(\omega) = i\omega \sum_{r=1}^{N} \frac{{}_rA_{ij}}{\omega_r^2 - \omega^2 + i\omega_r^2\eta_r}$$

The modal constant may be further described as the product of two of the mass-normalized eigenvector elements, thus :

$$_rA_{ij} = (_r\phi_i)(_r\phi_j)$$

It may be seen from this relationship that the modal constants for a particular mode determined from the four measurements Y_{ii}, Y_{ij}, Y_{ji} and Y_{jj} should be related by the identity

$$_rA_{jj} = (_rA_{ji})(_rA_{ij})/(_rA_{ii})$$

and this check was to be used to assess the overall quality of the modal properties produced.

3.2.2 Comparison of modal properties. In addition to the modal properties obtained by analyzing digital data furnished by the participants, further results could be submitted in the form of modal properties obtained by the participants themselves using their own modal analysis methods. The complete set of modal properties thus consisted of those supplied direct and those produced by analyzing appropriate measured data.

It was decided that the comparison of the modal properties should be confined to a relatively small number of modes in order to limit the quantity of data to be handled. Accordingly, it was decided to concentrate on the lowest three modes of structures I, IIA, IIB and IV, there being so little data submitted for structure III as to render a comparison inappropriate. For each such mode, four quantities were tabulated for each mobility parameter investigated. For mobility Y_{ij}, the four quantities for the r^{th} mode would be ω_r, η_r, $_rA_{ij}$, $_rD_{ij}$, where the last quantity is given by the expression :

$$_rD_{ij} = {}_rA_{ij}/\omega_r^2\eta_r$$

and represents the diameter of the circle curve-fit to the measured data points. This last parameter was included as its magnitude depends almost exclusively on the measured data themselves and does not depend on the performance of the modal analysis program which is used to extract the other three quantities. It may thus be regarded as a more appropriate way to compare the mobility measurements themselves in the region of a resonance. For each of these four quantities, it was proposed that a set of tables and histograms be used to present the comparisons of results from different sources.

In addition to comparing the results for individual mobility parameters, an opportunity exists for making an internal self-consistency check by examining the four results from each participant for the four components of the 2 x 2 mobility matrix measured between the two test points on each structure. This check consists of assessing the extent to which the relationship between $_rA_{ii}$, $_rA_{ij}$, $_rA_{ji}$ and $_rA_{jj}$ holds. An additional parameter, Δ_A, was introduced by the definition :

$$\Delta_A = 1 - \frac{{}_rA_{ij}\ {}_rA_{ji}}{{}_rA_{ii}\ {}_rA_{jj}}$$

and this quantity should be zero for a perfect set of results. It may also be seen that the same type of relationship must hold for the modal diameter D_{ij}, etc., and so a corresponding parameter Δ_D was also computed and included in the comparison. Thus, for each mode of each structure included in the comparison of modal properties, there exists a comprehensive set of tables and histograms and the latter are arranged in such a way that each individual histogram displays the different participants' estimates of a parameter or parameters, all of which should be identical.

3.3. Coupling Data

The basis for using the measurements requested for the coupling of structures IIA and IIB together to form the composite structure IIC is expressed in the single equation :

$$\left[Y_C\right]^{-1} = \left[Y_A\right]^{-1} + \left[Y_B\right]^{-1}$$

To be exact, each of these matrices should be of order 12 to include the six possible coordinates at each of the two connection points. In practice, one would not expect to include so many terms and the simplest form which could reasonably be used would be that based on just the translation coordinates x_1 and x_2. The pair of 2 x 2 mobility matrices that are required for this simplified case are those which are specified in the Instructions to Participants, measurements of which are requested at certain specific frequencies in the range 30-600 Hz. An additional comment was made to the effect that the participants could measure any additional data which they felt was necessary to complete the coupling process, and this was an invitation to measure any of the other 140 elements from the complete 12 x 12 matrix. In the event, no one did measure more than the basic 2 x 2 matrices, and so the processing necessary to couple the two structures together consisted simply of performing the calculation given in the above equation for each of the 115 specific frequencies measured.

A computer program was written which took as input the eight measured mobility curves and which computed the

necessary matrix inversions and addition, resulting in the calculation of a 2 x 2 matrix for the coupled system, $[Y_C]$. The results of this calculation were to be plotted and compared (a) by superimposing the results from all the contributing participants and (b) with some measured data obtained on the actual assembly.

4. RESPONSE TO THE SURVEY

4.1 General

The initial target was for a dozen or so participants in each of the parallel surveys and, in the event, results were obtained from 16 laboratories in the UK and from 15 in France. Representatives from a very wide range of industrial, educational and research establishments were included.

There are a number of statistics of the survey itself which it is worth recording in addition to the main body of technical results described below. These data are presented in Tables 1 and 2, showing the numbers of participants who tested each structure and the test (excitation) methods they used, and also indicating the degree of response in respect of the post-measurement analysis applications.

The timetable of the survey was well-respected at the measurement stage, although the data submission period (maximum of three months after testing) averaged out at six months, the quickest being three months and the longest, one year!

TABLE 1

Survey Response

	Number of Participants Who:								
	Received Structures	Submitted Data	Tested Structure I	II	III	IV	Submitted Modal Props
UK	18	16	12	15	5	9	5
F	19	14	13	14	3	3	8

TABLE 2

Test Methods Used for Primary Measurements

Structure \ Excitation		Sinusoidal Stepped	Sinusoidal Slow Sweep	Rapid Sine Sweep	Impact	Random
I	UK	3	1	1	6	3
	F	10		0	1	2
II	UK	5	2	1	6	4
	F	10		0	1	3
III	UK	2	2	0	1	2
	F	1		0	1	1
IV	UK	2	2	1	5	2
	F	1		0	0	2

4.2 Quality of Submitted Data

In addition to there being a very large quantity of data submitted, the task of processing and presenting the results was made even more arduous by the relatively poor quality and non-standardization of the data. The first problem was that the primary data for the mobility plots was only submitted in the standard format in about 50% of cases, the other 50% being plotted on slightly or considerably different graph sizes, requiring an additional stage of processing. The very high proportion of non-standard primary data necessitated the change in plan for presenting graphical data which resulted in the accumulation of a data bank, in which all the mobility plots were stored in digitized form on the mainframe CDC computer.

A second, but related problem arose with those data which were submitted in the form of paper tape or magnetic tape. In many cases, especially with the paper tape, there were many errors in the data as submitted. One of the direct results from this aspect of the survey is the clear indication of a need for duplicating or even triplicating data records so that real errors can be both located and corrected efficiently.

5. SUMMARY OF SUBMITTED DATA

5.1 Graphical Data

A series of plots were prepared, illustrating the primary graphical data submitted for all the structures in various combinations and detail. The main body of these graphs consists of 2 decades x 100 dB mobility modulus plots, produced directly by the CDC computer onto microfilm and subsequently printed photographically onto the 150 x 240 mm standard graphical layout. A number of additional plots were also produced to the same overall size, but covering different frequency ranges, there being a 1-decade plot for each structure and a number of much smaller frequency ranges to illustrate measurements in the vicinity of individual modes.

The selected results presented here include some data from each structure and are detailed below.

Structure 1 is represented by the point measurement at the central mass and the two plots, Figures 5.1 and 5.2, show the results from the UK and French surveys respectively. Similarly, a point measurement on Structure IIA is included in Figures 6.1 and 6.2.

Measurements on the simple structure, IIB, are shown in Figures 7.1 to 7.6, these being the point mobility at one end, Figure 7.1 (F), followed by replots of the same data, but this time including only those data obtained by sinusoidal excitation (Figure 7.2—UK and 7.5—F), random excitation (Figure 7.3—UK, 7.6—F) and transient excitation (Figure 7.4—UK). Figures 8.1 and 8.2 show details from a transfer measurement on IIB, covering different frequency ranges. Three plots are included for Structure III, Figures 9.1 and 9.2 showing the collected results for the axial transfer mobility, and Figure 10 showing the lateral point mobility (UK).

The format adopted for the majority of plots is one in which all the participants' data are plotted as individual points, exactly as they are stored in the data bank, (*Background Data*) but in order to provide a visual focus, one curve has been plotted as a continuous line (*Featured Data*). (One participant was selected somewhat arbitrarily for this role and it must not be inferred that that one single dominant

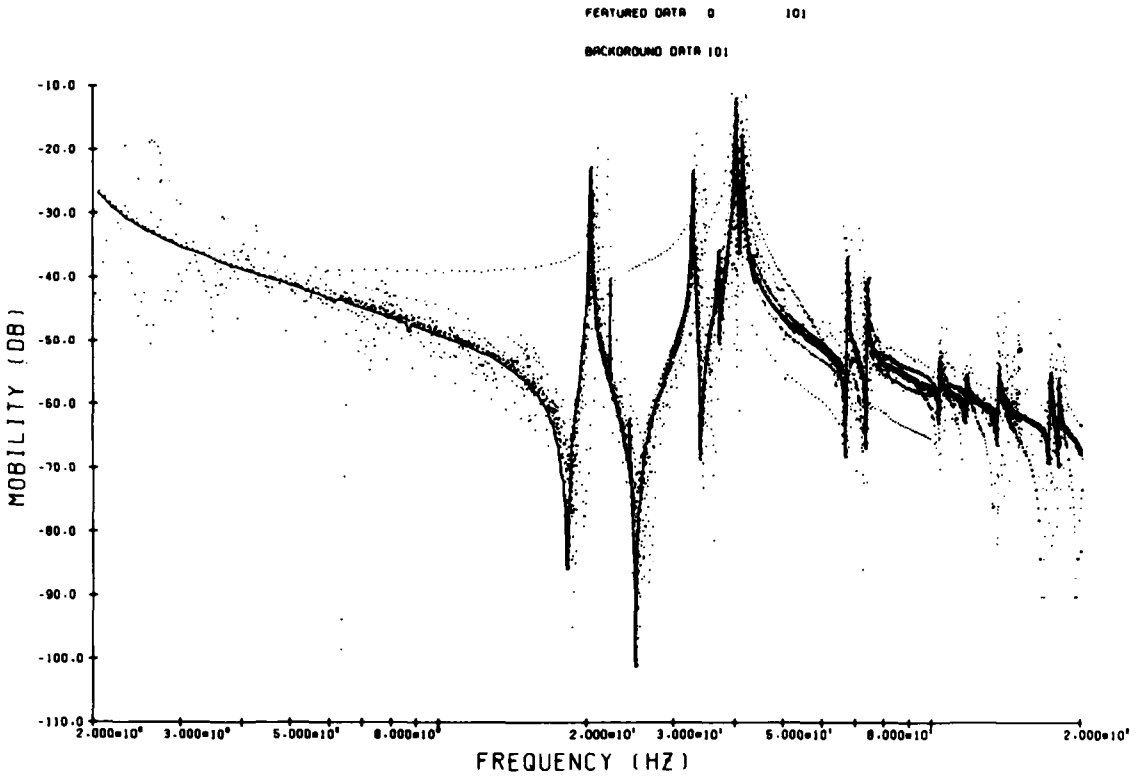

Figure 5.1 — Point mobility measurements on Structure I - all UK data (11 sets)

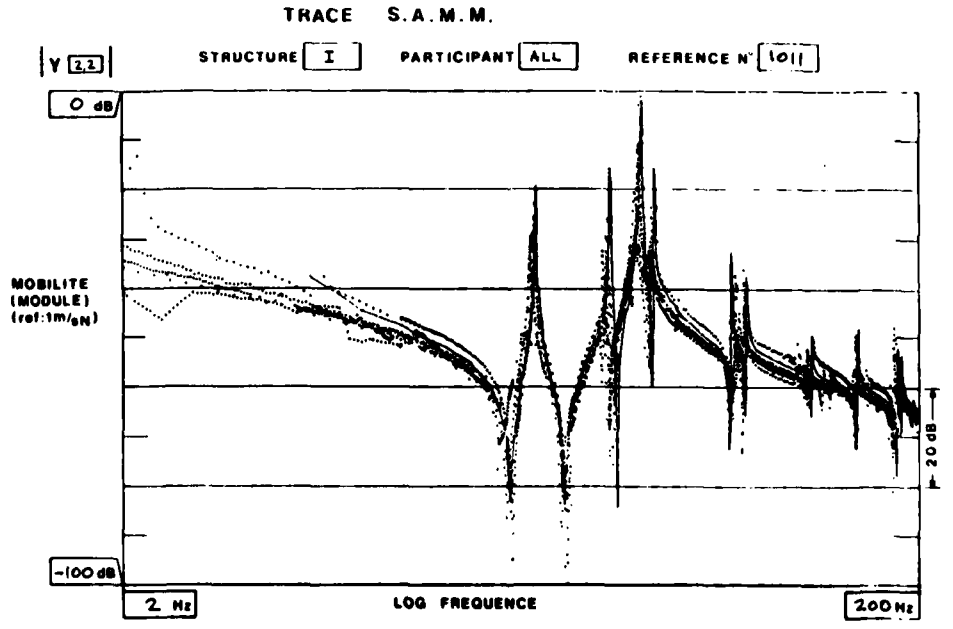

Figure 5.2 — Point mobility measurements on Structure I - all French data

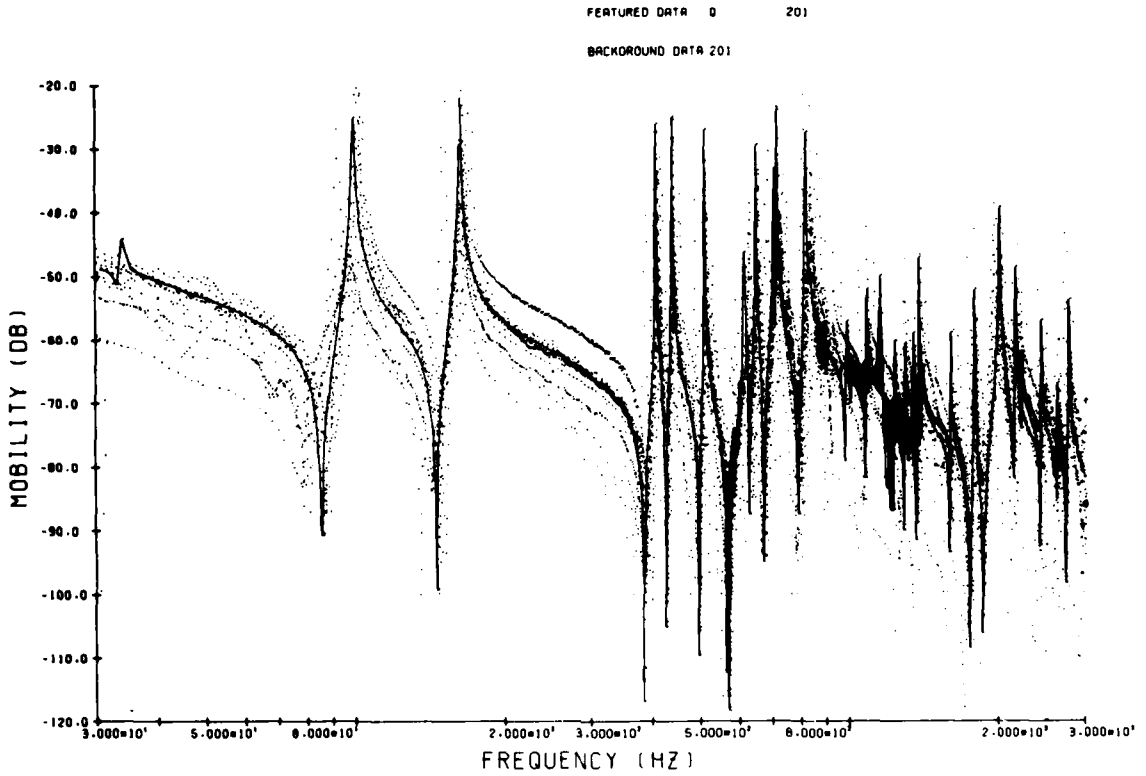

Figure 6.1 — Point mobility measurements on Structure IIA - all UK data (12 sets)

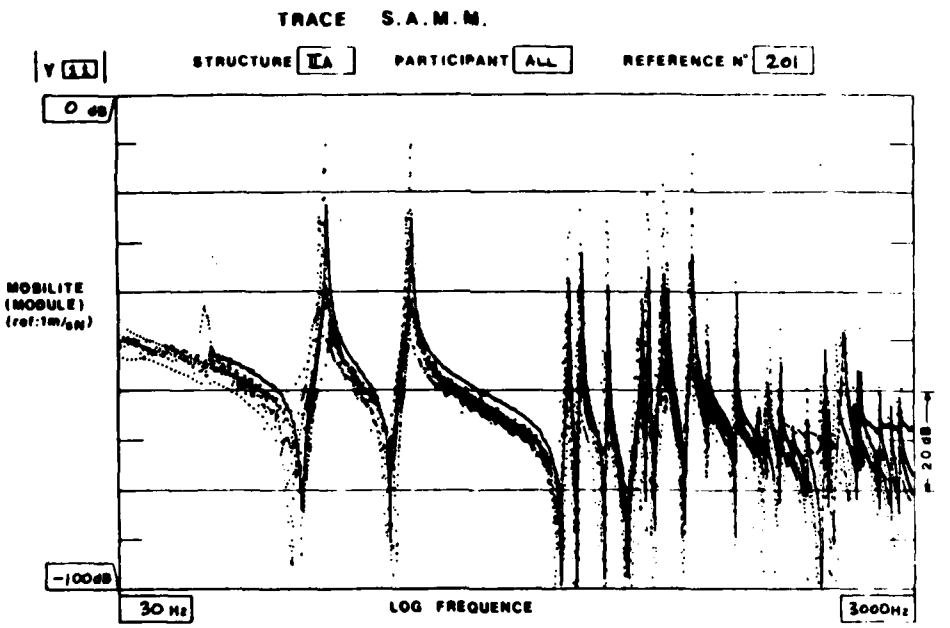

Figure 6.2 — Point mobility measurements on Structure IIA - all French data

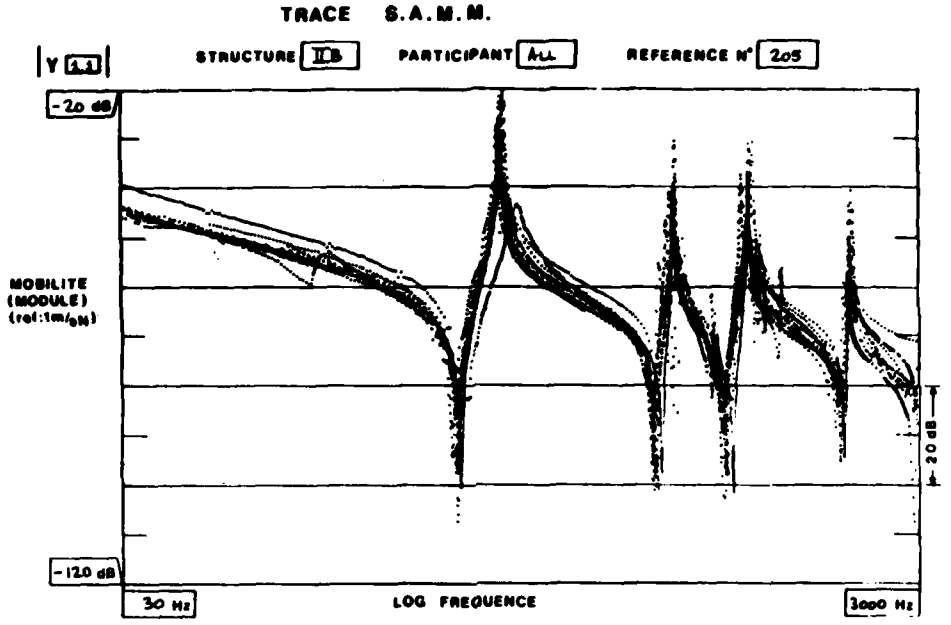

Figure 7.1 – Point mobility measurements on Structure IIB - all French data

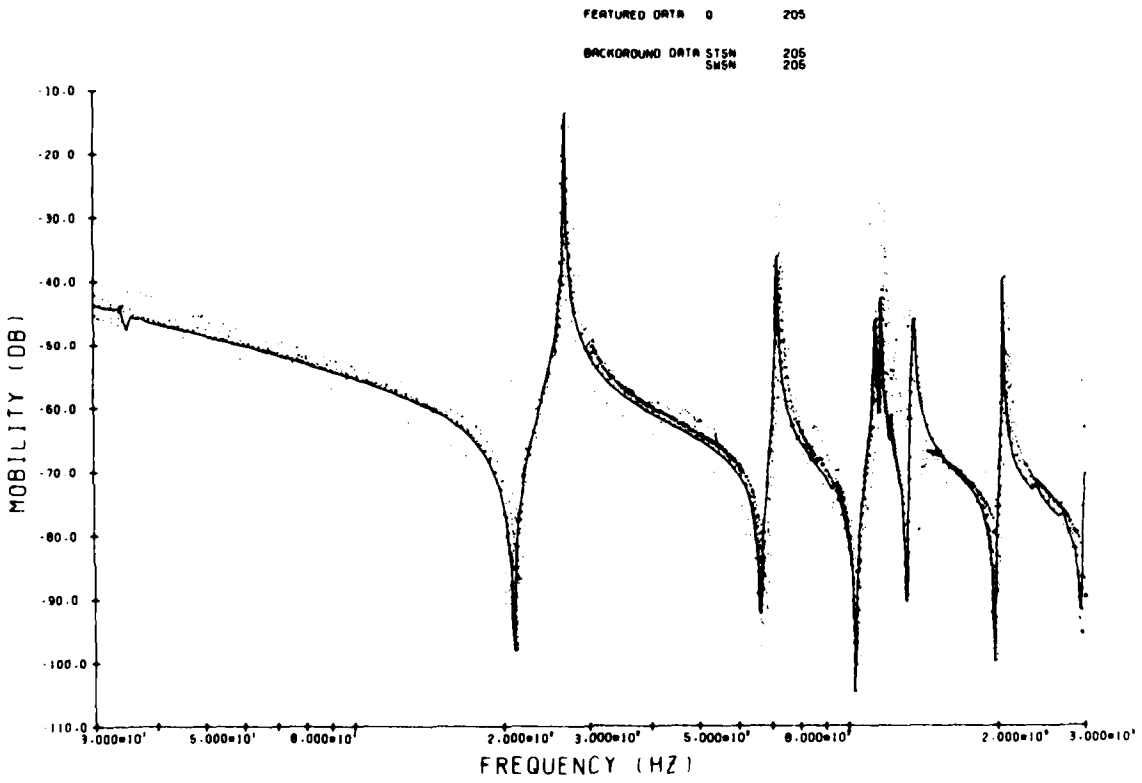

Figure 7.2 – Point mobility measurements on Structure IIB - UK data from sinusoidal excitation

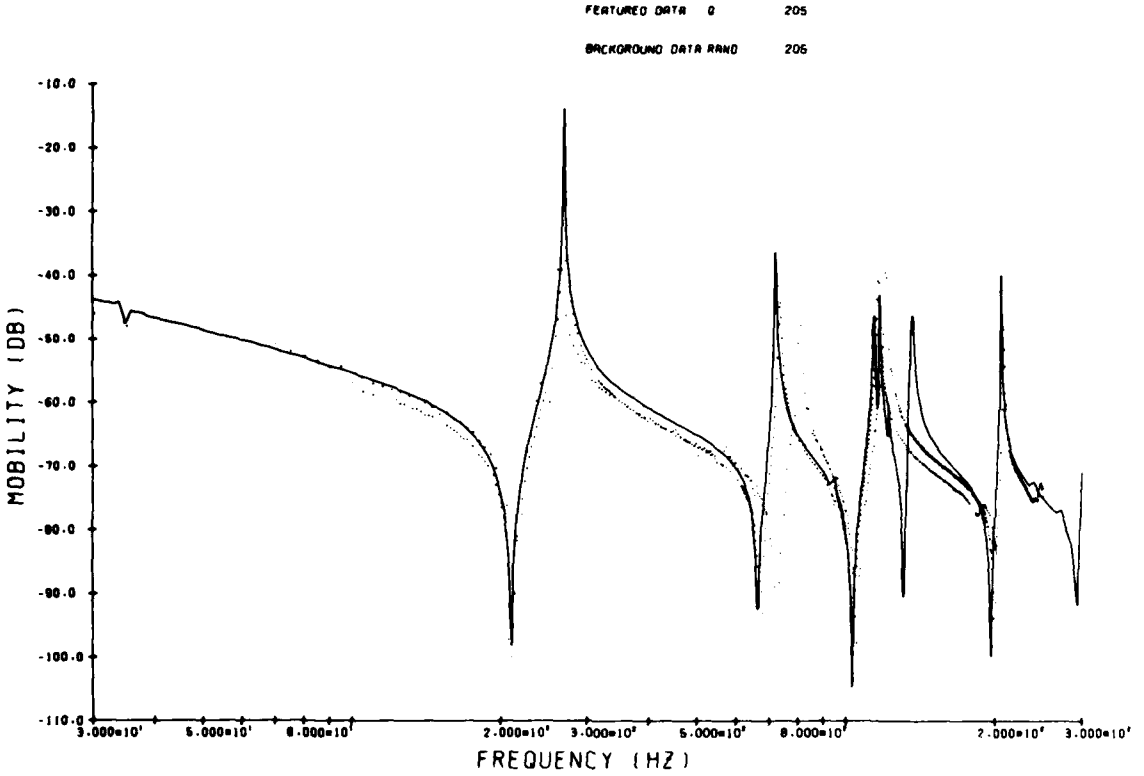

Figure 7.3 — Point mobility measurements on Structure IIB - UK data from random excitation

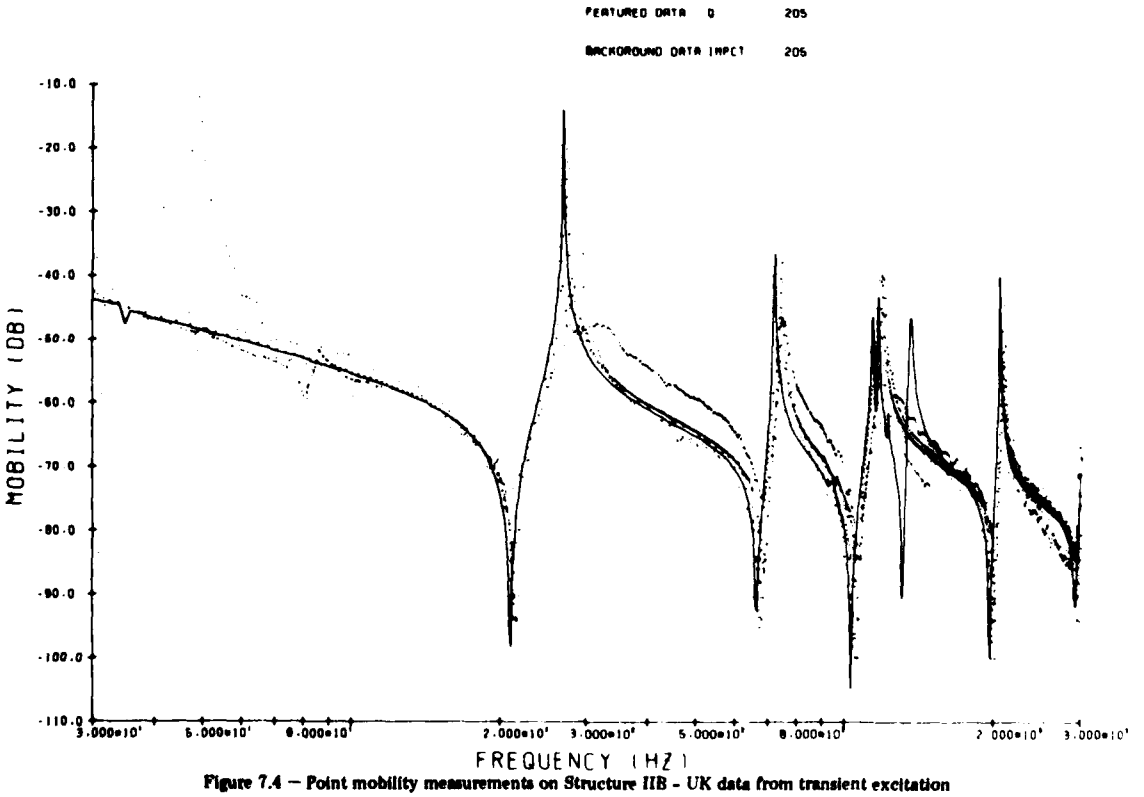

Figure 7.4 — Point mobility measurements on Structure IIB - UK data from transient excitation

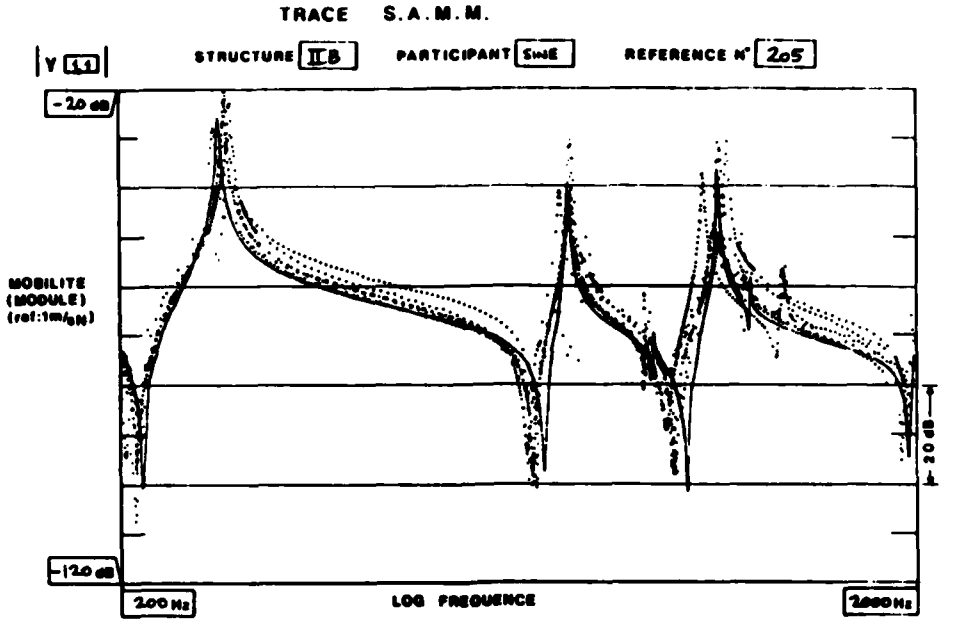

Figure 7.5 – Point mobility measurements on Structure IIB - French data from sinusoidal excitation

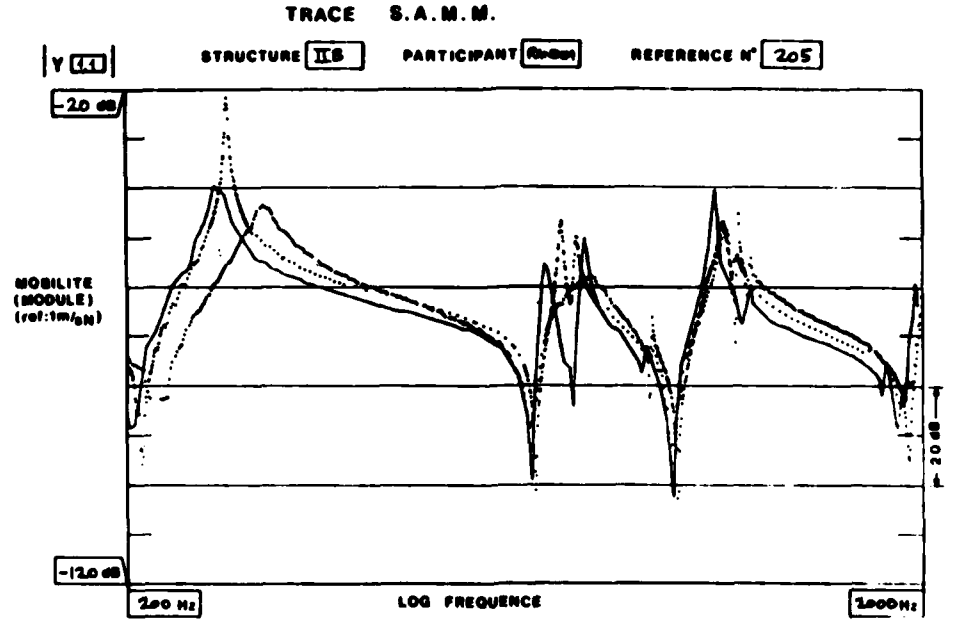

Figure 7.6 – Point mobility measurements on Structure IIB - French data from random excitation

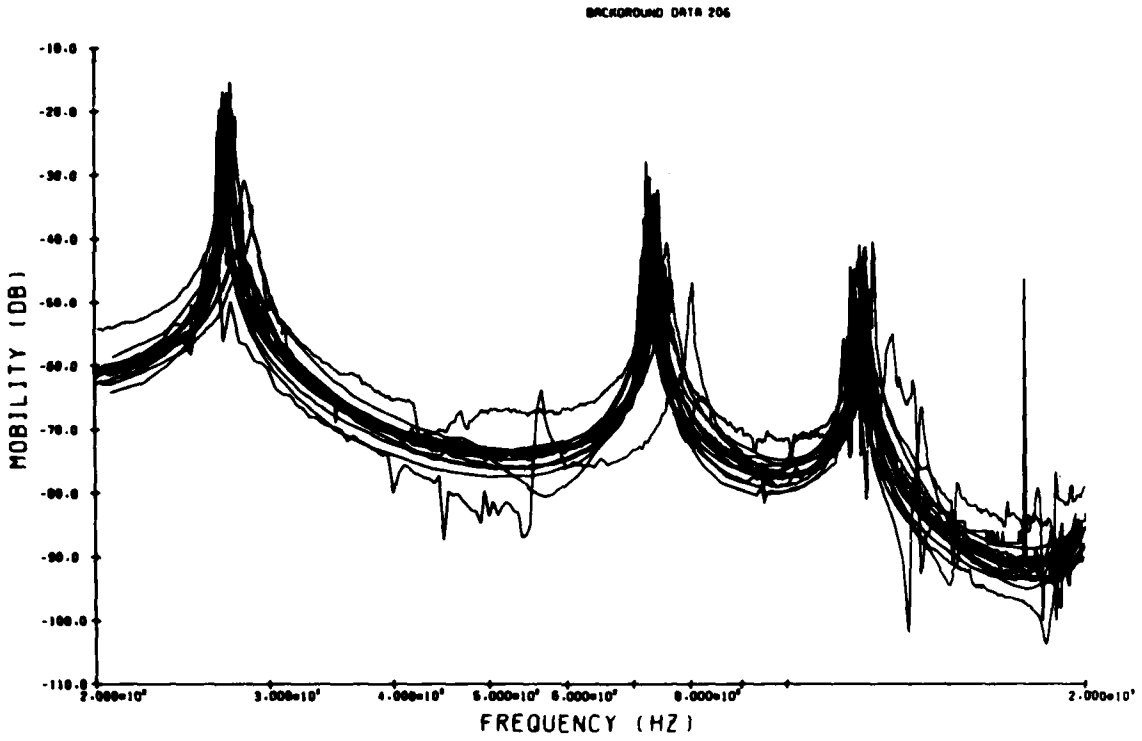

Figure 8.1 – Detail from transfer mobility measurements on Structure IIB - all UK data

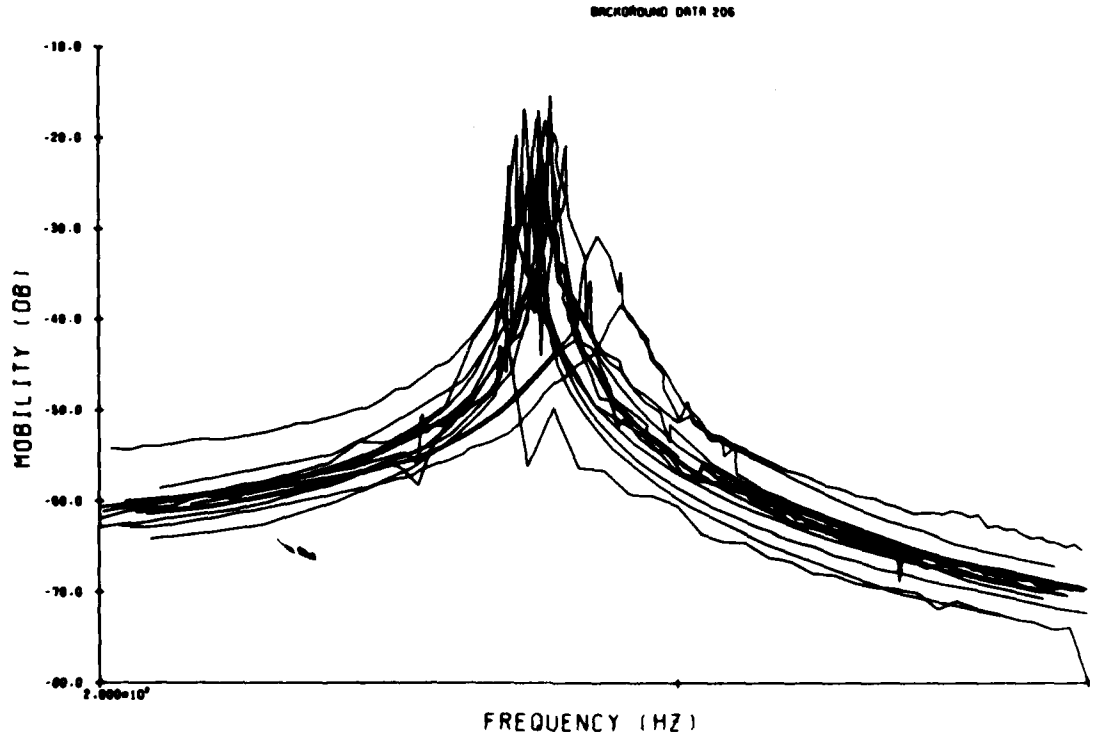

Figure 8.2 – Fine detail from transfer mobility measurements on Structure IIB - all UK data

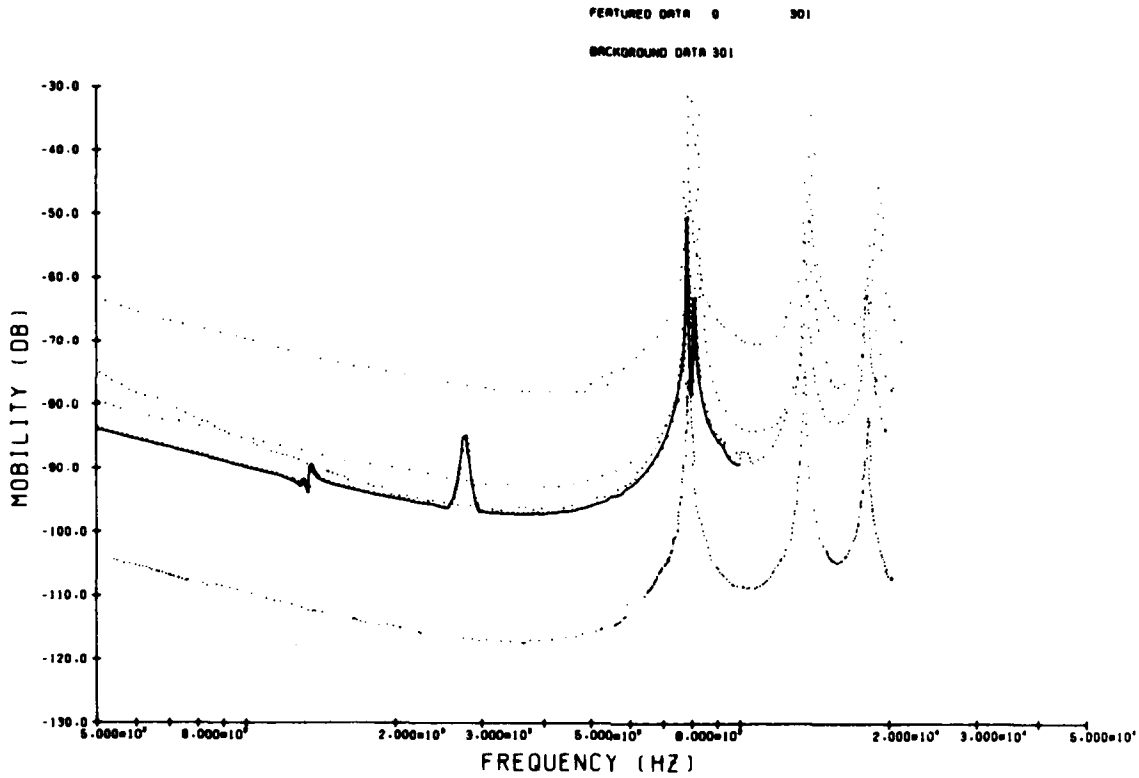

Figure 9.1 – Transfer mobility measurements on Structure III - all UK data

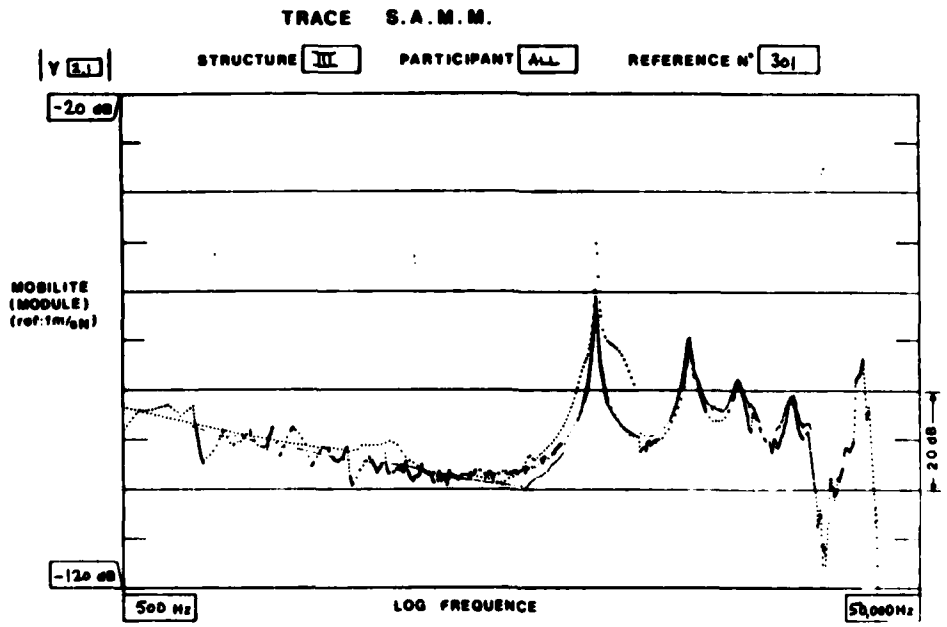

Figure 9.2 – Transfer mobility measurements on Structure III - all French data

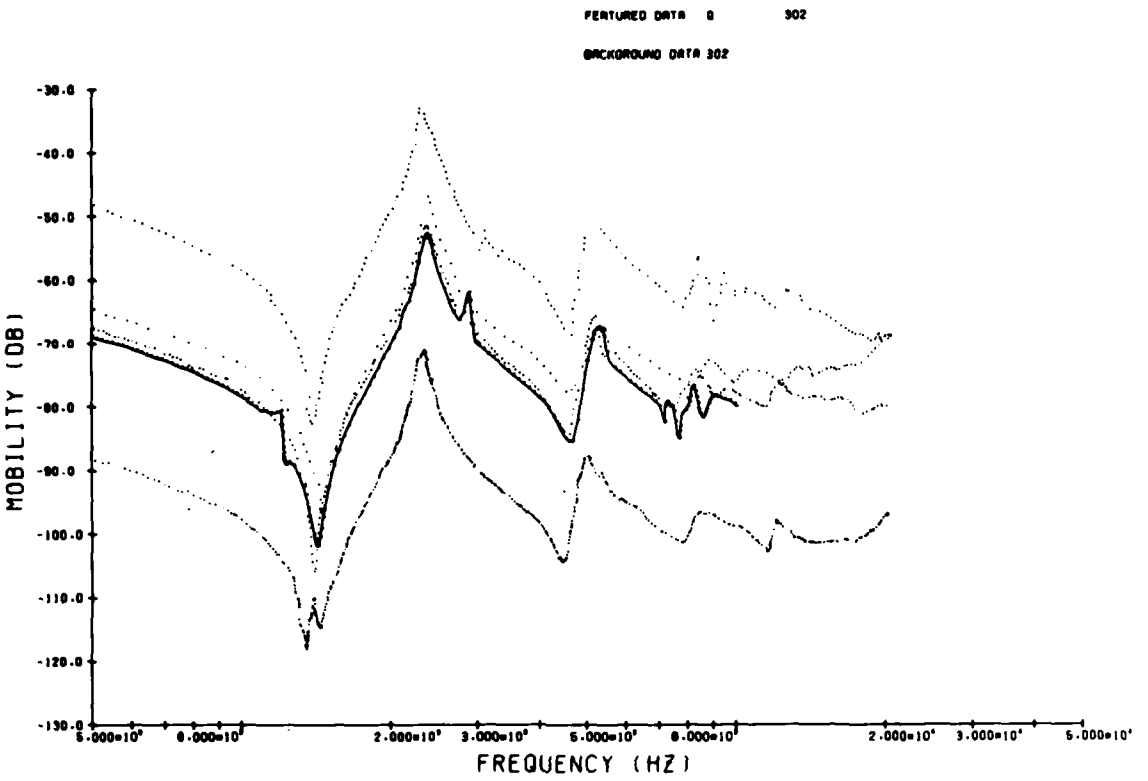

Figure 10 — Point mobility measurements on Structure III - all UK data

curve is in any way the correct or average result.) A number of the graphs show all the data as continuous lines where there is insufficient detail to result in this style of presentation being totally confusing. Finally, three plots are also included for Structure IV, Figures 11.1 and 11.2 being the UK and French measurements respectively of the point measurement on one side, and Figure 11.3 showing a transfer mobility between the two points of interest (UK only).

5.2 Repeatability Plots

The results shown in Figures 5-11 clearly indicate a fair degree of scatter and it is considered important that this be viewed alongside a series of plots (such as the one shown in Figure 12 for Structure IIA) which indicate the repeatability of one mobility parameter per structure when measured using exactly the same equipment and technique on a number of occasions encompassing the entire testing period. These measurements were made at Imperial College in February, July and September of 1978 and again in 1979 after all the participants had completed their testing. The five graphs obtained all show a relatively high degree of consistency when compared with the range of answers produced by different testers during the same period.

5.3 Modal Data

For each set of acceptable digital data submitted, modal analysis using the program POLAR was carried out and the results were recorded on standard tables, there being one such table for each mobility parameter studied. A corresponding table was also compiled for the submitted modal data where the modal properties had been supplied directly by the participants. From these two tables, the results were combined and are presented in the form of series of histograms, such as that shown in Figure 13 for Structure IIA.

Each such figure consists of ten individual histograms showing the collected results of both digital and modal data for an individual mode of a particular structure. The ten items displayed are the natural frequency and damping loss factor (of which there may be up to eight different estimates from each participant; four from digital data and four from modal data), the modal constants and modal circle diameters for the two point measurements (maximum two estimates per participant) and the pair of transfer mobilities (up to four estimates per participant) and, finally, the two histograms for the quantities Δ_D and Δ_A defined in Section 3.2.2 (up to two estimates per participant). For ease of identification, those results included in the histograms which come from Modal Data supplied directly by the participants are shaded, while those obtained by POLAR analysis of Digital Data are clear. Within each individual histogram, all of the data entries should theoretically have the same value, and in the case of the last two, this value should be zero.

Examination of the results of modal properties shows there to be a fairly wide range of values obtained for the various quantities. The spread of values for the natural frequency of the fundamental mode of the simple structure IIA covers a band 7% of the average value—at first sight, a somewhat large spread. The values obtained for the damping loss factor of

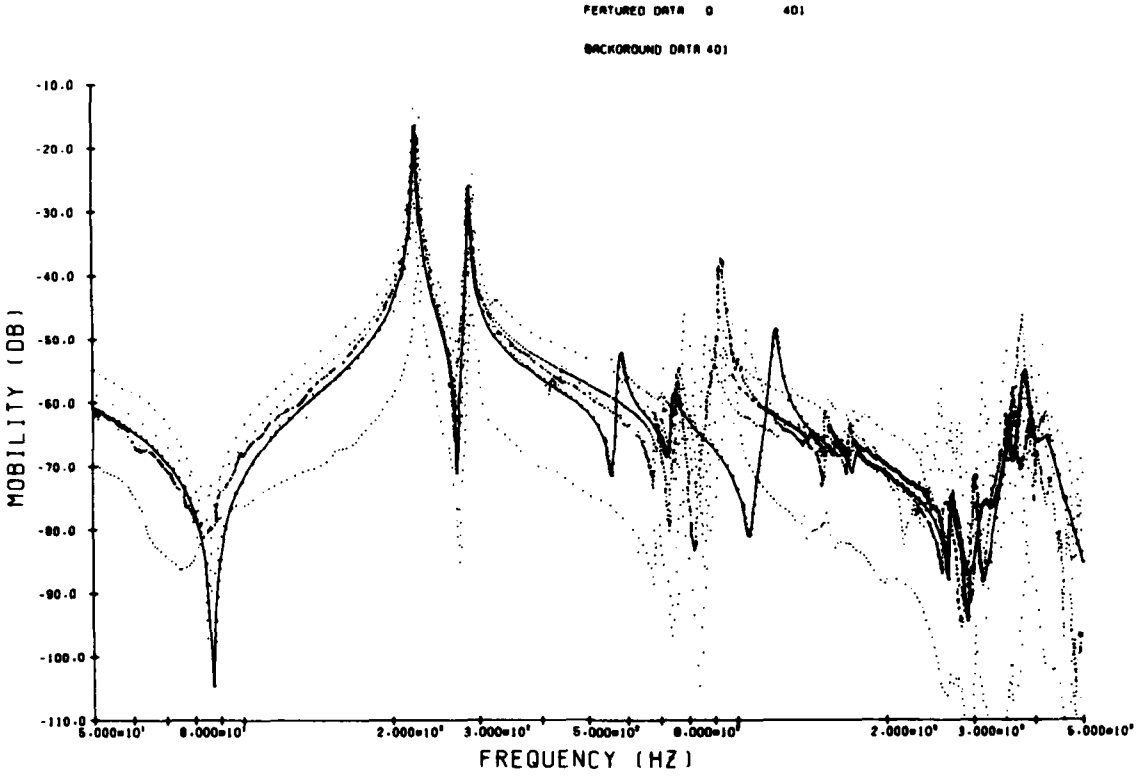

Figure 11.1 — Point mobility measurements on Structure IV - all UK data

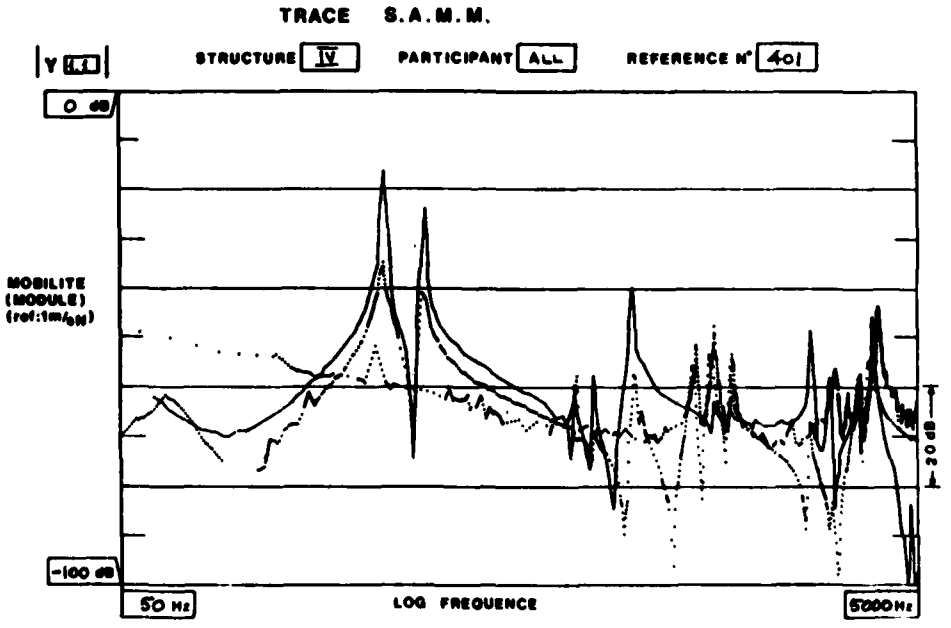

Figure 11.2 — Point mobility measurements on Structure IV - all French data

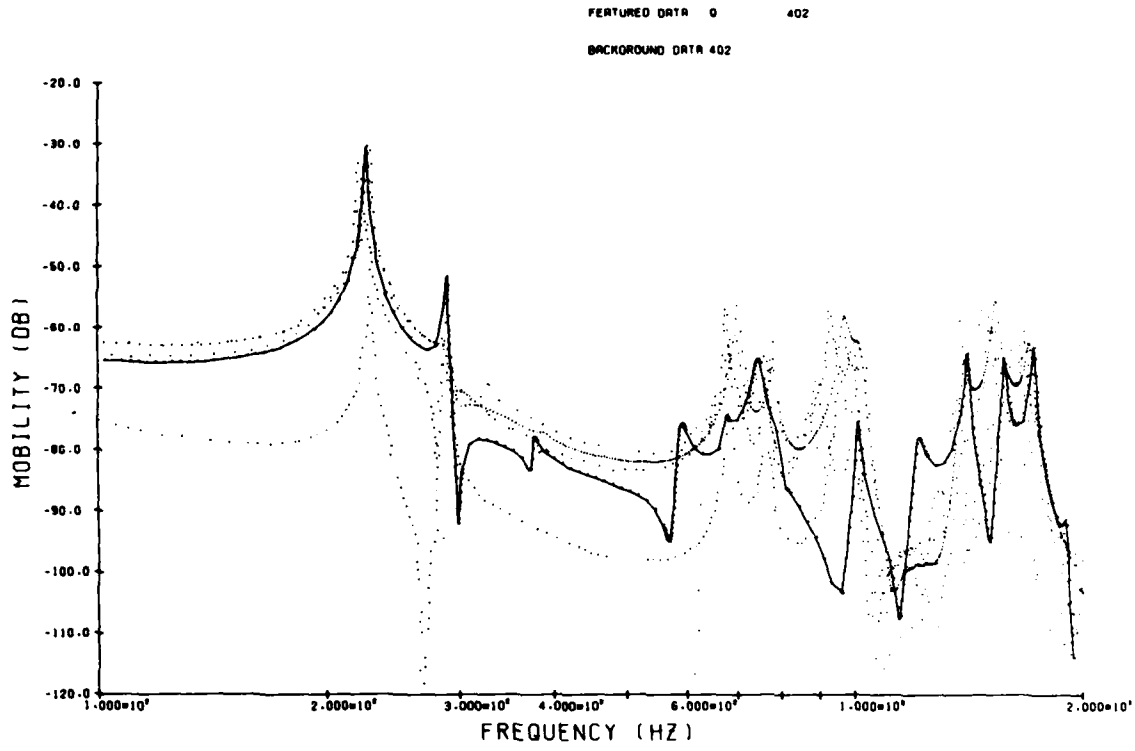

Figure 11.3 – Detail from transfer mobility measurements on Structure IV - all UK data

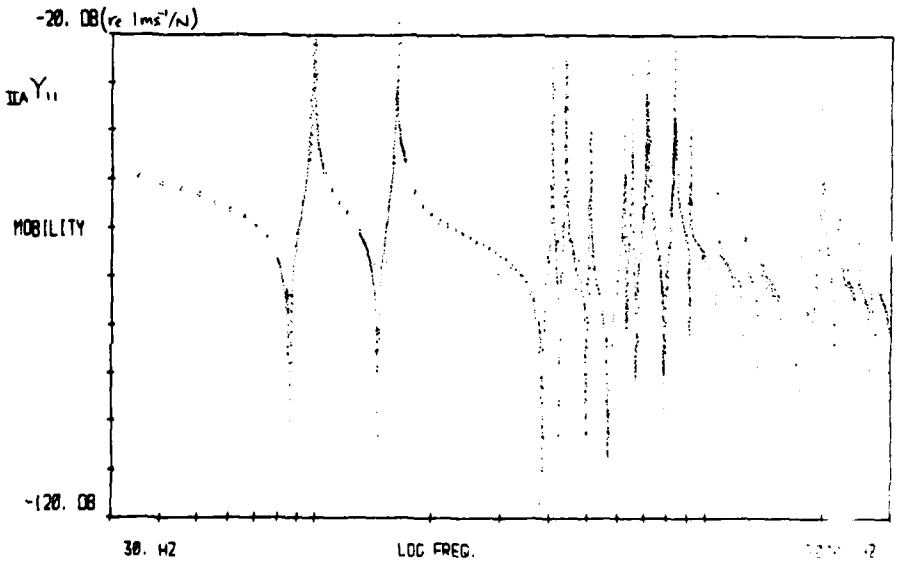

Figure 12 – Control measurements on Structure IIA

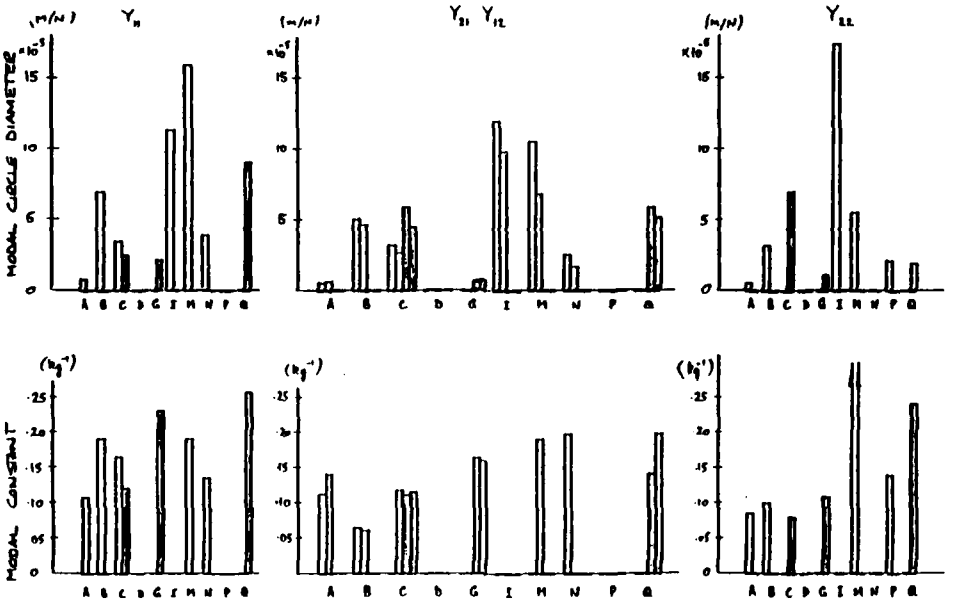

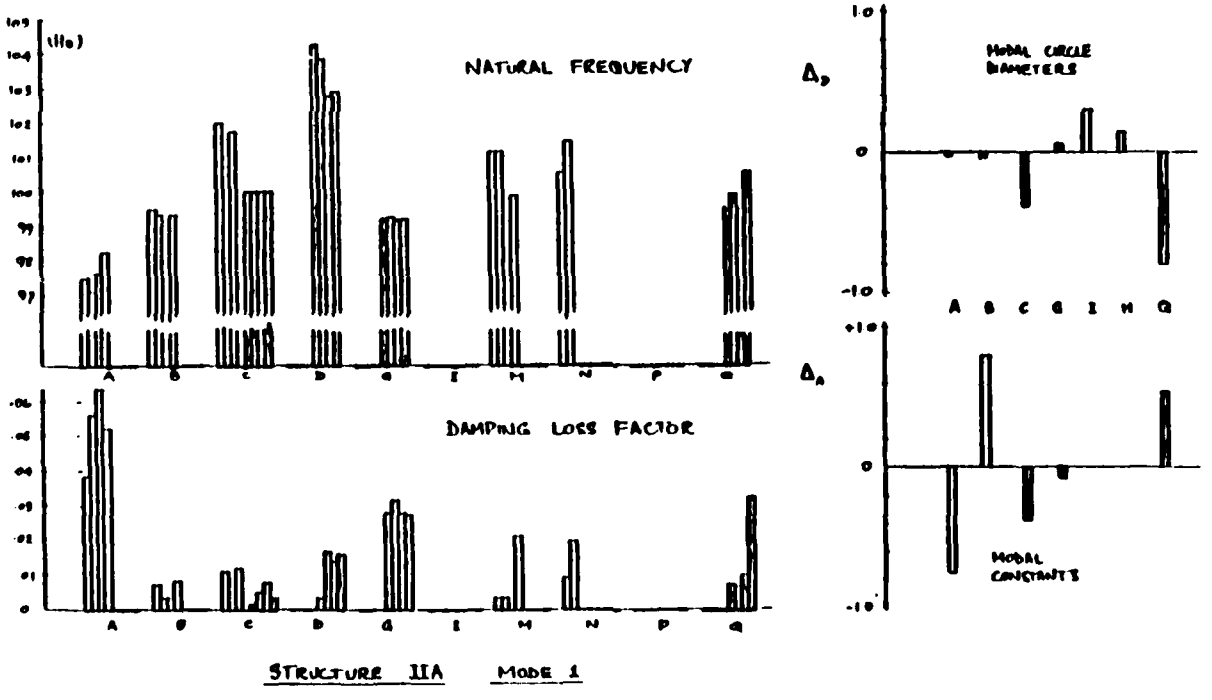

Figure 13 -- Modal properties of mode 1 Structure IIA

the same mode extend from .00128 to .0634, covering a range of 50 to 1. A table summarizing the data presented in the histogram of Figure 13 is given in Figure 14.

S.A.M.M.
Summary Table for Mode IIA - 1

	Participant Data	Polar Data	All
Minimum	99.138	97.12	97.12
Mean	100.607	99.843	100.28
Maximum	104.22	102.0	104.22
Spread	5.082 (5.0%)	4.88 (4.9%)	7.1 (7.1%)
Number of Items	16	12	28
Minimum	.00128	.00296	.00128
Mean	.0145	.0296	.0207
Maximum	.0320	.0634	.0634
Spread	.0307 (219%)	.06044 (204%)	.0621 (300%)
Number of Items	16	11	27

Figure 14 — Summary of modal properties for mode Structure IIA

5.4 Coupling Data

The results obtained from coupling measured 2 x 2 mobility matrices for each of the two substructures, IIA and IIB, constitute a group of four "predicted" mobilities for the coupled structure, IIC. One of these curves, ${}_{C}Y_{II}$, was selected and the prediction obtained from each of the four participants was plotted on the graph shown in Figure 15.1 and measurements have since been made of this same mobility on the assembled structure formed by bolting IIA and IIB firmly together with the adapters designed to give a contact surface between the two components which covered the same area as the adapters used to make the individual mobility measurements. The results of this measurement are shown in Figure 15.2 Some additional tests have been made using different types of connecting adapter, with the object of simulating different degrees of coupling, and some of these results are also given in Figure 15.2

6. REVIEW OF EXPERIMENTAL TECHNIQUES USED

It appears that there are too many factors in the detailed experimental techniques used by the different participants to permit a simple "explanation" of each curve produced during the survey. Nevertheless, from the data submitted it is possible to make some classifications for certain of the features used by the different laboratories. The four main points which can be identified as influencing the quality of the results are:

- the method of suspension of the structure,
- the method of attaching the shaker and/or the measuring transducers,
- The excitation techniques used to generate vibration in the structure,
- the total time taken by various methods to produce a good mobility measurement.

It is convenient to draw from the information and illustrations provided by the participants some general observations about the techniques currently in use.

6.1 Suspension Methods

The basic requirement of testing the structures in a free-free condition was met in one of two different ways, namely: by excitation *into* the suspension or *perpendicular* to it. In general, the latter approach is to be preferred, as it minimizes the influence which the suspension devices will have on the measured vibration.

6.2 Attachments

The two main variables in this area concerned the lightness (or otherwise) of the transducers and the attachment devices and the rigidity or flexibility of the drive rod connecting the shaker and the testpiece. The various solutions adopted for these two aspects of experimental technique resulted in some obvious differences in mobility characteristics, and especially in the natural frequencies found.

6.3 Excitation Methods

It is difficult and perhaps inappropriate to draw any major or general conclusions concerning the suitability of the different types of vibration excitation used throughout the survey, especially since only a fraction of the total set of results is presented here. Nevertheless, it is possible to report on some observations which have been made from a study of the full set of graphs (there are well over 100 in total: 20 are shown here).

One feature which was observed in a number of different cases was that the spread of N mobility curves measured by transient testing is consistently greater than that of N curves obtained by sinusoidal excitation. This trend is demonstrated in Figure 7 and is found in other examples on the other structures. Care must be taken not to conclude that transient testing is inaccurate—any one of the five curves in Figure 7.4 might be very accurate—but it is a fact that several experimenters obtain noticeably different results.

The other observation which can be made from closer scrutiny of these detailed plots is that many of the FFT-based measurements failed to resolve the relatively sharp resonance peaks on the lightly damped test-pieces. Although these instruments have the capability of sufficient resolution, it must be recorded that this is not always being used.

6.4 Testing Times

Another aspect of mobility measurement techniques which is always of considerable interest, and which was included in the survey, is the time it really takes to produce an acceptable or definitive mobility plot. Participants were

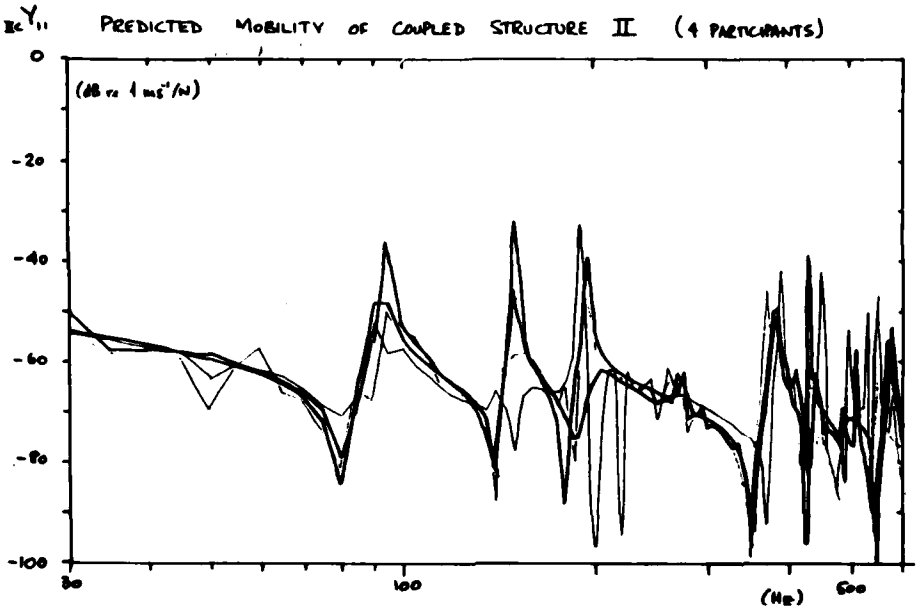

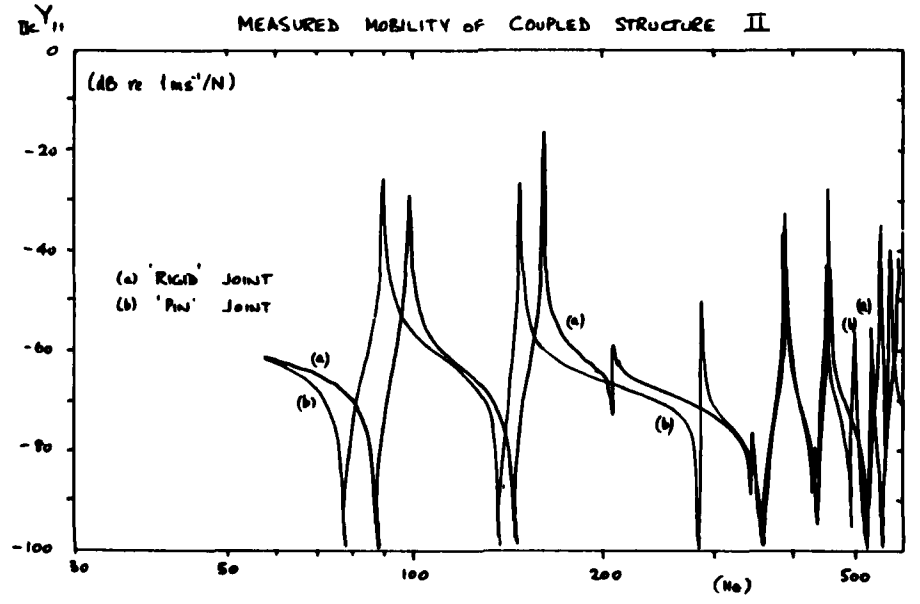

Figure 15 – Predicted and measured point mobilities for coupled Structure IIC

asked to record the time they took in various phases of the exercise, broken down into four categories: (a) overall time, (b) actual measurement time, (c) post-measurement plot preparation time, (d) modal analysis time. A significant proportion of the participants responded to this request and although it was not always possible to sub-divide their actual effort into these categories, it was found that sufficient information was available to investigate some of the statistics of the time requirements for various stages of mobility testing.

The procedure adopted was as follows: the total number of mobility plots which were submitted was recorded and the time requirements to produce these were estimated in four categories (not exactly the same ones as used on the log sheets), these being (i) the total time per plot, (ii) the testing or measurement time per plot, (iii) the data preparation time and (iv) the lost time per plot. Details of the information available to us presented in this way are included in Table 3, at the bottom of which are perhaps useful indications of the information sought. The most important of these results is the average time required to produce a mobility plot, which was found to be of the order of 2½ hours, drawn from a range which was in excess of one hour for the shortest and as much as five hours for the longest. The adjacent figures for the actual testing time show an average of just under half an hour from a range of one minute to one hour, and this illustrates clearly the significant amount of off-measurement time which is invariably incurred in the overall process of producing acceptable mobility plots.

TABLE 3
Mobility Measurement Times

	Total	Time/Plot minutes (No. of Items) Test	Lost
I	183 (18)	15 (14)	137 (14)
II	147 (76)	27 (68)	100 (68)
III	230 (11)	23 (8)	206 (8)
IV	156 (21)	27 (17)	121 (17)
Average	156 (126)	13 (126)	115 (107)
Range	80-320	1-60	50-280

7. CONCLUDING REMARKS

This survey set out to assess the state-of-the-art of mobility measurement techniques and we have tried to devise and conduct the exercise in such a way that we could achieve this objective. In particular, we have attempted to present the many results obtained during the survey in a number of ways to illustrate the various points of especial interest. To this end, a number of new procedures have been devised for comparing mobility data and for checking the measurements against each other using modal analysis methods.

We do not feel it is appropriate at this stage to draw any sweeping conclusions as to the "best" method for measuring mobility (there is almost certainly no single "best" method applicable to all situations anyway), but have concentrated on presenting all the data available to demonstrate the advantages and disadvantages of the various approaches which have been used.

It is appropriate, however, to summarize various conclusions which may be drawn about the conduct of the survey itself. The first and most positive of these is that it was found to be possible to conduct the exercise strictly according to the schedule drawn up at the outset and to obtain an enormous amount of valuable data from the many active participants who took part. The effort which they all made was clearly a very significant one. A second conclusion highlights a problem which obviously exists on a large scale; that being the difficulty encountered when trying to transmit mobility-type data from one place to another, or from one computer to another. Incompatible formats and apparently trivial handling problems combined to make the task of data transmission disproportionately great.

8. ACKNOWLEDGEMENTS

Inevitably, this report describes considerable effort expended by many people. In addition to all the participants, special adknowledgement is due to Mr. J. Griffin who processed the UK data, with assistance from Dr. P. T. Gleeson and Mr. D. A. Robb.

Continuing collaboration with Mr. R. Aquilina of CERT-SM, Toulon, France facilitated the direct comparison of results from both surveys.

Finally, thanks are given to the Ministry of Defence (P.E.) and the D.R.E.T. (France) who supported the whole project.

9. REFERENCES

1. Remmers, G. M. & Belsheim, R. O., "Effects of Technique of reliability of mechanical impedance measurement." SVB 34(3). 1964.

DEPARTMENT OF DEFENSE POLICY ON RELIABLIITY AND MAINTAINABILITY

Colonel Ben H. Swett, USAF
Director of Engineering and Standardization
Defense Industrial Supply Center, Philadelphia, PA

Thank you. A round of applause on introduction is enough to inspire any speaker. In any event, it's better than having people hiss and boo and stomp their feet. How many of you were at the IES Symposium in Philadelphia last spring? OK. I am using the same slides, but I will only point out how the DoD Directive on reliability and maintainability provides a better policy environment for shock and vibration engineers. As you know, I am concerned with environmental stress on military systems and equipment—but I am also concerned with the policy, procurement and psychological environments, and the stress they place on various people in various disciplines.

For example, consider the following scene. A GI supply sergeant is issuing uniforms to new recruits. As he hands out one stack of clothing, the recruit notices *something strange:* the buttons and the buttonholes are on the same side of the blouse. He hands it back to the sergeant, and asks, "What's this?" The sergeant says, "Right," gives him another blouse, and throws the defective blouse in the garbage can—thereby rewarding the manufacturer of the defective blouse by purchasing two blouses rather than one.

This scene repeats many, many times. Then, when some idiot like me goes to the manufacturer and asks him about his quality control, he says, "Get out of here." Of course, he may not know about the problem in the field—but if he does, he is not likely to see it as a problem, because his military customer buys more blouses when quality is lower.

His quality control people are highly dedicated—but highly frustrated, because nobody seems to listen to them. They do not realize their company is being rewarded for low quality, so they do not understand why the lack of emphasis on quality control. They do not know their corporate policy environment depends on a *military* policy that tells supply sergeants whether to throw a defective blouse in the garbage can or return it to the manufacturer for replacement.

This type of problem is not confined to the military. Take a look at some civilian products, such as light bulbs. Which manufacturer will sell more light bulbs per year: the one whose light bulbs last 100,000 hours, or the one whose light bulbs last 1,000 hours? Do you shop around for more reliable light bulbs, or just buy replacements? Most people just buy replacements. That is why we have, in our culture and in the DoD procurement system, a large tendency to reward poor quality and low reliability: the worse it is, the more we buy of it.

To the extent we can turn that cultural tendency around, we create a market for quality and reliability, and the environmental stress engineering that must support any sound quality or reliability program. Saying we need such a fundamental change and actually accomplishing it are two different things—as you are no doubt aware—but DoD Directive 5000.40 took a shot at it, via DoD policy on reliability and maintainability (R&M).

As I go through this discussion of 5000.40, you will see a sharp distinction between R&M engineering and R&M accounting. R&M accounting is what Will Willoughby refers to as "number crunching." R&M engineering is what he has been emphasizing for a number of years: reliability by design, test-fix-test, environmental stress screening, and so forth. There were some people who said, "The reliability discipline should be part of the product assurance. Leave engineering to the engineers." Then there were those who said, "The reliability discipline should be all engineering. We should hang or otherwise get rid of the number crunchers." The R&M Directive says, "A good reliability program has to have both engineering and accounting, and both must be tailored for return on investment."

Second, look for the distinction between two absolutely different kinds of testing: test-fix-test, and proof-testing.

Test-fix-test has many names. It is called development testing, growth testing, test-analyze-and-fix (TAAF), or test-analyze-find-fix (TAFF). The name doesn't matter: these are all generically the same kind of test, in which you are looking for trouble. In that kind of test, a failure is a good thing because you are looking for trouble. In that kind of a test, test realism—even over-stress—is a good thing because you are looking for trouble.

Proof-testing also has many names: qualification testing, acceptance testing, demonstration testing, compliance testing. In those tests, a failure is a bad thing because you are trying to determine compliance; you are deciding whether you are going to buy the item or not. In proof-testing, the manufacturer is not interested in finding failures. On the contrary, he hopes you don't find any. He's not interested in test realism; he would like the test to be as benign as possible. This is natural.

For many years, the DoD approach to reliability has emphasized proof-tests, but not test-fix-test. That policy affected you. Whether your bosses—your senior corporate managers,

and your government program managers—were interested in the services of environmental engineers depended on which type of testing was being emphasized. This is why your services have gone begging in many cases: only proof-testing was being emphasized, whereas environmental testing is inherently looking for trouble.

One last distinction to look for—5000.40 redefines "reliability," "time," and "failure." All of the "time" and all the failures that drive maintenance are now included. The classic definitions only addressed *mission* time and *critical* failures. As a result, "reliability by design" did not necessarily reduce maintenance or logistics support cost. For example: Does redundancy improve reliability? Yes, that is a correct answer. Now, next question: Does redundancy make reliability worse? Yes. That is *also* a correct answer. (It is a neat test where all the answers are correct.) The point is, there are two categorically different kinds of reliability. Redundancy helps Mission Reliability, but it hurts Maintenance related Reliability—which is also related to logistics, spare and repair parts cost, and life cycle cost—because redundancy means there are more parts to fail, and more demands on maintenance. Mission Reliability and Maintenance-related Reliability are two different animals, but the classic definition didn't make that distinction. Exclusive emphasis on Mission Reliability lead to a very strange design philosophy that says in effect, "If you have a bad part, use two of them. And if it's a really bad part, use three of them." So, efforts to enhance Mission Reliability have reduced Maintenance Reliability and increased—rather than reduced—maintenance and logistics support cost. By redefining basic reliability terms, DoD 5000.40 actually brought maintenance and logistics-related concerns into the reliability discipline for the first time.

DEPARTMENT OF DEFENSE POLICY ON RELIABILITY AND MAINTAINABILITY

Slide 1

As you know, that is my previous job title. I have been reassigned to the Defense Industrial Supply Center in Philadelphia.

1. OBJECTIVES OF R&M PROGRAMS

- INCREASE READINESS AND MISSION SUCCESS
- REDUCE MAINTENANCE & LOGISTICS SUPPORT COST
- LIMIT MANPOWER NEEDS
- PROVIDE MANAGEMENT INFORMATION
- ENSURE EFFICIENT INVESTMENT

Slide 2 – R&M policy

I'll only touch on the last bullet, where it says, "ensure efficient investment." That is really a very simple thought: What are we buying with each increment of cost and schedule investment in R&M? It also ties in with what I said a minute ago: your corporate manager has to ask that question, and if he's not—for example—getting any return defective, he's getting no return on his investment in quality so he's apt to reduce emphasis on quality control. That is something you might also keep in mind: what is your boss's return on his investment in you?

2. STRATEGY FOR R&M PROGRAMS

- INVEST IN DESIGN, DEVELOPMENT, AND MANUFACTURING TASKS THAT ACTUALLY IMPROVE R&M
- RETAIN, BUT LIMIT INVESTMENT IN R&M ACCOUNTING TASKS AND COMPLIANCE TESTS THAT DO NOT ACTUALLY IMPROVE R&M

Slide 3 – R&M policy

I would like to make a major point here, for those who are involved with or concerned with Mil Standard 810. Mil Standard 810 has been viewed as environmental *qualification* testing for many, many years. It has been restricted to qualification of first production units, or applied very late in the development process. That comes under Bullet 2, where it says, "Limit—hold down—restrain—restrict that kind of testing." As I've been telling the 810 community, they need to make sure that document is primarily applicable to test-fix-test early in the development process. That will not only provide a home for Mil Standard 810 in the policy environment, it is also good sense to run environmental tests early and then fix what fails. I am naive: I don't see the purpose of a test if you don't fix the failures you find.

3. TERMINOLOGY

- ESTABLISH R&M PARAMETERS IN UNITS OF MEASUREMENT DIRECTLY RELATED TO:
  - OPERATIONAL READINESS
  - MISSION SUCCESS
  - MAINTENANCE MANPOWER COST
  - LOGISTICS SUPPORT COST
- REDEFINE BASIC TECHNICAL TERMS:
  - MTBF = ALL TIME + ALL FAILURES*
  - MTTR = AT ALL LEVELS OF REPAIR

*FAILURE = PERFORMANCE OUT OF SPEC. BY ANY PART OF THE ITEM
RELEVANT = COULD OCCUR OR RECUR IN SERVICE
CHARGEABLE = WHO HAS TO FIX IT

Slide 4 — R&M policy

The first bullet addresses system level reliability and maintainability parameters. You are not primarily interested in that. You are primarily interested in the second bullet, because ultimately your job as testers is to produce failures—which is why you are sometimes unpopular in some quarters. Notice how "failure" has been redefined to include all failures that drive demand for maintenance. A relevant failure is any failure that could occur in the fleet; so the only non-relevant failures are those which are test-peculiar, or those that have been eliminated by a design change. A chargeable failure is a relevant failure within the responsibility of a given organization, whether government or commercial. A relevant failure could be charged to CFE hardware, GFE hardware, CFE or GFE software, or—if I can coin a term—CFE or GFE personnel. A GFE person is really what I am—an employee of the Government.

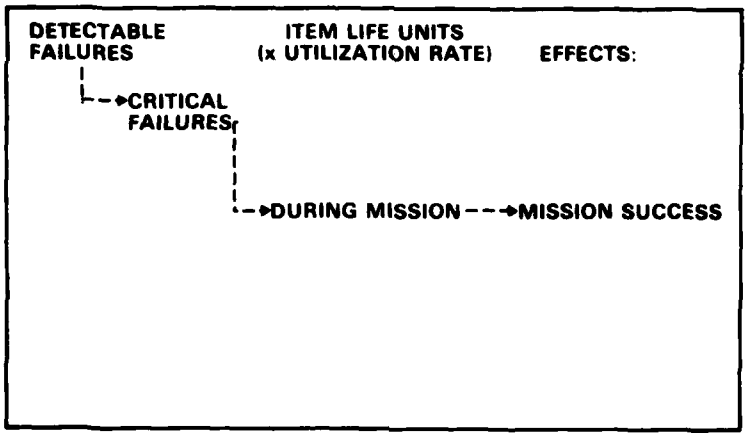

Slide 5 — Reliability audit trails

This is what reliability programs have been using to define such terms as "Mean-Time-Between-Failures (MTBF)." They only counted those failures, and that item operating time, which can effect mission success.

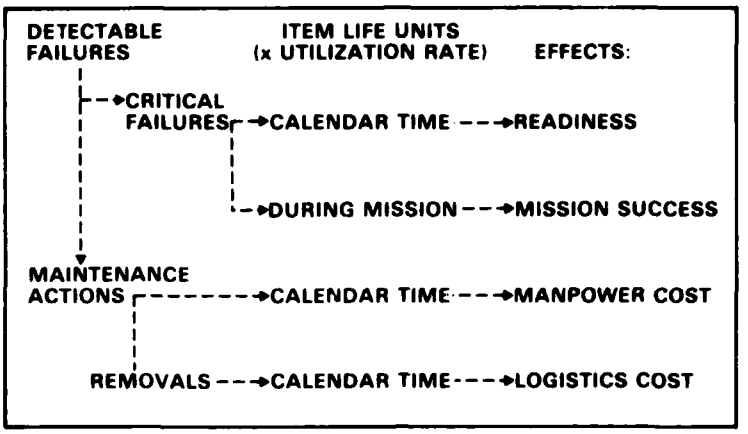

Slide 6 — Reliability audit trails

This is what the Directive does by expanding the definitions of "time" and "failure." Such terms as MTBF now include all of the item operating time, and all of the failures, that drive demand for maintenance. Critical failures are a subset of detectable failures, and removals are a subset of maintenance actions. Mission operating time is a subset of total operating time—during a given calendar period, at a given item utilization rate. So, by starting with the broadest and most basic units of measurement, we can get to these four different ways that item reliability effects the overall weapon system.

A LITTLE REDUNDANCY GOES A LONG WAY

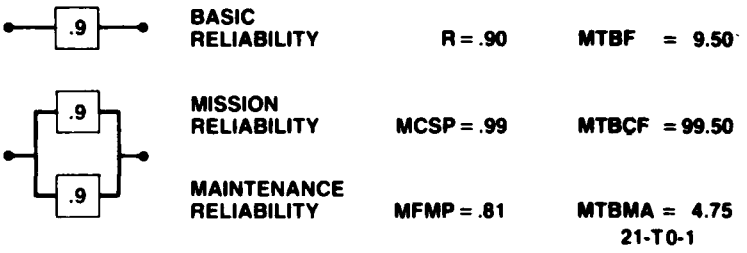

Slide 7 — R&M policy

This slide illustrates why efforts to enhance reliability—as previously defined—did not reduce demand for maintenance. Given an item with 90% probability of performing without failure for a 1-hour mission, Mean-Time-Between-Failures (MTBF) at a constant failure rate is 9½ hours; use of two such items in active redundancy increases Mission-Completion- Success-Probability (MCSP) to 99% for a 1-hour mission, and multiplies Mission-Time-Between-*Critical*-Failures (MTBCF) by a factor slightly greater than 10.0. However, that same redundancy *reduces* Maintenance-Free-Mission-Probability (MFMP) from 90% to 81%, and cuts Mean-Time-Between-Maintenance-Actions (MTBMA) in half. Therefore, this redundancy results in 21 times more maintenance actions than critical failures in any given amount of mission time. That is why "reliability" had to be redefined and the old definition had to be properly labeled, "*Mission* Reliability."

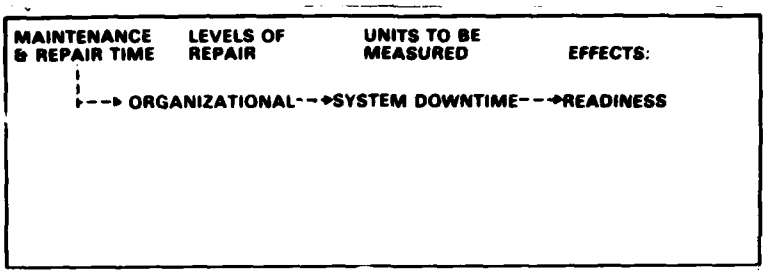

Slide 8 — Maintainability audit trails

This chart shows that the same kind of problem existed in the Military Standard definition of "Maintainability."

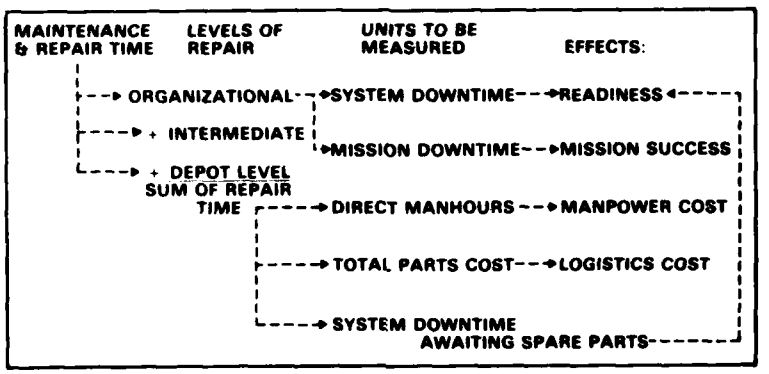

Slide 9 — Maintainability audit trails

The directive redefines "Maintainability" to include Mean-Time-To-Repair (MTTR) of detached components of a weapon system, at the intermediate and depot levels of repair. Notice how the effect of intermediate and depot-level repair time comes around to bite system readiness in the . . . flank. Downtime awaiting spare parts is usually blamed on the logistics system, but this chart shows it can also be due to poor maintainability of detachable system components.

OBJECTIVES	PARAMETERS	TERMS (EXAMPLES)
OPERATIONAL EFFECTIVENESS		
• READINESS, OR AVAILABILITY		
	– READINESS-RELATED RELIABILITY PARAMETER:	MEAN TIME BETWEEN DOWNING EVENTS (MTBDE)
	– READINESS-RELATED MAINTAINABILITY PARAMETER:	MEAN TIME TO RESTORE SYSTEM (MTTRS)*
• MISSION SUCCESS, OR DEPENDABILITY		
	– MISSION RELIABILITY PARAMETER:	MISSION TIME BETWEEN CRITICAL FAILURES (MTBCF)**
	– MISSION MAINTAINABILITY PARAMETER:	MISSION TIME TO RESTORE FUNCTIONS (MTTRF)

* CLASSIC USAGE OF "MEAN TIME TO REPAIR (MTTR)"
** CLASSIC USAGE OF "MEAN TIME BETWEEN FAILURES (MTBF)"

Slide 10 — System R&M parameters

This chart shows how the effects of basic reliability and maintainability relate to operational effectiveness of a weapon system.

OBJECTIVES	PARAMETERS	TERMS (EXAMPLES)

OWNERSHIP COST REDUCTION

- MAINTENANCE MANPOWER COST
  - MANPOWER-RELATED RELIABILITY PARAMETER: MEAN TIME BETWEEN MAINTENANCE ACTIONS (MTBMA)*
  - MANPOWER-RELATED MAINTAINABILITY PARAMETER: DIRECT MANHOURS PER MAINTENANCE ACTION (DMH/MA)**
- LOGISTIC SUPPORT COST
  - LOGISTICS-RELATED RELIABILITY PARAMETER: MEAN TIME BETWEEN REMOVALS (MTBR)
  - LOGISTICS-RELATED MAINTAINABILITY PARAMETER: TOTAL PARTS COST PER REMOVAL, AT ALL LEVELS OF REPAIR

* MTBF MUST INCLUDE ALL "TIME" AND "FAILURES" INCLUDED BY MTBMA.
** MTTR MUST INCLUDE ALL "MAINTENANCE/REPAIR TIME" INCLUDED BY DMH/MA.

Slide 11 — System R&M parameters

This chart shows how the effects of basic reliability and maintainability relate to ownership cost—and thus life cycle cost—of a weapon system. Notice that this whole chart addresses effects not included in the previous military standard definitions of reliability and maintainability.

4. PREREQUISITES TO R&M BY DESIGN

- FEED BACK PREDECESSOR EXPERIENCE
- CORRECT THE CAUSE OF THE DEFICIENCY:
  - DESIGN (HARDWARE AND SOFTWARE)
  - QUALITY (WORKMANSHIP AND MATERIAL)
  - CONCEPTS, POLICIES, PLANNING FACTORS
- TRADE OFF REQUIREMENTS:
  - PERFORMANCE VS RELIABILITY
  - SYSTEM R&M PARAMETERS
- SELECT RELIABLE, MAINTAINABLE GFE
- SPECIFY REALISTIC, INTEGRATED TESTS

Slide 12 — R&M policy

Mr. Willoughby has—for a number of years—put strong and proper emphasis on reliability by design. This Directive supports that emphasis and adds the requirement to feed back acquisition, operation and support experience as prerequisites for reliability by design, to include measured environmental stresses from similar equipment in similar applications. Where it says, "correct the cause of the deficiency," the policy states that operational problems of the predecessor must be analyzed to determine whether they were caused by hardware and software design, by quality of workmanship and material, or by operating and support concepts, policies, procedures or planning factors. It doesn't really help to hammer on the design if the cause of the problem is maintenance policy. That seems simple. The fourth bullet, "select reliable, maintainable Government Furnished Equipment," doesn't ping on you directly, but it sure does ping on the program managers. In many cases we are feeding back government furnished equipment because we have it; it is not always good equipment in the field, and its field reliability is not always looked at by the acquisition program manager. This policy says that the government program manager has to assume responsibility for the GFE.

"Specify realistic, integrated tests." We have had numerous debates about what is a realistic test. We heard an interesting talk yesterday about how accurately we can or can't measure vibration. Let me say it one more time: I am a pragmatist. I am not an idealist. I would be interested in a vibration test realistic enough to recognize that vibration induced failures are sensitive to frequency, and amplitude, and duration of exposure. When we get down to arguing about the exact signature of vibration, the details go beyond what I'm talking about. But I am concerned when a vibration test is considered realistic, because it covers the frequency and amplitude, but it doesn't pay any attention to the relative duration of exposure in the test and in the field. Again, I'm simple minded: I break a coat hanger by bending it, but it doesn't break the first time I bend it. The number of cycles, the duration of exposure, is an essential parameter of vibration as a stress, and it has not been considered in all cases. That is what I mean by realism. If the field environment is random vibration, I don't consider a single frequency sinusoidal vibration to be realistic. Integrated tests: the Directive says that performance, reliability, and environmental stress testing shall be integrated. This goes back to the presentation I gave at the IES Symposium several years ago, in which I pointed out that performance and reliability and environment stress are all essentially meaningless when addressed separately. I have not changed that opinion.

5. R&M GROWTH IS REQUIRED

- FSED, CONCURRENCY, INITIAL DEPLOYMENT
- INTERMEDIATE GOALS AND THRESHOLDS
- DESIGNATED TIME AND RESOURCES
- TEST-ANALYZE-AND FIX
- ALL APPLICABLE R&M PARAMETERS
- REDUCE ECP APPROVAL DELAYS
- ASSESS AND ENFORCE R&M GROWTH:
  - INTERMEDIATE GOALS BELONG TO PM
  - BREACH OF INTERMEDIATE THRESHOLD REQUIRES IMMEDIATE PROGRAM REVIEW

Slide 13 – R&M policy

I would like to expand on the third bullet. The Directive requires designated time and resources for test-fix-test reliability growth. That includes resources to fix the failures you find. One of the reasons that our testing has been under fire in the past—and especially our environmental testing—was because failures were discovered too late in the program, when there wasn't time or money to fix them. If you will recall, about ten years ago there was a study of environmentally induced failures in Naval aircraft. It said 50 percent of the environmentally induced failures in the fleet had been found during environmental tests, but had not been corrected because there was not sufficient time or resources in the acquisition program. That is not tolerable. Notice also the second bullet from the bottom: "Reduce Engineering Change Proposal (ECP) approval delays." One of the weird things in our policy environment is that, if you are testing and you find a failure, the contractor puts in an engineering change proposal, but it may take 14 to 18 months to get government approval of the engineering change. Just flat administrative delay. That is dumb on our part, especially when we are in a test-fix-test mode. I am recommending to our program managers that they not impose tight configuration controls until they are at least two thirds of the way through engineering development. During the first two thirds, we must get the fixes in as fast as we can.

6. COST-EFFECTIVE R&M DEMONSTRATIONS

- EMPHASIZE OPERATIONAL REALISM
- LIMIT THE COST OF CONFIDENCE
- COMPILE SYSTEM R&M ESTIMATES
- USE ALL RELEVANT DATA
- INDEPENDENT COMPLIANCE TESTS:
  - SEPARATE CONTRACT
  - HIGHER TIER CONTRACTOR
  - SUPPLIER, UNDER SURVEILLANCE (TECHNICAL OR FINANCIAL NECESSITY)

Slide 14 – R&M policy

I think that slide is fairly straightforward—which belies its controversial nature. The first bullet emphasizes operational realism, and gets translated into things like CERT. To say, "limit the cost of confidence," is a quick way to draw the wrath of a whole world of statisticians. The policy on independent compliance tests drew a great deal of fire from a great many people. What that policy actually says is very simple. It states that, insofar as possible, R&M compliance tests shall be conducted or controlled by someone other than the supplier whose compliance is being determined. That's what it says. Then it has a few other sentences that soften the thought, and permit waivers.

7. ACQUISITION PROGRAM PHASES

- MISSION AREA ANALYSIS: IDENTIFY NEEDS
- CONCEPTUAL PHASE: BASELINES AND GOALS
- D&V PHASE: DESIGN CFE, SELECT GFE, TAILOR CONCEPTS
- FSED PHASE: ENFORCE GROWTH TO MEET THRESHOLDS
- PRODUCTION & DEPLOYMENT: MEET THRESHOLDS IN SERVICE
- IN-SERVICE EVALUATION: ACHIEVE R&M GOALS
  - ACQUIRING AGENCY TO FIX DESIGN AND QUALITY
  - USER TO FIX CONCEPTS, POLICIES, PLANNING FACTORS

Slide 15 — R&M policy

Let me just point out where environmental testing fits in the phases of the acquisition process. It doesn't fit in the Mission Analysis phase, except grossly, as an overall look at the nature of system environments. In the Conceptual phase, where we are coming up with systems concepts, there may be a place to pay attention to environmental stress, but not too much. You really come in on the third bullet. The Demonstration and Validation phase is where someone must design the Contractor Furnished Equipment, select the Government Furnished Equipment, and tailor the operating and support concepts. That phase is where the input of measured environment becomes absolutely vital. The Full-Scale Engineering Development phase must emphasize test-fix-test reliability growth. If I were doing it, I would do it this way: I would use environmental stress screening at various levels of assembly during fabrication of full-scale prototypes. My best guess is that it would get rid of about 70 percent of the problems we would otherwise find in system level testing. Then I would go to Mil Standard 810 environmental tests, and fix the failures they produced. Then I'd go to CERT test-fix-test, and at the tail end of that I'd collect my demonstration data. That is how I'd run full scale development. Then I would use environmental stress screening to get weak parts and workmanship defects out of the production items—all of the production tests— and then require only a very few CERT production sampling tests.

8. OWNERSHIP

- REDUCE "RETEST OK" RATES
- REALISTIC TEST FACILITIES FOR TROUBLE-SHOOTING
- SPECIFICATIONS FOR SPARES, REPROCUREMENTS, AND MODS
- R&M DATA COLLECTION & FEEDBACK
- R&M "TIGER TEAMS"
  - ARMY "RISE"
  - NAVY "AERMIP"
  - AIR FORCE "PRAM"
- INCORPORATE R&M IMPROVEMENTS
  - HARDWARE AND SOFTWARE
  - CONCEPTS, POLICIES, PLANNING FACTORS

Slide 16 — R&M policy

I'd like to touch on the second bullet: realistic test facilities for trouble shooting. I mentioned this before. Our trouble-shooting facilities at maintenance and repair organizations by and large do not contain sufficient environmental stress, and as a result we don't find the failures we find in the fleet. We keep getting a very high "Retest OK" rate. One of the places we could use cheap random vibrators would be on a hot bench in a maintenance squadron, or in support of a maintenance squadron. There are just an awful lot of failure mechanisms that we can't find if we don't apply some environmental stress. Almost anything we can do to cut down the "Retest OK" rate is a very good investment. The charter of an R&M "Tiger Team" is to go after the problems in the fleet, track them to their sources, prototype a fix, and get it tested. Those teams have documented return on investment in the order of 30-to-1, which is a very good investment for the taxpayer. They go to specialized test labs and failure analysts as necessary in tracking down a problem. Some of you have probably encountered these teams at one time or another, as they go doggedly chasing down a problem. They are worthy of your support.

The last bullet on this slide is the bottom line. It summarizes the entire philosophy behind DoD Directive 5000.40: "Find the problem and fix it. Do it as early as you can; do it as efficiently as you can, but *do it*: Get the R&M deficiencies out of our military systems and equipment."

That concludes my presentation on the R&M directive. Now, if I may, I would like to say a few more things about your policy environment, as I see it.

Let's go back to 1973, when I first read Mil Standard 781B, saw the 2.2g sinusoidal vibration requirement, consulted with my airplane driver's innards, and said to myself, "No . . . that's not how airplanes feel." I made a few telephone calls, looking for measured vibration data, and wound up talking to Dave Earls at the Flight Dynamics Laboratory. They provided the data for those little briefing slides that said, in effect: "Here is the vibration we apply during Mil-Std-781B testing--and here is the vibration we measure in the A-7D fighter aircraft." Those simple little slides went up the chain of command to General Brown, who was at that time the Commander of Air Force Systems Command. He looked at them and digested the message. Somebody in the back of the room started yammering about what should be done, but General Brown turned and very quietly said, "I know how to do it right. I'm just concerned that we are doing it so very wrong."

That moment in time marked the beginning of a shift in the policy environment that governs demand from random vibration testing. Prior to that time, random vibration testing was available; a number of people were experts in the field; it was a potential solution to many problems, and it was being used in some places -but the demand had not been established as a matter of policy, so much of that technology, and that expertise, was not being utilized. Now there is an increased awareness and utilization of that not-so-new kind of testing. That is what I meant when I said the policy environment controls the market for your services.

Now let's look at what has happened in Japan over the past several years. The National Government and the major industries have established policy on the quality of Japanese products. That policy is not insignificant—for Japan, or for the rest of the world. To be blunt, they are blowing us out of one market after another. Our industries are just beginning to realize what that means to them, but they are increasingly aware that something has changed, and I believe they will move to re-establish their markets. So this emphasis on quality, coming essentially out of Japan, is a major wave of change, sweeping through the policy environments of the industrialized world. Don't fail to pay attention to it. It is important, and it bears on your discipline.

Environmental testing necessarily causes problems, stimulates failures, discloses defects in item design and manufacture. Whether or not your services are popular, in demand, and therefore supported and financed, depends on how well you fit into the policy environment. I believe you should hitch your wagon to the star of quality control—by emphasis on environmental stress screening as a way to disclose weak parts and workmanship defects in support of timely quality control. Don't forget the full-scale prototype: environmental stress screening during the fabrication of full-scale prototypes will pay high dividends, primarily by avoiding subsequent costs and schedule delays at the higher levels of assembly. You have a good market there.

You also have a potential market in test facilities for trouble-shooting items in the fleet, but I think it may be a little harder to get into, at least right now. Management is not yet as sensitive to the "Retest OK" problem as it is to the quality control problem.

I recommend that you align yourselves with the test-fix-test concept, whatever it may be called in a specific program. Those tests are inherently looking for trouble. They are part of the policy environment that bodes well for your discipline, which is by its very nature trouble-seeking. Don't tie yourselves to the qualification tests, the proof-tests, where the unwritten policy is "pass the test any way you can." Nobody wants test realism there; nobody wants to find a failure in a proof-test; neither the contractor nor the Government. So go with your natural market. Point out the real benefits you have to offer, wherever anyone is serious about finding and fixing the quality and reliability problems of systems and equipment.

That is what I came here to say; so with that, I will conclude this presentation and make myself available for questions for the remainder of the hour.

DISCUSSION

Mr. Kilroy (Naval Ordnance Station): I would like you to say a few words about specification control drawings, source control drawings, and purchasing departments.

Colonel Swett: OK. When you say drawings, specification drawings, and so forth, what immediately pops into my mind is a situation we had in Viet Nam. I was in a special operations wing, an air commando operation, flying C-123 aircraft. It was a very ugly, but very rugged airplane: I loved it. But one day a flap hinge broke on one of the airplanes, and we lost a crew. The flap was in assault position, the hinge broke, and the aircraft was impossible to control. Two days later we

lost another one. The flap hinge broke. We had a total of 19 incidents over the next few weeks, although we developed tactics to work around the problem until we could get replacement hinges. I was on board during one of those incidents. We were going in on a bundle drop, just leveling off at 300 ft., and as we were bringing up the flaps something went snap. Due to the skill of my pilot, I am still here, but it was a sporting go there for a minute, as our British friends say.

The solution to that whole problem was accomplished by a draftsman who changed the radius of one part of the flap bracket, on the specification drawing. What they found was a tight radius in one corner. After prolonged exposure to vibration, the bracket had cracked at that point. The solution was to increase the radius by some very small amount. That is what I think of when I think of specification drawings.

The second thing I think of is that, in my present assignment, I am involved with a large number of such drawings. And if I read the implication of your question correctly, I would say you are right. You are looking at the cutting edge of how your disciplines and the policy environment actually gets put into effect. Management of specification drawings is too often remote from the operational problem, from the policy environment, and from the technical expertise. Now, there are a lot of those drawings, but the way you eat an elephant is one bite at a time. I am in the process of nibbling on a large stack of them, but I believe that if problems are not corrected in the drawings, nothing much is going to happen. I would also like to add: if the things I have been talking about don't show up on the government check list at final source selection—the criteria, the drawings and the specifications by which a company does or does not win a contract—nothing much is going to happen. That is the cutting edge. Question? *(There were no further questions.)*

Well, let me conclude by saying that, six years ago, in 1974, Henry Pusey contacted me and invited me to speak at the Shock and Vibration Symposium in Dayton, Ohio. I checked around Headquarters, Systems Command, to find out what a S&V Symposium was. I was told that it was a bunch of weird but basically friendly engineers. That appealed to me, because I had been briefing hostile audiences for a long time, so I went. I reported to a large auditorium in Dayton and heard Jack Short give his Rivet Gyro pitch. That was interesting because the guy flipping the slides came out with the two packets of slides and said, "Who's is which, and which goes on first?" Before I could open my mouth, Jack Short said, "It doesn't matter. He can brief mine and I can brief his." Which was true. We had brief back to back for about six weeks. I got up to speak. The temperature was approximately 30 degrees Fahrenheit, the Air Force Band was performing on the other side of a curtain, at about 130 decibels. I didn't know what a decibel was in those days but I thought, "These people are serious about shock and vibration." Anyway, I looked at the script, said, "Oh, what the hell," threw the script away, and told war stories. Afterward, I got the first friendly round of applause I had during that whole briefing tour. As a result, I have a fond spot in my heart for this organization and the people in it, and that is why I am most pleased to be here. I appreciate a thinking audience. I feel I have accomplished some things in the R&M Directive that create a home for the technical expertise and the services represented by this audience, but there is nothing altruistic in that. I believe there is a real need for your services, and that need has to be stated in policy and contracting documents or the value of your services will not come to fruition. So with that, I'll conclude and give you time for a cup of coffee before the next round. Ladies and Gentlemen, I thank you.

NECESSARY AND SUFFICIENT QUALIFICATION FOR SHOCK

Mr. Robert Dyrdahl
The Boeing Company
Seattle, Washington

It is a pleasure to be here this morning to discuss shock problems, and I do think that we have some problems to talk about even though "shock" has been with us a long time. I believe that we can do something to improve the state of our ability to support preliminary and final design with better analyses and simpler, more realistic, and more straightforward shock specifications. We also must become much more efficient in transferring important technology to all users, so that everyone may benefit by having the latest and most accurate information. A very important part of the solution to the United States balance of trade deficit is major improvements in our technology and major improvements will occur easier if we do not have to "re-invent the wheel."

When I remark about shortcomings in our "shock" work, I am including myself. I have been in charge of the dynamics and loads work for the Boeing Aerospace Company for many years, with the responsibility to see that only the necessary and sufficient qualification for shock was included in each of our products. I have to admit that, at the present time, our analysis capability could be better and some of the shock specifications that we use need updating and simplification. For some of our programs, we are not sure our methods result in only the necessary and sufficient conditions, but these sometimes may be more than what is actually necessary. We also have some difficulty in transferring our technology to other engineers because of different programs and work locations.

Most of our aerospace equipment that is exposed to shock is complicated with many, many parts so that a credible analysis is not easy. Complex equipment such as electronic racks (Figure 1) is difficult, sometimes even impossible, to model. Usually there is a poor definition of the dynamic environmental loads, hence some question about the validity of various applicable specifications. However, with computer capability increasing at a very rapid rate, and by getting a better handle on some of the other problems, we will have the means to make major improvements, if we try.

Consider the design process as shown in Figure 2. In the past, we have supported concept development for critical structural sizing of the major elements of an equipment assembly by minor calculations and a very crude "rule of thumb" estimation of the modes and modal participation factors for establishing equivalent static design loads for use by designers and stress engineers. This crude estimation has been successful in that the hardware passed the qualification test, but we could not evaluate the degree of conservatism

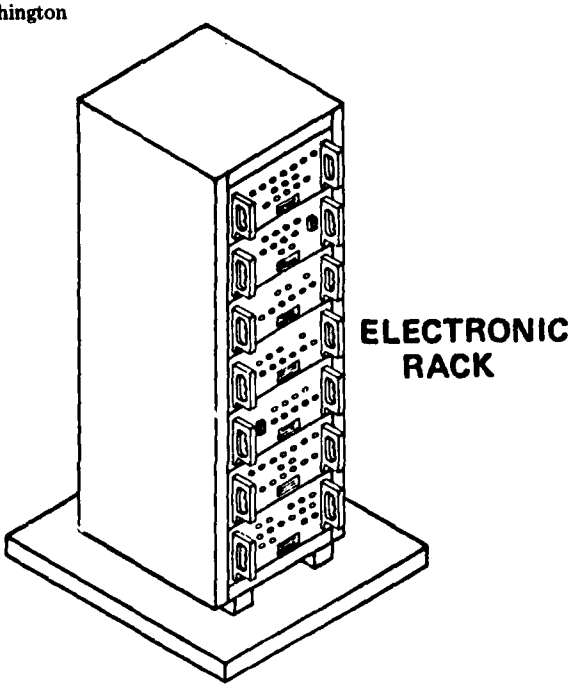

Figure 1 — Typical equipment

inherent in the design. The question was not answered in the final qualification either because lack of instrumentation precluded an understanding of the stress levels. For some of our equipment, we used more complex analyses: component mode synthesis and, in some cases, elaborate finite element analyses. Even then, the conservatism question was not answered.

For any loads work we must have an understanding of the environment, so a complete review of the mission requirements is necessary as soon as possible, including an assessment of the fatigue load cycle spectrum. From the mission requirements we establish the analysis and test requirements and, unfortunately, it is at this time that we lock-up permanently the specifications, at a time when our knowledge of the environment is not complete. The shock environment must represent that expected in the field. The birth of a weapons system often makes this task difficult. For example, in the early phases of a task, the contracting agency defines preliminary requirements, often without input from the user organization. These preliminary requirements become the

	ANALYSIS METHOD
CONCEPT DEVELOPMENT	"RULE OF THUMB" MINOR CALC'S
PRELIMINARY DESIGN	
FINAL DESIGN	COMPONENT MODE SYNTHESIS OR ELABORATE FINITE ELEMENT DYNAMIC ANALYSIS
QUALIFICATION	

Figure 2 — Design process

basis for mil-std specifications levied in the request for proposal. The proposal and follow on contract award are based on these preliminary requirements. At this point the logical step would be a thorough examination of the requirements from a systems engineering approach, and then a renegotiation of the contract to adjust the environments to the maximum expected levels. Unfortunately the step is often poorly executed for several reasons, such as:

- The lead time on vendor items often require that specifications for purchase orders are released immediately after award of the prime contract.
- The mil-std type environments are "traditional" and there is considerable inertia against striking out on your own with new unconfirmed environments.
- Human nature may lead one into hiding behind a "traditional" environment.
- The end item user is not available for definitive identification of requirements.
- Typical schedules for preliminary design do not always allow time for a job. The program is in the "manning" stage during this period and a dynamics staff is not fully effective.

Regardless of the reasons, the facts are that the original conservative envelope-type specifications often become "fixed" with long term effects on cost and integrity.

At Boeing we design the inertical upper stage (IUS) which is a space tug that goes in the space shuttle or on a Titan booster to low earth orbit, and then transports various spacecraft to their destination. A shock environment occurs from ordnance devices used during safe and arm and staging. Figure 3 illustrates the IUS qualification test process. We are able to define accurately, by actual test on representative hardware, the shock environment and yet, because of the critical nature of the mission, the customer wants the reliability assurance gained by the 6 dB increase over the maximum expected exvironment for all qualification tests. We also have various degrees of conservatism introduced in the test method. The design of the test fixture hardware has important effects on the response of the test article. NASA and the Air Force use different degrees of conservatism in the factor between qualification test environment and maximum predicted environment, as indicated in Table 1. The Air Force uses a factor of 2 and NASA uses a factor of 1.0.

Conservatism in test levels generally improves the reliability of a system although, when the conservatism results in a requirement to shock isolate to pass the test, some careful consideration must be given to ensure that adding isolator

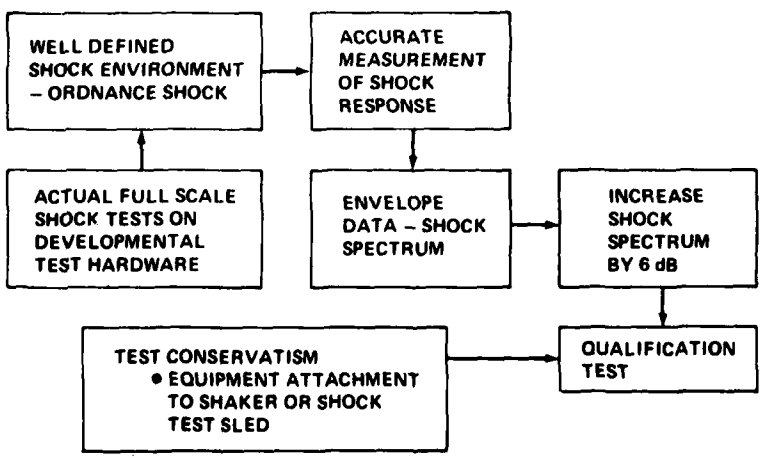

Figure 3 — IUS qualification test

Table 1 — Shock Test Factors

	FACTOR ON MAXIMUM EXPECTED ENVIRONMENT
	QUALIFICATION
USAF (MIL-STD-1540A)	2.0 (6 dB)
NASA – GSFC (-320-G-1)	1.0
NASA – JSC (MF 0004-014)	1.0
NASA – MSFC (TMX-64868)	1.0

hardware does not cause additional reliability problems. For example, isolators may be affected by temperature extremes which need careful attention to ensure a satisfactory design. Also, use of isolators may be affected by temperature extremes which need careful attention to ensure a satisfactory design. Also, use of isolators may eliminate a major heat sink path which in turn will result in the requirement to provide a thermal shunt around the isolator, resulting in an extra item of hardware that will need to be qualified to achieve the required reliability. Also, the conservatism impacts the test facilities and method of test, because the test cannot be done by using the actual device that caused the shock environment.

There is evidence that use of the Mil-std-1540A qualification test factors results in lower on-orbit defects for space systems. This may be a very important and necessary part of the design of space-craft to achieve the required reliability, but it is critical enough to warrant continuing review to ensure that only the necessary and sufficient conditions are imposed on the hardware. Now if we dynamics engineers were really on our toes and knew with considerable certainty what was required for the necessary and sufficient qualification for the IUS equipment, we could have prevented some concern, coordination, time delay, and cost in establishing the test and design requirements. I suppose the necessary knowledge to accomplish this exists piecemeal with various engineers, but the total integrated picture, test results vs. on-orbit defects, is not available for use by the community. We may have only a vague knowledge how on-orbit defects are related to shock environments. It is very important that dynamics engineers understand this thoroughly and completely, so that positive and definite advice and guidance can be given to equipment managers and military and government leaders.

It may seem a little odd to talk of United States balance of trade deficits when talking about "shock," but it is part of the overall picture, the concern that technology improvement can reduce our balance of trade problems. We can only improve our technology overall by efficient transfer of information and engineering techniques in order to maximize technical competence in a time of increased cost. We just cannot afford to keep "re-inventing the wheel."

To improve our capability to make this happen, I would like to challenge the shock and vibration information center to become the driver for a unified, concise procedure and guidelines for the necessary and sufficient analysis and test of equipment exposed to shock and vibration. The SVIC has access to all of the world's experts and is in the unique position to make it happen and disseminate the information to all users. The result will be a joy to managers because they will have confidence that we will be using the correct information and procedures. It will also be very useful during on-the-job training of new engineers.

The analysis and test procedure will include various degrees of complexity for supporting concept development, preliminary design, final design, and qualification testing. The procedure will be related to the type of produce to be produced and, I suppose, for a large complex product like an airplane or a ship, it will address equipment only and not the overall design. The overall design may be too complex and is usually well established and documented in most companies.

As indicated in Figure 4, the procedure should include answers to the following questions:

- How is a design load defined when the environment in the specification is defined by a shock spectrum, random vibration or sine sweep?
- When is it reasonable and acceptable to use (a) traditional load factors, (b) analyses with a statistical basis, (c) test data extrapolation, or (d) a combination of methods?

We like to think that we define a load with a certain probability and confidence level, but in truth this rarely happens. Even the most sophisticated analysis is not nearly as definitive as the usual material allowables data, that is the other half of the structural integrity problem. Aerospace structural dynamics have popularized the 3 sigma loads definition with defined confidence levels, but how do we really know that a 3 sigma rather than 2.5 sigma factor is appropriate? How many engineers consider the reliability requirement before defining the loads criteria? The service life is often used in

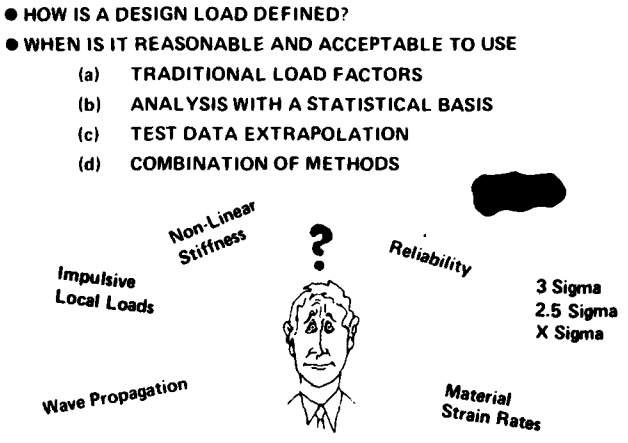

Figure 4 — Analysis and test methods content

adjusting allowables (especially fatigue), but is rarely consciously used in specifying loads.

Traditional load factors are so commonplace that one often assumes they are beyond question. Such things as airplane flight load factors or hoisting factors are just accepted. There was undoubtedly good rationale for the factors at one time but have conditions changed? Often the tendency is to hide behind a code and blame the contracting agency for high load factors and over-design.

The point of all of the above is that I believe that the industry is "shabby" when viewing the state-of-the-art in design (dynamics) loads. Certainly we are far behind the linear statics disciplines and possibly even the non-linear statics analysis. Until some guidelines are established, it will be status quo, that is, if you have a situation that is covered by the book—use it. If your situation is not covered by the book, you are on your own. Invent it! And we find that we invent a lot of our methods.

Another problem is impulsive type "very local" loads. There are everyday type loads such as a door opening against a stop with wind and an assist spring, or a missile wing "popping" open when in flight and impacting against a stop. It seems that no matter how careful one makes the loads analysis, the results are still conservative. By "careful," I mean the care of defining the stiffness characteristic and damping. The part of the problem that is often forgotten is the material strain rates, stress wave propagation, localized impact stresses, non-linear stiffness, etc. What happens if you go to the literature? Usually it is a textbook problem, examining one phenomena only under idealized conditions that allow the mathematics to yield reasonable predictions. Again, I realize that the usage and reliability requirements determine the sophistication of analysis. However, there seems to be no "middle ground" for analyses of shock loads that have a rise time of less than one millisecond.

So, the challenge to the shock and vibration center is to establish a document that will provide explanations, guidelines, and methods for establishing design loads and dynamics requirements and specifications for necessary and sufficient qualifications for shock and vibration. The document must be arranged so that it can be modified easily and it can, of course, refer to other applicable basic books such as the shock and vibration handbook. Then, I would recommend that each year some of the symposium papers would address certain aspects of the document to provide additional verification that the methods are correct or that modifications and additions are necessary, and that the specifications truly represent the necessary and sufficient qualification. The document would be modified and updated each year along with the bulletin.

The result will be a tool that will provide a large increase in confidence that we are using the best available approach to our particular job. Our managers, who have never quite understood some of our flounderings and uncertainties, will be comfortable that their product is receiving the necessary and sufficient attention and is therefore cost effective. This document will also be very useful for on-the-job training of new engineers. It will not be an easy task but I think it can be done in stages, with an initial incomplete release to start and with each succeeding symposium focusing attention to make improvements. The current method of publishing papers in the Bulletin is worthwhile, but over the years becomes somewhat bewildering to find useful information in a timely manner. I have a cabinet full of bulletins in my office for use by all engineers, but it is difficult to wade through them to find applicable information. Usually I end up calling the SVIC and asking for help to locate the applicable paper.

The result of such an effort will be an accurate road map for use by engineers, managers and government leaders that will provide a major improvement in the efficiency of technology transfer to all users, and a major improvement in the confidence that their shock and vibration plans will include only the necessary and sufficient conditions to qualify their product.

Myths and Sacred Cows in Shock and Vibration

Henry Caruso
Westinghouse Electric Corporation

Introduction

The start of a new decade that will be characterized by limited resources and funding is a most fitting time to critically evaluate where we are letting our profession take us. What are we doing from habit or tradition that's a waste of time and money? What should we be doing that we aren't? Why aren't we? The following discussion will deal with these and other important issues responsible for myths and sacred cows in shock and vibration.

What Is A Sacred Cow?

Webster's Third New International Dictionary defines a sacred cow as:

> *A person or thing so well established in and venerated by a society that it seems unreasonably immune from criticism, even of the honest or justified kind.*

But to truly understand what a sacred cow is in practical terms, we need more than a dictionary definition. For the purposes of this discussion, I have adopted the following working definition:

> *Sacred Cow: 1. A tradition, common practice or accepted condition that lacks technical or rational substantiation; 2. A deeply rooted, unquestioned philosophy that prevents or discourages the adoption of more sensible and efficient practices.*

But where do sacred cows come from and how do they survive? This paper considers these questions through the use of actual cases and suggests a practical means by which we may deal with them.

Where Do They Come From?

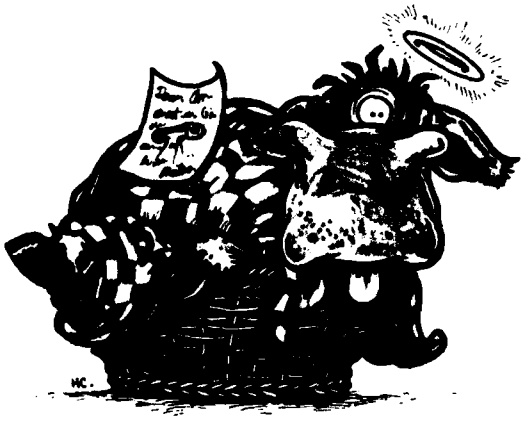

Sacred cows rarely begin their lives in a way which gives any indication of their future status. They attract little attention initially and usually have a legitimate, if limited, reason to exist. They fill small but real knowledge gaps or describe valid, if specialized, philosophies. In some cases they represent early test facility or instrumentation limitations. But regardless of their origin, each sacred cow eventually becomes "standardized." And with standardization comes the sacrosanct status of the true sacred cow.

Standardization (a sacred cow in its own right) may be thought of as that process by which we too often sacrifice the identity and practical value of knowledge on the alter of expediency. Standardization seems to provide exemption from the normal pragmatic, scientific scrutiny that our profession demands we exercise. And the respectability associated with standardization automatically causes otherwise rational professionals to doubt the validity of information not blessed with such privileged status.

What sort of information merits this reverence? An examination of some representative cases will provide a better insight into the real nature of these sacred cows.

Case Number 1: Orthogonal Axis Testing

Most standardized shock and vibration tests prescribe applying vibration in the three orthogonal axes of the hardware being tested. Test engineers routinely perform orthogonal axis tests and debate the pros and cons of multi-axis vs. single-axis testing. But

discussions of the necessity and *effectiveness* of orthogonal axis testing are rare.

What does orthogonal axis testing represent? Are all natural and induced dynamic forcing functions conveniently (and sequentially) aligned along hardware orthogonal axes? Hardly. Instead, we have institutionalized a test artifice introduced to facilitate the separation of vibration modes at a time before the development of modern fast Fourier Analyzers and sophisticated modal analysis software.

Recent comparative experiments with orthogonal and diagonally applied force vector vibration (Ref. 1) have shown that orthogonal axis testing may be less effective than expected or desired. These results reflect the fact that the hardware structures aligned along orthogonal axes in some cases are the least capable of transmitting the forces needed to excite internal hardware components and assemblies. When the goal of dynamic testing is the realistic simulation of real-world situations (Development/ Qualification) or thorough internal structural excitation (Stress Screening), is orthogonal axis testing really what we need? Shouldn't we consider tailoring input force vectors to the structural characteristics of the hardware to be tested?

Case Number 2: 2000 Hz

Standardized broadband random vibration tests (Refs. 2, 3) are almost invariably specified with a 2000-Hz upper limit. But again we must ask, "What does 2000 Hz really represent?"

Do all natural and induced dynamic forcing functions have a built-in cut-off point of 2000 Hz? Do all man-made structures cease to vibrate at 2000 Hz? Obviously not. We are not dealing with a natural physical law or universal mechanical property. Rather, we have institutionalized a test equipment characteristic: The natural frequency of many electrodynamic vibration exciter armature structures lies just beyond 2000 Hz. A test equipment capability has been turned into an implied description of hardware physical behaviour. Isn't it time we questioned the validity of a universal frequency spectrum that ignores hardware impedance?

Case Number 3: 15 g's, 11 ms

Many test engineers would be hard pressed to recall a dynamics qualification test program in which a 15-g, 11-ms shock test was not required. Most of these same test engineers would be equally hard pressed to recall the significant failures resulting from this test, especially when performed after vibration testing. And an exhaustive search of the literature shows only the conspicuous absence of supporting rationale and data for these 35-year old test parameters. Yet procuring agencies seem to regard this test with particular reverence and become uneasy when its deletion is suggested.

In one recent representative shock and vibration test program, an avionics pod spent 18 days in random vibration testing and 6 days in shock testing. The vibration test disclosed 30 defects requiring design or process modification, quality control action or inspection attention; the shock test disclosed none.

This is certainly not to say that shock testing is unimportant. But in light of current Department of Defense policy (Ref. 4) which requires that ". . . qualification tests . . . be tailored for effectiveness and efficiency (maximum return on cost and schedule investment) . . .," can we really justify the rote application of such an apparently unproductive test?

What Are The Consequences?

In spite of their seemingly innocuous nature, sacred cows can have an enormous impact upon the way we conduct our profession. They impede and discourage technical innovation and, in general, make life very unpleasant and unnecessarily expensive.

- How many engineer hours have been wasted in trying to design massive vibration fixtures with natural frequencies above 2000 Hz when the hardware being tested could not transmit energy above 500 Hz? (Refs. 1, 5)
- How much schedule time has been lost performing 15-g, 11-millisecond shock tests that have produced little or no new design defect disclosures because prior vibration testing was more effective?
- Should we continue to standardize without question the artificiality of dynamic testing along three orthogonal axes (Refs. 2, 3) when the real world acts differently and produces dynamic responses that orthogonal-axis testing, in some cases, cannot? (Ref. 8)
- How many nonproductive, and in many cases, counterproductive standardized tests have been performed because other, more effective but nonstandard tests have been stigmatized as being noncompliant?

While it would be impossible to quantify the answers to these questions, anyone familiar with environmental testing will recognize these penalties as being very large indeed.

Why Do They Persist?

Given the scientific arguments that can be brought to bear upon these sacred cows and their demonstrated inefficiency and costliness, we must seriously question why they continue to exist. Indeed, sacred cows are not only hard to get rid of, *they actually become more enduring when challenged*.

There are undoubtedly many interrelated reasons for the persistence of sacred cows in the environmental sciences, but the most appropriate ones for this discussion are ignorance, insecurity, and misplaced reverence.

In many cases, ignorance of a sacred cow's true origin provides an effective barrier to rational treatment. But even worse, when the truth is made known, the errors are so obvious and the respectability of standardization so strong that there is a common tendency to assume that there must be more to the explanation. In this peculiarly intractable situation, *technical knowledge cannot dispel technical ignorance, it only intensifies it.*

Contributing to this situation is the basic human insecurity that manifests itself whenever a change from the familiar is suggested. This insecurity will often win out even when there is conscious realization that what is familiar may be a mistake. In fact, this insecurity is so deep-seated that some will go to great lengths to discover the unique combination of circumstances in which the sacred cow is valid. Then, in a sweeping perversion of statistical abuse, they will adamantly assert that this unique occurrence demonstrates the universal relevance of the 5-σ case.

Finally, there is the proven reverence given (albeit subconsciously) to the printed word, regardless of its pedigree. In fact, because of the bizarre character of human nature, the strength of our reverence varies directly with the anonymity of the source; *the less we know of the source of a statement, the greater the reverence afforded the information.* This leaves us in the curiously contradictory position of being most skeptical of or unsympathetic towards that information in which we should logically have the most confidence.

It is for these reasons that sacred cows persist with a life of their own, even to the point of breeding new strains.

Sacred Calves

Sacred cows are always being born, although our familiarity with our own profession often makes the birth difficult to notice. However, if we are ever to reverse the trend towards costliness and ineffectiveness engendered by blind standardization, we must be both technically prepared and psychologically willing to admit to the existence of these new sacred cows, the sacred calves. Briefly, four of these sacred calves are described below, but it would be reckless to assume that there are no others.

The End-Use Syndrome

While bringing with it definite practical benefits, the crusade for test realism has also begun to create a myopia that recognizes only the end-use or intended service environment as being of concern in environmental design and testing. However, the opposite is all too often true. That is, the end-use environment can be relatively benign when compared to environmental stresses routinely found in other areas of service use and deployment not directly involving the hardware's intended mission function (Ref. 6). For example, natural and induced environmental stresses experienced by an airborne radar may be far less severe than those normally imposed during handling and transportation. Schafer (Ref. 7) urges that we distinguish between complete life-cycle profiles and specific mission (sortie) profiles. Adoption of such a view would do much to stunt the growth of this sacred calf.

The "6-g" Test

How many of us would describe a Superbowl playoff as a 36-point game without regard for the point distribution? Undoubtedly none. Yet there seems to be a distinct trend towards standardizing "the 6-g vibration test" as a stress screening canon, when it should be obvious that no one test can uniquely satisfy this description. The stress characteristics, and therefore the test effectiveness, will vary widely with the frequency distribution imposed.

This is not to say that the 6-g test of NAVMAT P-9492 (Ref. 3) cannot be used effectively. Rather, the caution being offered is that, because of the associated 2000-Hz bandwidth, we are ignoring the true dynamic nature of most assembled hardware which generally attenuates well below this frequency (Refs. 1, 5). As a consequence, we may be overlooking valid stress screening approaches that capitalize on the unique dynamic characteristics of the hardware under test. In addition, we will be effectively barring the use of valid, lower cost alternative stress-generation facilities (Refs. 1, 8) with reduced, but nevertheless adequate, capabilities.

It will indeed be regrettable if a verbal convenience is allowed to become a standardized methodology.

Data

Data is the foundation of the engineering sciences, the lifeblood of the technical literature. Data is a commodity in constant demand and much of the test engineer's time is spent in data acquisition. But data is a double-edged sword: it can just as easily hinder progress as help it.

Data that is not being actively applied to the solution of problems does little good for anyone. This is not to belittle the value of pure research and development, but somewhere in the data acquisition process, professional judgement must face up to the obligation to *turn data into information* by identifying its utility and applicability. The perpetual accumulation of data as an end in itself is wrong. Simply stated,

$$\text{Data} - \text{Intelligence} = \text{Noise}$$

Even greater damage is done when data is used as a weapon to deliberately impede progress. All too often, insistence upon ever-increasing accuracy and statistical rigor is in reality an unjustifiable pretense to avoid committing to a decision. In this no-win situation, the existing information can never be enough and complete ignorance becomes more credible than partial knowledge. Even worse, any additional data, instead of strengthening the information base, only increases the perceived opportunities for uncertainty. The trend towards perpetual study without resolution can only paralyze technological advancement. This conscious abuse of data is inexcusable.

Official Laboratory Tests

The final irony is that some persons feel that the ability of hardware to perform in field service can only be demonstrated in the test laboratory. I was recently made aware of this attitude when a laboratory transportation vibration test was portrayed as being "more official" than a real-world test in which the hardware would be loaded on a truck and driven over rough road. The real-world test apparently seemed too unsophisticated to be reassuring.

Let's not lose sight of the fact that laboratory testing evolved only because real-world testing was not always repeatable or affordable. Test laboratories are certainly here to stay. But in some cases, the real-world test is cheaper and more accurate and should be used. We must not let laboratory testing for its own sake become another sacred cow.

What Can Be Done?

At the beginning of this discussion, I stated that I would offer some practical suggestions for dealing with sacred cows. These suggestions may be somewhat anticlimatic, but simple, direct approaches are usually the best.

First, I believe that the deeply rooted vagaries of human nature and continuously changing personnel populations will effectively doom any proposed solution based primarily upon education of acquisition personnel. Similarly, I don't believe that the facts will always speak for themselves...or at least not loudly enough to be heard over the background noise of preconception and personal motivations. But if these traditional approaches will not work, what will?

The most effective, if undramatic, campaign that can be mounted against the sacred cow is direct involvement in the development process of the environmental test standards themselves. *The sacred cows must never make it into print.* Once they do, it will be too late for they will have established their territory and will not easily be budged.

Professional societies such as the Institute of Environmental Sciences, IEEE, AIA, and EIA are actively involved in the writing and review of key standards defining industry and military-wide environmental test methods. The direct participation of so many competent and experienced professionals is the best assurance that these documents will be written in such a way that they cannot be misapplied, for if they can be, they will be. I have been privileged to participate in this process and have seen it work. This effort must be continued and strengthened if the sacred cow is to be put to pasture.

References

1. "A Rational Approach to Stress Screening Vibration," W. Silver, H. J. Caruso, Westinghouse Electric Corporation; 1981 Annual Reliability and Maintainability Symposium.
2. MIL-STD-810C, "Environmental Test Methods," 10 March 1975.
3. NAVMAT P-9492, "Navy Manufacturing Screening Program," Naval Material Command, May 1979.
4. Department of Defense Directive 5000.40, "Reliability and Maintainability"; 8 July 1980.
5. "Determining Stress Screening Levels from Preproduction Test Experience," H. J. Caruso, W. Silver, Westinghouse Electric Corporation; Journal of Environmental Sciences; Jan/Feb 1980.
6. "The Perils and Pitfalls of Low-Cost Vibration Alternatives," H. Caruso, Westinghouse Electric Corporation; Proceedings, 24th Institute of Environmental Sciences Annual Technical Meeting, April 1978.
7. "Reliability Specifications, Rethinking Mission Profile Testing," H. C. Schafer, Naval Weapons Center; Proceedings, 1978 Annual Reliability and Maintainability Symposium.
8. "Electrohydraulic — The Most Versatile Shaker?" Bruce Huntley, Team Corporation; Journal of Environmental Sciences, March/April 1979.

DAMPING

ON MODELING VISCOELASTIC BEHAVIOR

Dr. Lynn Rogers
Flight Dynamics Laboratory
AFWAL/FIBA
Wright-Patterson AFB, Ohio 45433

The modeling of viscoelastic behavior under sinusoidal, relaxation, creep, constant strain rate, or any other condition is unified. The areas of polymer dynamics, solid mechanics, system dynamics, structural analysis and feedback control systems are drawn upon to construct a unified mathematical treatment which is consistent with observed behavior. A procedure is established to synthesize a stress-strain constitutive differential equation appropriate for more rigorous system dynamics studies. The fractional derivative representation is established as attractive and feasible.

INTRODUCTION

Damping technology is being rapidly advanced and is becoming more widely known. Applications of damping technology to emerging aerospace systems for vibration and noise control have resulted in substantial payoff to systems in terms of cost, weight, and reliability. One key area in the acceleration of the development and application of damping technology is an improved understanding of the behavior of viscoelastic materials. This facilitates the gathering of data to characterize materials and the processing, storing, retrieving, transmitting and utilizing of the data.

Another motivation for this paper is the enabling of more rigorous, accurate and tractable studies of the dynamics of systems and/or structures which incorporate viscoelastic materials. In particular, many studies are based on the fourier transform of systems of differential equations which implicitly assume that structural damping and other system parameters do not vary with frequency. [1] However, it is well known that viscoelastic material properties vary significantly with frequency. As a consequence, past studies are not as a rule based on rigorous methods.

The present paper unifies treatment of all the types of behavior of viscoelastic material, including dynamics (sinusoidal), relaxation, creep and constant strain rate. It draws on the areas of polymer dynamics, solid mechanics, structural analysis, system dynamics, and feedback control systems. As a result, system studies based on more rigor are possible. Furthermore, the full spectrum of effort from characterizing material properties to the design of integrally damped structural components is facilitated. This paper also reveals several areas of research needs.

COMPLEX MODULUS

The well-known complex modulus approach [2] is outlined here. Consider a viscoelastic element undergoing shear strain

$$\gamma = \gamma_A \sin \omega t \qquad (1)$$

which lags the shear stress by phase angle δ

$$\tau = \tau_A \sin (\omega t + \delta) \qquad (2a)$$

$$= \tau_A \cos \delta \sin \omega t + \tau_A \sin \delta \cos \omega t \qquad (2b)$$

$$= \tau_s \sin \omega t + \tau_c \cos \omega t \qquad (2c)$$

The sinusoidal strain and stress may be represented in complex notation

$$\gamma = \gamma_A e^{j\omega t} \quad (3a)$$

$$\tau = \tau_A e^{j(\omega t + \delta)} \quad (3b)$$

and the complex shear modulus may be formed as the ratio

$$G^* = \frac{\tau}{\gamma} = \frac{\tau_A e^{j\delta}}{\gamma_A} = |G^*| e^{j\delta} \quad (4a)$$

$$= \frac{\tau_A \cos\delta}{\gamma_A} (1 + j \tan \delta) \quad (4b)$$

$$= G_R + j G_I = G_R(1 + j \eta_{VEM}) \quad (4c)$$

Solving (1) and (2c) for the sine and the cosine respectively, squaring, adding, etc., leads to the commonly presented ellipse or hysteresis loop

$$\tau = \frac{\tau_s}{\gamma_A} \gamma \pm \frac{\tau_c}{\gamma_A} \sqrt{\gamma_A^2 - \gamma^2} \quad (5)$$

The instantaneous work is proportional to

$$w \propto \int_o^t \tau \frac{d\gamma}{dt} dt \quad (6a)$$

which leads to

$$w \propto \frac{\gamma_A \tau_c}{2} \omega t + \frac{\gamma_A \tau_s}{4} \left[1 - \frac{\cos(2\omega t + \delta)}{\cos \delta}\right] \quad (6b)$$

and the work (or energy dissipated) per cycle is proportional to

$$W \propto \pi \gamma_A \tau_c = \pi \gamma_A \tau_A \sin \delta \quad (6c)$$

and the reason for referring to the real and imaginary parts of the complex modulus as storage modulus and loss modulus respectively is immediately obvious.

It is well known that the dynamic complex modulus for a particular material is strongly dependent on temperature and significantly dependent on frequency over ranges of engineering interest.

For some circumstances it is appropriate to adjust the modulus for temperature

$$G_A = G_{exper} \frac{T_o}{T} \quad (7)$$

REDUCED FREQUENCY

For vibration damping applications, it is commonly accepted that the complex modulus is a function only of reduced frequency for a large class of materials

$$f_R = f \cdot \alpha_T \; ; \; \omega_R = \omega \cdot \alpha_T = \frac{f_R}{2\pi} \quad (8)$$

which expresses the temperature-frequency equivalence principle. [3] Materials which obey Equation 8 are called thermorheologically simple.

The temperature shift parameter is expressed by the WLF equation

$$\log \alpha_T = \frac{-C_1(T - T_o)}{C_1 D_2 + (T - T_o)} \quad (9)$$

(whose form is theoretically justified [4]) where T_o is the reference temperature and where C_1 and D_2 are constants. In practice, C_1 and D_2 may or may not be constants, while T_o is selected in the processing of material dynamic modulus data. In the literature the constant in the denominator is written $C_2 = C_1 D_2$, but the form E9 is preferred because of the relationship between C_1 and C_2 evident in Fig. 1a and b.[5] The use of Equations 7-9 is often advocated for extrapolation of material properties outside the range of temperatures and frequencies of measurement; however, the validity of this process has not been fully experimentally established for a wide range of temperature and frequency. Fig. 2 is an example of material properties derived from sandwich cantilever beam data using the classic Ross-Ungar-Kerwin fourth order theory.

TEMPERATURE NOMOGRAM

The temperature nomogram [6] is a major advance in processing and interpreting VEM complex modulus data. A standard [7] has been proposed to use it in presenting material data. The reading of real modulus and loss factor from graphical presentations is greatly facilitated by its use. In Fig. 2 a vertical scale for frequency is included, as are a number of diagonal lines. Each diagonal line represents a particular temperature. The WLF equation, 9, relates the temperature, frequency and reduced frequency. A reduced frequency value (vertical line) is defined by the intersection of a frequency value

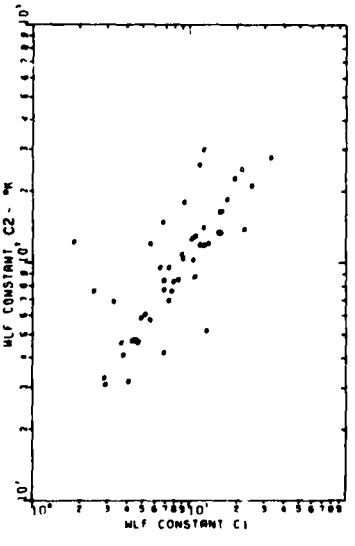

Fig. 1a - Williams-Landell-Ferry Constants

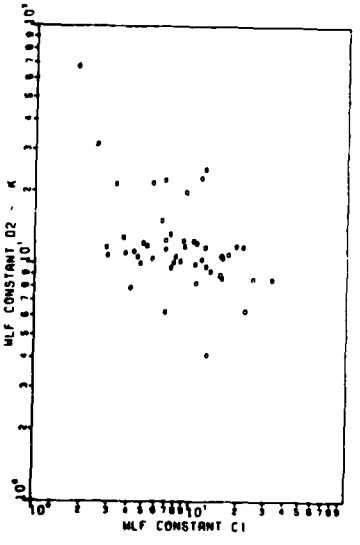

Fig. 1b - Williams-Landell-Ferry Constants

(horizontal line) and a temperature value (diagonal line). This scheme also greatly facilitates any necessary manual plotting of data.

EMPIRICAL CURVE FITTING

It has become common practice [8] to use a standard temperature shift curve, e.g.

$$C_1 = 12.0;\ C_2 = 291.7^{\circ}K \qquad (10)$$

in Equation 9 and select T_o to simultaneously define G_R and η_{VEM} curves and minimize data scatter. A logarithmic least squares fit is used to select parameter values in the empirical equations given in Fig. 2, where M is the real modulus and ETA is the loss factor. Data in this form has been published for a number of polymers [9] and enamels. [10]

Note that the real part of shear modulus, GR, asymptotically approaches G_{RBR} for low values of reduced frequency, F_R, (in the rubbery region). GR increases monotonically with increasing F_R (through the transition region) and asymptotically approaches G_{GLS} for high values of F_R (in the glassy region). The above procedure is well established and serves well for much design work.

REAL-IMAGINARY RELATIONSHIPS

It has been stated by Carson [11] that the behavior of a linear, constant-coefficient, stable system is completely determined if either the real or the imaginary component of the frequency response function is known over the entire frequency range. This leads to the relationships developed by Gross [12].

$$G_R(\omega) = \frac{2}{\pi} \int_o^{\infty} G_I(\xi)\, \frac{\xi}{\omega^2 - \xi^2}\, d\xi \qquad (11a)$$

$$G_I(\omega) = \frac{2}{\pi} \int_o^{\infty} G_R(\zeta)\, \frac{\omega}{\zeta^2 - \omega^2}\, d\zeta \qquad (11b)$$

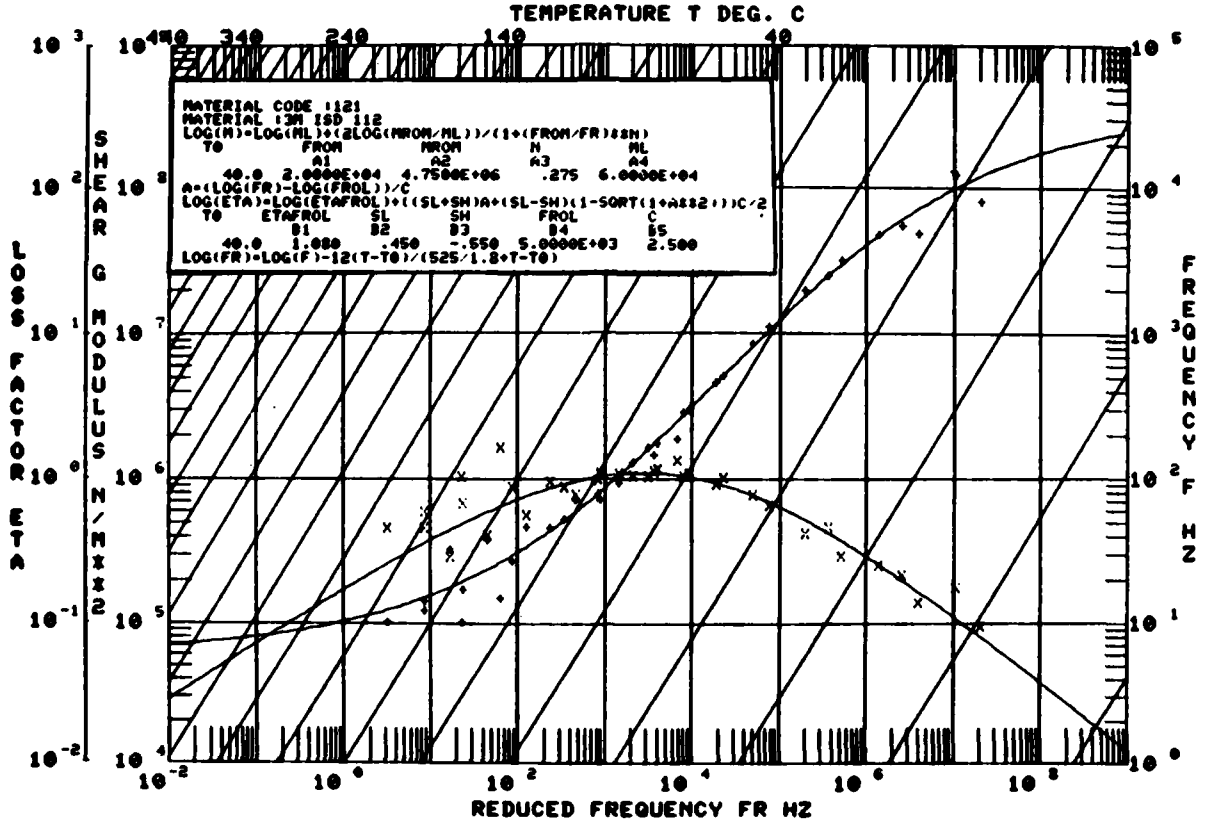

Fig. 2 - Empirical Representation of Complex Modulus

Another useful relationship is

$$\frac{\pi}{2} \frac{d \ln G_R}{d \ln \omega_R} \simeq \eta \qquad (12a)$$

which has been reported by Staverman and Schwarzl [13]. Since for a stable (passive, dissipative, or physically realizable) system

$$\eta > 0 \qquad (12b)$$

it follows that G_R monotonically increases with reduced frequency.

THEORETICAL CONSIDERATIONS

The form of the standard viscoelastic model [3, 14] for a constitutive relation is

$$\tau + a_{D_1} \alpha_T \frac{d\tau}{dt} + a_{D_2} \alpha_T^2 \frac{d^2\tau}{dt^2} + \ldots = G_{RBR}\left[\gamma + a_{N_1} \alpha_T \frac{d\gamma}{dt} + a_{N_2} \alpha_T^2 \frac{d^2\gamma}{dt^2} + \ldots\right] \qquad (13a$$

or in operator form

$$\left[\sum_{k=0}^{N} a_{D_k} \alpha_T^k D^k\right] \tau(t) = G_{RBR}\left[\sum_{\ell=0}^{N} a_{N_\ell} \alpha_T^\ell D^\ell\right] \gamma(t); \qquad (13b)$$

$$a_{D_0} = a_{N_0} = 1.$$

Here the derivatives are of integer order, but fractional order [15] derivatives are a viable (perhaps even preferred) generalization. The inclusion of α_T in the coefficients is believed to be original to this paper and their usefulness will become obvious. With appropriate assumptions invoked, the laplace transform of Equation 13b is

$$\left[\sum_{k=0}^{N} a_{D_k} \alpha_T^k s^k\right] \bar{\tau}(s) =$$

$$G_{RBR}\left[\sum_{\ell=0}^{N} a_{N_\ell}\,\alpha_T^{\ell}\,s^{\ell}\right]\bar{\gamma}(s) \qquad (14)$$

The transfer function, G(s), associated with Equations 13-14 is defined as the ratio of the laplace transform of the output, $\bar{\tau}(s)$, to that of the input, $\bar{\gamma}(s)$

$$G(s) = \frac{\bar{\tau}(s)}{\bar{\gamma}(s)} = G_{RBR}\,\frac{\sum_{\ell=0}^{N} a_{N_\ell}\,\alpha_T^{\ell}\,s^{\ell}}{\sum_{k=0}^{N} a_{D_k}\,\alpha_T^{k}\,s^{k}} =$$

$$G_{RBR}\,\frac{P_N(\alpha_T\, s)}{P_D(\alpha_T\, s)} \qquad (15)$$

If the system represented by Equation 13 is subjected to a sinusoidal input Equation 1, then after transients subside, the steady-state response will be

$$\tau(t) = \gamma_A|G(j\omega)|\,\sin\,(\omega t + \delta) \qquad (16)$$

where $|G(j\omega)|$ and δ are the magnitude and argument, respectively, of the complex quantity $G(j\omega)$, which is called the frequency response function. It is obtained from Equation 15 by replacing the laplacian variable s with $j\omega$.

$$G(j\omega) = G_{RBR}\,\frac{\sum a_{N_\ell}\,(j\omega\cdot\alpha_T)^{\ell}}{\sum a_{D_k}\,(j\omega\cdot\alpha_T)^{k}} =$$

$$G_{RBR}\,\frac{P_N(j2\pi f_R)}{P_D(j2\pi f_R)} \qquad (17)$$

It is obvious at this juncture that $G(j\omega)$ as represented by Equation 17 is the complex modulus Equation 4 and f_R is the reduced frequency Equation 8. Moreover, from a theoretical basis, a ratio of polynomials [14] in $(j2\pi f_R)$ is established as appropriate to represent complex modulus experimental data. It is seen that at the extremes

$$G(jf_R)\Big|_{f_R \to 0} = G_{RBR} \qquad (18a)$$

$$G(jf_R)\Big|_{f_R \to \infty} = G_{RBR}\,\frac{a_{N_N}}{a_{D_N}} = G_{GLS} \qquad (18b)$$

and that the equal order operators in Equation 13 provide the required asymptote.

Equation 13 is variously viewed as a representation of a finite order network of discrete springs and dashpots which approximates viscoelastic behavior or as a truncation of an infinite order process.

BODE PLOTS

The previous development briefly illustrates the procedure for determining the transfer function and the frequency response from the basic differential equation. It is clear that if this equation is of the linear constant coefficient type, then G(s) will be a rational algebraic function consisting of a ratio of polynomials in s. The object here, however, is the reverse operation, i.e. to synthesize the governing differential equation [16] from an experimentally determined frequency response curve. The technique of Bode plots [17] provides a very useful tool for this purpose.

The Bode plot of an arbitrary frequency response function $|G(j\omega)|$ consists of two separate graphs: the magnitude $|G(j\omega)|$ and the phase angle arg $G(j\omega)$. Typically, both the magnitude in db units, called the "log magnitude", and the phase angle in degrees, are plotted vs. frequency on a logarithmic scale. The log magnitude, denoted by Lm is defined as

$$\text{Lm } G(j\omega) \equiv 20\,\log_{10}|G(j\omega)|$$

The use of logarithmic scales leads to a considerable simplification in the construction and interpretation of the plots. This is particularly true when $G(j\omega)$ consists of products and ratios of factored terms. In this case, the total or composite Bode magnitude plot is obtained by simply adding or subtracting those of the individual terms. The same rule applies to the Bode phase angle plots according to the theorems of complex algebra.

In feedback control systems and most frequency response functions, the independent variable is the circular frequency; in the present application it is the reduced circular frequency. The terms most often encountered in the functions $G(j\omega)$ are the polynomials of various degrees in $j\omega$. Their Bode magnitude and phase angle plots have been systematically tabulated in standard reference works such as D'Azzo and Houpis [17]. These plots form the basis of approximating a given experimental frequency response curve in terms of

factored polynomials. A list of typical factors, together with plots of their low-frequency and high-frequency asymptotes is contained in the literature. The corresponding plots of the reciprocal terms are obtained by simply reflecting the given curves about the ω_R axis. The abscissa in these plots is the frequency ω_R plotted on a log scale.

The technique for fitting experimental data is to select factors for the numerator and denominator, such that their asymptotes for magnitude and phase simultaneously approximate the corresponding experimental curves. With reference to Fig. 3, the following expression is easily developed:

$$G^*(j\omega_R) = G_{RBR} \frac{\left(1 + j\frac{\omega_R}{z_1}\right)\left(1 + j\frac{\omega_R}{z_2}\right)\cdots\left(1 + j\frac{\omega_R}{z_N}\right)}{\left(1 + j\frac{\omega_R}{p_1}\right)\left(1 + j\frac{\omega_R}{p_2}\right)\cdots\left(1 + J\frac{\omega_R}{p_N}\right)} \tag{19a}$$

$$= G_{RBR} \frac{\prod_{\ell=1}^{N}\left(1 + j\frac{\omega_R}{z_\ell}\right)}{\prod_{k=1}^{N}\left(1 + j\frac{\omega_R}{p_k}\right)} \tag{19b}$$

It is apparent that

$$G^*(j\omega_R)\Big|_{f_R \to 0} = G_{RBR} ;$$

$$G^*(j\omega_R)\Big|_{f_R \to \infty} = G_{RBR}\prod_{k=1}^{N}\left(\frac{p_k}{z_k}\right) = G_{GLS} \tag{19c}$$

In the present context, the use of the technique to determine values for the constants is inappropriate because the reduced frequency scale (and therefore the slopes) are dominated by the values of the WLF, Equation 9, constants.

In factored polynomial form the transfer function is

$$G(s) = G_{RBR} \frac{\prod_{\ell=1}^{N}\left(1 + \frac{\alpha_T s}{z_\ell}\right)}{\prod_{k=1}^{N}\left(1 + \frac{\alpha_T s}{p_k}\right)} \tag{20}$$

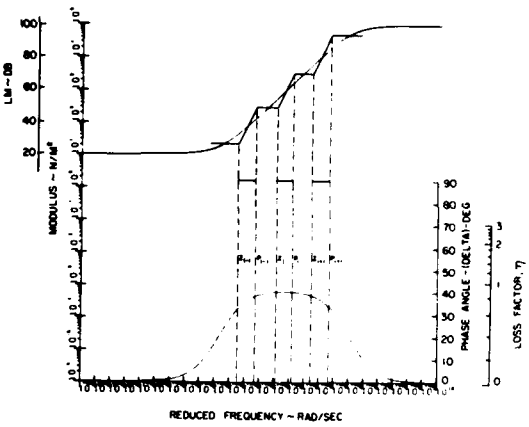

Fig. 3 - Bode Diagram Representation of Complex Modulus

STRESS RELAXATION

When a specimen is subjected to a step shear strain input

$$\gamma(t) = \gamma_o \ , \ t \geq 0 \ ; \ \bar{\gamma}(s) = \frac{\gamma_o}{s} \tag{21}$$

and the relaxation shear modulus is defined from the resulting stress

$$G_{relax}(t) \equiv \frac{\tau_{relax}(t)}{\gamma_o} \ ; \ \bar{G}_{relax}(s) = \frac{\bar{\tau}_{relax}(s)}{\gamma_o} \tag{22}$$

From Equation 15 and Equation 22 we may obtain

$$G(s) = s\, G_{relax}(s) \tag{23}$$

Shapery [14] has assumed a series

$$G_{relax}(t) = G_{RBR}\left[1 + \sum_{k=1}^{N} G_k\, e^{\frac{-p_k t}{\alpha_T}}\right] \tag{24a}$$

where, for vanishing time,

$$G_{relax}(0) = G_{GLS} = G_{RBR}\left[1 + \Sigma\, G_k\right] \tag{24b}$$

The laplace transform of Equation 24a is

$$G_{relax}(s) = G_{RBR}\left[\frac{1}{s} + \Sigma \frac{G_k \alpha_T / p_k}{1 + \frac{\alpha_T s}{p_k}}\right] \quad (25)$$

from which

$$G(s) = G_{RBR}\left[1 + \sum_{k=1}^{N} \frac{G_k \frac{\alpha_T s}{p_k}}{1 + \frac{\alpha_T s}{p_k}}\right] \quad (26)$$

The associated complex modulus is given by

$$G(j\omega) = G_{RBR}\left[1 + \sum_{k=1}^{N} \frac{G_k \frac{\omega_R^2}{p_k^2} + j\, G_k \frac{\omega_R}{p_k}}{1 + \frac{\omega_R^2}{p_k^2}}\right] \quad (27)$$

The expression Equation 26 may be rewritten by letting

$$\Pi = \prod_{k=1}^{N}\left(1 + \frac{\alpha_T s}{p_k}\right) \quad (28)$$

and substituting

$$G(s) = G_{RBR}\left[\frac{\Pi + \sum_{k=1}^{N} G_k \frac{\alpha_T s}{p_k} \prod_{\substack{\ell=1 \\ \ell \neq k}}^{N} 1 + \frac{\alpha_T s}{p_\ell}}{\Pi}\right] \quad (29)$$

When Equations 29, 15, and 20 are compared, it is seen that they are different expressions for the same quantity and the p_k's in Equations 24-29 are seen to be the same as those in Equations 19-20.

Alternatively, Equations 20 and 2[illegible] may be used to express the laplace transform of the relaxation modul[illegible] as

$$G_{relax}(s) = G_{RBR} [illegible]$$

This equation [illegible] of Equation 2[illegible] partial fract[illegible] expansion form[illegible] laplace transforms) and may be used to obtain the values for

$$G_k = -\frac{\prod_{\ell=1}^{N}\left(1 - \frac{p_k}{z_\ell}\right)}{\sum_{\substack{\ell=1 \\ \ell \neq k}}^{N}\left(1 - \frac{p_k}{p_\ell}\right)} \quad (31)$$

Equation 26 can be considered to represent a Wiechert model where the G_k's are proportional to the relaxation times for the individual Maxwell elements in the array [14]. Parenthetically, it is noted that since relaxation times are positive, again the storage modulus is monotonic. Letting

$$\tau_k = \frac{1}{p_k} \; ; \; G_k = \frac{H(\tau_k)\ \Delta_k\ \tau}{\tau_k} \quad (32)$$

and substituting into Equation 26 gives

$$G(j\omega_R) = G_{RBR}\left[1 + \Sigma \frac{H(\tau_k)\ \Delta_k\ \tau}{\tau_k (j\omega_R + 1)}\ j\omega_R\right] \quad (33)$$

In the limit the summation becomes an integral [14]. When the modified power law is used to represent the relaxation spectrum

$$H(\tau) = c\left(\frac{\tau_o}{\tau}\right)^n e^{-\frac{\tau_o}{\tau}} \quad (34)$$

Equation 33 becomes

$$G(j\omega_R) = G_{RBR}\left[1 + \Sigma \frac{c\left(\frac{p_k}{p_o}\right)^n e^{-\frac{p_k}{p_o}} \Delta_k \frac{1}{p}}{\frac{j\omega_R}{p_k} + 1}\ j\omega_R\right] \quad (35)$$

Use of Equation 35 would permit a reduction in the number of parameters required to represent a particular material. It also appears desirable to express p_k as a function of k.

[illegible]

[illegible] when a specimen is subjected [illegible] stress

$$[illegible](s) = \frac{[illegible]_o}{s} \quad (36)$$

[illegible]ance is defined

$$D_{CRP}(t) \equiv \frac{\gamma_{CRP}(t)}{\tau_o} \; ; \; \bar{D}_{CRP}(s) = \frac{\bar{\gamma}_{CRP}(s)}{\tau_o} \qquad (37)$$

the laplace transform of the compliance is

$$\bar{D}(s) = s\,\bar{D}_{CRP}(s) = \frac{1}{\bar{G}(s)} \qquad (38)$$

Knaus [14], following Schapery, has worked with the series

$$D_{CRP}(t) = D_{GLS}\left[1 + \sum_{k=1}^{N} D_k\left(1 - e^{\frac{-tz_k}{\alpha_T}}\right)\right] \qquad (39a)$$

where

$$D_{CRP}(\infty) = D_{RBR} = D_{GLS}\left[1 + \Sigma\, D_k\right] \qquad (39b)$$

The laplace transform of Equation 39a is

$$\bar{D}_{CRP}(s) = D_{RBR}\left[\frac{1}{s} - \Sigma\, \frac{D_k \alpha_T / z_k}{1 + \frac{\alpha_T s}{z_k}}\right] \qquad (40)$$

or

$$D(s) = D_{RBR}\left[1 - \sum_{k=1}^{N} \frac{D_k \alpha_T s / z_k}{1 + \frac{\alpha_T s}{z_k}}\right] \qquad (41)$$

which may be placed in the form

$$D(s) = D_{RBR}\,\frac{\Pi - \sum_{k=1}^{N} \frac{\alpha_T D_k}{z_k} s \prod_{\substack{\ell=1 \\ \ell \neq k}}^{N} \left(1 + \frac{\alpha_T s}{z_k}\right)}{\Pi} \qquad (42a)$$

where

$$\Pi = \prod_{k=1}^{N} \left(1 + \frac{\alpha_T s}{z_k}\right) \qquad (42b)$$

It may be seen that the z_k's are the same as in the previous development and that

$$D_{RBR} = \frac{1}{G_{RBR}} \; ; \; D_{GLS} = \frac{1}{G_{GLS}} \qquad (42c)$$

The coefficients may be obtained

$$D_k = \frac{\prod_{\ell=1}^{N} \left(1 - \frac{z_k}{p_\ell}\right)}{\prod_{\substack{\ell=1 \\ \ell \neq k}}^{N} \left(1 - \frac{z_k}{z_\ell}\right)} \qquad (42d)$$

Constant strain rate test data [14] is an easy extension. The above developments unify the theory of handling various types of test data. Fig. 4 illustrates the flow from any formulation to any other.

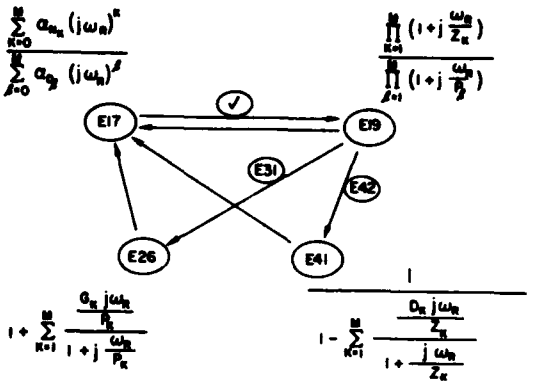

Fig. 4 - Interrelationships of Complex Modulus Expressions

GENERALIZED DERIVATIVES

Bagley [15] had success in fitting 3M-467 complex modulus data with the expression

$$G(j\omega) = \frac{\mu_o + \mu_1 (j\omega)^{\alpha_1}}{1 + b_1 (j\omega)^{\beta_1}} \qquad (43a)$$

where

$$\mu_o = 1.0 \text{ lb/in}^2$$
$$\mu_1 = 7.3 \text{ lb-sec}^{.56}/\text{in}^2$$
$$b_1 = .0008 \text{ sec}^{.51}$$
$$\alpha_1 = .56$$
$$\beta_1 = .51 \qquad (43b)$$

When the experimental data was fitted, only these five parameters were varied and the parameters in the WLF Equation 9 were not adjusted. Together with proper selection of values for the WLF constants, an equation of the form

$$G(jf_R) = \frac{G_{RBR} + G_{GLS}\left(\frac{jf_R}{f_{R_o}}\right)^{\beta}}{1 + \left(\frac{jf_R}{f_{R_o}}\right)^{\beta}} \qquad (44a)$$

is appropriate. This expression satisfies all of the characteristics of observed data mentioned above. To simplify, the complex quantity may be written

$$(j)^{\beta} = \left(e^{j\frac{\pi}{2}}\right)^{\beta} = \cos 90\beta + j \sin 90\beta$$

$$= c + js$$

and Equation 44a becomes

$$G^* = G_{RBR}\left[\frac{1 + \frac{G_{GLS}}{G_{RBR}}\left(\frac{f_R}{f_{R_o}}\right)^{\beta}(c + js)}{1 + \left(\frac{f_R}{f_{R_o}}\right)^{\beta}(c + js)}\right] \qquad (44b)$$

which may be placed in the form

$$G^* = G_{RBR}\,\frac{Re + jIm}{1 + 2\cos 90\beta\left(\frac{f_R}{f_{R_o}}\right)^{\beta} + \left(\frac{f_R}{f_{R_o}}\right)^{2\beta}} \qquad (44c)$$

where:

$$Re = 1 + \cos 90\beta\left(\frac{G_{GLS}}{G_{RBR}} + 1\right)\left(\frac{f_R}{f_{R_o}}\right)^{\beta} + \left(\frac{G_{GLS}}{G_{RBR}}\right)\left(\frac{f_r}{f_{R_c}}\right)^{2\beta}$$

and

$$Im = \sin 90\beta\left(\frac{G_{GLS}}{G_{RBR}} - 1\right)\left(\frac{f_R}{f_{R_o}}\right)^{\beta}$$

It is apparent that the quantities

$$\beta \longleftrightarrow \left(\frac{G_{GLS}}{G_{RBR}}\right) \qquad (44d)$$

are interrelated through the Gross-Staverman-Schwarzl relationships [12,13] or through the inherent dynamic characteristics of polymers.

Equation 44a may be written

$$G(s) = G_{RBR}\left[1 + \frac{\left(\frac{G_{GLS}}{G_{RBR}} - 1\right)\left(\frac{\alpha_T s}{\omega_{R_o}}\right)^{\beta}}{1 + \left(\frac{\alpha_T s}{\omega_{R_o}}\right)^{\beta}}\right] \qquad (44e)$$

by way of analogy to Equation 26. Provided the ratio of moduli is large compared to unity, this is approximated when the viscous damper in the standard three-element model [14] is replaced by a hybrid-spring-damper-element whose force is proportional to the fractional derivative of the relative displacement of its ends. On the Bode diagram this hybrid element would have a constant phase angle of 90β degrees, and the log magnitude would have a constant slope of 20β db per decade. For visualization by polymer chemists and dynamicists, it may be desirable to represent this hybrid element as an infinite array of springs and viscous dampers. In the Bode diagram this array would have stepped log magnitude asymptotes with slopes of 20 and zero db/decade and phase angle asymptotes at 90° for 100β% of the logarithmic reduced frequency scale and at zero degrees for the remainder. An infinite order expression of the form of Equation 19a would result with

$$p_{i+1} = c\,p_i;\; z_i = \beta c p_i \qquad (44f)$$

where a smaller value for c would result in smaller steps and smoother curves closer to the hybrid element. It may happen that these relationships hold only in an average sense and also that pairs of polynomial factors represent local distributed transitions with individual characteristics.

With an understanding of the behavior of polynomial factors having fractional exponents in the Bode diagram, it becomes an easy matter to write expressions for a two-transition material

$$G(j\omega_R) = G_o\,\frac{\left[1 + \frac{G_1}{G_o}\left(\frac{j\omega_R}{\omega_1}\right)^{\beta_1}\right]\left[1 + \frac{G_2}{G_1}\left(\frac{j\omega_R}{\omega_2}\right)^{\beta_2}\right]}{\left[1 + \left(\frac{j\omega_R}{\omega_1}\right)^{\beta_1}\right]\left[1 + \left(\frac{j\omega_R}{\omega_2}\right)^{\beta_2}\right]} \qquad (44g)$$

or for a material which exhibits a rubbery plateau and which flows at zero

frequency or under sustained stress

$$G(j\omega_R) = G_1 \frac{\left[\left(\frac{j\omega_R}{\omega_1}\right)^{\beta_1}\right]}{\left[1+\left(\frac{j\omega_R}{\omega_1}\right)^{\beta_1}\right]} \frac{\left[1+\frac{G_2}{G_1}\left(\frac{j\omega_R}{\omega_2}\right)^{\beta_2}\right]}{\left[1+\left(\frac{j\omega_R}{\omega_2}\right)^{\beta_2}\right]} \quad (44h)$$

or any given proper complex modulus function. In this regard, data which cannot be fit in the Bode diagram is suspect. For selected values of parameters Equation 44a, g, and h are plotted in Fig. 5a, b, and c to illustrate various types of complex modulus curves.

It may be shown that

$$\eta_{max} = \frac{(G_{GLS} - G_{RBR})\ s}{2\sqrt{G_{RBR}G_{GLS}} + (G_{GLS} + G_{RBR})\ c} \simeq \tan 90\beta \quad (45a)$$

from which

$$\beta \simeq \frac{\arctan \eta_{max}}{90} \quad (45b)$$

It also may be shown that the maximum G_I occurs at $f_R = f_{R_o}$ (which serves to define a value for f_{R_o}) and that

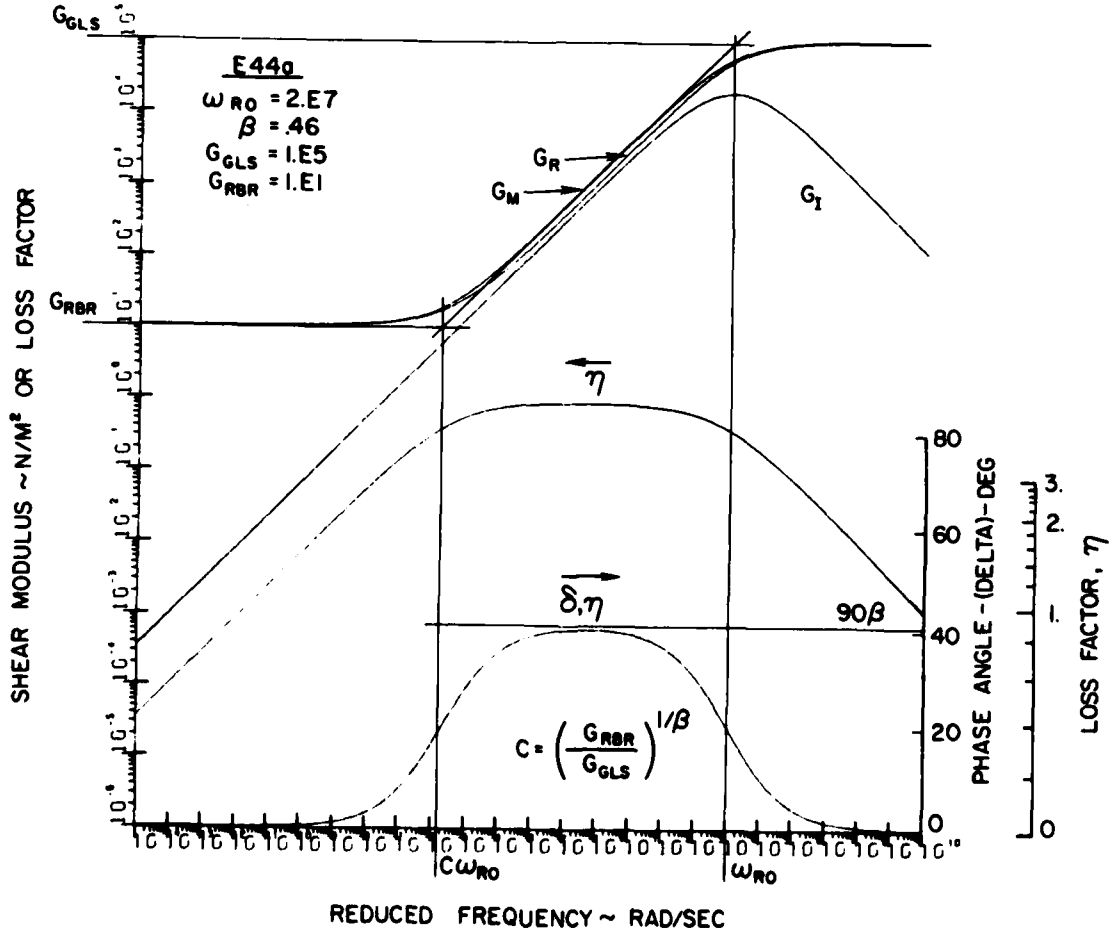

Fig. 5a - Fractional Derivative Representation of Complex Modulus

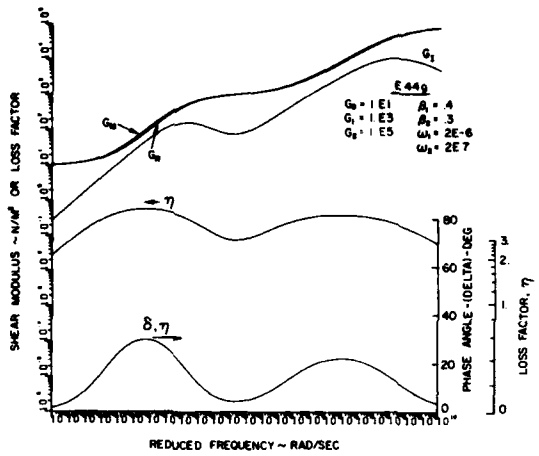

Fig. 5b - Fractional Derivative Representation of Complex Modulus

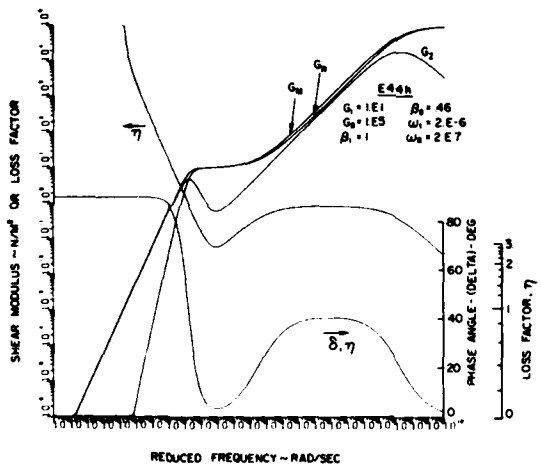

Fig. 5c - Fractional Derivative Representation of Complex Modulus

$$G_{GLS} = \frac{2(1 + c)G_{I_{max}}}{s} + G_{RBR} \qquad (45c)$$

The interrelationships of Equation 45a - c assume $G_{GLS} >> G_{RBR}$ and are approximated in Fig. 6 and may be used to select initial values of parameters for curve-fitting purposes.

Equation 44b may be used for manual fitting of data with the following procedure:

1. Select an initial T_o and plot data (using standard WLF constants)
2. Select β and (G_{GLS}/G_I) from Fig. 6.
3. Set $f_{R_o} = f_R$ @ $G_{I_{max}}$
4. Select G_{RBR} for low asymptote
5. Plot curves
6. Iterate T_o and replot data until slope of data matches curves
7. Iterate all parameters as necessary.

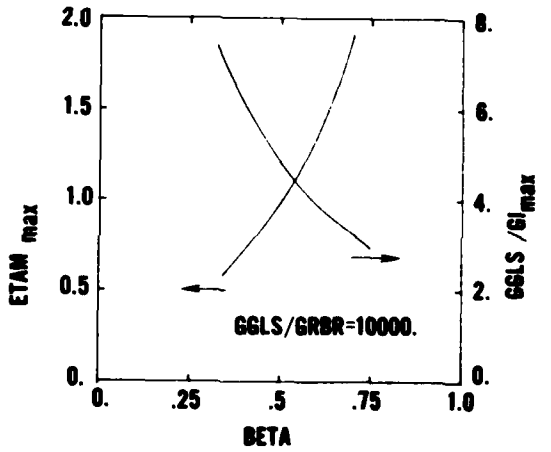

Fig. 6 - Relations of Fractional Derivative Parameters

EXPERIMENTAL DATA FITTING

Because Schapery had success in manually fitting Equation 41 to complex compliance data by collocating at discrete points [14], Equation 27 is used here for complex modulus data to preserve the manual option. The manual collocation process may be used to obtain initial values for the least squares data fitting. The real part of Equation 27 is written

$$\frac{G_N \frac{\omega_R^2}{p_N^2}}{1 + \frac{\omega_R^2}{p_N^2}} + \ldots + \frac{G_2 \frac{\omega_R^2}{p_2^2}}{1 + \frac{\omega_R^2}{p_1^2}} + \frac{G_1 \frac{\omega_R^2}{p_1^2}}{1 + \frac{\omega_R^2}{p_1^2}} = \frac{G_R(\omega_R)}{G_{RBR}} - 1 \qquad (46)$$

The collocation is performed at specific values of reduced frequency, f_{R_i}, and

the p_i's are taken as the same values.

For the curve in Fig. 2 the following is selected

$$\omega_{R_i} = p_i = 10^{i-1} \; ; \; i = 1,2,\ldots 10 \qquad (47)$$

For i=1, Equation 46 becomes

$$\frac{G_{12}\,\frac{.1^2}{10^{18}}}{1+\frac{.1^2}{10^{18}}} + \ldots + \frac{G_2\,\frac{.1^2}{1^2}}{1.01} + \frac{G_1\,\frac{.1^2}{.1^2}}{1+\frac{.1^2}{.1^2}} = \frac{G_R(\omega_{R_1})}{G_{RBR}} - 1 \qquad (48a)$$

or approximately

$$G_1 \simeq 2\left[\frac{G_R(\omega_{R_1})}{G_{RBR}} - 1\right] \qquad (48b)$$

For i=2, Equation 46 yields

$$\ldots \tfrac{1}{2} G_2 + \frac{G_1\,\frac{1^2}{.1^2}}{1+100} = \frac{G_R(\omega_{R_2})}{G_{RBR}} - 1 \qquad (48c)$$

or again approximately

$$G_2 \simeq 2\left[\frac{G_R(\omega_{R_2})}{G_{RBR}} - 1 - G_1\right] \qquad (48d)$$

or, in general,

$$G_\ell \simeq 2\left[\frac{G_R(\omega_{R_\ell})}{G_{RBR}} - 1 - \sum_{i=1}^{\ell-1} G_i\right] \qquad (49)$$

If it is desired to use a large digital computer to solve for the G_ℓ's, the collocation matrix equation becomes

$$\{G\} = [A^{-1}]\left\{\frac{G_{R_i}}{G_{RBR}} - 1\right\} \qquad (50)$$

It may be desirable to collocate on G_I or some combination of G_I and G_R.

The imaginary part of Equation 27 may be written

$$\frac{G_N\,\frac{\omega_R}{p_k}}{1+\frac{\omega_R^2}{p_k^2}} + \ldots + \frac{G_2\,\frac{\omega_R}{p_2}}{1+\frac{\omega_R^2}{p_2^2}} + \frac{G_1\,\frac{\omega_R}{p_1}}{1+\frac{\omega_R^2}{p_1^2}} = \frac{G_I(\omega_R)}{G_{RBR}} \qquad (51a)$$

or, for ω_{R_j}

$$\ldots + .01G_{j+2} + .099G_{j+1} + .5G_j + .099G_{j-1} + .01G_{j-2} + \ldots = \frac{G_I(\omega_{R_j})}{G_{RBR}} \qquad (51b)$$

Fig. 7a, b, and c are plots of the storage modulus, loss modulus and loss factor from Equation 26. Fig. 7a is derived from collocating Equation 46 on the storage modulus from Fig. 2. Fig. 7b is derived from a collocation of both storage and loss modulus, and while not a good representation of this material, suggests that this method may represent materials with two transitions. Further work in this area would be desirable. Fig. 7c shows a representation of storage modulus which is not monotonic and, therefore, is unacceptable. This illustrates the need for care with this method.

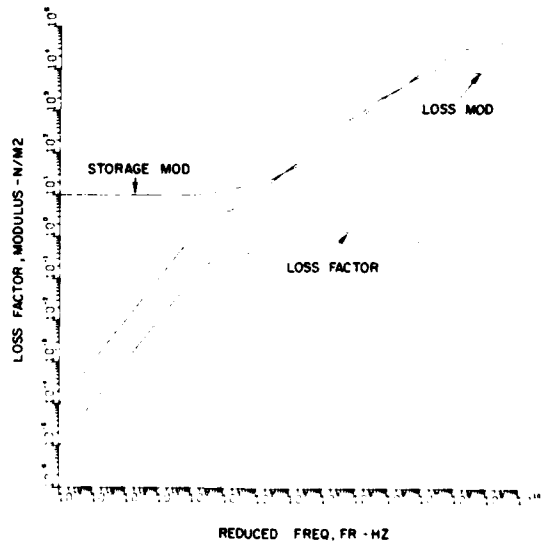

Fig. 7a - Collocation Representation of Complex Modulus

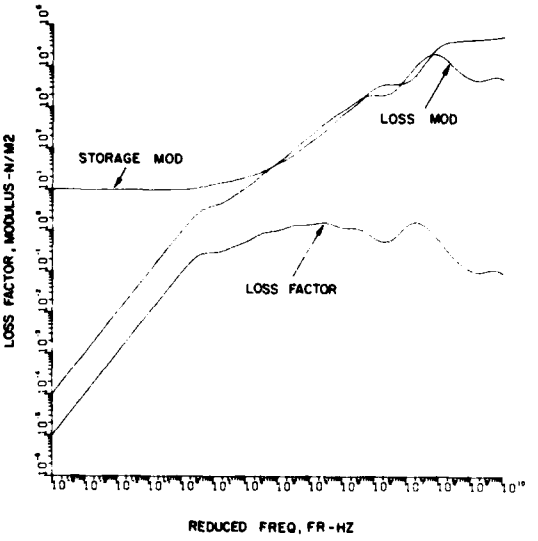

Fig. 7b - Collocation Representation of Complex Modulus

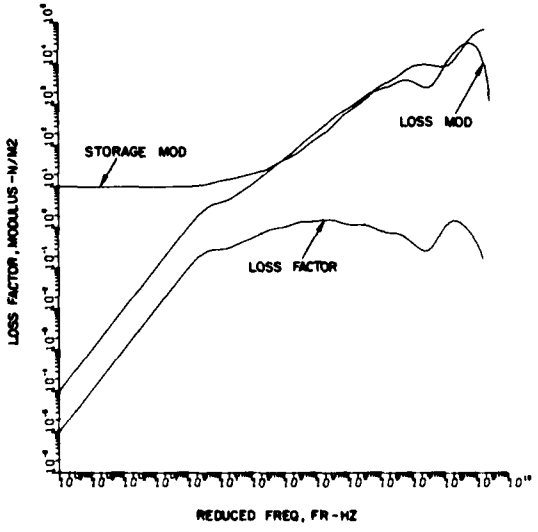

Fig. 7c - Collocation Representation of Complex Modulus

The lack of smoothness in Fig. 7a, b, and c may be explained in terms of the Bode diagram asymptotes. The break frequencies being one decade apart gives too coarse a representation especially at the low values of phase angle (see Fig. 3). The desirability of the most separation of break frequencies at max phase angle and progressively closer symmetric spacing on both sides is indicated. This rationale also has ramification in the logarithmic time spacing for taking creep and relaxation data.

Fig. 8 presents data points and a least squares fit curve of the type Equation 44a.

NEEDED FUTURE WORK

In performing this work, a number of needed and fruitful areas for future development have been indicated. A computer program to go from any representation to any other (Equations 17, 19, 26 and 41) as illustrated in Fig. 4, together with the fractional representation (Equation 44), would be very useful.

A very simple least squares fit computer program was written and used several times to determine parameter values in Equation 44 from experimental data. For each parameter in turn, the merit function is evaluated at the current value of the parameter and at ± 10%. The value for zero slope of a quadratic through the three points is computed; parameter increments are limited to 10%. The procedure is iterated many times. It would be desirable to have an interactive graphics program which incorporated this least squares aspect and also a feature which permits giving less weight to data points where there is less confidence. The small number of parameters in the fractional representation makes it attractive and it should be thoroughly investigated for available material data. It appears possible to include additional terms and represent materials with more than one transition. The polynomial representation should be evaluated for a number of materials. The polynomial form, at least for the near term, would facilitate system eigen-problem studies to investigate complex modulus vs. frequency independent fourier transform approaches.

More data is needed such as dynamic, creep, relaxation, and constant strain rate information for the same material, a variety of specimen types, a wide range of temperature and frequency to investigate G vs. GT_o/T, and Poisson's ratio and other three-dimensional effects.

Sources of data scatter should be studied. It may be, for example, that even very small temperature rise from energy conversion may lead to gradients in modulus and material loss factor in the specimen and consequent scatter.

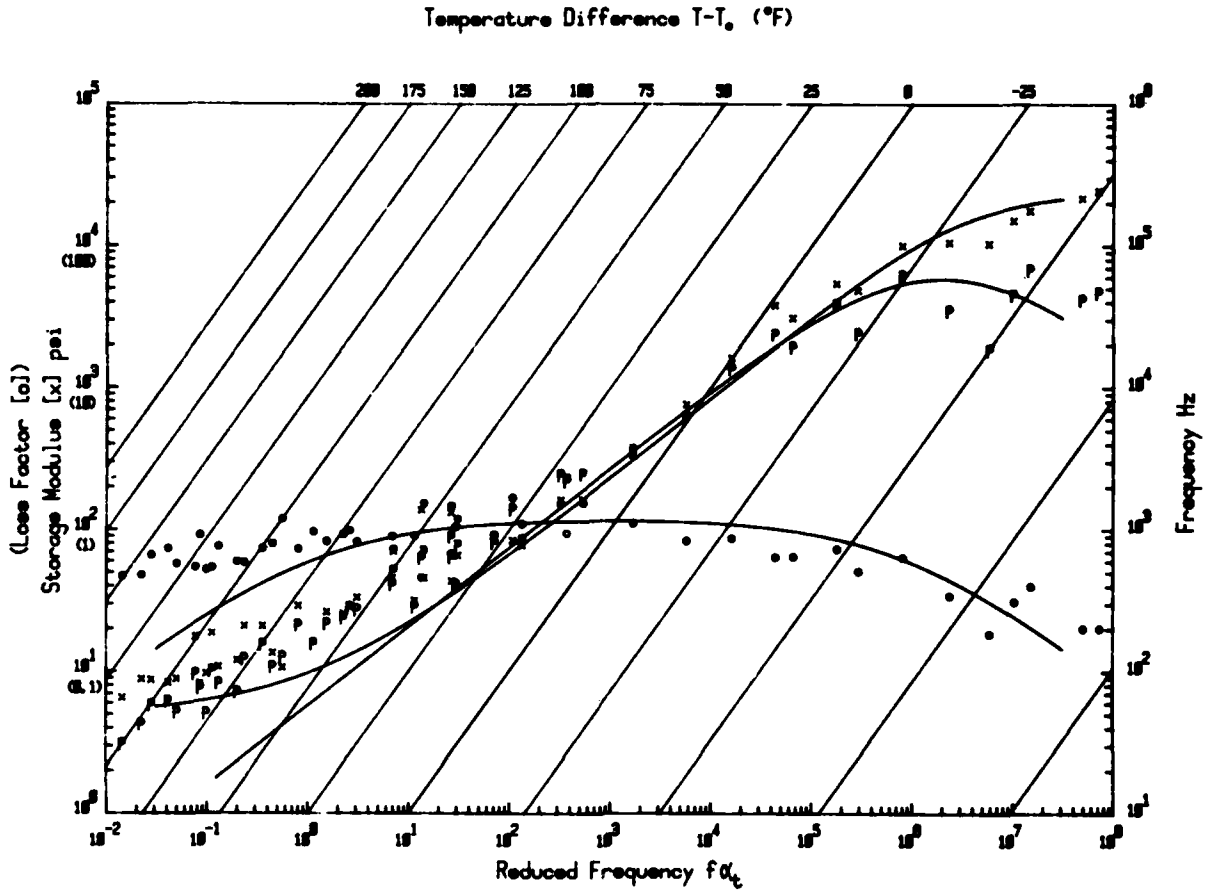

Fig. 8 - Least Squares Fractional Derivative Fit of Complex Modulus Data

It also may be possible to develop other specimens which are less sensitive to workmanship and spurious damping. In this regard, a free-free, unsymetrical sandwich either suspended by threads from an edge or perhaps magnetically levitated should be investigated.

The relationship among the parameters of the fractional derivative representation has been mentioned above. It appears possible to use the Gross relations to obtain an explicit interrelationship. Another possibility is a closed form solution for the inverse laplace transform of the fractional representation for the relaxation, creep, and constant strain rate cases.

CONCLUSIONS

This paper establishes a procedure for the synthesis of constitutive equations. A ratio of polynomials, either of integer or fractional order, is established as appropriate to fit complex modulus material property data. Also, viscoelastic behavior under dynamic, relaxation, creep and constant strain rate test is unified. Because of the small number of parameters, the fractional derivative representation is attractive and limited data fitting indicates that it is a viable approach.

Because this paper provides a unifying foundation for the modeling of viscoelastic behavior by drawing on the areas of polymer dynamics, solid mechanics, structural analysis, and feedback control systems analysis, much needed future work is indicated.

ACKNOWLEDGEMENT

Of many, many individuals and organizations contributing to this paper, the contributions of Ms. Karen Hall, structural vibration analysis consultant, Capt. Ron Bagley, PhD, AF Academy,

Dr. D.I.G. Jones and Dr. J.P. Henderson, Materials Lab at Wright-Patterson AFB, A.D. Nashif, President of Anatrol, and M.L. Drake of University of Dayton Research Institute are especially noteworthy. Reproduction for any purpose of the U.S. Government is permissible.

REFERENCES

1. P.C. Hughes, "Passive Dissipation of Energy in Large Space Structures", J. Guidance and Control, Vol. 3, No. 4, July-Aug. 1980.

2. B.J. Lazan, Damping Materials and Members in Structural Mechanics, Pergamon, New York, 1968.

3. R.M. Christensen, Theory of Viscoelasticity, An Introduction. New York: Academic Press, 1971.

4. J.J. Aklonis, W.J. MacKnight, and M. Sher, eds., "Introduction to Polymer Viscoelasticity", Wiley-Interscience, 1972, p. 52.

5. Roger N. Capps, and F.J. Weber, Handbook of Passive Sonar Transducers (Draft), Naval Research Laboratory, Orlando, FL, 1980.

6. D.I.G. Jones, "A Reduced-Temperature Nomogram for Characterization of Damping Material Behavior", 48th Shock and Vibration Symposium, October 1977.

7. J.P. Henderson, D.I.G. Jones, et al, Characterization and Graphical Representation of Linear Damping Material Properties, ANSI S2-73 Working Group Proposed Standard, Draft No. 3, Sep 1980.

8. C.S. King, Computerized Processing and Graphic Representation of Viscoelastic Material Property Data, University of Dayton Research Institute, AF Materials Lab-TR-79-4099, 1979 (Available from Defense Technical Information Center as ADA 079914).

9. M.L. Drake and G.E. Terborg, Polymeric Material Testing Procedures to Determine Damping Properties and the Results of Selected Commercial Material, AFWAL-TR-80-4093, Apr 1980.

10. G.A. Graves, Jr., C. Cannon, and B. Kumar, A Study to Determine the Effect of Glass Compositional Variations on Vibration Damping Properties, AFWAL-TR-80-4061, May 1980.

11. John R. Carson, Electric Circuit Theory and the Operational Calculus, McGraw-Hill, 1926, p.180.

12. B. Gross, On Creep and Relaxation II, J. Appl. Phys, v 19, Mar 1948, pp. 257-264.

13. A.J. Staverman and F. Schwarzl, Linear Deformation Behavior of High Polymers, Chapter 1, in H.A. Stuart, ed., Die Physik der Hochpolymeren (Springer, Berlin, 1956).

14. M.L. Williams, Structural Analysis of Viscoelastic Materials, AIAA Journal, v 2, n 5, May 1964, pp. 785-808.

15. R.L. Bagley, Applications of Generalized Derivatives to Viscoelasticity, AF Materials Lab TR-79-4103, Nov 1979. (Available from Defense Technical Information Center - ADA 081131).

16. L.C. Rogers and H.K. Brewer, Synthesis of Tire Equations for Use in Shimmy and Other Dynamic Studies, J. Aircraft, v 8, n 9, Sep 1971, pp. 689-697.

17. J.J. D'Azzo, and C.H. Houpis, "Feedback Control System Analysis and Synthesis", 2nd ed., McGraw-Hill, New York, 1966, pp. 175-194.

FINITE ELEMENT PREDICTION OF DAMPING

IN BEAMS WITH CONSTRAINED VISCOELASTIC LAYERS

Conor D. Johnson and David A. Kienholz
Anamet Laboratories, Inc.
Applied Mechanics Division
San Carlos, California

and

Lynn C. Rogers
Air Force Wright Aeronautical Laboratories
Flight Dynamics Laboratory
Wright-Patterson AFB, Ohio

Vibration control in structures by means of viscoelastic material in constrained layers has gained wide acceptance, particularly in the aerospace industry. A key to increased use of damping technology is the ability to analyze and define the candidate viscoelastically damped structure accurately and efficiently in a project environment. This paper describes and establishes the validity of the modal strain energy approach, implemented with finite element techniques, for damped, laminated beams. The modal strain energy approach uses the modal strain energy distributions, obtained by purely elastic analysis, to predict modal damping (loss) factors. These distributions may also be used by a designer as a tool to choose the best location and material for optimum damping. The approach described in the paper may easily be extended to complex structures.

INTRODUCTION

The use of additive or integral viscoelastic damping treatments has steadily gained acceptance in the last two decades as a means of controlling the resonant response of elastic structures. It is especially popular in the aerospace industry where the need for low structural weight often leads to various types of vibration problems. Fatigue failures, excessive noise, or structures which simply deform too much to perform their intended function are the most common examples. Damping can be effective if the undesired motion is known to be of a resonant character. That is, the vibration is characterized by a power spectral density which has most of its area in narrow peaks around natural frequencies of the structure. If such a situation exists, and if the inherent damping of the structure (without any specific damping treatment) is known to be small, the use of constrained viscoelastic layers can often produce a dramatic reduction in vibration.

Examples of the successful use of layered viscoelastic damping material are common in the engineering literature [1,2]. However, the prediction of damping in practical structures is by no means a routine activity. While mass and stiffness properties of complex assemblages are accurately modeled by finite element methods, the inclusion of damping into such models is generally left to simple ad hoc methods which yield solvable equations of motion but do not necessarily agree with physical reality. The situation is unfortunate because if it is known in advance that resonant response will predominate, the prediction of that response can be no better than the prediction of damping. The situation is summarized well by Fahy [3] in a survey article on Statistical Energy Analysis (SEA), a branch of sound and vibration analysis concerned exclusively with resonant response. He states, "the estimation of internal loss factors is the major uncertainty in the application of SEA, as it is in most calculations of dynamic response of mechanical systems. The magnitude of this uncertainty is often such as to make quibbles regarding the finer points of analysis pale into insignificance."

In this paper a method is presented whereby the tools of modern finite element analysis, and in particular the MSC/NASTRAN code, can be used

to estimate damping in certain types of structures. The class of structure to be considered is that which includes layered viscoelastic material, either in a constrained or unconstrained configuration. The assumption is made that the loss factor of the viscoelastic is much higher than that of the metal, and that damping mechanisms other than material damping in the viscoelastic material can be neglected. The emphasis here is on the development of a method which is applicable to a wide range of structures, which is economical enough for design purposes, and which is sufficiently accurate to give useful, though not necessarily exact, damping predictions. The last requirement is reasonable, given the difficulty of characterizing the viscoelastic material itself.

The basic approach is called the modal strain energy method. It is based on the principle that the ratio of composite structural loss factor to viscoelastic material loss factor for a given mode of vibration can be estimated as the ratio of elastic strain energy in the viscoelastic to total elastic strain energy in the entire structure when it deforms into the particular undamped mode shape.

Practical considerations are discussed for finite element modeling of structures with viscoelastic layers. Comparisons of calculated damping are given between modal strain energy results and analytical complex eigenvalue results for simple three-layer beams. Finally, a design example is given to illustrate how the modal strain energy method might be used when viscoelastic material properties are known to vary with frequency.

BACKGROUND

Most methods for finite element analysis of structures with distributed viscoelastic damping fall into one of three categories. For the purposes of this paper they will be called (1) the direct frequency response method, (2) the complex eigenvalue method, and (3) the modal strain energy method.

The direct frequency response method is based on the so-called correspondence principle of linear viscoelasticity [4]. The equations of motion for a structure or structural element are derived in the usual way with the Young's modulus of all materials treated as real. They are then solved for the case of an applied load which varies sinusoidally in time. The Young's modulus of the viscoelastic is then taken to be complex with the ratio of imaginary to real part being called the material loss factor. This implies that stress and strain in the viscoelastic can be out of phase and thus energy can be dissipated. The storage and loss moduli of the viscoelastic are generally obtained as functions of frequency by experiments on material specimens using an imposed sinusoidal stress or strain. For the direct frequency response method, a finite element model of a structure containing a viscoelastic material produces a system of equations of the following form:

$$[-\omega^2 \underset{\sim}{M} + j \underset{\sim}{K}_2(\omega) + \underset{\sim}{K}_1(\omega)]\{X\} = \{F\} \qquad (1)$$

where

$\{F\}$ = vector of amplitudes of imposed sinusoidal forces, usually taken as real

$\{X\}$ = vector of complex response amplitudes

$\underset{\sim}{M}$ = mass matrix

ω = radian frequency of forcing and response

$\underset{\sim}{K}_1(\omega)$ = stiffness matrix which depends on the storage moduli measured at frequency ω for all materials in the structure

$\underset{\sim}{K}_2(\omega)$ = hysteretic damping matrix which depends on loss moduli measured at frequency ω for all materials in the structure

$j = \sqrt{-1}$

In addition to questions of theoretical consistency for nonsinusoidal forcing, the above method has a clear drawback for applied work. The complex coefficient matrix on the left must be formed, inverted, and stored for each frequency of interest in order to obtain a complete solution. This is generally impractical for any but very small problems. The storage requirement can be eliminated if only a few input and output degrees of freedom are required but the cost remains high for problems of practical size.

The complex eigenvalue method is similar to the direct frequency response method in that a complex Young's modulus is assumed. Stiffness and damping matrices are taken to be constant, however. The following system of equations for free vibration of the hysteretically damped system is then obtained:

$$[-\omega^2 \underset{\sim}{M} + j \underset{\sim}{K}_2 + \underset{\sim}{K}_1]\{X\} = \{0\} \qquad (2)$$

If viscous damping forces are known to exist, another term may be added to the matrix equation.

$$[-\omega^2 \underset{\sim}{M} + j \omega \underset{\sim}{D} + j \underset{\sim}{K}_2 + \underset{\sim}{K}_1]\{X\} = \{0\} \qquad (3)$$

Now, if the matrices $\underset{\sim}{M}$, $\underset{\sim}{D}$, $\underset{\sim}{K}_2$, and $\underset{\sim}{K}_1$ are taken as constant, Eqs. (2) or (3) may be recast as an algebraic eigenvalue problem with complex eigenvalues and eigenvectors [5]. The forced response for any input may then be calculated as a weighted sum of the free responses, just as one does in undamped analysis by the normal mode method. The damping ratios of the complex modes are obtained from the complex eigenvalues.

In addition to the difficulty of obtaining realistic damping matrices $\underset{\sim}{D}$ and $\underset{\sim}{K}_2$, the complex eigenvalue method is generally too costly for most design situations. While MSC/NASTRAN provides subroutines for complex eigensolving, the matrices which must be handled are at least double the order of the associated undamped problem. The resulting cost for computing renders the method of little use for models which are already large in undamped form.

The third approach is the modal strain energy method and is the basis of the work reported here. Its mathematical statement is very simple and has already been mentioned. It is

$$\frac{\eta_s^{(r)}}{\eta_v} = \frac{V_v^{(r)}}{V_s^{(r)}} \tag{4}$$

where

$\eta_s^{(r)}$ = loss factor for thr r'th mode of the composite structure

η_v = material loss factor for the viscoelastic material

$V_v^{(r)}$ = elastic strain energy stored in the viscoelastic material when the structure deforms in its r'th undamped mode shape

$V_s^{(r)}$ = elastic strain energy of the entire composite structure in the r'th mode shape

Equation (4) has long been the basis of damping estimates for simple systems [6]. Finite element technology allows it to be extended to much more general structures. One simply computes the undamped mode shapes of the composite structure with the viscoelastic material treated as if it were purely elastic with a real stiffness modulus. The right hand side of Eq. (4) is then calculated as

$$\frac{V_v^{(r)}}{V_s^{(r)}} = \frac{\sum_{e=1}^{n} \underset{\sim}{\phi}_e^{(r)} \underset{\sim}{k}_e \underset{\sim}{\phi}_e^{(r)}}{\underset{\sim}{\phi}^{(r)T} \underset{\sim}{K} \underset{\sim}{\phi}^{(r)}} \tag{5}$$

where

$\underset{\sim}{\phi}^{(r)}$ = r'th mode shape vector

$\underset{\sim}{\phi}_e^{(r)}$ = subvector formed by deleting from $\underset{\sim}{\phi}$ all entries not corresponding to motion of nodes of the e'th viscoelastic element

$\underset{\sim}{k}_e$ = element stiffness matrix of the e'th viscoelastic element

$\underset{\sim}{K}$ = stiffness matrix of the entire composite structure

n = number of viscoelastic elements in the model

Combining Eqs. (4) and (5) we have

$$\frac{\eta^{(r)}}{\eta_v} = \frac{\sum_{e=1}^{n} \underset{\sim}{\phi}_e^{(r)} \underset{\sim}{K}_e \underset{\sim}{\phi}_e^{(r)}}{\underset{\sim}{\phi}^{(r)T} \underset{\sim}{K} \underset{\sim}{\phi}^{(r)}} \tag{6}$$

Several points pertaining to Eq. (6) are worth noting:

(1) It is remarkable in that it relates the real eigenvector $\underset{\sim}{\phi}^{(r)}$ obtained from an undamped model with $\eta^{(r)}$, a quantity obtained from the complex eigenvalue characteristic of a damped model.

(2) It implies that damping of a structure can be described by associating a single number, called a modal loss factor, with each undamped natural mode shape and frequency. This is equivalent to assuming that the damping matrices $\underset{\sim}{D}$ and $\underset{\sim}{K}_2$ were proportional to some linear combination of the undamped mass and stiffness matrices.

(3) The composite loss factor for every mode is taken to be proportional to the material loss factor for the viscoelastic portion of the structure. In the examples to follow, it is shown that this is not precisely true. $\eta^{(r)}$ and η_v are proportional only for $\eta_v << 1$. However, Eq. (6) is shown to be accurate enough for practical purposes even for η_v in excess of unity.

FINITE ELEMENT MODELING

The method used for finite element modeling of a viscoelastic layer constrained between two metal face sheets is illustrated in Fig. 1. The

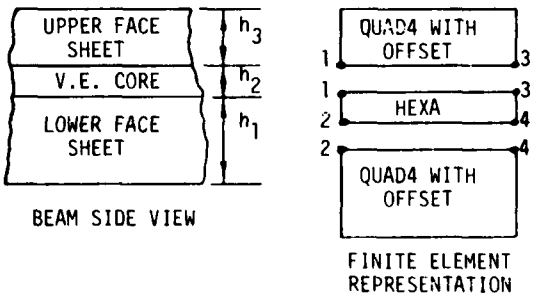

Fig. 1 - Finite element modeling of a sandwich plate with viscoelastic core.

viscoelastic core is modeled with three-dimensional isoparametric solid elements called HEXA elements in MSC/NASTRAN. Each element has eight to twenty nodes with three translational degrees of freedom defined at each node. In this work eight corner nodes were defined for each element. The face sheets are modeled with quadrilateral shell elements called QUAD4's [7]. These utilize three translations and two rotations (about in-plane axes) at each of four corner nodes. An important feature of the QUAD4 element for this work is its ability to account for coupling between bending and stretching. This allows the nodes to be at the surface of the face sheet in contact with the viscoelastic rather than at the midplane of the face sheets. The usefulness of membrane-bending coupling is obvious from the geometry of constrained-layer dampers.

After a model is assembled, a standard normal mode extraction run is executed including calculation of elastic strain energy in each element for each mode. The fraction of total energy within a group of elements corresponding to the viscoelastic is obtained by calling another standard option. Multiplying this value for each mode by the viscoelastic material loss factor yields the modal loss factors. These are then input via a damping vs. frequency table for subsequent forced response calculations.

COMPARISON TO ANALYTICAL RESULTS

A number of simple test cases were run to assess the accuracy of the modal strain energy method and to investigate any unforeseen problems prior to application to a real structure. The test problems were simple sandwich beams with a variety of geometries, material properties, and boundary conditions. An exact complex eigenvalue solution due to Rao [8] was used as the standard for comparison. It is based on a numerical solution of the differential eigenvalue problem obtained from a sixth order differential equation of motion for a sandwich beam [9]. An older, more widely-known solution based on a fourth order governing equation with an equivalent complex flexural stiffness was also used for comparison [10].

The sixth order formulation allows three independent boundary conditions to be specified at each end of the beam. These can be either kinetic or natural boundary conditions on the transverse displacement, slope, and shear in the core layer. The latter is of particular importance since the shearing of the viscoelastic core produces the damping. The older fourth order theory simply assumes a sinusoidal mode shape (in the lengthwise direction) and does not allow for general boundary conditions. It agrees with the sixth order theory for simply supported ends with unrestrained shearing strain, but differs somewhat for other cases. The finite element model retains rotations and displacements of both upper and lower face sheets as separate degrees of freedom and is therefore capable of representing even more general boundary conditions than the sixth order theory. This generality is quite important in modeling of real sandwich structures.

It has been found that some care is required in restraining lengthwise displacements in the finite element model when results are to be compared to those for the sixth order beam theory. The restrained point must be at or near the beam neutral axis (which varies somewhat from mode to mode) [10] since this condition is implicit in the analytical model. Furthermore, the restraint on lengthwise motion must be imposed without inadvertently altering the restraint on relative lengthwise displacements of the upper and lower face sheets (i.e., the core shear). The implementation of boundary conditions has been found to be of particular importance in modeling sandwiches with unequal face sheet thicknesses.

A typical beam geometry is shown in Fig. 2 The dimensions correspond to the standard test specimens used to obtain material properties of viscoelastics by controlled vibration tests [11]. Prior to dynamic analysis of this layered beam, several checks were made on the model. These included calculation of static displacement due to dead weight and calculation of undamped frequencies and mode shapes for two limiting cases. These were for $G_2=0$ (uncoupled face sheets) and $G_2=G_1=G_3$ (all-metal beam). Results were checked against solutions for simple uniform beams and found to be satisfactory.

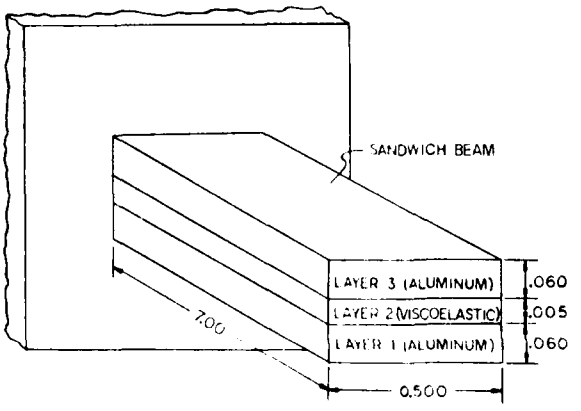

Fig. 2 - Cantilever sandwich beam example.

A number of runs were also made to determine the numerical error which might be introduced by the extreme aspect ratio of the solid elements used to model the viscoelastic core. This was considered a potential problem since core layers of a few mils are commonly used in practice. Aspect ratios between 20 and 5,000 were run by using different beam lengths with all other features of the beam (including the number of elements in the lengthwise direction) held constant. No problems were ever encountered

which could be traced to aspect ratio. It was found during this exercise that energy ratios below about .01 could not always be calculated accurately. Thus, care must be exercised in interpreting very low damping predictions. This was not considered a problem since presumably a designer would not be interested in configurations producing such low damping.

Figure 3 shows a comparison between results for a cantilever sandwich beam as obtained from sixth order theory, fourth order theory, and a NASTRAN model having 20 elements in the lengthwise direction. The 7 inch long cantilever beam has equal aluminum face-sheets 0.060 inches thick, and a viscoelastic core 0.005 inches thick. Results are given in terms of η/η_2, the composite loss factor normalized on the material loss factor of the core, and in terms of natural frequency for each of the first four modes. A value of core material loss factor much smaller than unity ($\eta_2 = 0.01$) was used in the fourth order and sixth order analyses. The ratio η/η_2 is obtained from the finite element results simply as the ratio of core-to-total elastic strain energies (Eq. (6)) and thus does not depend on η_2.

Similar calculations were made for a variety of boundary conditions with similar results. The sixth order and NASTRAN results for damping and frequencies were, for practical purposes, identical for the first six modes. Results from the fourth order theory differed somewhat for certain boundary conditons as would be expected based on the built-in assumptions.

The shear parameter g, shown as the abscissa in Fig. 3, may be thought of as a normalized shear modulus of the core material. It is defined [8] as

$$g = \frac{G_2^*}{(1 + j\eta_2)} \frac{A_2 L^2}{t_2^2} \frac{(E_1A_1 + E_3A_3)}{E_1A_1E_3A_3} \quad (7)$$

where

G_2^* = complex shear modulus of core material

η_2 = loss modulus of core material

A_2 = cross-sectional area of core

t_2 = thickness of core

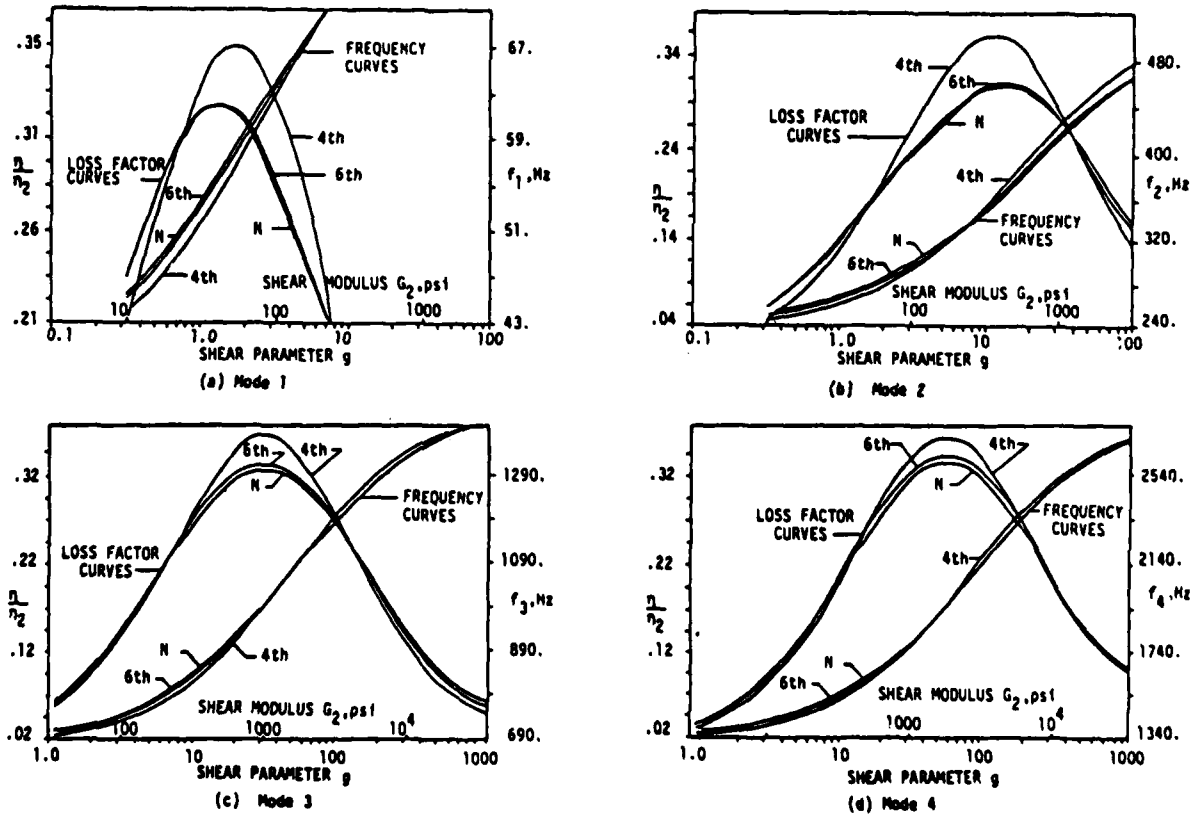

Fig. 3 - Modal loss factors and natural frequencies of sandwich cantilever beam as computed by 4th Order Theory, 6th Order Theory, and NASTRAN.

L = beam length

E_1, E_3 = elastic moduli of face sheets

A_1, A_3 = cross-sectional area of face sheets

The quantity $g(1 + j\eta_2)$ occurs as a coefficient in the nondimensional sixth order differential equation of motion [8].

Figure 4 illustrates the effect of core material loss factor on composite loss factor for the fairly high values of η_2 which one would wish to use in practice. It may be seen that η increases less than linearly with η_2 but that the deviation is not as great as to be of much practical concern. This is particularly true given the dependence of η_2 on structure temperature which is not usually well controlled anyway.

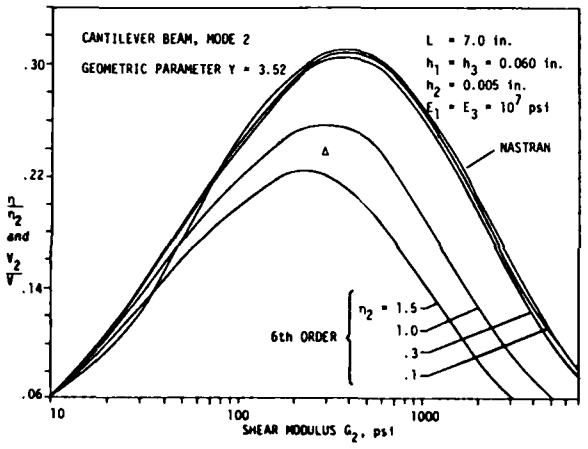

Fig. 4 - Composite loss factor for various core loss factors as computed by Modal Strain Energy Method(NASTRAN) and 6th Order Beam Theory.

The significance (or insignificance) of error in the modal strain energy method may be evaluated in another way. Figure 5 shows a driving point displacement admittance of the cantilever beam of Fig. 2 calculated by two methods. The direct frequency response method (dashed curve) accounts for the material loss factor directly and does not require the assumption that η and η_2 are proportional. The solid line was calculated by summing the modal frequency responses of the first six modes with the modal damping ratio obtained via the modal strain energy method (Eq. (6)). A fairly high value of material loss factor (η_2 = 1.35) was used in both methods. It may be seen that the difference is quite small even in the neighborhood of resonance. This is due partly to the fact that the modal loss factors obtained by Eq. (6) were not far off to begin with, and partly

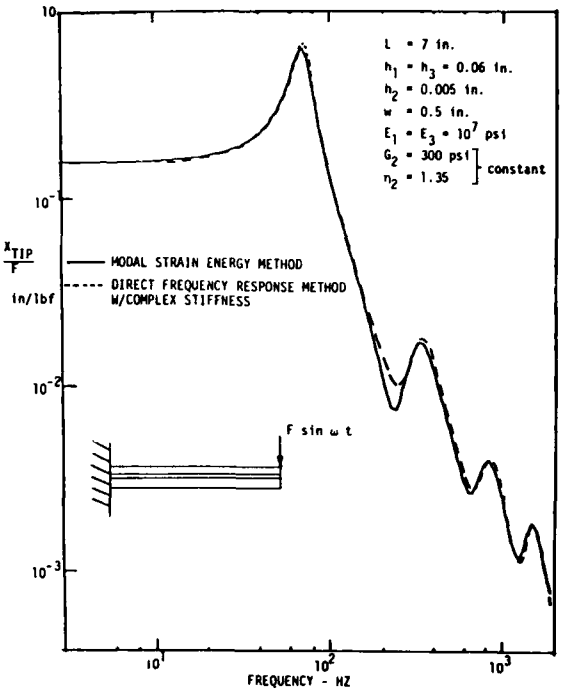

Fig. 5 - Frequency response of sandwich beam calculated by direct and modal strain energy methods.

to the fact that as damping increases, a greater fraction of the total response at any frequency (including a resonance) is due to off-resonant modes.

Figure 6 shows the strain energy distribution in the cantilever beam of Fig. 2 for various values of core shear modulus. In this case, both the top and bottom face sheets are restrained at the root of the beam and, therefore, the core strain is zero at this location. In design work, a plot of the strain energy distribution could be very helpful in determining where viscoelastic layers should be located in a structure to provide maximum damping for the modes or frequency range of interest.

DESIGN EXAMPLES

Figure 7 illustrates the logic which might be used by a designer in specifying a damping treatment. Suppose it is desired to damp the second, third, and fourth bending modes of a uniform cantilever, but to minimize the added weight of the damping treatment. An initial finite element model is constructed with a constrained layer treatment applied over the entire surface. The plots in Fig. 7 illustrate the lengthwise distribution of core strain energy for the first four modes. In this case, the constrained layer is an add-on treatment, and therefore is not fixed at the root of the beam. The strain energy distribution for this

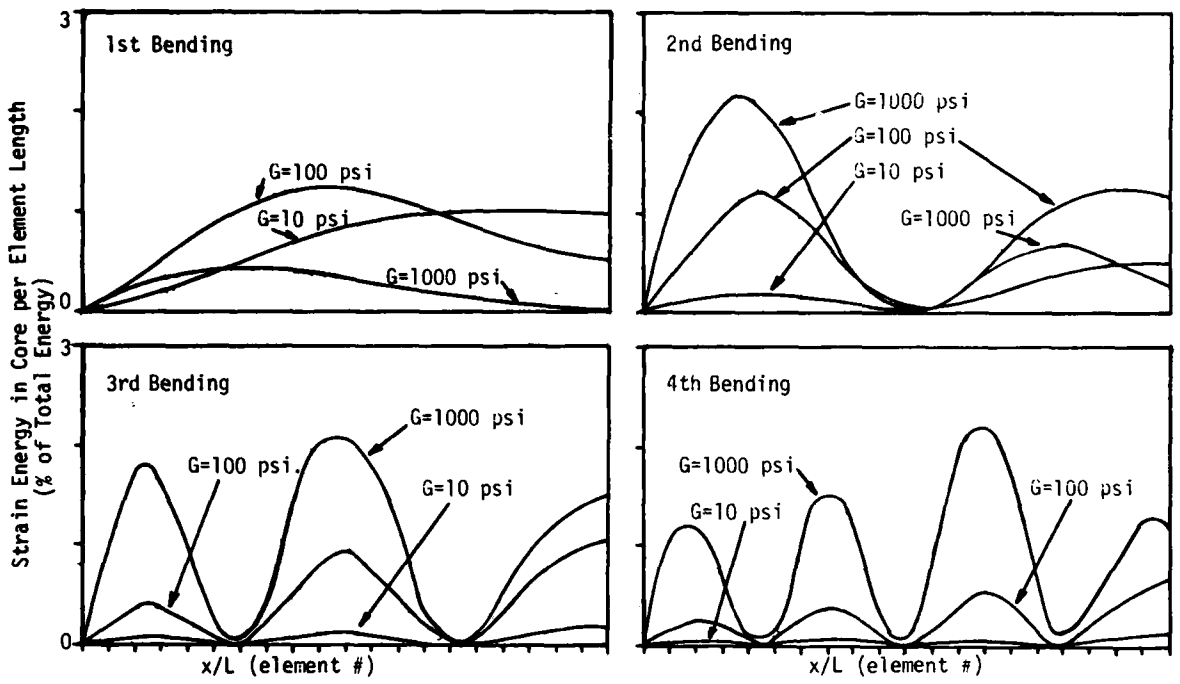

Fig. 6 - Strain energy distribution in a cantilever beam for various values of core shear modulus.

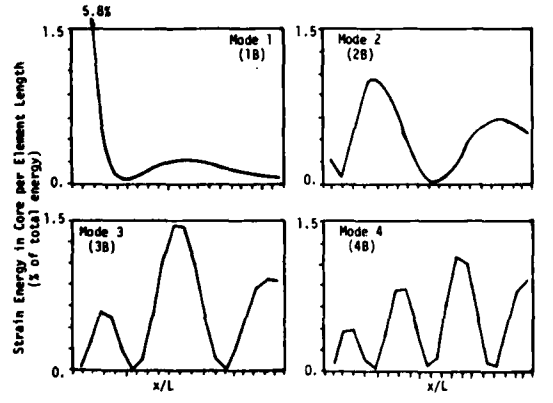

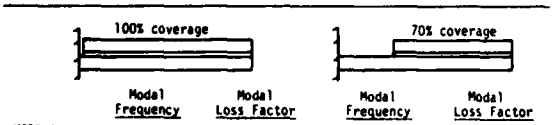

	Modal Frequency	Modal Loss Factor	Modal Frequency	Modal Loss Factor
MODE 1	16.9	.110	14.7	.020
MODE 2	107.9	.107	104.0	.104
MODE 3	285.6	.132	286.1	.091
MODE 4	538.9	.107	549.8	.087

BEAM PARAMETERS

L = 10.00 in. $E_1 = E_3 = 10 \times 10^6$ psi
t_1 = 0.50 in. G_2 = 100 psi
t_2 = .005 in. γ = 0.974
t_3 = .010 in.

Fig. 7 - Use of modal strain energy distributions in damping design.

case should be compared to that given in Fig. 6 for the case of an integral damping treatment. It may be seen from these plots in Fig. 7 that weight can be reduced by removing the damping layer from a portion of the beam near the root where there is little strain energy for the modes of interest. This can be expected to reduce the damping of the modes in question only moderately, although the fundamental bending mode will lose most of its damping. The tables at the bottom of Fig. 7 verify that this is in fact the case.

A second example will illustrate the use of materials with frequency-dependent properties. It is well known that the loss and storage moduli of viscoelastic materials show significant variation with frequency when measured under sinusoidal excitation; however, the modal strain energy method is based on solving a constant-coefficient eigenvalue problem. It is natural to ask how this basic contradiction can best be accommodated while retaining the simplicity and economy of analysis by proportionally damped normal modes. In this section an ad hoc method is presented which has given encouraging results for simple problems.

The method is based on solving one pair of simultaneous equations for each normal mode of interest. The equations are the constant-coefficient eigenvalue problem for the particular mode number and the material property-

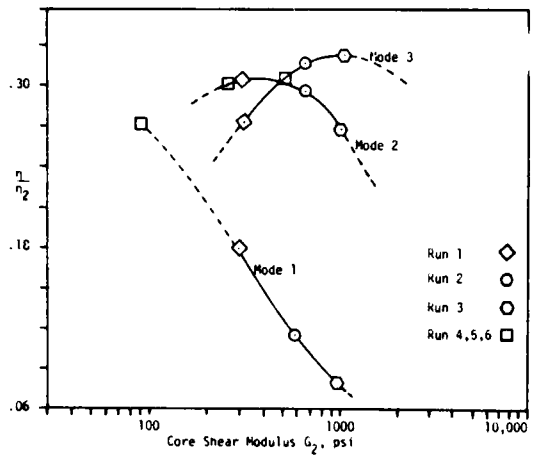

(a) Composite loss factor vs. core shear modulus

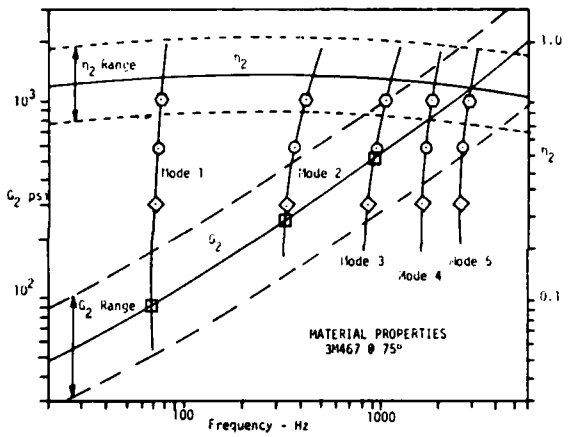

(b) Material properties

Fig. 8 - Design method for sandwich beam with viscoelastic core (frequency-dependent material properties).

frequency relation. The procedure is illustrated in Figs. 8a and 8b. It is desired to select a viscoelastic material and predict the response of the cantilever beam of Fig. 2 when the design criterion is to maximize damping for the frequency range of 300 to 1100 Hz. The approach will be to model the cantilever in terms of a set of normal modes calculated from a sequence of finite element models. Each model will be consistent with the core material properties only for one mode. That is, the model for mode n will have values of G_2 and η_2, which are characteristic of the core material at frequency f_n, the calculated n'th natural frequency. It is clear that an iterative solution will be required

One begins by making several normal mode runs for a range of different core shear moduli. A set of natural frequencies and damping ratios is obtained for each value of G_2. The normalized structural damping factor and first few natural frequencies are plotted vs. G_2 as shown in Figs. 8a and 8b, respectively. As can be seen from Fig. 8b, the second and third modes occur in the frequency range of interest (300 to 1100 Hz). Figure 8a shows that $200 < G_2 < 1{,}000$ psi will optimize damping for modes 2 and 3. Therefore, a material should be selected that has a high loss factor for the frequency range of 300 to 1100 Hz and a shear modulus between 200 and 1,000 psi in this frequency range. Using this criterion, the material 3M-467 was selected, and its properties are shown in Fig. 8b. Also in Fig. 8b, the natural frequencies of modes 1 though 5 are plotted vs. G_2. Curves are drawn for each mode, and the intersections with the material property curve are found as shown. Each intersection represents the G_2 value which is appropriate for calculating the damping of the associated mode. This set of runs is denoted as 4, 5 and 6 in Fig. 8. One of these runs, usually with an intermediate value of core shear stiffness (hereinafter called G_{ref}), is selected as the source for the final values of modal stiffnesses, masses and shapes which are used in subsequent response calculations.

When modal parameters obtained by the above procedure were used to calculate frequency responses, it was found that the result differed from those obtained by the direct frequency response method with variable core properties. Modes below the frequency corresponding to G_{ref} showed too much damping, and modes above it showed too little. A simple empirical correction, which was found to work well, was to multiply the damping ratios obtained by the iterative modal strain energy method by $\sqrt{G(\omega_n)/G_{ref}}$. The results are shown in Figs. 9a and 10a. These figures give a comparison of the displacement and acceleration admittance calculated by the modal strain energy method and a direct-frequency response method with frequency dependent material properties. It may be seen that the comparison is quite good, particularly around the second and third modes. The static stiffness and first natural frequency obtained by the modal strain energy method are somewhat high because G_{ref} is substantially higher than $G(\omega_1)$.

It is not known precisely why the above correction works so well. It was originally introduced on the theory that one should try to adjust the entire coefficient of modal velocity ($2\omega_n n_n$) in the modal equation of motion to account for frequency-dependent properties; however, this reasoning is questionable since ω_n depends also on face sheet stiffness, and is not simply proportional to $\sqrt{G}$ of the core. Present plans are to test this correction factor for more general structure geometries and, if it works, pursue a more thorough investigation of why.

Also plotted in Fig. 8b is the variation in G_2 and η_2 for the material 3M-467 at 75 degrees

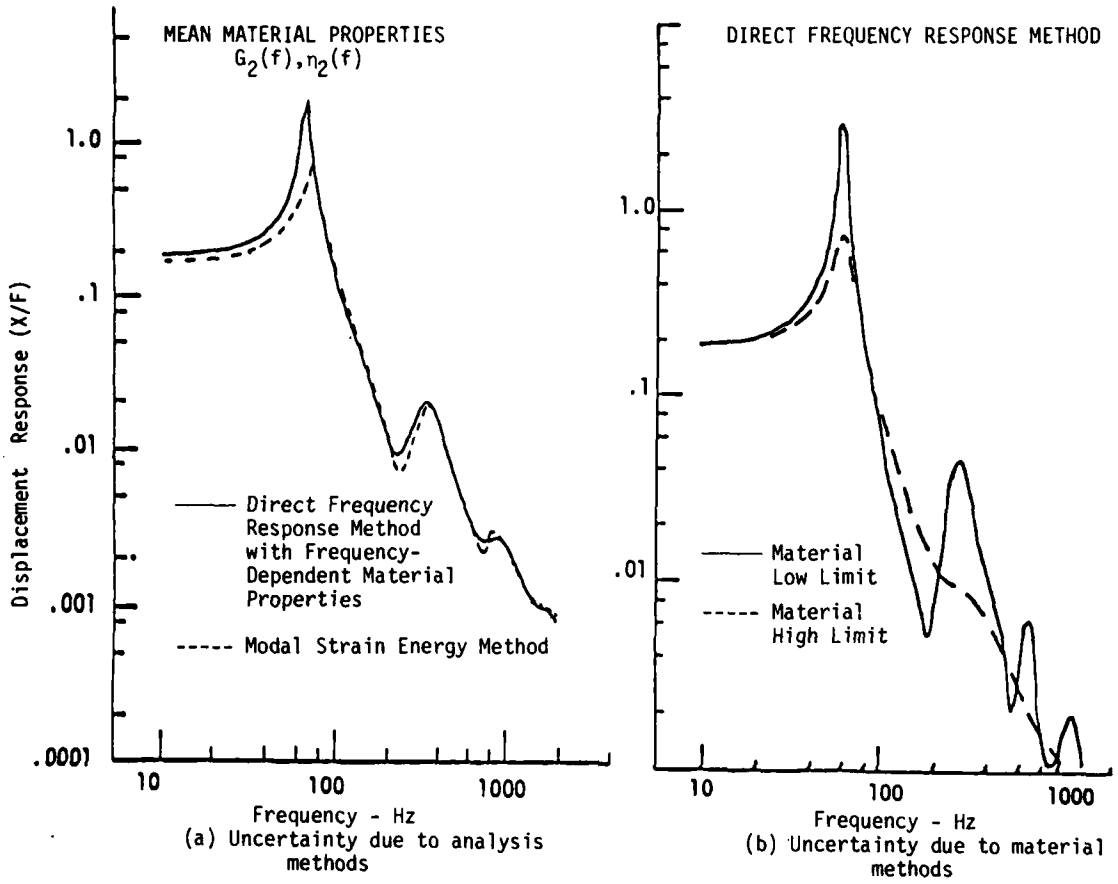

Fig. 9 - Displacement admittance of a sandwich cantilever beam with frequency-dependent core material properties.

Fahrenheit. This variation is due to the scatter in material test data. It was of interest to compare the uncertainty due to material properties with the uncertainty due to the analysis methods. Figures 9b and 10b give the displacement and acceleration admittance functions obtained by the direct frequency response method using the material high and low limits. Comparing Fig. 9a with Fig. 9b, and Fig. 10a with Fig. 10b shows that the uncertainty due to material properties outweighs the uncertainty due to the analysis methods.

CONCLUSION

The modal strain energy method has numerous attractive features as a means of estimating damping in structures with constrained viscoelastic layers. Primary among these is the fact that it may be implemented with a modern finite element code which is widely accessible and familiar to a large number of engineers. The method would fit quite naturally into the design process for structures with integral or added damping. It provides information of direct usefulness in designing a damping treatment.

The use of only undamped mode properties in estimating modal loss factors is essential if computation costs are to be kept within reasonable limits. It has been demonstrated here that this economy can be obtained without unacceptable loss of accurary relative to complex eigenvalue methods. The basic energy ratio relation is valid even for viscoelastic loss factors of 1.0 - 1.5, which are desirable and common in current damping materials.

The basic method can obviously be implemented with any of a number of commercial finite element codes. However, certain features of MSC/NASTRAN make it well suited to the analysis of viscoelastic sandwiches. In particular, the QUAD4 shell element with offset capability allows modeling of constraining and base layers with a minimum of artifice. Calculation of element strain energies and energy distributions are available as a standard option. The extensive selection of elements allows the method to be applied to a wide range of structures, although constrained layer viscoelastic is most commonly employed for controlling flexural vibration of plate sections.

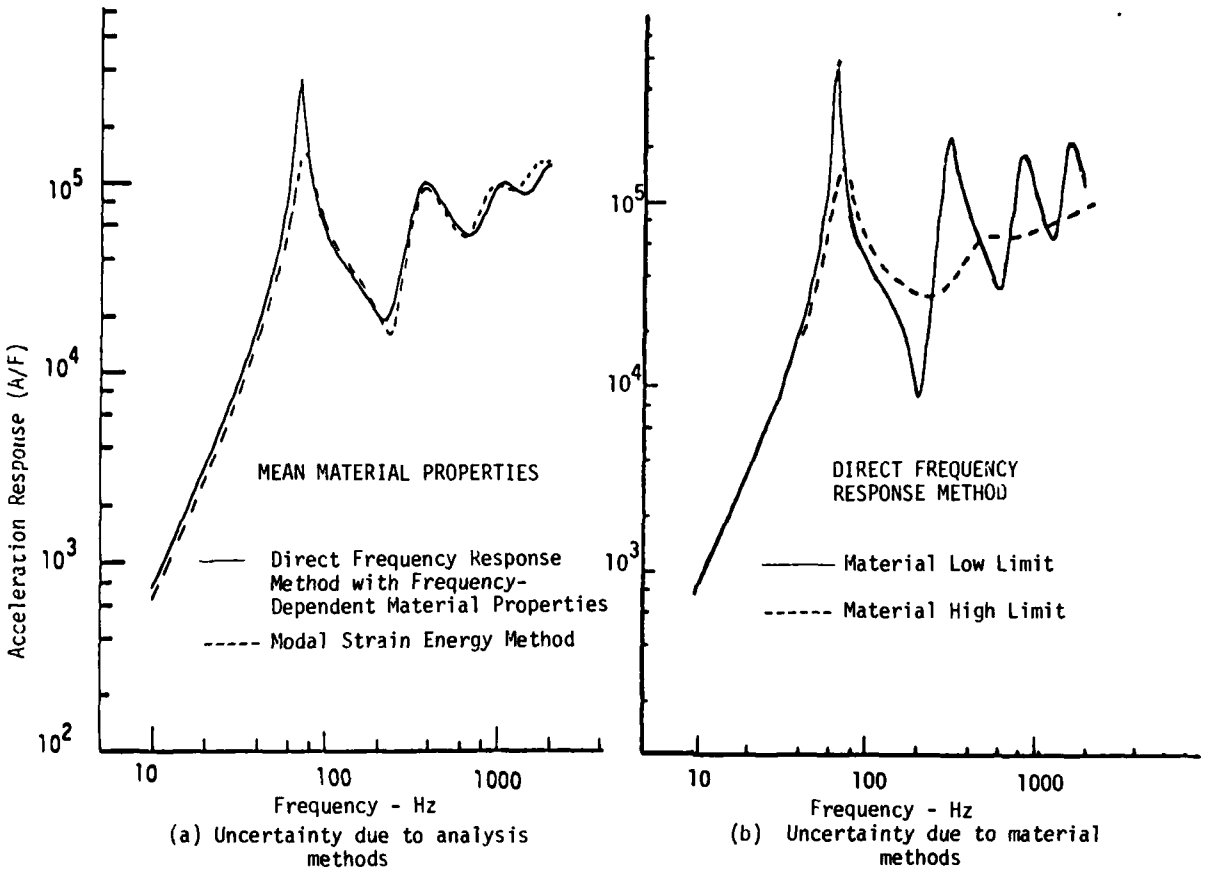

Fig. 10 - Acceleration admittance of a sandwich cantilever beam with frequency-dependent core material properties.

Plans for future work include analysis and comparison to experiment for several real structures. Among these will be a doubly curved thin shell and a stiffened tube. The tube will be modeled and tested with and without an add-on constrained layer damping treatment.

ACKNOWLEDGMENT

A portion of the work reported in this paper was sponsored by the Flight Dynamics Laboratory, Air Force Wright Aeronautical Laboratories, Air Force Systems Command, Wright-Patterson Air Force Base, Ohio. The authors would like to express their gratitude to Captain Salvatore Cusamano of the Air Force Weapons Laboratory, Kirtland Air Force Base, New Mexico, who provided the computer time for this study.

REFERENCES

1. Rogers, L., editor, Proceedings of the Conference on Aerospace Polymeric Viscoelastic Damping Technology for the 1980's. Air Force Flight Dynamics Laboratory Technical Memorandum 78-78-FBA, July 1978.

2. Course notes from Vibration Damping Short Course given by the University of Dayton Research Insititute, Dayton, Ohio, November 1979. Dale Whitford, Course Director.

3. Fahy, F. J., "Statistical Energy Analysis - A Critical Review," Shock and Vibration Digest, Vol. 6, No. 7, July 1974.

4. Bland, D. R., The Theory of Linear Viscoelasticity, Chap. 3, Pergamon Press, 1960.

5. Foss, K. A., "Coordinates Which Uncouple the Equations of Motion in Damped Linear Dynamic Systems," Journal of Applied Mechanics, Vol. 25, 1958, pp. 361-364.

6. Ungar, E. E., and Kerwin, E. M., Jr., "Loss Factors of Viscoelastic Systems in Terms of Energy Concepts," J. Acoust. Soc. Am., Vol. 34, 1962, pp. 954.

7. MacNeal, R. H., "A Simple Quadrilateral Shell Element," Computers and Structures, Vol. 8, 1978, pp. 175-183.

8. Rao, D. K., "Frequency and Loss Factors of Sandwich Beams Under Various Boundary Conditions," J. of Mechanical Engineering Science, Vol. 20, No.5, 1978, pp. 271-282.

9. DiTaranto, R. A., "Theory of Vibratory Bending for Elastic and Viscoelastic Layered Finite Length Beams," Journal of Applied Mechanics, Vol. 32, 1965, pp. 881-886.

10. Ross, D., Ungar, E. E., and Kerwin, E. M., Jr., "Damping of Plate Flexural Vibrations by Means of Viscoelastic Laminae," Section 3 of Structural Damping, ASME, 1959.

11. Parin, M. L., "Material Property Measurement and Data Reduction; Resonant Beam Technique," Course Notes from Vibration Damping Short Course given by the University of Dayton Research Institute, Dayton, Ohio, November 1979.

DYNAMIC BEHAVIOR OF LATHE SPINDLES WITH ELASTIC SUPPORTS INCLUDING DAMPING BY FINITE ELEMENT ANALYSIS

A.M. Sharan, T.S. Sankar, S. Sankar
Department of Mechanical Engineering
Concordia University, Montreal, Canada

This paper presents the free-vibration behavior of a lathe spindle-workpiece system using finite element analysis. The investigation is carried out in three parts which are: (1) The classification of the end condition at the running center, (2) The determination of the undamped natural frequencies and the corresponding mode shapes, and (3) The effect of bearing stiffness on the natural frequencies as well as the mode shapes. The theoretically computed natural frequencies are compared with the experimentally obtained frequencies. The end condition at the running center is classified based on the sum of the squares of the residues between the experimental and the theoretically obtained natural frequencies. The undamped mode shapes are explained in terms of the interacting play between the inertia forces, the flexural rigidity of the system, and the spring forces.

INTRODUCTION

Improving the accuracy and surface finish of a machined product has always been the objective in manufacturing engineering. The accuracy and the surface finish are greatly affected by the vibrations arising in the machine operating. A proper design of a machine tool spindle would greatly reduce the vibration levels and hence would improve the quality of the workpiece produced. Some of the factors which influence the static and the dynamic stiffness of the spindle are: (a) sectional rigidity, (b) spacing of the bearings, and (c) the stiffness of the bearings.

The spindle-workpiece system is subjected to a combination of harmonic and random forces [1], during a turning operation. Therefore, a good design would require a high dynamic stiffness in the spindle-workpiece system having elastic supports with damping. In a lathe, the equivalent stiffness of the spindle-workpiece is usually considerably less than that of the other parts of the machine [2]. Several authors [3-5] have developed mathematical models of the machine tool under self-exited and forced vibrations, and established stability criterion in terms of the rotational frequency of the system. Studies using pulse technique [6] and an analog computer technique [7] have been used to explain the dynamic behavior of the spindle.

The purpose of the present paper is

a) To investigate the nature of the end conditions of the workpiece supported at the running center i.e. to determine whether the end condition can be classified as hinged or clamped support.

b) To calculate the undamped natural frequencies and mode shapes of the spindle-workpiece system using finite element analysis.

c) To compare experimentally obtained frequencies with the theoretically computed natural frequencies.

d) To study the effect of the bearing stiffness on the natural frequencies and the mode shapes of the spindle-workpiece system.

FORMULATION OF THE MATHEMATICAL MODEL

A typical lathe spindle is shown in Figure 1a and its discretized model is shown in the Figure 1b. A schematic model of the spindle-workpiece system is shown in the Figure 2a, where one end of the workpiece is held in the chuck, and the other end is supported by the running center. The two bearing supports, in both Figures 1b and 2a, are considered to be flexible with elastic support and damping.

The equation of motion of the lathe spindle-workpiece system supported by elastic bearings with damping can be written as [8]:

$$\frac{\partial^2}{\partial x^2}\left[EI(x)\,\frac{\partial^2 U(x,t)}{\partial x^2}\right] = a_1 + a_2 + a_3 + a_4 \qquad (1)$$

where $a_1 = -\,m(x)\,\dfrac{\partial^2 U(x,t)}{\partial t^2}$

$a_2 = -\,k(x)U(x,t)$

$a_3 = -\,c(x)\,\dfrac{\partial U(x,t)}{\partial t}$

$a_4 = f_{ext}(x,t),$

and the associated boundary conditions.

In equation (1) it is assumed that the effect of rotary inertia and shear deformation are negligible. The terms on the right-hand side are the inertia forces, the spring forces at the bearings, the damping forces, and the externally applied forces. Referring to the Figure 2a, the system has been subdivided into 12 parts. Since the main objective of this paper is to investigate the nature of the end condition at the running center, the fourth order partial differential equation (1) has to be solved for the different sets of the boundary conditions at the running center. In this paper as a first case, the workpiece has been assumed to be hinged at the running center and therefore, the boundary condition would be

$$U(x,t)\Big|_{x=0} = 0, \text{ and } EI(x)\,\frac{\partial^2 U(x,t)}{\partial x^2}\Big|_{x=0} = 0 \qquad (2a)$$

In the second case, the workpiece has been assumed to be clamped instead of hinged therefore, the corresponding set of boundary conditions can be written as

$$U(x,t)\Big|_{x=0} = 0, \text{ and } \frac{\partial U(x,t)}{\partial x}\Big|_{x=0} = 0 \qquad (2b)$$

The boundary condition for the free end of the spindle in either of the above mentioned cases would be

$$EI(x)\,\frac{\partial^2 U(x,t)}{\partial x^2}\Big|_{x=L} = 0 \quad \text{and} \qquad (3)$$

$$\frac{\partial}{\partial x}\left[EI(x)\,\frac{\partial^2 U(x,t)}{\partial x^2}\right]_{x=L} = 0$$

where L is the total length of the combined spindle-workpiece system.

The finite element model of a shaft-element of the spindle-workpiece system is shown in Figure 2b. The partial differential equation (1) along with the boundary conditions (2a), (2b) and (3) has been solved by expressing the displacement at any point in the system as

$$y(x_1,t) = \sum_{i=1}^{4} \phi\,(x_1)\, w_i(t) \qquad (4)$$

where $\phi_i(x_1)$ is the shape function, x_1 is the local position coordinate, and $w_i(t)$ is the joint displacement function.

For a free vibration problem, the equation (1) and (4) can be combined and after some mathematical operations [9] can be written as:

$$y(x_1,t) = \left(1 - \frac{3x_1^2}{\ell^2} + \frac{2x_1^3}{\ell^3}\right) w_1(t) + \qquad (5)$$

$$\left(\frac{x_1}{\ell} - \frac{2x_1^2}{\ell^2} + \frac{x_1^3}{\ell^3}\right) \ell\, w_2(t) + \left(\frac{3x_1^2}{\ell^2} - \frac{2x_1^3}{\ell^3}\right)$$

$$w_3(t) - \left(\frac{x_1^2}{\ell^2} - \frac{x_1^3}{\ell^3}\right) \ell\, w_4(t)$$

where ℓ is the length of the element.

Now using equation (5) in the Lagrange's equations of motion of the element will yield the elemental inertia matrix [m], stiffness matrix [k], and damping matrix [c] as:

$$[m] = \frac{m\ell}{420}\begin{bmatrix} 156 & 22\ell & 54 & -13\ell \\ 22\ell & 4\ell^2 & 13\ell & -3\ell^2 \\ 54 & 13\ell & 156 & -22\ell \\ -13\ell & -3\ell^2 & -22\ell & 4\ell^2 \end{bmatrix}$$

$$[k] = \frac{EI}{\ell^3}\begin{bmatrix} 12+k & 6\ell & -12 & 6\ell \\ 6\ell & 4\ell^2 & -6\ell & 2\ell^2 \\ -12 & -6\ell & 12+k & -6\ell \\ 6\ell & 2\ell^2 & -6\ell & 4\ell^2 \end{bmatrix}$$

$$[c] = \begin{bmatrix} c & 0 & 0 & 0 \\ 0 & 0 & 0 & 0 \\ 0 & 0 & c & 0 \\ 0 & 0 & 0 & 0 \end{bmatrix}$$

Adding the contributions due to all the elements, the equation of motion of the spindle-workpiece system can be represented by the matrix differential equation

$$[M] \{\ddot{U}\} + [C] \{\dot{U}\} + [K] \{U\} = f_{ext}(t) \qquad (6)$$

where [M], [C] and [K] represent the global mass, damping and stiffness matrices (26 x 26) respectively obtained by assembling the elemental matrices.

The homogeneous part of the matrix differential equation (6) was solved by modal analysis [10], utilizing the two sets of boundary conditions given in the equations (2a), (2b), and (3). The variation of the mass and the stiffness along the spindle-workpiece system used in the analyses are shown in the Figures 3(a) and 3(b) respectively. It should be noted that in these two figures, both the mass and stiffness of all sections have been normalized with respect to the mass and the stiffness of the chuck. Also, the front end (chuck) bearing stiffness k_7, has been taken as 3.19 times the rear bearing stiffness k_{11}, in all computations. (Refer to Figure 2(a)). In other words, the ratio of the stiffness of the front- and the rear bearing has been held constant while the front bearing stiffness has been varied, thus the effect of the bearing stiffness on the natural frequencies and the corresponding mode shapes can be studied.

EXPERIMENTAL SET-UP

In order to estimate the nature of the boundary condition at running center, a 12 hp Demoor type Lathe, Model No. 821A, was selected. A workpiece, AISI 1020 steel, 0.051 m (2 in.) diameter, 0.302 m (13 in.) long was selected and held between the chuck and a running center. An electromagnetic shaker, type B & K - 4812 with a specification of maximum force of 44.5 N (100 lb_f) and displacement limit of 0.013 m (0.5 in.) was selected to provide sinusoidal force excitation to the spindle-workpiece system through a push rod. A schematic diagram of the experimental set-up is shown in Figure 4. A pictorial view of the actual instrumentation and the workpiece-shaker system is shown in Figures 5(a), and 5(b) respectively.

An accelerometer, B & K - 8302, having a sensitivity of 10 pc/g was mounted to the chuck. The output signal of the accelerometer was conditioned using a charge amplifier B & K 2626 and then amplified by a Kistler 504E voltage amplifier. The amplified signal was plotted on a H.P. 7004-B x-y plotter, and at the same time it was recorded on B & K 7000, 4 channel tape recorder. An oscilloscope, Tektronic Model 201-2 was also used to observe the signal which was being recorded. One end of a Kistler 931A force transducer was screwed on to the push rod of the exciter, and the other end of the force transducer was rigidly connected to the workpiece. The output signal from the force transducer was conditioned and connected to the shaker exciter control in order to maintain a constant excitation force. The exciter was statically loaded at first, and then the spindle-workpiece system was excited within the range of 25 Hz to 1500 Hz with a constant dynamic force of 44.5N (100 lb_f), and at a sweep rate of 1000 Hz/minute.

RESULTS AND DISCUSSION

The finite-element analysis of the spindle-workpiece system outlined in equation (6) was solved for free vibration using a CDC Cyber 174 with zero damping. The parameters used in the analysis are shown in Table 1. The theoretically calculated values of the undamped natural frequencies for both types of end condition for the running center are listed together with the experimentally obtained values in Table 2. These results are also plotted in Figure 6. The variation of the first five natural frequencies as a function of bearing stiffness is shown in Figure 7. Figures (8) to (12) show the first five undamped mode shapes.

Since the electro-dynamic shaker has a low frequency limitation (i.e. to maintain a constant force in the low frequency region, the exciter displacement will exceed the maximum allowable limit), the first two natural frequencies were not detected experimentally. Referring to Table 2, theoretically calculated values of the undamped natural frequencies for hinged and clamped support conditions lie in the close proximity of the experimentally obtained values. Based on a comparison of the percentage error in the first five natural frequencies, the hinged condition has an error of less than 8% in comparison to the clamped condition which as a maximum error of 20%. Considering the twelve theoretically calculated natural frequencies, the calculation of the root sum squared (RSS) error for hinged and clamped conditions also show that the hinged condition has an error of 3.3% less than the clamped condition. Based on this, it is possible to conclude that the hinged support at the running center for a spindle-workpiece system is a better representation of the actual system. This indicates that there is a significant resistance to bending moment at the running center.

In order to study the influence of bearing stiffness on the free vibration of the spindle-workpiece system, the finite-element analysis was repeated for variations in the front end bearing stiffness, keeping the stiffness ratio of the two bearings a constant. The results are illustrated in Figure (7) which indicate that

the first natural frequency increases rapidly at first and then reaches a constant value for values higher than 4 times the original stiffnes.

The second, the third, and the fourth natural frequencies are quite sensitive to the change in the stiffness of the bearings. They show quite a large change due to the variation of the bearing stiffness. On the other hand, the fifth natural frequency remains almost unaltered due to the change in the bearing stiffness.

The undamped mode shapes can be best understood by referring to the Figures 2(a), 3(b), 6, 7 and any particular mode shape such as Figure 8. In the free vibration of the spindle-workpiece system under consideration, there is an interaction between the inertia forces, the spring forces of the bearings, and the flexural rigidity of the system. The deflection of any section is governed by the above mentioned forces. For the mode shapes as shown in Figure 8, the hinged end is on the right and the free end is on the left. In the first mode, for low values of front bearing stiffness, there is considerable bending in the workpiece due to its slenderness, and at the same time the spindle remains unbent. This results in the large deflection at the free end. The spring forces due to the bearings are not large enough to introduce any bending in the spindle which has considerable flexural stiffness. However, as the bearing stiffness is increased, the deflections at the bearing locations decrease, and consequently there is bending in the spindle. This results due to the fact that the natural frequency increases with the increase in bearing stiffness. Also in the first mode, due to large inertia forces at the chuck, the deflection at the front bearing is larger as compared to the rear-bearing even though the front bearing is 3.19 times stiffer than the rear bearing. Referring to the first mode it can also be seen that increasing the stiffness of the bearings increases the deflection in the workpiece and has little variation in the mode shape for large stiffness values. Based on these results, it should be noted that the selection of bearing stiffness based on the first mode is not straight forward.

Figures 9, 10, and 11 show the second, the third and the fourth mode shapes and have considerable change in the mode shapes due to variation of the bearing stiffness. The explanation of this can be detected from Figure 7, where one can see that the corresponding natural frequencies undergo large variation as the bearing stiffness changes. As a consequence, there would be a larger change in the inertia forces. Since the system has complex distribution of the stiffness along its length, the interacting forces result in the complicated mode shapes which are quite sensitive to any change in the bearing stiffness.

It can be seen that for second, third and fourth modes as the front end bearing stiffness increases, the maximum deflection of the workpiece increases initially and then decreases with the minimum value of the peak deflection occurring in the fourth mode. Comparing the deflection at the bearing locations, the amplitude increases and then decreases for the third and fourth modes at front end bearing while for the second mode, the deflection decreases initially and then increases. Increasing the stiffness of the rear end bearing, increases the deflection in the third and fourth modes, but the second mode, the deflection increases initially and then decreases.

The fifth mode which is shown in the Figure 12 is almost insensitive to changes in the bearing stiffness. This is due to the fact that the fifth natural frequency is almost not influenced by any change in the bearing stiffness. Therefore, the inertial forces do not change very much.

CONCLUSIONS

This paper presents the dynamic behavior of the lathe spindles with elastic supports including damping by finite element analysis. The equation of motion representing the spindle-workpiece system is characterized by a fourth order partial differential equation with its associated boundary conditions. A finite element analysis using cylindrical (shaft) elements are used in conjunction with the modal analysis to compute the undamped mode shapes and the natural frequencies of the spindle-workpiece system. The workpiece support at the running center has been modelled as hinged or fixed support and the theoretical results were compared with the laboratory experiments to classify the nature of the support condition. The effect of varying the spindle-bearing stiffness on the natural frequencies and modes shapes are also presented.

Based on this investigation, the following conclusion can be drawn:

1. A conceptional model of the spindle-workpiece system is developed which utilizes finite element and the modal analysis techniques.

2. The end condition of the workpiece supported by the running center can be better represented by hinged condition as compared to the clamped condition.

3. The first natural frequency is sensitive to any changes in the low bearing stiffness at the lower range but reaches a constant value at the higher bearing stiffness range.

4. The second, the third, and the fourth natural frequencies are very sensitive to any changes in the bearing stiffness.

5. The fifth natural frequency is insensitive to any changes in the bearing stiffness.

REFERENCES

1. Maragos, S.K., "Measurement and Modeling of Cutting Force Fluctuations During Machining", M.Eng. Thesis, 1973, Sir George Williams University, Montreal, Quebec, Canada.

2. Tobias, S.A., "Machine Tool Vibration", Blackie & Son Ltd., Glasgow, U.K., 1965, p. 245.

3. Tobias, S.A., and Fishwick, W., "Theory of Regenerative Machine Tool Chatter", Engineer, London, Vol. 205, 1958, p. 199.

4. Cook, N.H., "Self-Excited Vibrations in Metal Cutting", Journal of Engineering for Industry, Trans. of the A.S.M.E., Series B, Vol. 81, 1959, p. 183.

5. Gurney, J.P. and Tobias, S.A., "A Graphical Analysis of Regenerative Machine Tool Instability", Journal of Engineering for Industry, Trans. of the ASME, Vol. 84, No. 1, 1962, p. 103.

6. Allemang, R.J., Thomas Graef, H., and Powell, C.D., "Dynamic Characteristics of Rotating and Nonrotating Machine Tool Spindles", a paper presented at the Design Engineering Technical Conference, Cincinnati, Ohio, September 9-12, 1973.

7. Bollinger, J.G., and Geiger, G., "Analysis of the Static and Dynamic Behavior of Lathe Spindles", Int. J. Mach. Tool Des. Res., Vol. 3, 1964, pp. 193-209.

8. Thomson, W.T., "Theory of Vibration with Applications", Prentice-Hall, Inc., Englewood Cliffs, N.J., U.S.A., 1972, p. 272.

9. Meirovitch, L., "Elements of Vibration Analysis", McGraw-Hill Book Company, New York, U.S.A., 1975, p. 311.

10. Meirovitch, L., "Analytical Methods in Vibrations", The Macmillan Collier-Macmillan Canada Ltd., Toronto, Ontario, 1969, p. 410.

NOMENCLATURE

$[\ ]$	Matrix
$\dot{}$	Differentiation with respect to time
E	Modulus of elasticity
I	Diametral moment of inertia
L	Total length of the spindle-workpiece system
U	Global displacement coordinate.
$[m],[k],[c]$	Mass, stiffness, and damping matrices respectively
c	Damping at the bearings
f_{ext}	Externally applied force
k	Stiffness of the bearings
ℓ	Element, length
m	Mass per unit length
t	Time
w	Joint displacement coordinate
x	Global displacement coordinate along spindle-workpiece system
x_1	Local displacement coordinate along spindle-workpiece system
y	Displacement in the local coordinate
ϕ	Shape function

TABLE 1
Parameter Values of Spindle-Workpiece System

PARAMETERS	VALUES OF THE PARAMETERS
Modulus of Elasticity	(30 x 10^6 lbs/inch) 206.456 x 10^9 N/m
Mass of the Chuck	(75 lbs) 33.975 kg.
Diameter of the Chuck	(10") 0.254 m
Stiffness of the Front Bearing	(8.74 x 10^6 lbs/inch) 1514 x 10^6 N/m
Stiffness of the Rear Bearing	(2.741 x 10^6 lbs/inch) 474.81 x 10^6 N/m

TABLE 2
Undamped Natural Frequencies of the System

Freq. Number	Finite-Element Analysis		Experimental Hz	% Error = (F.E. Analysis-Exp)x100 / Exp	
	Hinged Support, Hz	Clamped Support, Hz		Hinged Support	Clamped Support
1	20	28	-	-	-
2	30	31	-	-	-
3	55	72	58	5.2	17.2
4	83	91	77	7.8	15.4
5	178	210	175	1.7	20.0
6	234	246	275	14.9	10.5
7	377	424	425	11.2	0.23
8	455	471	465	2.1	1.3
9	659	726	545	20.9	33.2
10	772	780	985	21.6	20.8
11	1082	1150	1075	0.3	7.0
12	1178	1352	1295	9.03	3.3

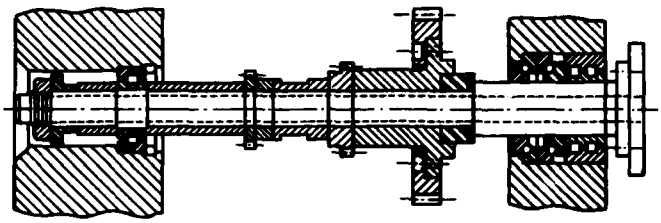

Fig. 1a: Lathe spindle system.

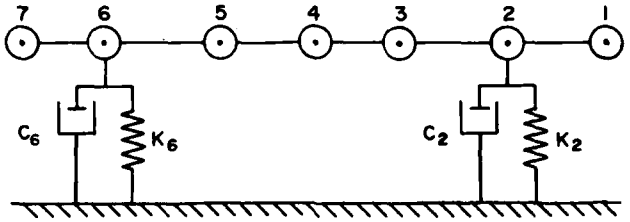

Fig. 1b: Discretized 7-mass spindle system.

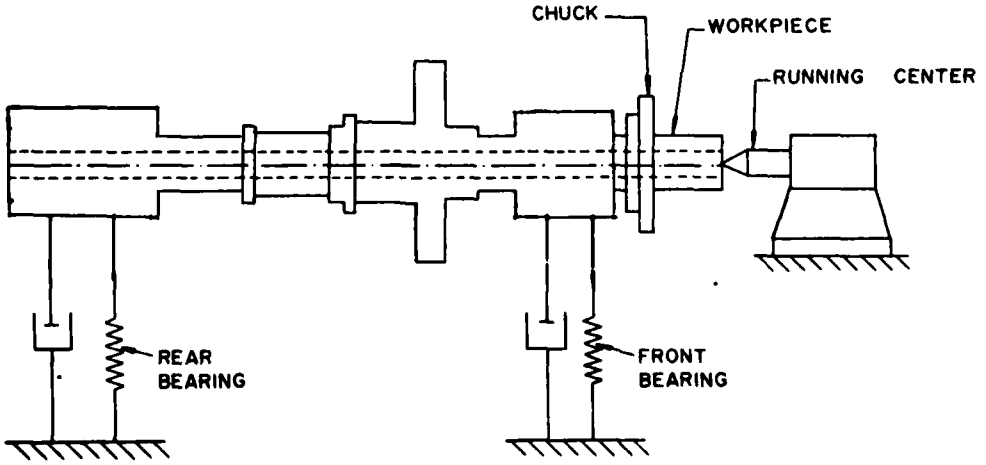

Fig. 2a: 12-mass spindle-workpiece system.

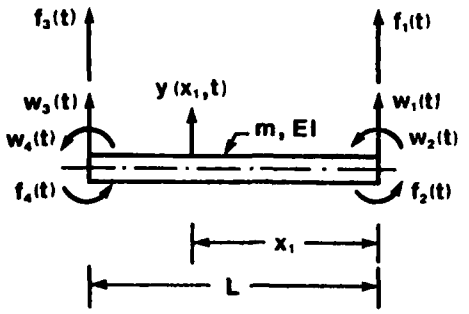

Fig. 2b: Finite element model of one of the elements of the system.

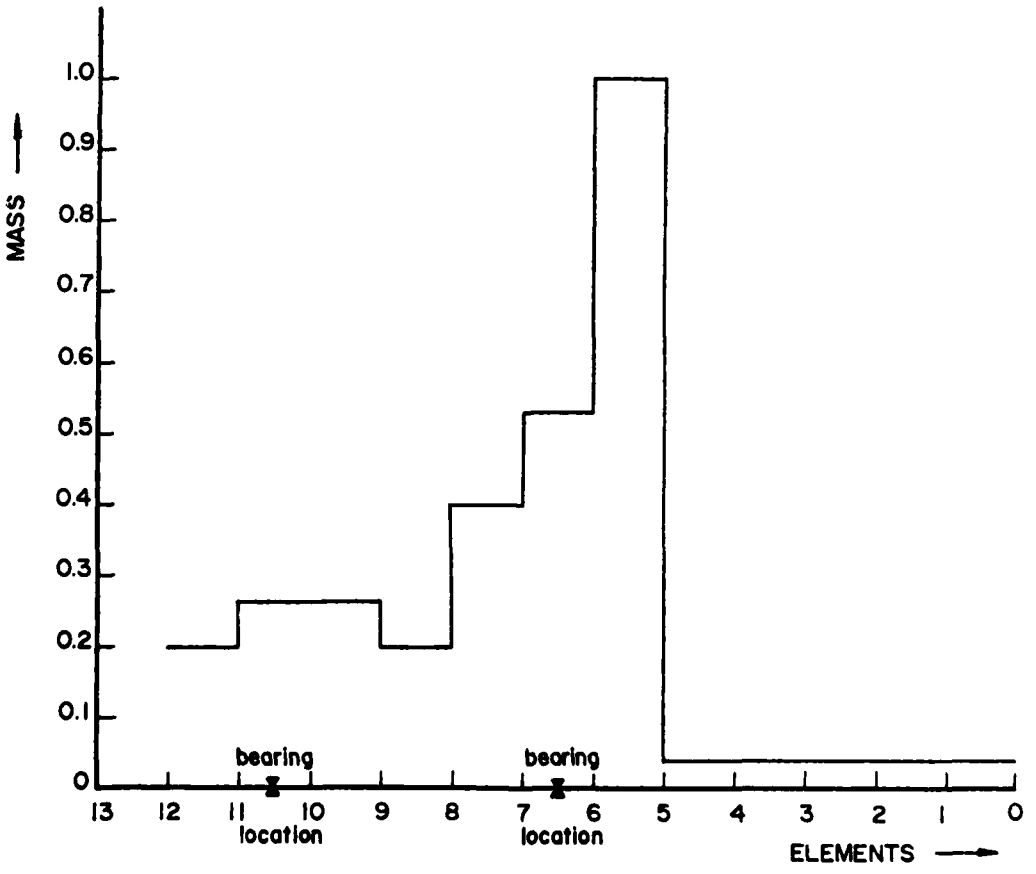

Fig. 3a: Normalized mass distribution of the spindle-workpiece system.

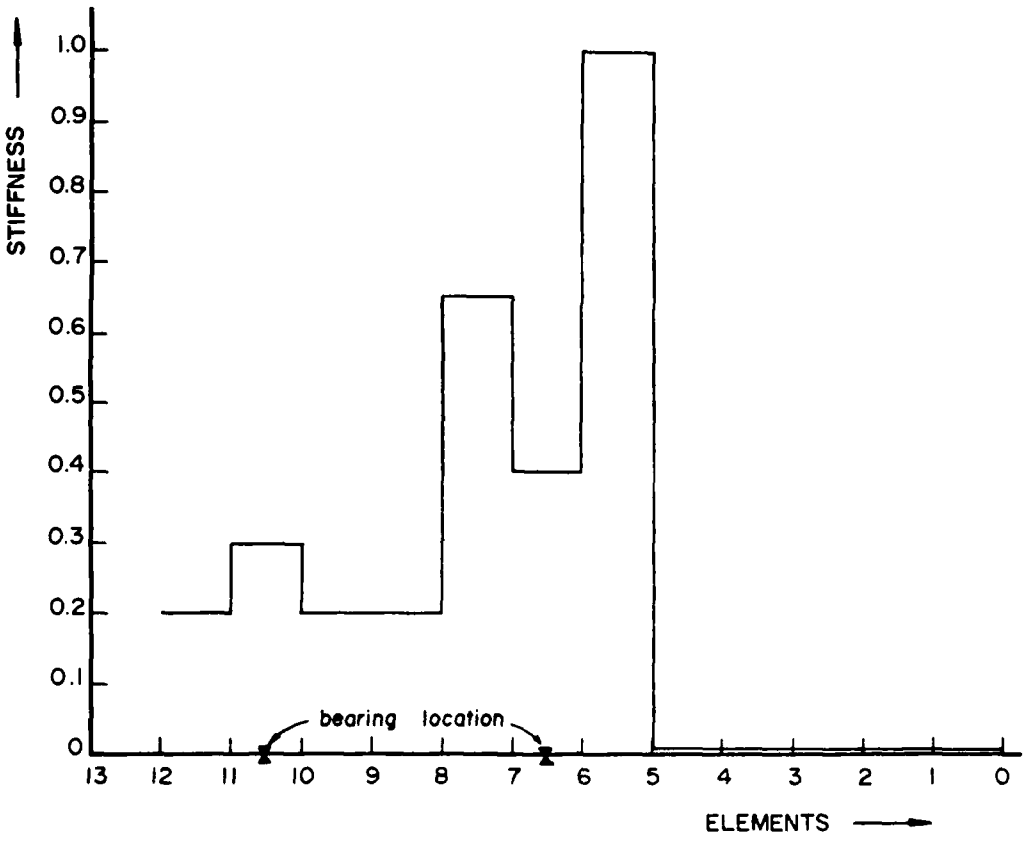

Fig. 3b: Normalized stiffness distribution of the spindle-workpiece system.

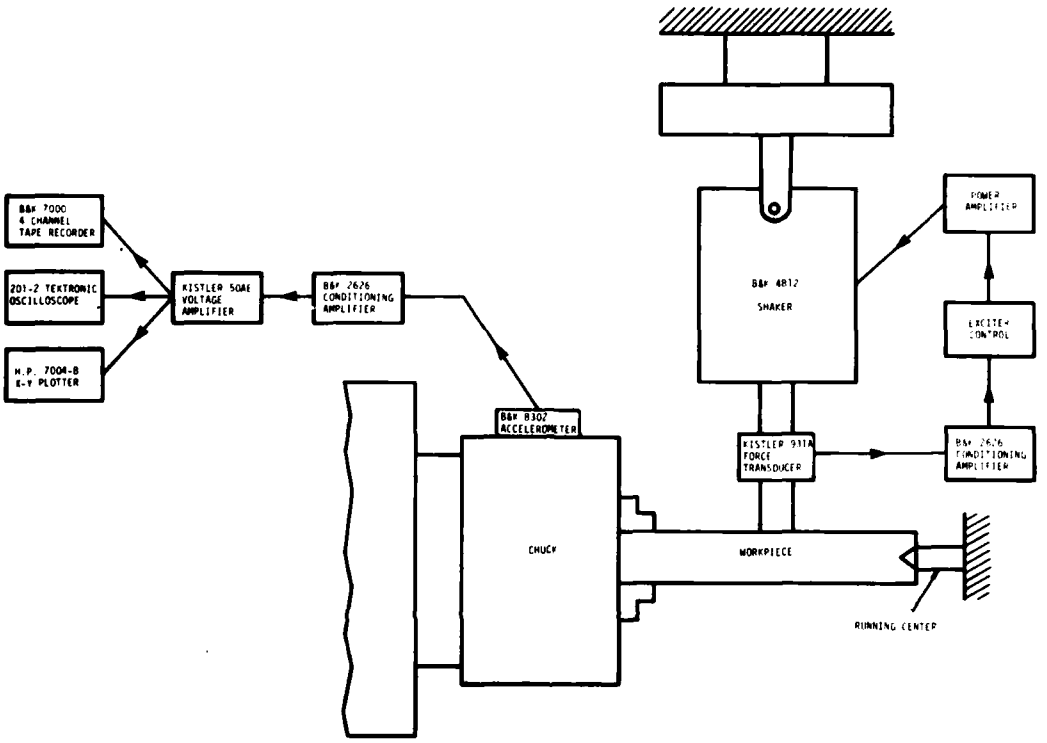

Fig. 4: Schematic diagram for the experimental set-up.

Fig. 5a: Pictorial view of the instrumentation for frequency analysis.

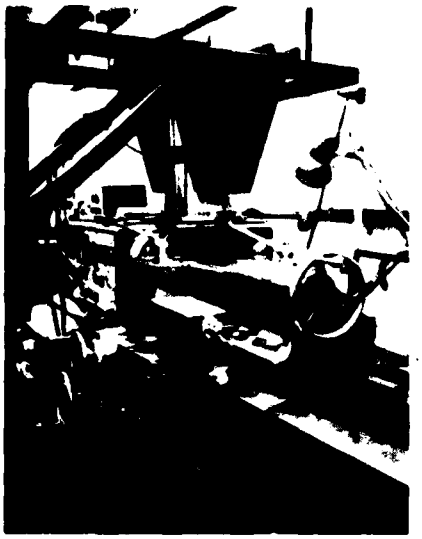

Fig. 5b: Pictorial view of the shaker, work-piece for frequency analysis.

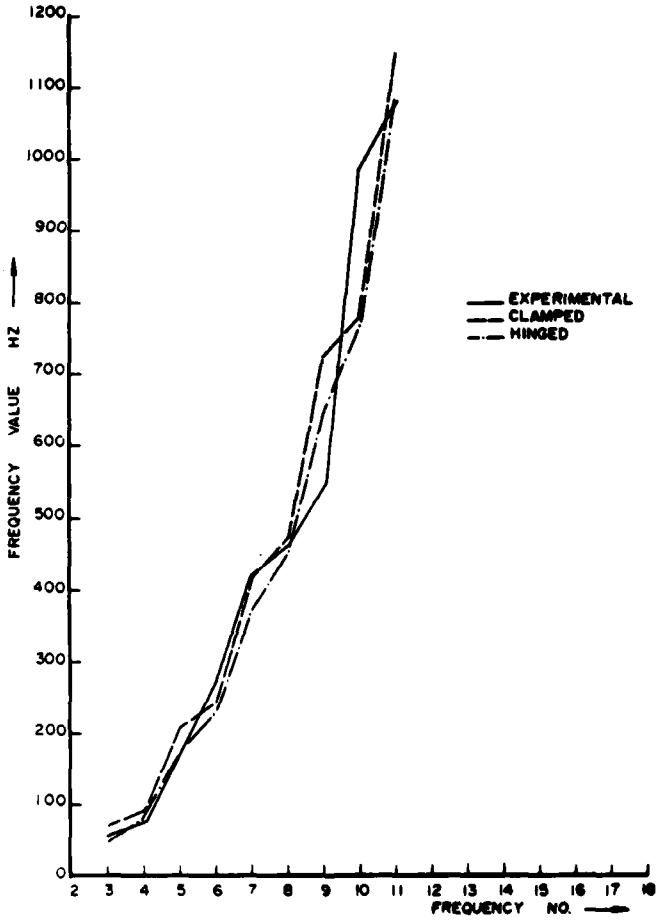

Fig. 6: Hinged, clamped experimental frequency versus frequency number.

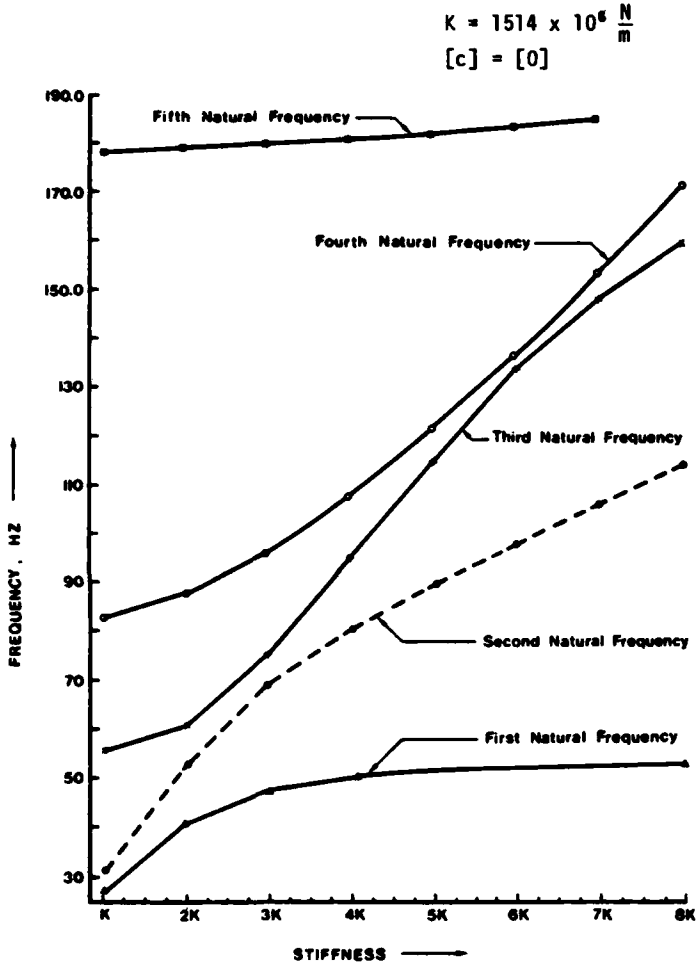

Fig. 7: First five natural frequency versus front bearing stiffness.

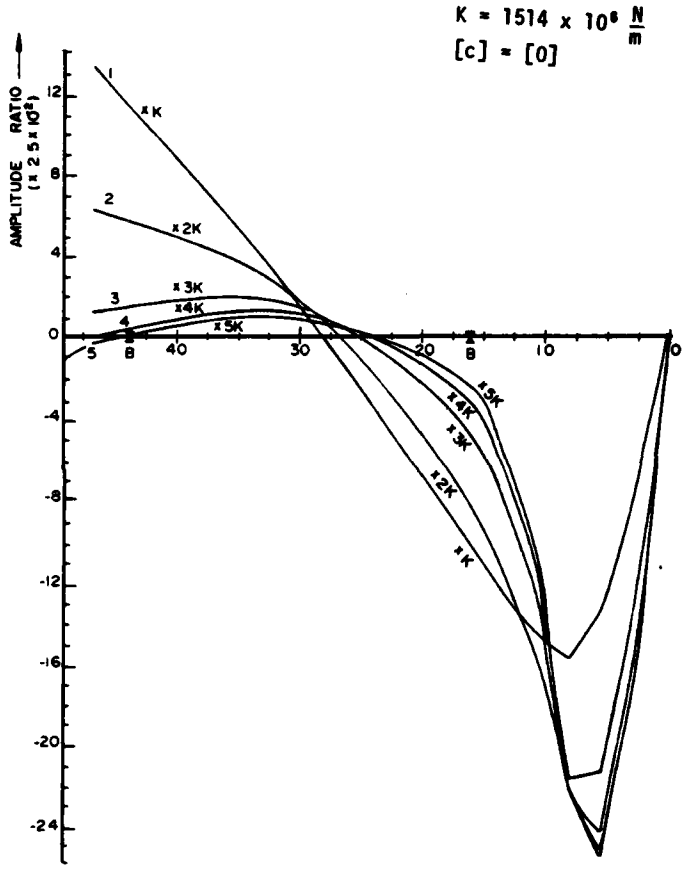

Fig. 8: First mode shape versus front bearing stiffness.

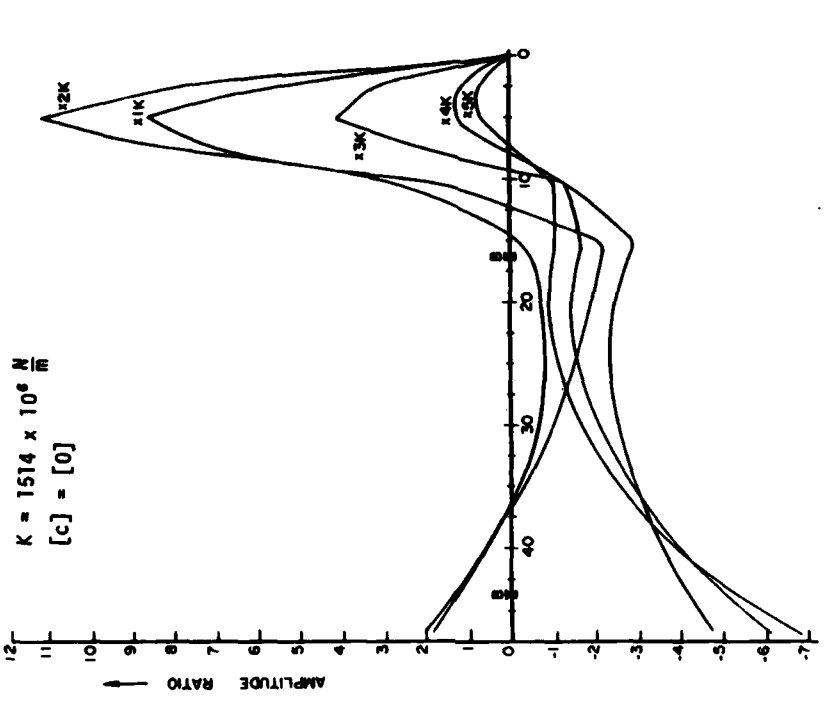

Fig. 10: Third mode shape versus front bearing stiffness.

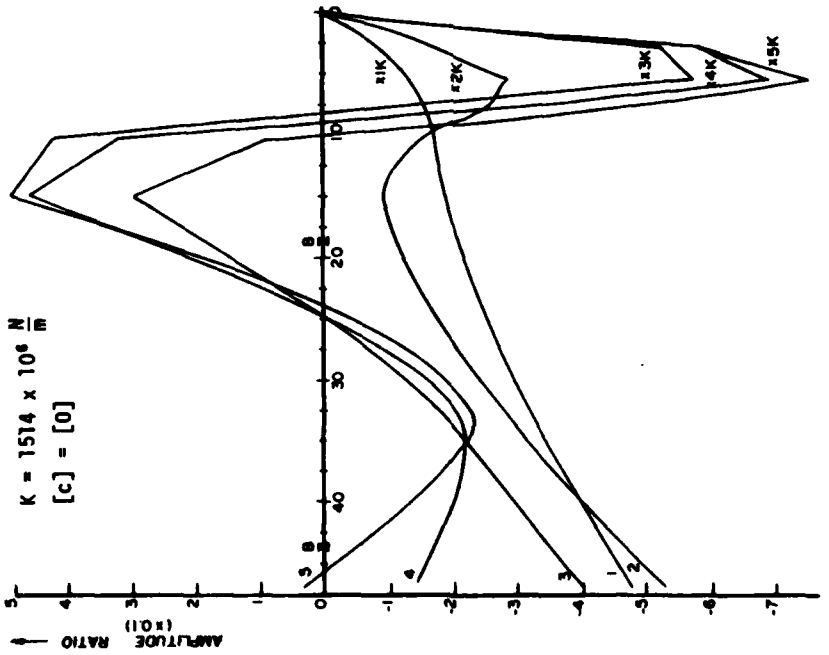

Fig. 9: Second mode shape versus front bearing stiffness.

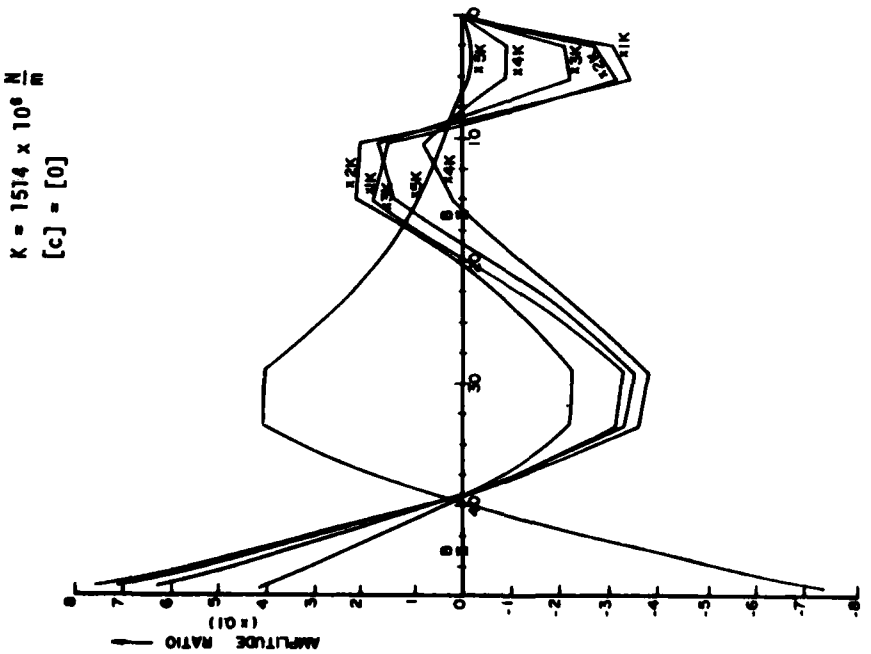

Fig. 11: Fourth mode shape versus front bearing stiffness.

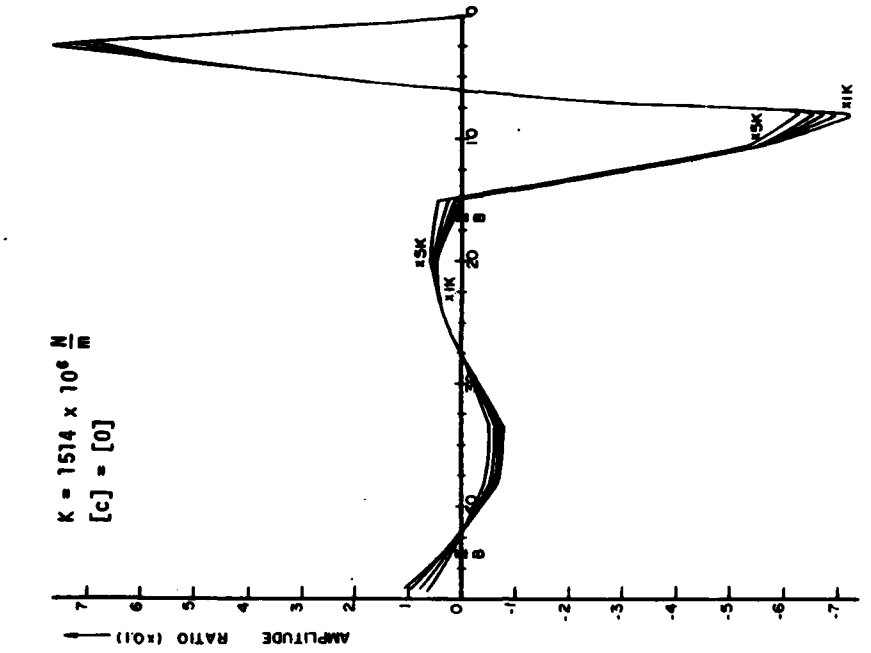

Fig. 12: Fifth mode shape versus front bearing stiffness.

FINITE ELEMENT ANALYSIS OF VISCOELASTICALLY DAMPED SANDWICH STRUCTURES

M. L. Soni
University of Dayton Research Institute
Dayton, Ohio

This paper addresses the problem of finite element modeling of the sandwich type structures typical of constrained layer damping designs. Existing modeling techniques are examined and a new finite element program with improved modeling capabilities is described. The new program is applied to the frequency domain vibration analysis of viscoelastically damped sandwich structures. Damped resonance frequencies and modal loss-factors are obtained from the direct solution of complex structural equations of motion. Modal loss-factors are also calculated from the energy weighted loss-factors of components. Damped deflection shapes rather than classical normal modes are used for this purpose. The application of the developed program is demonstrated in two typical damping analyses.

INTRODUCTION

The application of surface damping treatments consisting of one or more layers of energy absorbing viscoelastic material is a common device for reducing vibration-induced stress and displacement amplitudes in many aerospace structures [1]. Due to the wide variety of possible damping treatment designs, reliable methods for the analytical determination of resonant frequencies and overall damping properties of the resulting structure are required to determine the most effective damping treatment.

Methods of elastic analysis together with the closed form solution techniques have been in use in the layered damping analysis for over two decades. A review of the literature on this subject is given in [2]. These analytical models are applied within the restrictions of a particular set of layered geometry, boundary conditions and assumed modes of deformation; and intractable difficulties are encountered when extended to multilayer treatments, complex geometries and boundary conditions. The method of finite element analysis has been successfully employed in solving boundary and initial value problems from diverse areas of mechanics. However, its application in damping analysis is relatively recent [3,4,5,6] and as such some problems particular to damping analysis have not received enough attention.

Figure 1 shows some typical sandwich constructions encountered in constrained layer damping design. In each case the relatively soft viscoelastic material (called the core) is sandwiched between thin, high modulus constraining layers (the face sheets). Direct stresses are resisted primarily by the face sheets while the core layer separates the faces and acts primarily in transverse shear. Typically, shell elements are used to discretize the constraining layers and either solid or shear panel elements are used to discretize viscoelastic layers [7,8]. The shell elements available im most programs utilize translation as well as rotations as nodal degrees of freedom whereas the solid or shear panel elements employ translation alone as the nodal degrees of freedom. Furthermore, the shell element represents the midsurface of the structure (layer) it is used to model, the thickness is treated as constant and edges are

Viscoelastic Core and
Branched Shell Structure

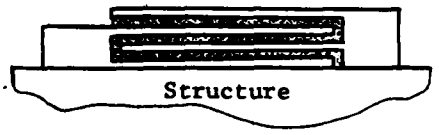

Multilayer Anchored Treatment

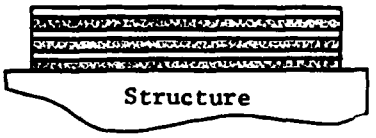

Multiple Constrained Layer

Multilayer Spaced Treatment

Fig. 1 - Typical Sandwich Constructions in Constrained Layer Damping Treatment.

required to be normal to the midsurface. Difficulties in modeling geometry and boundary conditions are encountered when one attempts to use these elements to discretize the sandwich structures such as those shown in the figure. Enforcement of displacement compatibility at shell-solid interfaces requires the use of linear constraints between the shell displacements and rotations and the pure translational degrees of freedom of solid elements. This is a tedious and error prone process. For branched shell structures shown in the figure enforcement of displacement constraints produces rigid links at sharp discontinuities in the surface shape leading to artificially stiff solutions. Furthermore, due to the two dimensional nature of these shell elements the treatment of sandwich damping designs requires the use of offsetting the shell element from the grid points of adjoining solid elements. For multilayer damping designs this may be unduly cumbersome.

This paper describes the formulation of the forced damped vibration problem and its finite element implementation. A finite element library with improved geometric modeling capabilities developed for general nonlinear transient stress analysis in [9,10] is used in the finite element implementation of the present formulation. Next, a method is described for calculating modal damping using the forced damped response, followed by a description of two sample damping analyses demonstrating the application of the developed program.

FORMULATION

The formulation is based on the virtual work equation

$$\int_V (\sigma_{ij}\delta e_{ij} + \rho u_i \delta u_i)dv = \int_V \bar{b}_i \delta u_i dv + \int_{\partial V} \bar{f}_i \delta u_i dA \qquad (1)$$

where σ_{ij}, e_{ij} and u_i are respectively the stress, strain, and displacement at a point within the body V of the viscoelastic structure with surface ∂V, and $\bar{b}_i$ and $\bar{f}_i$ are prescribed body and surface forces, respectively. For the steady state dynamic equilibrium of the body undergoing time harmonic motion,

$$\begin{aligned} \bar{f}_i &= F_j \exp(i\omega t) \\ u_j &= U_j \exp(i\omega t) \\ e_{jk} &= \varepsilon_{kj} \exp(i\omega t) \\ \sigma_{jk} &= S_{jk} \exp(i\omega t) \end{aligned} \qquad (2)$$

where $i = \sqrt{-1}$ and ω is the vibration frequency. The multipliers of the exponential functions in Equation 2 are the peak amplitudes and are in general complex quantities. The viscoelastic

damping behavior is accounted for through the stress-strain law

$$\underline{S} = (\underline{\underline{E}}^R + i\,\underline{\underline{E}}^I)\,\underline{\varepsilon} \qquad (3)$$

where $\underline{\underline{E}}^R$ and $\underline{\underline{E}}^I$ respectively are the tensors characterizing energy storage and dissipative behavior of the material. In the present work the above equality is specialized to that for the material with proportional damping, thus replacing $\underline{\underline{E}}^I$ by $\eta(\omega,t)\underline{\underline{E}}^R$, where η is the material loss-factor, a function of both the vibration frequency ω and the temperature T. The loss-factor is assumed to be the same in both dilatation and shear. The case of distinct dilatational and shear loss-factor, and also that of nonproportional damping, can be introduced through appropriate $\underline{\underline{E}}^I$ without sacrificing the computational advantages of the above stress-strain law.

Combining Equations 1, 2 and 3, we obtain

$$\int_V (E_{ijk\ell}\varepsilon_{k\ell}\delta\varepsilon^*_{k\ell} - \rho\omega^2 u_i\, U_i^*)dV = \int_{\partial V} F_j \delta U_j^* dA \qquad (4)$$

where $E_{ijk\ell}$ represents the complex modulus tensor of Equation 3, and the asterisk denotes complex conjugation.

The general procedure for formulating finite element equations from the virtual work principle is well known and is only briefly described here. The finite element formulation used here seeks to find the displacement field U_i such that it satisfies the displacement constraints imposed on the boundaries of the structure and satisfies the above virtual work equality. The finite element equations are obtained by discretizing the domain V into elements and approximating the displacement distribution within each element. For arbitrary values of virtual displacements, this procedure then leads to a complex set of linear algebraic equations of the form

$$[\underline{\underline{K}} - \omega^2\underline{\underline{M}}]\tilde{\underline{U}} = \tilde{\underline{F}} \qquad (5)$$

where, $\underline{\underline{K}}$ is the complex structural stiffness matrix, $\underline{\underline{M}}$ is the mass matrix, $\tilde{\underline{U}}$ is the vector of complex nodal displacements and $\underline{F}$ is the vector of nodal forces.

The complex structural stiffness matrix $\underline{\underline{K}}$ is obtained by summing up the individual element stiffness matrices, i.e.,

$$\underline{\underline{K}} = \underline{\underline{K}}^R + i\underline{\underline{K}}^I$$

and

$$\underline{\underline{K}}^R = \sum_{e=1}^{n} \Lambda^T \underline{\underline{K}}^e \Lambda$$

$$\underline{\underline{K}}^I = \sum_{e=1}^{n} \Lambda^T (\eta^e \underline{\underline{K}}^e) \Lambda$$

Similarly,

$$\underline{\underline{M}} = \sum_{e=1}^{n} \Lambda^T \underline{\underline{M}}^e \Lambda$$

where $\underline{\underline{K}}^e$ is the element stiffness matrix, n is the number of elements, Λ is a matrix defined from element nodal connectivities, η^e is the element material loss-factor, and $\underline{\underline{M}}^e$ is the element mass matrix. For a typical element with the shape function matrix $\underline{N}$ and the strain-displacement relation matrix $\underline{\underline{D}}$, the element matrices are of the form

$$\underline{\underline{K}}^e = \int_{V_e} \underline{\underline{D}}^T \underline{\underline{E}}^R \underline{\underline{D}} dV$$

and

$$\underline{\underline{M}}^e = \int_{V_e} \rho \underline{N}^T \underline{N} dV$$

where ρ is the material density and V_e represents the volume of the element. The above procedure allows the formulation of response problems where all or part of the structure is damped. The frequency dependence of material properties is implemented in the program through user supplied frequency versus material property tables or appropriate equations. The details of the derivation of various matrices are given in [11], wherein a general case of viscoelastic structures vibrating about an initially stressed state such as that due to rotation is considered.

Equation 5 yields the complex eigenvalue problem of damped vibrations by setting the nodal force vector to zero. In this paper the complex eigenvalue problem is not solved. Instead, the damped resonant frequencies and

corresponding modal damping factors are obtained by solving Equation 5 for a number of frequencies at constant magnitude of excitation force. The loss-factors of the built-up structure are also obtained as the weighted sum of the loss factors of the individual components (elements), the weighting factors being the energy stored in each of the components, i.e,

$$\eta_{si} = \frac{\sum_{j}^{n} \eta_j \, W_{jmax}^{(i)}}{\sum_{j}^{n} W_{jmax}^{(i)}} \qquad (6)$$

where η_{si} is the structure loss-factor, η_j is the material loss-factor of element j and $W_{jmax}^{(i)}$ is the peak elastic strain energy of element j in the i^{th} mode. In the calculation of $W_{jmax}^{(i)}$, the damped deflection shapes are used rather than the undamped normal modes used in [7] and [13].

MAGNA-D COMPUTER PROGRAM

The finite element program MAGNA-D has been specifically developed for steady-state dynamic analysis of large three-dimensional structures vibrating about initially stressed configuration. The program modules include static stress analysis, eigenvalue analysis and damped forced vibration analysis. The program uses out-of-core skyline matrix storage and factorization scheme. The eigenvalues are extracted using a simultaneous iteration method. The unique features of the program are its modular programming and element library. In the following the finite elements used in the discretization procedure are described.

FINITE ELEMENT LIBRARY

The finite elements currently implemented in the MAGNA-D vibration analysis program are:

1. Three-Dimensional, Isoparametric Solid with Variable Number of Nodes. This element is based upon a variable order of interpolation for both geometry and displacements and may contain from eight nodes (trilinear, eight-node brick) to 27 (triquadratic, 27 node brick). The nodal configuration for the element is shown in Figure 2. The vertex nodes (1 through 8) are the minimum number required to define the element geometry. Each of the nodes 9 through 27 are optional, to permit a great variety of local node patterns. The flexibility afforded by this element is particularly useful in constructing transitions between coarse and fine regions of finite element models. Typical uses of this element are in the modeling of solid continua, and thick to moderately thin shells.

2. Three-Dimensional, Isoparametric Eight-Node Brick. This element is a specially programmed version (for more efficient computations) of the variable-node solid element. Both the geometry and displacement field of an element are represented by trilinear polynomials. Nodal configuration of the element is shown in Figure 2. This element models simple states of stresses accurately and performs very well in layered sandwich constructions where the core layer acts primarily in transverse shear. The core

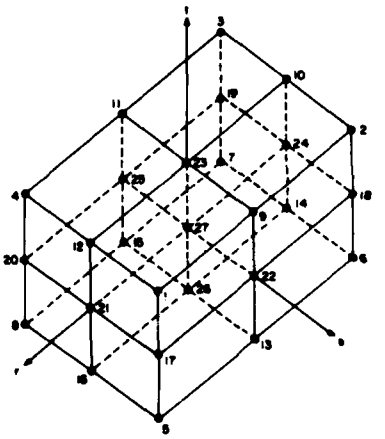

Variable Node Solid Element

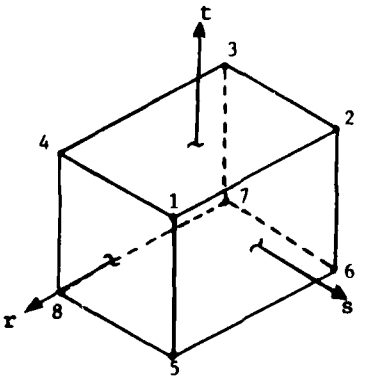

Eight-Node Solid Element

Fig. 2 - MAGNA-D Finite Element Library.

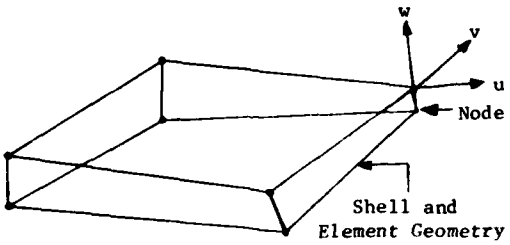

Penalty-Function-Based Shell Element

Fig. 2 - (concluded).

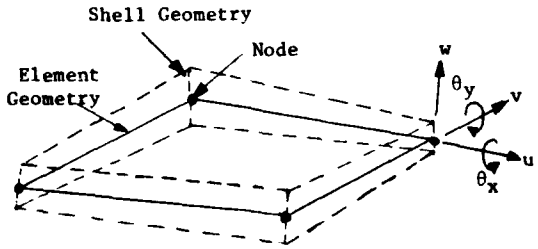

Fig. 3 - Conventional Shell Element

layer can be effectively modeled with this element using one point integration.

3. Isoparametric, Eight-Node Thin Shell Element. The eight-node thin shell element shown in Figure 2 is an isoparametric element similar in its geometry, nodal configuration and nodal variable definition to the eight-node brick element. The element has nodes at the upper and lower surfaces rather than at the shell midsurface. Each node point is permitted three nodal translation degrees of freedom. In the formulation of this element the constraints of transverse normal and shear beahvior of the Kirchoff shell theory are enforced through the use of penalty function. The details of the penalty function formulation and the development of the shell element are given in [9]. Briefly, a penalty function, which consists of terms appended to the usual element strain energy, associates a high level of strain energy with elements directly from three-dimensional elasticity theory, and thus permits the shell element to be based upon displacement degrees of freedom only. In contrast, in the formulation of conventional shell elements, the behavioral constraints of shell theory are introduced through the use of either additional unknowns as nodal rotational degrees of freedom or through the use of gradients of transverse displacements. Figure 3 shows a conventional shell element for comparison. The choice of nodal locations and the degrees of freedom make the penalty function shell element fully compatible on all exterior surfaces with other shells (of the penalty-function type) and with the conventional solid isoparametric elements. The shell element can be of variable thickness and the lateral boundaries of the element need not lie along the normal to the shell midsurface. Layered shells, sandwich constructions, transition between shells and solids or branched shells are thus easily modeled without special constraints.

All of these elements are fully compatible, isoparametric elements with arbitrary orientation in three-dimensional space. A unique feature of the element library is the exclusive use of nodal translations as external degree of freedom in all element types. With this convention, any two elements of different types having similar nodal configurations may be joined directly, providing complete compatibility of displacements of interelement boundaries. This com-

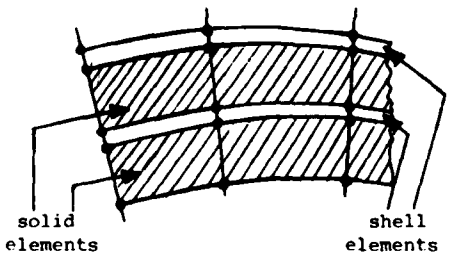

LAYERED/SANDWICH STRUCTURES

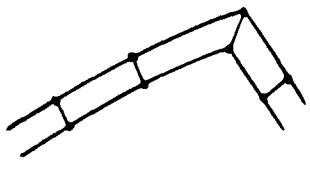

GENERAL SHELL JOINTS/BOUNDARIES

FULL COMPATIBILITY WITH SOLIDS

Fig. 4 - Typical Modeling Capabilities of MAGNA-D Element Library.

patibility provides a greater flexibility over the existing finite elements in the modeling of practical structures and eliminates the possibility of incorrect definition of constraints at element interfaces and the specification of artificial stiffness. Figure 4 shows some of the modeling capabilities of the above element library.

NUMERICAL EXAMPLES

Two sample applications of the finite element program developed are presented to demonstrate its accuracy and modeling capabilities.

1. Sandwich Cantilever Beam. The first case considered is that of a cantilever beam with constrained layer damping treatment. This problem has been studied extensively in various analyses and experiments [2]. The effect of shearing capability of the viscoelastic layer upon the damped frequency and loss-factor of the composite beam was first analyzed for infinite length beams in [12] using an effective stiffness method and the classical fourth order theory of elastic plates. In [13] energy approach was introduced to define the beam loss-factor. For finite length beams a sixth order theory was derived in [14], however, the loss-factor versus natural frequency behavior was shown to be independent of the boundary conditions. The theory has been further refined and solved for various boundary conditions in [15,16]. The problem has also been analyzed using various finite element programs [6,7,8,17]. More recently the sandwich beam has been used in damping characterization of polymeric materials [18].

The geometry and material properties of the beam shown in Figure 5 are those used in an actual test specimen [18]. Two different cases of damping layer materials are considered. In the first the damping layer is taken to be 3M-ISD468 adhesive with the frequency and temperature dependent material properties found in [18]; in the second case a hypothetical damping material with frequency-invariant material properties is used [7,17].

The base and the constraining layers are discretized using the eight-node thin shell elements and the solid element with eight corner nodes and reduced integration are used to model the damping layer; each layer employed 22 elements of respective type. A total of 184 nodes with 440 active degrees of freedom were used in the model. Damped

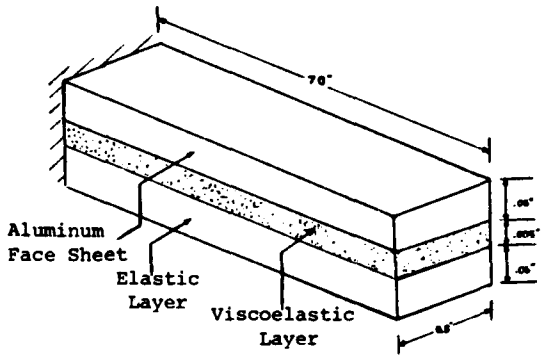

MATERIAL PROPERTIES

FACE SHEETS: $E = 10 \times 10^6$ psi
$\nu = 0.3$
$\rho = .1$ lbs/in^3

DAMPING LAYER:

(a) Constant Material Properties
$G = 100$ psi
$\rho = 0.035$ lbs/in^3
$\eta = 0.01, .1, .2, .3, .6, 1., 1.5$

(b) Material ISD 468 at 0°F

Fig. 5 - Cantilevered Beam with Constrained Layer Damping Treatment.

forced response is obtained using the complex stiffness method for the first six flexural modes of vibrations.

Figure 6 shows the amplitude-frequency response for the beam with ISD-468 as the damping layer material. The frequency dependent shear modulus and loss-factor for the material are obtained from the reduced temperature nomogram shown in Figure 7. The damped frequencies and corresponding modal loss factors obtained from the finite element analysis are compared to those of laboratory experiment in the following table.

TABLE I

Mode	Frequency (HZ)		Modal Loss Factor	
	FEA*	Experiment	FEA	Experiment
1	82.	-	.0049	-
2	505.	510.	.0101	.006
3	1394.	1402.	.0123	.009
4	2690.	2699.	.0148	.014
5	4375.	4380.	.017	.018

*FEA = Finite Element Analysis

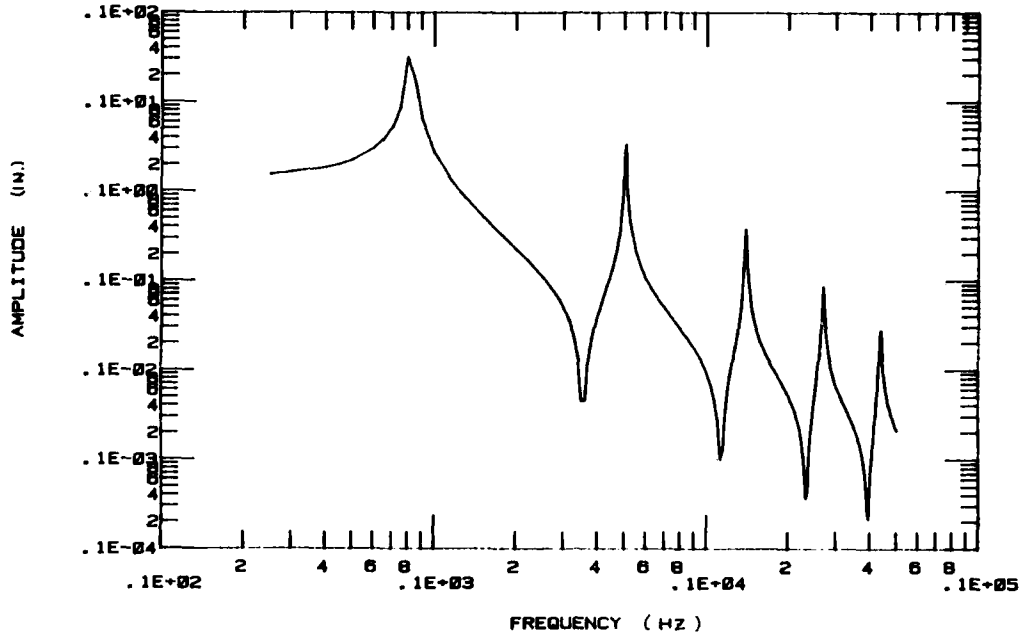

Fig. 6 - Frequency Response of Cantilevered Sandwich Beam with Constrained Layer Damping Treatment (Material ISD468).

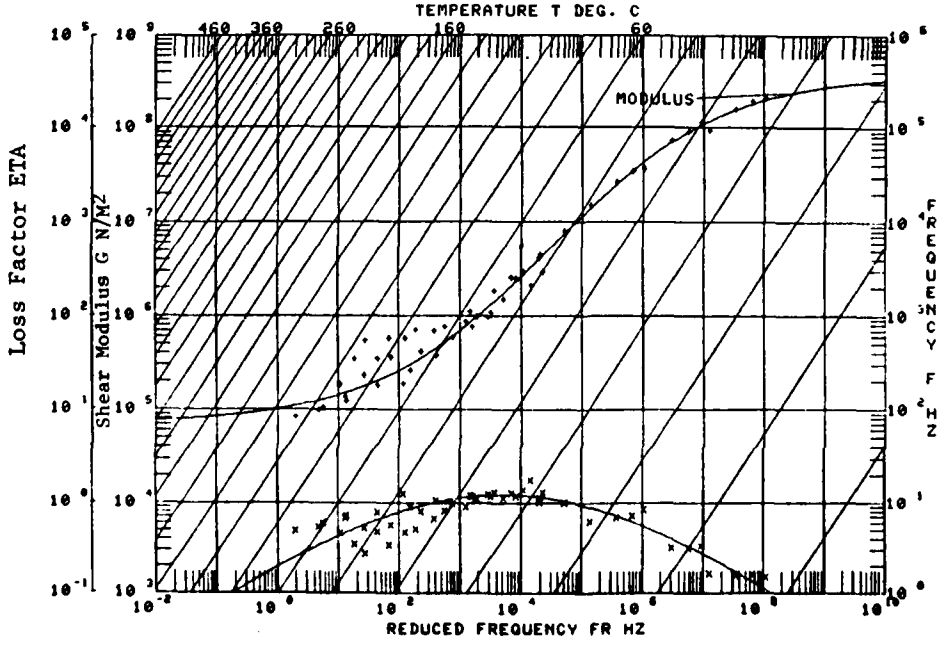

Fig. 7 - Reduced Temperature Nomogram for ISD468 Damping Material.

TABLE II

CORE LOSS-FACTOR AND MODAL PROPERTIES OF CANTILEVERED BEAM WITH CONSTRAINED LAYER DAMPING

η_2	Mode	1		2		3		4		5		6	
		ω	$\bar{\eta}$	ω	$\bar{\eta}$	ω	$\bar{\eta}$	ω	$\bar{\eta}$	ω	$\bar{\eta}$	ω	$\bar{\eta}$
.1	sixth order theory	64.075	.2815	296.41	.2424	743.7	.154	1393.9	.0889	2261.09	.0573	3343.6	.0390
	FEA	64.2	.285†	297.	.2424	747.2	.154	1408.3	.090	2304.	.0573	3446.1	.038
			.2817*		.2425		.1534		.0878		.0559		.0377
.2	sixth order theory	64.21	.2779	296.64	.2415	743.85	.154	1394.	.0888	2261.15	.0572	3343.6	.039
	FEA	64.4	.283	297.6	.2416	748.	.1537	1409.	.0889	2304.	.0562	3446.4	.038
			.2782		.2416		.1533		.0878		.0559		.0372
.3	sixth order theory	64.43	.2723	.297.01	.2399	744.1	.1538	1394.	.0888	2261.24	.0572	3343.7	.039
	FEA	64.7	.2750	298.	.2383	748.2	.1533	1409.5	.0882	2305.	.056	3447.	.038
			.2725		.2401		.1531		.0878		.056		.0372
.6	sixth order theory	65.48	.246	298.9	.2323	745.48	.1528	1394.9	.0886	2261.7	.0572	3344.	.0390
	FEA	65.5	.2487	301.	.227	753.	.149	1414.	.087	2310.	.0563	3450.	.0378
			.2462		.2326		.1521		.0876		.056		.0377
1.0	sixth order theory	67.41	.2022	302.8	.2177	748.6	.1502	1396.6	.0881	2262.88	.0570	3345.	.0389
	FEA	67.4	.1957	307.	.203	762.	.141	1422.	.086	2316.	.056	3455.	.0382
			.2019		.218		.15		.0873		.056		.0377
1.5	sixth order theory	69.88	.1531	308.85	.1975	75.4	.146	1399.7	.0873	2265.	.0568	3346.	.0389
	FEA	70.	.1555	315.	.1767	774	.132	1433.	.0826	2328.	.0553	3468.5	.0383
			.1522		.1952		.1457		.0868		.0559		.0378

η_2 = Core Loss Factor ω = Damped Resonance Frequency † Half Power Bandwidth Method

$\bar{\eta}$ = Loss Factor Parameter (= modal loss factor/core loss factor) * Strain Energy Method, Equation 6

The values of damped resonance frequencies are in excellent agreement and the modal loss-factor also compare well except at very low damping. This discrepancy may be attributed to the errors in the measurement. At very small damping the sharpness of the amplitude-frequency response curve makes it difficult to locate the half power bandwidth points. For further comparisons, the beam problem with frequency independent material properties is solved for various values of core loss-factor. The results are presented in Table II where the corresponding results of sixth order theory [17] are also shown. The two analyses are excellent agreement for the range of frequencies and core loss-factors considered.

The modal loss factors are obtained with good accuracy using the strain energy method Equation 6, whereas those obtained using the half-power bandwidth method are sometimes in error depending upon the accuracy of curve fit. For most practical values of the composite loss-factors, however, the ratio of energy (loss-factor parameter) stored in the damping layer to the energy stored in the entire structure is independent of the core loss-factor as seen in Figure 8 and, therefore, the procedure using undamped normal modes, obtained from the eigen-solution of the corresponding undamped system as suggested in [7] may be more economical to use. However, within the limitations of proportional damping, the method used in this paper to calculate modal damping, yields results consistent with the sixth order theory.

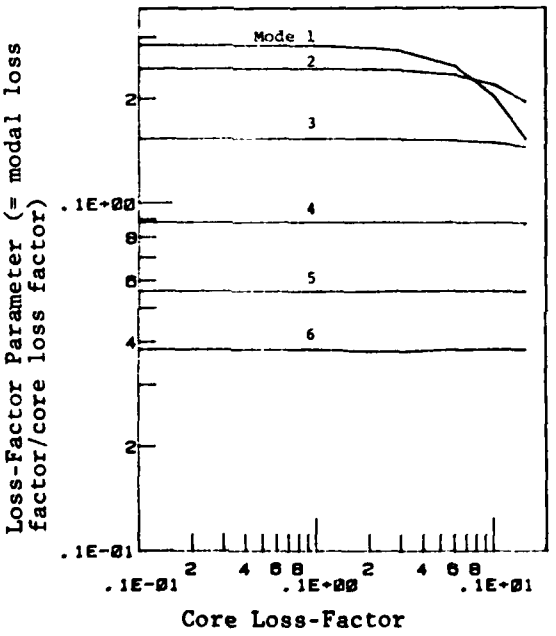

Fig. 8 - Loss Factor Parameter Versus Core Loss Factor Behavior of Sandwich Beam.

2. Enamel Coated Turbine Blade. This example illustrates the capability of the developed program to predict natural frequency and damping of a structure having complex geometry and anisotropic material properties. Figure 9 shows a jet engine turbine blade. High cycle fatigue in a high temperature and centrifugal force environment causes the blade to fail. The feasibility of using inorganic glass and vitreous enamel surface coatings to alleviate this problem is currently being studied [18]. In the following the preliminary results of the analysis of the damped nonrotating blade is presented and where available the comparison is made with experimental results. The finite element program described in this paper was used in the analysis [18].

The blade considered in this study has a sawtooth root, a rectangular extended hollow neck, a platform and a hollow airfoil. The pressure and suction sides of the airfoil are connected through 74 pins (.049 in.O.d). The blade is made from a directionally solidified nickel base alloy giving it anisotropic elastic properties. For this study, only the airfoil section of the blade is discretized and total displacement fixidity is imposed at the platform section. Instead of modeling each of the 72 pins connecting the two airfoil sections, a volume-average-effective-modulus approach is used to replace the bars with an equivalent homogeneous anisotropic elastic solid 'core' occupying the space between the airfoil sections. Surface coating of .01 inch thickness of glass enamel is used as a damping material, .005" inch thick layer of nickel is used in the constraining layer. Shell elements of the present program are used to model airfoil and the constraining layer whereas solid elements with reduced integration are used to model the core and damping layer. Figure 10 shows the finite element model. A total of 928 degrees of freedom were used in the model. The natural frequencies and damping factors obtained from amplitude-frequency response for the blade with and without constrained layer damping treatment at room temperature are shown in Table III. A value of .002 for

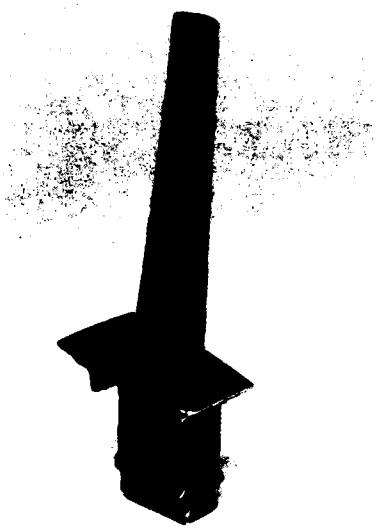

Fig. 9 - Directionally Solidified, Cooled Turbine Blade.

material loss-factor was used for all the materials involved.

Figure 11 shows the amplitude frequency response of the blade with enamel coating only (free layer treatment) taking into account the frequency and temperature sensitivity of the glass enamel. The response was obtained at three different temperatures shown in Figure 11. The material properties for the Corning glass 8463 used in the analysis were obtained from the reduced temperature nomogram shown in Figure 12. The frequency response shows maximum attenuation of resonant amplitudes and also the maximum modal loss factor for a temperature of 925°F for the frequency range under consideration. From Figure 12 it is also the temperature at which the loss-modulus (loss-factor times the Young modulus) is maximum. Analysis of the detailed model along with the effects of centrifugal forces will be presented at a later date.

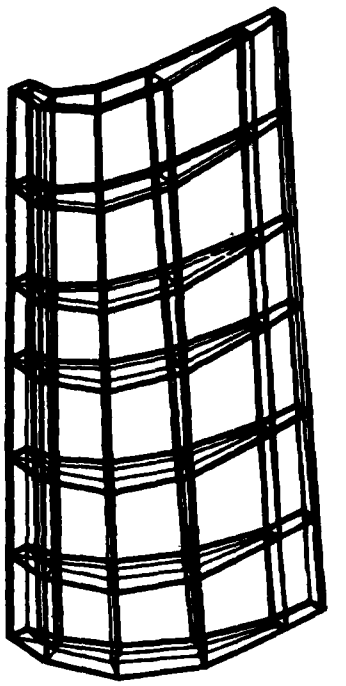

View From Convex Side

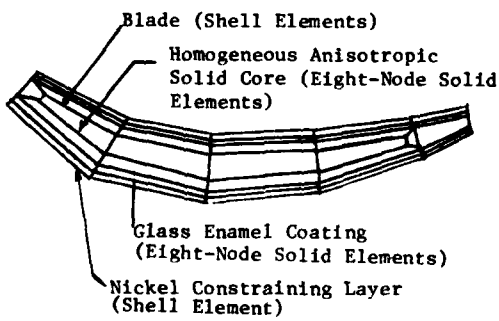

Cross Section

Fig. 10 - Finite Element Model of Blade (Airfoil) with Constrained Layer Damping Treatment.

TABLE III

	Bare Blade		Coated Blade	
	FEA	Experiment	FEA	Experiment
Frequency (HZ)	1085.4	1002.	1050.2	-
Modal Loss Factor	.002	.002-.004	.002	.002-.004

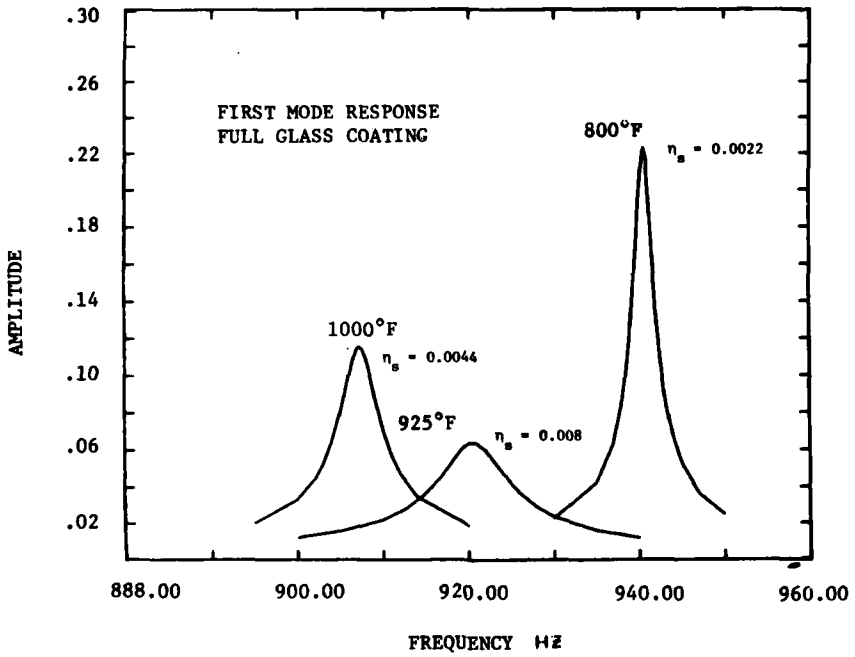

Fig. 11 - Amplitude Frequency Response of Glass Coated Blade at Three Different Temperatures.

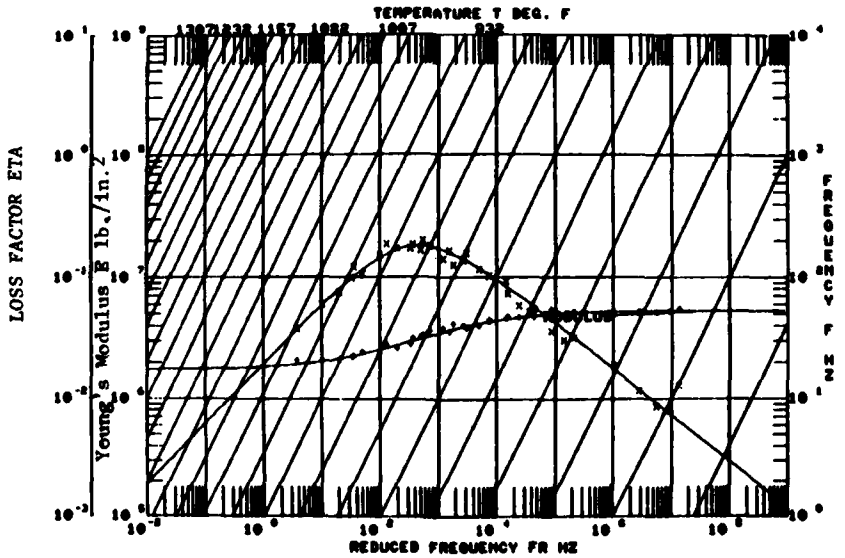

Fig. 12 - Reduced Temperature Nomogram for Corning glass 8463.

SUMMARY

In this paper the current modeling practices of layered damping analysis are reviewed. A finite element program, MAGNA-D with improved modeling capabilities for the damped forced harmonic response analysis of sandwich structures is presented and the accuracy and modeling capabilities of the developed program are illustrated.

ACKNOWLEDGEMENT

This work was supported in part by the Air Force Materials Laboratory and Air Force Flight Dynamics Laboratory.

REFERENCES

1. D.I.G. Jones, J.P. Henderson, L.C. Rogers, "Viscoelastic Damping in USAF Applications," in Damping Effects in Aerospace Structures, AGARD Conference Proceedings, No. 277, April 1979.

2. B.C. Nakra, "Vibration Control with Viscoelastic Materials," The Shock and Vibration Digest, Vol. 8 (6), 1975.

3. R. MacNeal (Ed), NASTRAN Theoretical Manual, MacNeal Schwendler Corporation, May 1974.

4. R.A. Brockman, "Finite Element Analysis of Forced Vibration in Viscoelastic Layered Panel Structures," UDR-TR-78-31, University of Dayton Research Institute, Dayton, Ohio, March 1978.

5. ANSYS Theoretical Manual, Swanson Analysis Systems, Inc., May 1978.

6. T. Carne, "Constrained Layer Damping Examined by Finite Element Analysis," Proceedings of the Society of Engineering Science, 12th Annual Meeting, Austin, Texas, October 1975, p. 567-576.

7. L.C. Rogers, C.D. Johnson, D.A. Keinholtz, "The Modal Strain Energy Finite Element Analysis Method and its Application to Damped Laminated Beams," 51st Shock and Vibration Symposium, October 21-23, 1980, San Diego, California.

8. M. Lalanne, M. Paulard, P. Trompette, "Response of Thick Structures Damped by Viscoelastic Material with Application to Layered Beams and Plates," Shock and Vibration Bulletin, 45, pp. 65-71, 1975.

9. R.A. Brockman, "A Penalty Function Approach to the Nonlinear Finite Element Analysis of Thin Shells," Ph.D. Dissertation, University of Dayton, July 1979.

10. R.A. Brockman, "MAGNA: A Finite Element Program for the Materially and Geometrically Nonlinear Analysis of Three-Dimensional Structures Subjected to Static and Dynamic Loading," University of Dayton Research Institute report UDR-TR-79-45, October 1979.

11. M.L. Soni, "Finite Element Analysis of Initially Stressed Viscoelastic Solids," University of Dayton Research Institute report UDR-TR-79-113, November 1979.

12. E.M. Kerwin, "Damping of Flexural Waves by a Constrained Viscoelastic Layer," The Journal of the Acoustical Society of America, Vol. 31, No. 7, pp. 952-962, 1959.

13. E.E. Ungar, "Loss Factors of Viscoelastically Damped Beam Structures," The Journal of the Acoustical Society of America, Vol. 14, No. 8, pp. 1082-1089.

14. R.A. Ditaranto, "Theory of Vibratory Bending for Elastic and Viscoelastic Layered Finite Length Beams," Journal of Applied Mechanics, Vol. 32, Transactions of the American Society of Mechanical Engineers Series E, Vol. 87, pp. 881-886, 1965.

15. D.J. Mead, S. Markus, "Loss Factors and Resonant Frequencies of Encastré Damped Sandwich Beams," Journal of Sound and Vibration, Vol. 12 (1), 1970, pp. 99-112.

16. D.K. Rao, "Frequency and Loss Factors of Sandwich Beams Under Various Boundary Conditions," Journal of Mechanical Engineering Science, Vol. 20, No. 5, 1978, pp. 271-282.

17. L.C. Rogers, R. Gordan, C.D. Johnson, "Seminar on Damped Laminated Beams," Wright-Patterson Air Force Base, Ohio, March 19, 1980.

18. M.L. Drake, G.E. Turborg, "Polymeric Materials Testing Procedures to Determine the Damping Properties and the Result of Selected Commercial Materials," University of Dayton report UDTR-80-40, 1980.

19. M.F. Kluesener, Personal Communication, January 1981.

DISCUSSION

Mr. Nicholson (Naval Surface Weapons Center: I would like to know first of all how you did your finite element analysis. Did you use a standard code? The second question is did you put any damping in your beams? I assume not.

Mr. Sharan: No I didn't use any damping on the beams as such. But it can be easily incorporated because all the materials are metal and they have very, very low structural damping. However, the main object of our investigation was to study the possibility of improved surface finish on these work pieces so that we can easily apply some external damping - say at the bedding locations or at the ends. We have done some studies on that by putting damping at certain definite locations. The finite element analysis has all been done using standard techniques.

Mr. Nicholson: Did you use a standard code?

Mr. Sharan: I have done my own analysis. I wrote my own program so I haven't used any of these standard systems.

PNEUMATIC VIBRATION CONTROL USING ACTIVE FORCE GENERATORS

S. Sankar and R.R. Guntur
Department of Mechanical Engineering
Concordia University, Montreal, Canada

In this paper, various design aspects of an active vibration control system are considered. Three of the design alternatives currently available are reviewed. It is shown that these three vibration control systems use either explicicly or implicitly a force generator concept. In the proposed system a general expression for the control force is chosen so that this system is representative of not only all the above three systems but also a passive system. Transmissibility characteristics of this system are studied. The results obtained indicate that by proper choice of various feedback gains it is possible to design an active vibration control system that will give the desired transmissibility characteristics.

INTRODUCTION

A vibration control system performs the important task of isolating a certain system from vibrating environment. Vibration control systems can be classified into two groups: passive systems and active systems. Passive systems make use of simple mechanical elements like springs and dampers and they do not need additional sources of energy for the purpose of controlling vibrations. However, passive systems have some fundamental limitations [1].

Active vibration control systems offer considerable potential for overcoming the limitations of passive systems. Active systems also offer greater flexibility of design and better performance than passive systems do. These systems can be designed to produce forces which are functions of any system variables, for example, output acceleration, output velocity or output displacement. However, it must be admitted that active systems in general are more costly, more complex and therefore often less reliable than the passive systems. Therefore, the use of active means of vibration control also has been limited to the cases in which performance gains outweigh the disadvantages of increased cost, complexity and weight.

Calcaterra described an active vibration control system designed for aircraft pilot protection [2]. An active pneumatic control system employing a three-way servo-valve for ground vehicles has been described by Esmail-zadeh [3]. An active pneumatic suspension applicable to passenger rail car is described by Klinger [4]. Yoshiaki [5] applied an active vibration absorber to a preview control syst of a vehicle suspension. Suggs et al [6] developed an electro-hydraulic seat suspensic system. Karnopp [8] described a means by whi the desired performance of a vibration contro system could be obtained with the aid of semi-active force generators.

In this paper an active vibration control system using a pneumatic force generator has been described. Transmissibility characteristics of this active pneumatic vibration control system are obtained. A generalized control policy from which other control policies can be derived as special cases has been considered. It is shown that a pneumatic vibration control system can be designed to give any shape of the transmissibility characteristic.

CONTROL FORCE DEVELOPED BY A PASSIVE SYSTEM

A simple passive vibration control system of a mass spring and a damper is shown in Fig. 1.

The equation of motion of the system is given by,

$$m \ddot{y}_1 + c (\dot{y}_1 - \dot{y}_2) + k (y_1 - y_2) = 0 \qquad (1)$$

or $$m \ddot{y}_1 + F_c = 0 \qquad (1a)$$

where $$F_c = c (\dot{y}_1 - \dot{y}_2) + k (y_1 - y_2)$$

The control force offered by a passive vibration control system, F_c is dependent on the damping coefficient c, the relative velocity $(\dot{y}_1 - \dot{y}_2)$, the spring stiffness k and the relative displacement $(y_1 - y_2)$.

A low value of k will increase the static deflection and may not be suitable.

A high value of k will increase the natural frequency and may lend to high transmissibility (ratios) in the low frequency range.

A low value of c will increase the magnitude of the resonance peak and thus it will increase the transmissibility in the low frequency range.

A high value of c will increase the transmissibility in the high frequency range.

The above performance limitations of passive vibration control systems render them unsuitable for applications where optimal performance is desired over a wide range of frequency.

CONTROL FORCE DEVELOPED BY SOME ACTIVE SYSTEMS

In addition to the simple passive elements used in the system, one may use active elements which alter the control force to suit the requirements. Since a given set of values of c and k is not suitable over a wide range of frequency, one can think of altering the values of c and k and make them frequency dependent. An alternative approach is to make the control force dependent on other variables different from relative velocity, $\dot{y}_1 - \dot{y}_2$ and relative displacement $y_1 - y_2$. This second approach is commonly used in active vibration control systems.

Karnopp et al [8] advocated the use of a force generator that produces a damping force that is dependent an $\dot{y}_1$. In this case the control force F_{ck} is given by the following equation:

$$F_{ck} = c_k \dot{y}_1 + k_k (y_1 - y_2) \qquad (2)$$

The term $c_k \dot{y}_1$ in the above equation is conceived to be due to a ficticious damper known as a Skyhook damper [8].

Klinger [4] suggested a slightly different approach. He used the following relation to calculate the control force. Then he allowed the control system to compare the calculated control force and the measured control force and to take the appropriate action.

$$F'_{ck} = - m\ddot{y}_c + c'_k (\dot{y}_1 - \dot{y}_2) + k'_k (y_1 - y_2) \qquad (3)$$

Esmailzadeh [3] studied a servo controlled pneumatic suspension system in which he used the output displacement and output velocity for feedback control purposes. Considering the linearized version of Esmailzadeh's system, one obtains the following equation for the control force, if there is no surge tank in the system,

$$F_{CE} = \frac{(C_e D + k_e)\, y}{(1 + \tau_e D)} \qquad (4)$$

VIBRATION CONTROL SYSTEM USING A PNEUMATIC FORCE GENERATOR

A schematic diagram of the suspension system using a pneumatic force generator is shown in Fig. 2a. In this system the mass is attached to the cylinder of a pneumatic actuator. The cylinder of the pneumatic actuator is connected with two springs to the frame that is being subjected to input excitation. The piston of the pneumatic actuator is also connected to the frame. The piston divides the cylinder into two chambers. The lower chamber is sealed while the upper chamber is connected to air supply through an electro-pneumatic servo-valve.

Control Policy. The pressure in the upper chamber of the pneumatic actuator is changed by connecting it either to the air supply or to the atmosphere. The position of the electro-pneumatic servo valve is made to vary linearly with the sum of signals proportional to output displacement, output velocity, output acceleration and relative velocity. In other words the control law for the electro-pneumatic valve can be stated as follows (see equation A.8).

$$\Delta x_v = - k_4 D \Delta h - (k'_1 D^2 + k'_2 D + k'_3) \Delta y_1 \qquad (5)$$

A block diagram of the control system is shown in Fig. 2b.

Mathematical analysis is presented in Appendix 1. This analysis is based on the assumption that only small changes in pressure and volume of air in chambers one and two occur. From this linearized analysis an expression for the control force has been obtained and it is as follows:

$$F_{cs} = \frac{k'_4 (\dot{y}_1 - \dot{y}_2) + k''_1 \ddot{y}_1 + k''_2 \dot{y}_2 + k''_3 y_2}{(1 + \tau_s D)} + k_5 (y_1 - y_2) \qquad (6)$$

Since equation (6) gives the control force in its most general form in that by appropriate selection of parameters k_4, k_5, k'_1, k'_2, k'_3 and τ_s expressions for F_{ck}, F'_{ck} and F_{CE} can be obtained from equation (6). In this paper, an attempt is made to study in detail the transmissibility characteristics of the proposed pneumatic vibration control system.

The transmissibility ratio T_r of the pneumatic active suspension system shown in Fig. 2

is given by the following equation (see also equation A.12)

$$T_r = \frac{\alpha^{\frac{1}{2}}}{[\beta^2 + \nu^2]^{\frac{1}{2}}}$$

$$\alpha = \left(\frac{\tau}{\tau_2^2} + \frac{\tau}{\tau_1^2} + \frac{k_4^2}{\tau_v^2}\right)\omega^2 + \frac{1}{\tau_2^4} \qquad (7)$$

$$\beta = \frac{k_3'}{\tau_v^2} + \frac{1}{\tau_2^2} - \left(\frac{k_1'}{\tau_v^2} + 1\right)\omega^2$$

$$\nu = \left(\frac{k_2'}{\tau_v^2} + \frac{\tau}{\tau_1^2} + \frac{\tau}{\tau_2^2} + \frac{k_4}{\tau_v^2}\right)\omega - \tau\omega^3$$

To investigate the effects of various feedback terms, it is proposed to draw the transmissibility ratio vs frequency plots for different cases.

DISCUSSION OF RESULTS

In Fig. 3 are shown the transmissibility plots when the control force is given by the following relation and the feedback gain k_4 is varied. In this case, other feedback gains are set to zero.

$$F_{csk_4} = \frac{k_4'(\dot{y}_1 - \dot{y}_2)}{(1 + \tau_s D)} + k_5(y_1 - y_2) \qquad (6a)$$

When k_4' is zero, the pneumatic system reduces to a simple mass spring system without any damping and the transmissibility ratio increases as frequency increases until resonance peak occurs and then transmissibility decreases as frequency increases. However, when k_4 is zero, equation (6a) reduces to the following form (see Appendix 1)

$$F_{csk_4} = \frac{P_1 A_1^2}{RT_1 K_b}\frac{(\dot{y}_1 - \dot{y}_2)}{(1 + \tau_s D)} + k_5(y_1 - y_2) \qquad (6b)$$

The transmissibility characteristic if k_4 is zero is given in Fig. 3. The system in this case behaves like a simple mass-spring-damper system with a damping coefficient that is very small. However, if k_4 is not zero, the transmissibility ratio increases slowly as the frequency increases.

When $\tau_s D \ll 1$, the feedback term (the first term on the right-hand side of equation (6a)) is equivalent to a conventional viscous damper and when $\tau_s D \gg 1$, the feedback term is equivalent to that of a conventional spring. Thus as the frequency increases the natural frequency of the pneumatic suspension system is altered. For this reason k_4 is equal to 0.01 the resonance peak is not within the frequency range of interest and transmissibility ratio varies from 1.0 - 1.8 when frequency is increased from 0 - 60 rad/s. As k_4 increases, the range within which transmissibility ratio varies becomes smaller. However, the transmissibility ratio within the frequency range of interest is not less than 1.0 when $k_4 = 1.0$. When $k_4 = 1.0$ the transmissibility characteristic is flat. Thus, if a flat transmissibility characteristic at a value of 1.0 is desired a suitable value of k_4 may be chosen.

In Fig. 4 are presented the transmissibility plots when the control force is given by the following relation and the feedback again k_2' is varied. In this case k_4, k_1' and k_3' are all equal to zero.

$$F_{csk_2} = \frac{\frac{P_1 A_1^2}{RT_1 K_b}(\dot{y}_1 - \dot{y}_2) + k_2''\dot{y}_1}{(1 + \tau_s D)} + k_5(y_1 - y_2) \qquad (6c)$$

In this case the feedback term $k_2''\dot{y}_1/(1+\tau_s D)$ is equivalent to a Sky-hook damper $\tau_s D \ll 1$ and when $\tau_s D \gg 1$ it is equivalent to a 'Sky-hook spring' (the feedback is proportional to the output displacement, y_1).

The transmissibility ratio is equal to 1.0 at zero frequency, but it decreases to a low value as frequency increases. Thus by employing the velocity feedback term it is possible to get a flat transmissibility characteristic in such a way that the transmissibility ratio is close to zero at all frequencies except at near zero frequency.

The results in Figs. 3 and 4 indicate that with proper choice of feedback terms such as k_4 and k_2, an active vibration control system can be designed to yield any one of the two distinct transmissibility characteristics of Figs. 3 and 4.

Thus far the effects of feedback gains k_2' and k_4 on the transmissibility ratio have been investigated. Irrespective of the values of k_2' or k_4 the transmissibility ratio is unity at zero frequency in Figs. 3 and 4. To decrease the transmissibility ratio at zero frequency, the feedback term $k_3''y_1/(1 + \tau_s D)$ can be used. In this case the control force is given by the following equation ($k_3' \neq 0$, $k_4' = 0$, $k_1' = 0$, $k_2' = 0$).

$$F_{csk_3'} = \frac{\frac{P_1 A_1^2}{RT_1 k_b}(\dot{y}_1 - \dot{y}_2) + k_3'' y_1}{(1 + \tau_s D)} + k_5(y_1 - y_2) \qquad (6d)$$

Thus when $\tau_s D \ll 1$ $k_3'' y_1/(1 + \tau_s D)$ represents a 'Sky-hook spring' (this feedback term is proportional to the output displacement) and when $\tau_s D \gg 1$, $k_3'' y/(1 + \tau_s D)$ represents integral control or this feedback term is proportional to the integral of the output displacement.

The transmissibility plots when the control force is given by equation (6d) are presented in Fig. 5. From the results in Fig. 5, it is noted that as k_3' is increased the transmissibility ratio at zero frequency is decreased. When k_3' is equal to 0.1 the transmissibility ratio reaches its maximum value of 0.56 at a frequency at 41 rad/s. As k_3' is increased the transmissibility ratio at zero frequency decreases, for example, when k_3' is changed from 0.5 to 2.0, the transmissibility ratio at zero frequency changes from 0.030 to 0.0175. As k_3' is increased the transmissibility characteristic becomes flat. When k_3' is equal to 0.5 the transmissibility ratio varies from 0.030 to 0.140 in the frequency range of interest 0 - 60 rad/s. In this frequency range when k_3' is equal to 2.0 the transmissibility ratio varies from 0.0175 to 0.0375.

To study the effect of the acceleration feedback term, $k_1'' \ddot{y}_1/(1 + \tau_s D)$ the transmissibility plots for various values of k_1 are obtained and presented in Fig. 6. The control force in this case is given by the following relation ($k_1' \neq 0$, $k_4 = 0$, $k_2' = 0$, $k_3' = 0$).

$$F_{csk_1'} = \frac{\frac{P_1 A_1^2}{RT\, k_b} (\dot{y}_1 - \dot{y}_2) + k_1'' \ddot{y}_1}{(1 + \tau_s D)} + k_5 (y_1 - y_2) \quad (6e)$$

Thus when $\tau_s D \ll 1$ the feedback term is proportional to the output acceleration and when $\tau_s D \gg 1$, it is proportional to the output velocity (or equivalent to a Sky-hook damper).

Since k_1' is zero, the transmissibility ratio at zero frequency is equal to 1.0 for all values of k_1' in Fig. 6. When k_1' is equal to 0.1 the transmissibility ratio reaches a value of 35.0 at a frequency of 0.5 rad/s and it drops to a value of 0.6 at a frequency of 1.0 rad/s (this result is not shown in Fig. 6). In the frequency range of 10-60 rad/s the transmissibility ratio is constant and has a value close to zero, (this result is not shown in Fig. 6). When k_1' is equal to 0.5 the transmissibility ratio at zero frequency is equal to 1.0. By increasing the value of k_1' the lower limit of the frequency range in which the transmissibility ratio becomes constant can be made smaller. However, since k_3' is not equal to zero transmissibility ratio at zero frequency is still equal to 1.0. It is also noted that except at frequencies near to zero frequency, the transmissibility characteristics obtained with acceleration feedback are similar to those obtained with velocity feedback. A resonance peak at near zero frequency is a drawback of this form of control.

If it is required to design an active vibration control system with transmissibility ratio close to zero in the frequency range of interest, 0-60 rad/s, the output displacement feedback and the output velocity feedback terms should be used for control purposes. To illustrate the effect of acceleration feedback on a system that has both output displacement and output velocity feedback, a system is considered in which the control force is given by the following equation.

$$F'_{csk'} = \frac{\frac{P_1 A_1^2}{RT_1 k_b} (\dot{y}_1 - \dot{y}_2) + k_1'' \ddot{y}_1 + k_2'' \dot{y}_1 + k_3'' y_1}{(1 + \tau_s D)} + k_5 (y_1 - y_2) \quad (6f)$$

In the present example $k_3' = 1.5$, $k_2' = 1.0$, $k_4 = 0$ and k_1' is varied. The results in Fig. 7 indicate that acceleration feedback term helps in making the lower limit of the frequency range in which transmissibility ratio is constant smaller. In addition, an increase in the value of k_1' decreases the transmissibility ratio except at near zero frequency.

Finally, the transmissibility characteristics for a system in which control force is given by equation (6) are presented in Fig. 8. The relative velocity feedback term $k_4' (\dot{y}_1 - \dot{y}_2)/(1 + \tau_s D)$ seems to have an adverse affect on the transmissibility characteristics in that as k_4 increases the maximum value of the transmissibility ratio increases. It is also noted that as k_4 increases the frequency range in which transmissibility ratio is constant becomes smaller.

CONCLUSIONS

Active vibration control system using a pneumatic force generator is presented. A linearized analysis of the pneumatic vibration control system is carried out and it is shown that the force generator in this case is capable of producing a control force of a passive system and a wide variety of control forces. It is shown that a pneumatic vibration control system can be designed to give any desired transmissibility ratio.

Based on the results, it can be concluded that the relative velocity feedback term if used alone keeps the transmissibility ratio close to unity in the desired frequency range if the value of k_4 is properly selected. The displacement feedback term is useful in giving a low transmissibility at zero frequency. A flat transmissibility characteristic at the higher end of the frequency can be obtained by properly selecting output velocity and

and acceleration feedback terms. For a low transmissibility ratio throughout the frequency range, the pneumatic vibration control system must be designed without the relative velocity feedback terms, but with proper values of output displacement, velocity and acceleration terms.

ACKNOWLEDGEMENT

This investigation is supported through grants A-3685 and U-0061 from the Natural Sciences and Engineering Research Council of Canada.

REFERENCES

[1] Bender, E.K., "Some fundamental limitations of active and passive vehicle suspension systems". Transactions of the Society of Automotive Engineers Paper No. 680750, 1968.

[2] Calcaterra, P.C., "Research on Vibration Isolation Techniques for aircraft pilot protection". Air Force Report AMRL-TR-67-138.

[3] Esmailzadeh, E., "Servovalve Controlled Pneumatic suspensions", Journal of Mechanical Engineering Science, Vol. 21, no. 1, 1979.

[4] Klinger, D.L., and A.J. Calzado, "A Pneumatic on-off vehicle suspension system", Transactions of ASME, June 1977. Journal of Dynamic Systems Measurement and Control.

[5] Iwata Yoshiaki and Mitsuo Nakno, "Optimum preview Control of Vehicle air suspensions", Bulletin of the JSME V19, no. 138, Dec. 1976.

[6] Young, R.E., and Suggs, C.W., "Seat Suspension System for isolation of roll and pitch in off-road vehicles", Transactions of ASAE, 1973, p. 876-880.

[7] Grimm, E.A., Huff G.J., and Wilson, J.N., "An Active seat suspension for off-road vehicles". Univ. of Saskatchewan, Sask.

[8] Karnopp, D. et al, Crosby, M.J., and Harwood, R.A., "Vibration Control using semi-active force generators", Transactions of ASME, Journal of Engineering for Industry, 1974.

APPENDIX A

Mathematical Analysis In the following analisis it is assumed that only small changes occur in the values of P_1, P_2, V_1 and V_2.

Considering the mass flow from chamber 1 [3]

$$\Delta\dot{m}_1 = \frac{P_1}{R\,T_1} D\,(\Delta V_1) + \frac{V_1 D}{nRT_1}(\Delta P_1) \qquad (A.1)$$

where, $\Delta V_1 = A_1\,\Delta h$ (A.2)

$$\Delta h = \Delta y_1 - \Delta y_2 \qquad (A.3)$$

Considering the mass flow from chamber 2

$$\Delta\dot{m}_2 = \frac{P_2}{RT_2} D\,(\Delta V_2) + \frac{V_2}{nRT_2} D\,(\Delta P_2) = 0 \qquad (A.4)$$

$$\text{or} \quad \Delta P_2 = \frac{n P_2 A_2}{V_2}\Delta h \qquad (A.5)$$

mass flow from the servo-valve [3]

$$\Delta\dot{m}_1 = K_a\,\Delta X_v - K_b\,\Delta P_1 \qquad (A.6)$$

Equating $\Delta\dot{m}_1$ given by (A.1) and (A.6)

$$\frac{P_1 A_1 D\,\Delta h}{RT_1} + \frac{V_1}{nRT_1} D\,\Delta P_1 = K_a\,\Delta X_v - K_b\,\Delta P_1 \qquad (A.7)$$

$$\text{or} \quad \left(\frac{V_1 D}{nRT_1 K_b} + 1\right)\Delta P_1 = K_v\,\Delta X_v - \frac{P_1 A_1 D\,\Delta h}{RT_1 K_b} \qquad (A.7a)$$

$$\Delta P_1\,(1 + \tau D) = K_v\,\Delta X_v - \frac{P_1 A_1 D\,\Delta h}{RT_1 K_b} \qquad (A.7b)$$

The following control law has been used to monitor the movement of the spool of the servovalve.

$$\Delta X_v = -k_4 D\,\Delta h - (k_1' D^2 + k_2' D + k_3')\,\Delta y_1 \qquad (A.8)$$

Substitution of the above expression for ΔX_v in equation (A.7b) yields the following equation

$$\Delta P_1 = \left[- K_v k_4 \frac{P_1 A_1}{RT_1 K_b} \right] D \, \Delta h / (1 + \tau D)$$

$$- K_v \left[k_1' D^2 + k_2' D + K_3' \right] \Delta y_1 / (1 + \tau D) \quad (A.9)$$

Considering the changes in forces in the vertical direction

$$m D^2 \Delta y_1 = A_1 \Delta P_1 - A_2 \Delta P_2 - k \Delta h \quad (A.10)$$

Substituting for ΔP_1 and ΔP_2 from equations (A.5) and (A.9) and simplifying, one obtains the following equation:

$$\frac{\Delta y_1}{\Delta y_2} = \frac{A + B}{\tau D + C + E + F} \quad (A.11)$$

where $A = \left(\frac{\tau}{\tau_1} + \frac{k_4}{\tau^2} \right) D$

$$B = \left(\frac{1 + \tau D}{\tau_2^2} \right)$$

$$C = \left(\frac{k_1'}{\tau_v^2} + 1 \right) D^2$$

$$E = \left(\frac{k_2'}{\tau_v^2} + \frac{\tau}{\tau_1^2} + \frac{\tau}{\tau_2^2} + \frac{k_4}{\tau_v^2} \right) D$$

$$F = \left(\frac{k_3'}{\tau_v^2} + \frac{1}{\tau_2^2} \right)$$

$$\left| \frac{\Delta y_1}{\Delta y_2} \right| = \frac{\alpha^{\frac{1}{2}}}{[\beta^2 + \nu^2]^{\frac{1}{2}}} \quad (A.12)$$

where

$$\alpha = \left(\frac{\tau}{\tau_2^2} + \frac{\tau}{\tau_1^2} + \frac{k_4}{\tau_v^2} \right)^2 \omega^2 + \frac{1}{\tau_2^4}$$

$$\beta = \frac{k_3'}{\tau_v^2} + \frac{1}{\tau_2^2} - \left(\frac{k_1'}{\tau_v^2} + 1 \right) \omega^2$$

$$\nu = \left(\frac{k_2'}{\tau_v^2} + \frac{\tau}{\tau_1^2} + \frac{\tau}{\tau_2^2} + \frac{k_4}{\tau_v^2} \right) \omega - \tau \omega^3$$

The magnitude of the control force is given by the magnitude of the expression on the right-hand side of equation (A.10)

$$F_{cs} = - A_1 \Delta P_1 + A_2 \Delta P_2 + k \Delta h \quad (A.13)$$

Substituting the expression for ΔP_1 and ΔP_2 in equation A.13 and simplifying

$$F_{cs} = \frac{k_4^1 (\dot{y}_1 - \dot{y}_2) + k_1'' \ddot{y}_1 + k_2'' \dot{y}_1 + k_3'' y_1}{(1 + \tau D)}$$

$$+ k_5 (y_1 - y_2) \quad (A.14)$$

where, $k_4^1 = A_1 K_v k_4 + \frac{P_1 A_1^2}{RT_1 K_b}$

$$k_1'' = K_v A_1 k_1'$$

$$k_2'' = K_v A_1 k_2'$$

$$k_3'' = K_v A_1 k_3'$$

$$k_5 = \frac{n P_2 A_2^2}{V_2} + k$$

In the example given,

$\tau_1 = 0.062$ s

$\tau_2 = 0.044$ s

$\tau_v = 0.00539$ s

$\tau = 0.0487$ s

NOMENCLATURE

A_1 area of chamber 1 (see Fig. 2)

A_2 area of chamber 2

c damping coefficient in a passive system

c_k damping coefficient of a sky-hook damper

$c_{k'}$ damping coefficient in Klinger's active system

c_e coefficient of output velocity feedback term in Esmailzadeh's active system

F_{cE} control force in Esmailzadeh's active system

F_{ck} control force in Karnopp's active system

F'_{ck} control force in Klinger's active system

F_{cs} control force in the active system

Δh $\Delta y_1 - \Delta y_2$, a small change in the position of actuator piston w.r.t. to its cylinder

k spring constant

k_e coefficient of output displacement term in Esmailzadeh's active system

k_k spring stiffness in Karnopp's system

k_4 coefficient of relative velocity feedback term in this paper

k_5 spring stiffness in this paper

k'_k spring stiffness in Klinger's system

k'_1 coefficient of output acceleration feedback term in this paper

k'_2 coefficient of output velocity feedback term in this paper

k'_3 coefficient of output displacement feedback term in this paper

$$k'_4 = A_1 K_v k_4 + \frac{P_1 A_1^2}{RT_1 k_b}$$

$$k''_1 = K_v A_1 k'_1$$

$$k''_2 = K_v A_1 k'_2$$

$$k''_3 = K_v A_1 k'_3$$

$$K_a = (\partial \dot{m}/\partial x_v)_{p=p_1} = \text{constant}$$

$$K_b = (\partial \dot{m}/\partial P_1)_{x_v} = \text{constant}$$

$$K_v = K_a/K_b$$

m mass of the system

n ratio of specific heats of air (C_p/c_v)

P_1 pressure of air in chamber 1

ΔP_1 a small change in the pressure of air in chamber 1

P_2 pressure of air in chamber 2

ΔP_2 a small change in the pressure of air in chamber 2

R universal gas constant

S_1 $n P_1 A_1^2/V_1$

S_2 $n P_2 A_2^2/V_2$

T_1 temperature of air in chamber 1

T_2 temperature of air in chamber 2

V_1 volume of air in chamber 1

ΔV_1 a small change in the volume of air in chamber 1

V_2 volume of air in chamber 2

ΔV_2 a small change in the volume of air in chamber 2

ΔX_v a small change in the movement of the spool of the servo-valve

τ $V_1/K_b\, n\, RT_1$

τ_e time constant of Esmailzadeh's active system equivalent to τ

τ_v $\sqrt{\frac{m}{K_v A_1}}$

τ_1 $\sqrt{m/S_1}$

τ_2 $\sqrt{\frac{m}{(k + S_2)}}$

τ_s time constant of the present active system (equal to τ)

$(\cdot)$ a dot represents differentian with respect to time

$\ddot{y}_c$ represents input acceleration signal after it has been passed through a filter

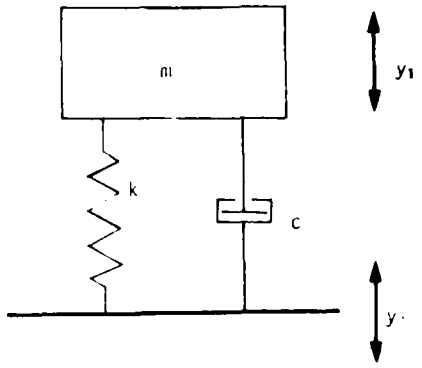

Fig. 1 A Simple mass-spring-damper system

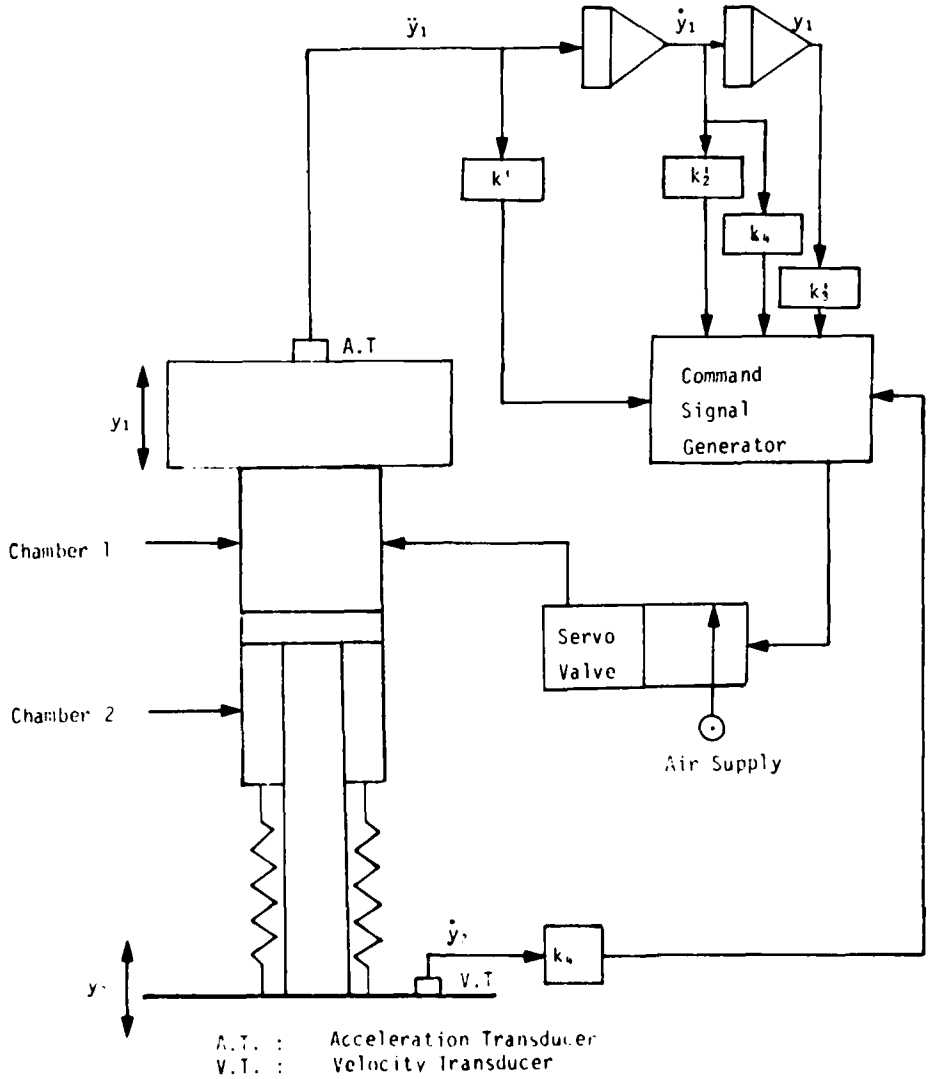

Fig. 2a Schematic diagram of the active vibration control system

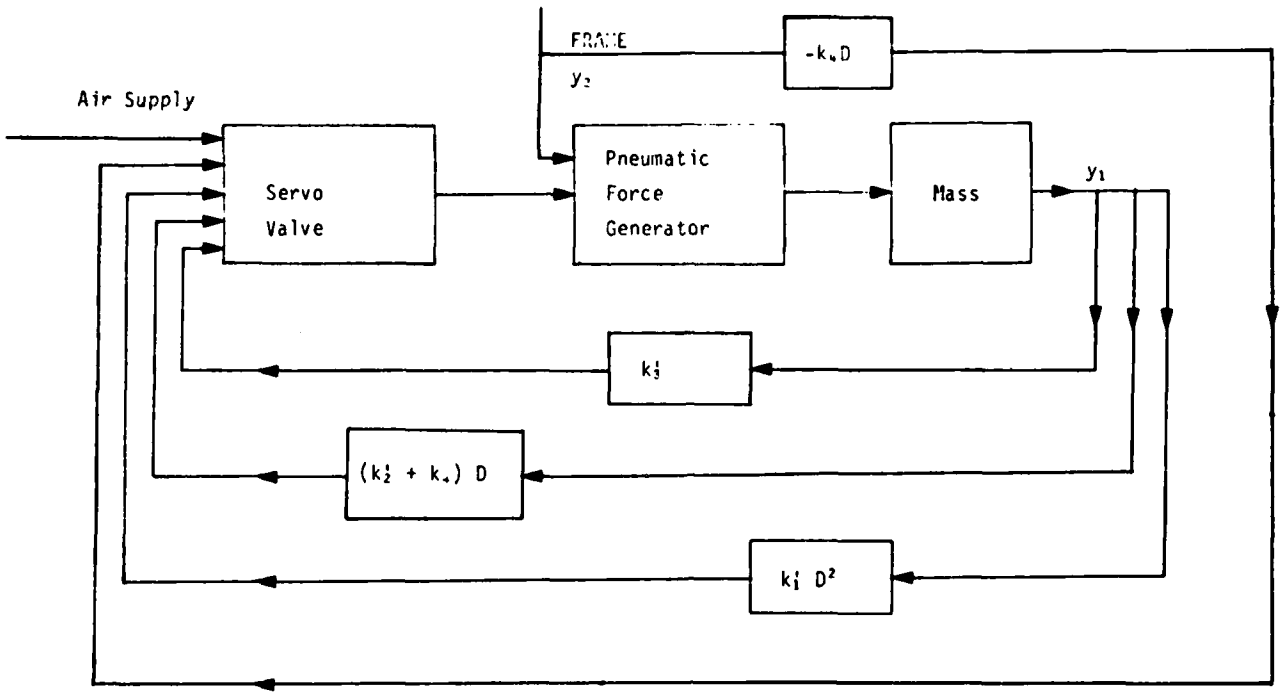

Fig. 2b Block diagram of the active vibration control system

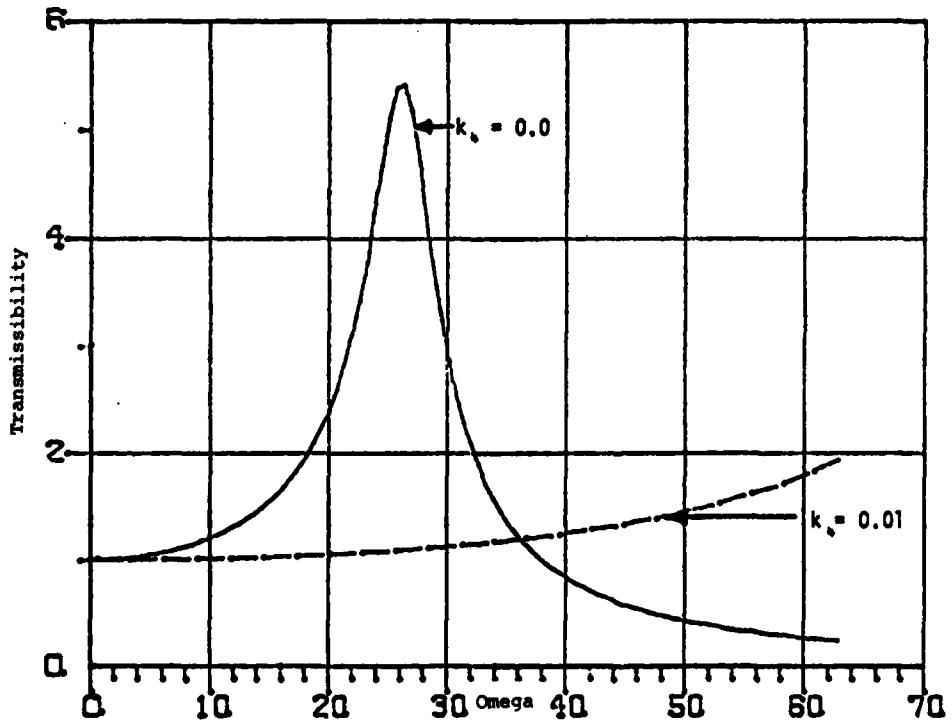

Fig. 3a Transmissibility vs frequency (ω: rad/s) curves when $k_3' = 0$, $k_2' = 0$, $k_1' = 0.0$, $k_4 = 0.0$ and 0.01.

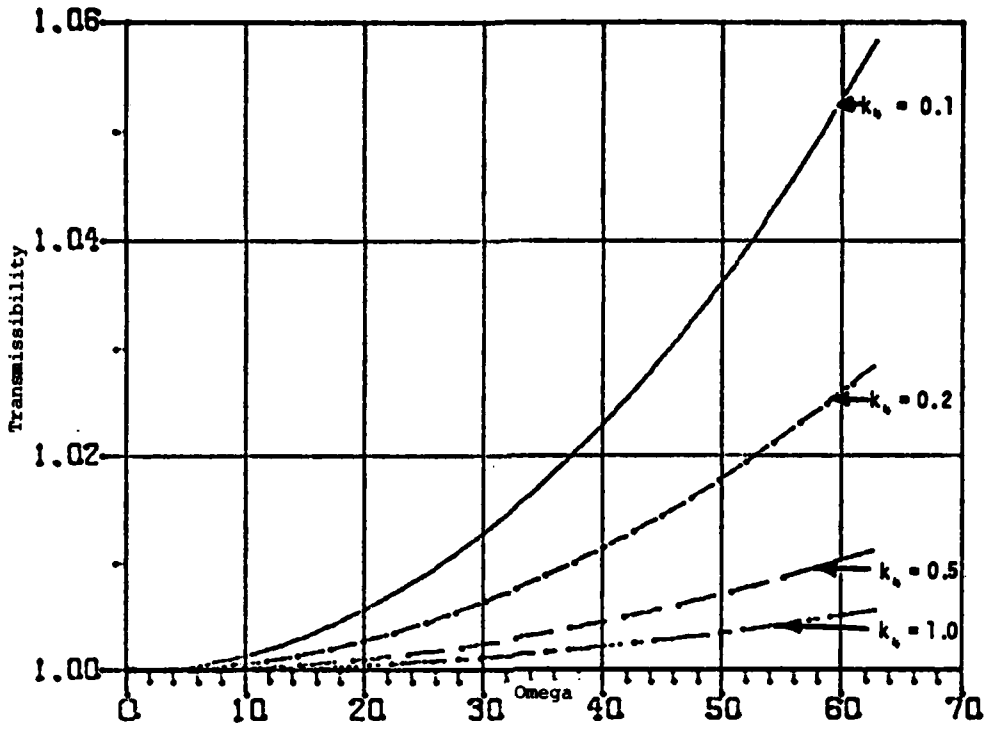

Fig. 3b Transmissibility vs frequency (ω: rad/s) curves when $k_3 = 0.0$, $k_2' = 0.0$, $k_1' = 0.0$; $k_4 = 0.1$, 0.2, 0.5 and 1.0.

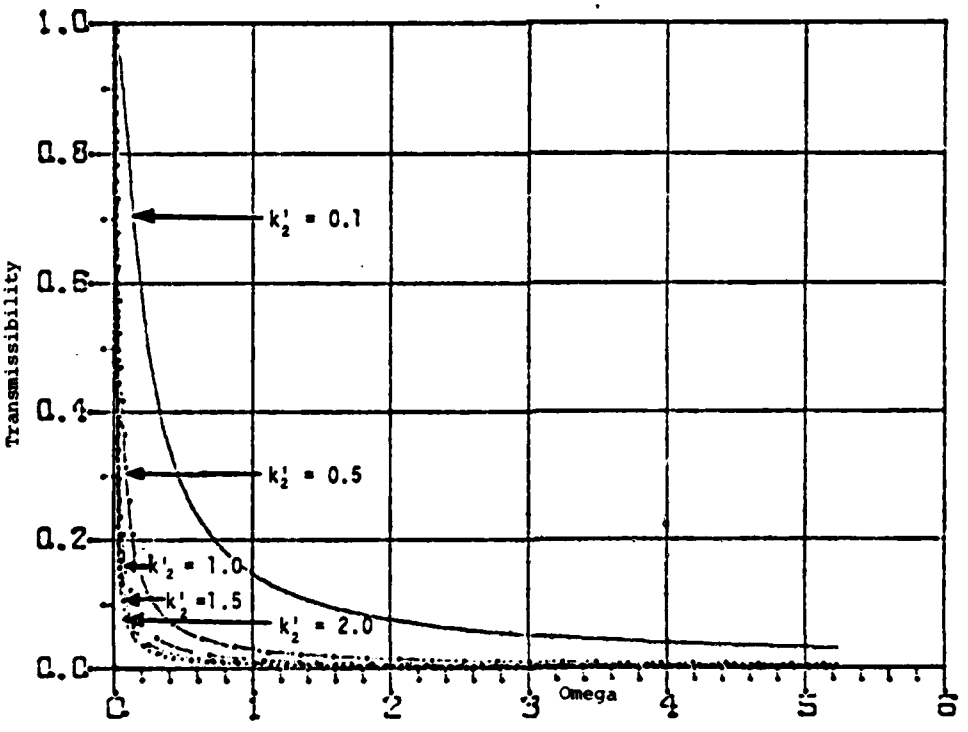

Fig. 4 Transmissibility vs frequency (ω: rad/s) curves when $k_3' = 0.0$, $k_4 = 0.0$, $k_1' = 0.0$; $k_2' = 0.1$, 0.5, 1.0, 1.5 and 2.0.

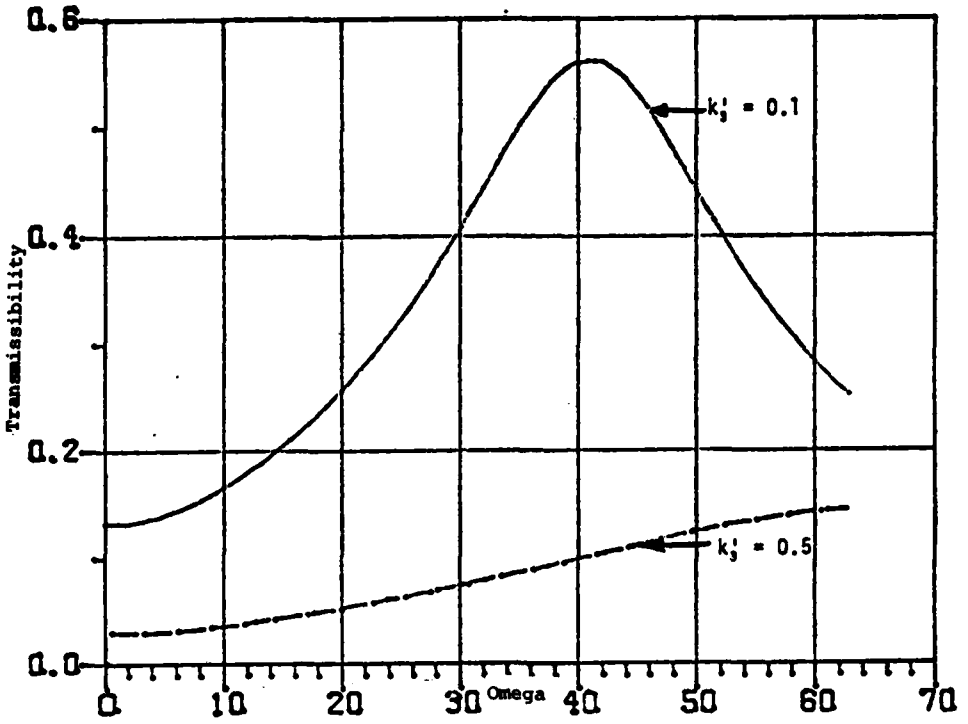

Fig. 5a Transmissibility vs frequency (ω: rad/s) curves when k_4 = 0, k_2' = 0, k_1' = 0; k_3' = 0.1 and 0.5.

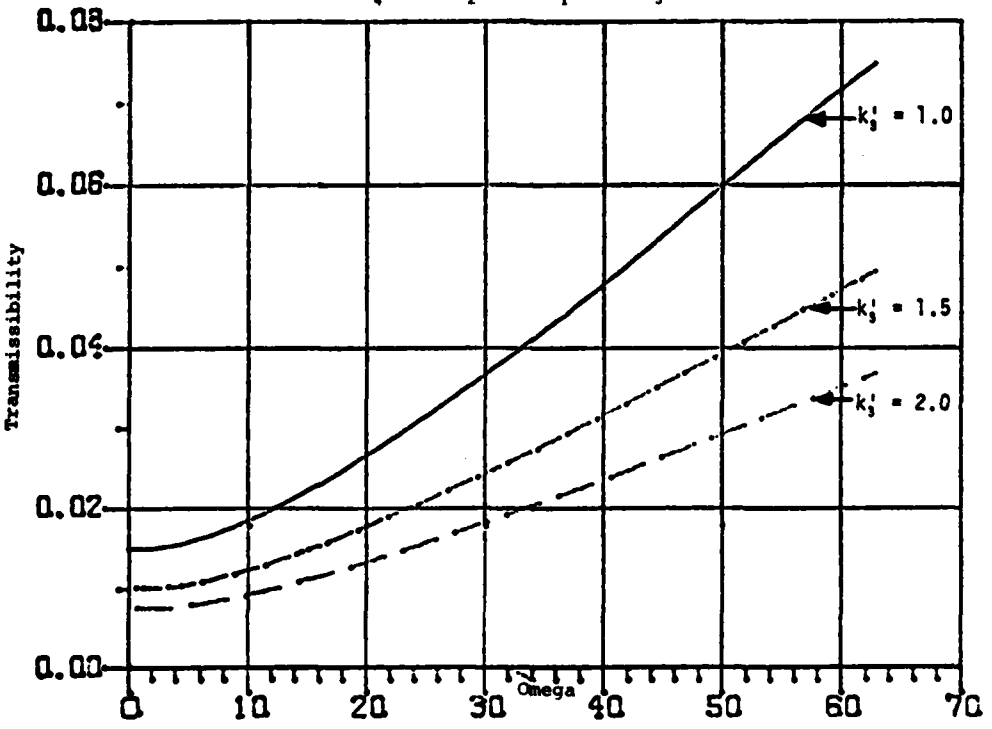

Fig. 5b Transmissibility vs frequency (ω: rad/s) curves when k_4 = 0, k_2' = 0, k_1' = 0, k_3' = 1.0, 1.5 and 2.0.

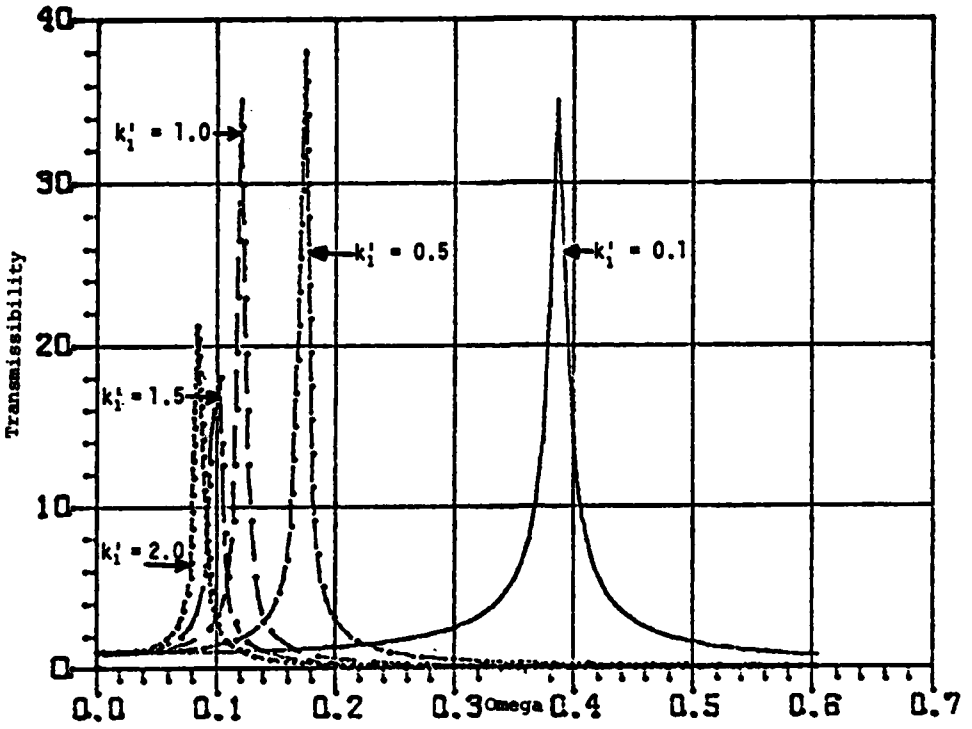

Fig. 6 Transmissibility vs frequency (ω: rad/s) curves when $k_3' = 0$, $k_4 = 0$, $k_2' = 0$; $k_1' = 0.1$, 0.5, 1.0, 1.5 and 2.0.

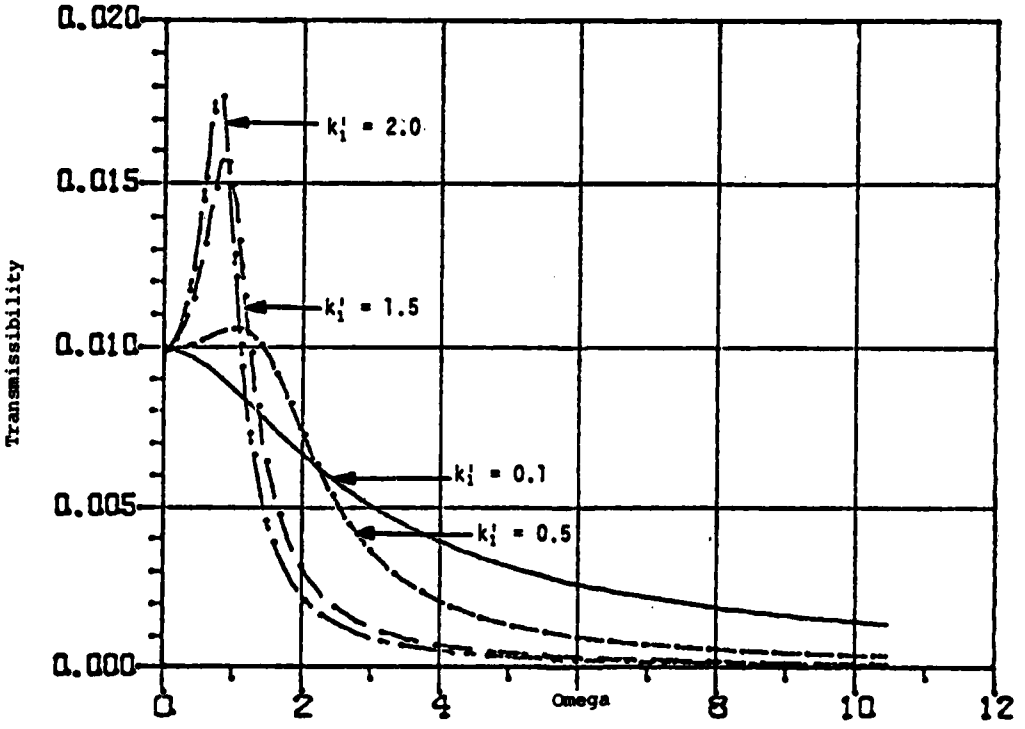

Fig. 7 Transmissibility vs frequency (ω: rad/s) curves when $k_3' = 1.5$, $k_4 = 0$, $k_2' = 1.0$; $k_1' = 0.1$, 0.5, 1.5 and 2.0.

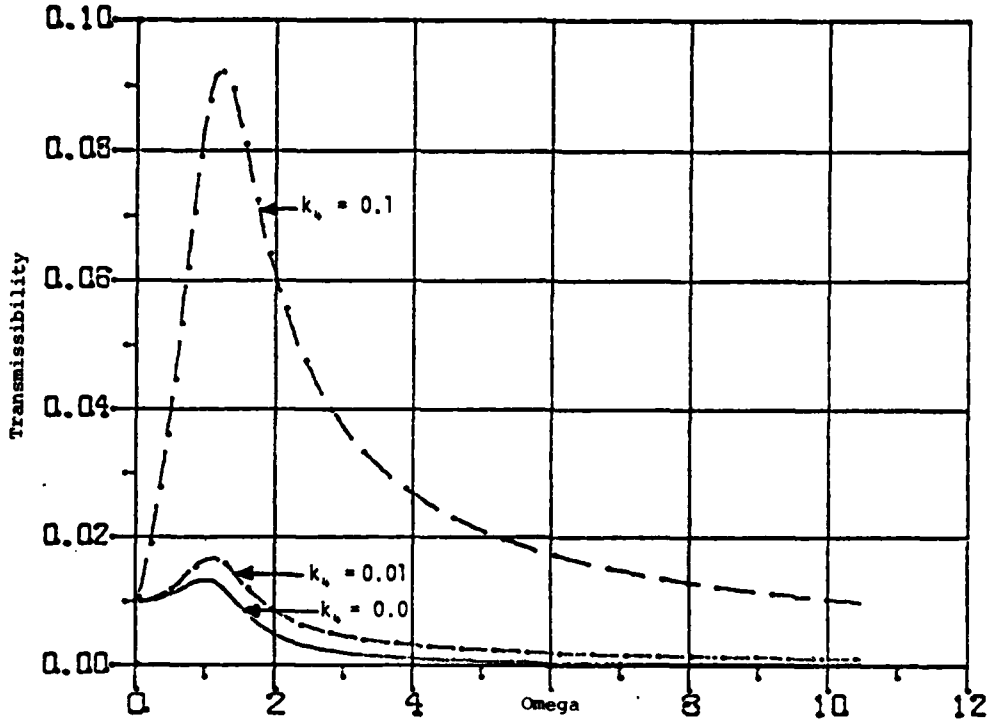

Fig. 8a Transmissibility vs frequency (ω: rad/s) curves when $k_3' = 1.5$, $k_2 = 0$, $k_1' = 1.0$; $k_4 = 0.0$, 0.01 and 0.1.

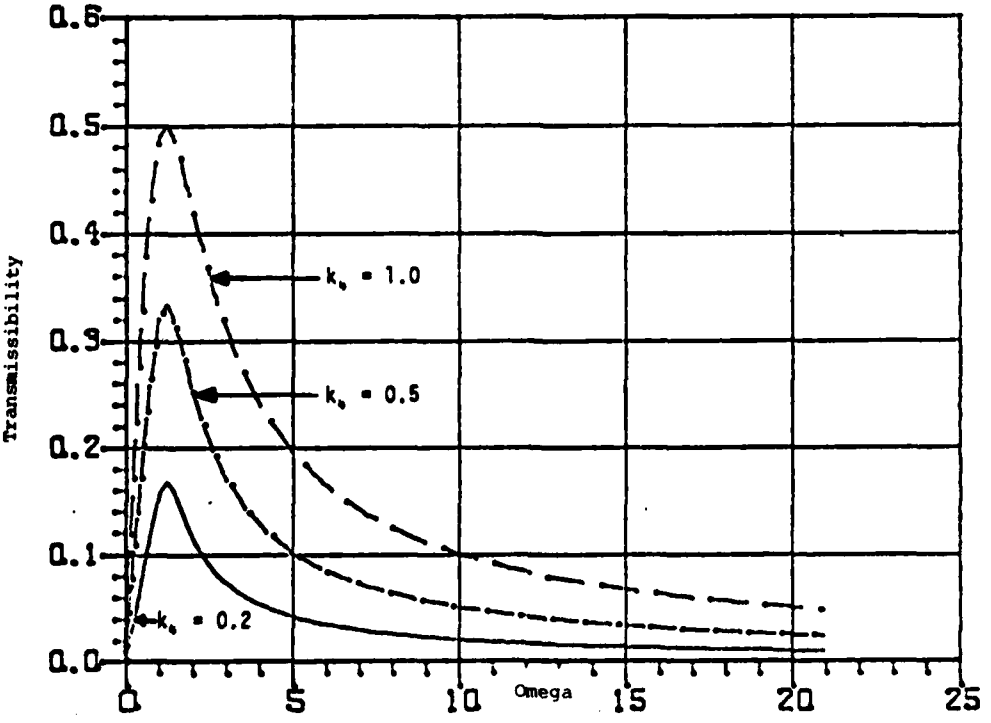

Fig. 8b Transmissibility vs frequency (ω: rad/s) curves when $k_3' = 1.5$, $k_2' = 1.0$, $k_1' = 1.0$; $k_4 = 0.2$, 0.5 and 1.0.

THE EXPERIMENTAL PERFORMANCE OF AN "ON-OFF" ACTIVE DAMPER

E. J. Krasnicki
Lord Kinematics
Erie, Pennsylvania

The experimental performance advantages of the "On-Off" active damper used in a single degree of freedom vibration isolation system have been successfully demonstrated. Utilization of the "On-Off" control scheme simplifies the hardware implementation and reduces the cost of the active damper to a point where general industrial use is feasible. In spite of its simple control scheme, the "On-Off" active damper out-performs conventional passive isolation systems with damping ratios sufficient to limit mass motion amplification at resonance. This paper illustrates the experimental performance of the "On-Off" active damper compared to analytical simulations, passive isolation systems, and experimental "Skyhook" active damper performance.

INTRODUCTION

The active damper concept developed in 1973 by M. Crosby of the Lord Corporation and D. Karnopp of the University of California has since been extensively studied and documented both analytically and experimentally. Reference 1 describes in detail the history, operation, analytical performance, and potential hardware configurations of the active damper. The first hardware prototype of a single degree of freedom system employing a "skyhook" active damper used as a semi-active vibration isolation device was successfully constructed and tested in 1979 at Lord Corporation. The experimental performance of this active damper prototype is presented and compared to the experimental performance of passive isolation systems as well as the analytical performance of passive, active, and semi-active vibration isolation systems in Reference 2.

The active damper, as described in References 1 and 2, has been shown to provide improved vibration and shock isolation approaching that of a fully active system through appropriate modulation of the damping characteristics of a passive viscous damper. The control strategy has been to modulate the passively generated damper force to equal the force that would be generated by a damper to ground ("skyhook" damper) if one were present. This can only be done, of course, when the actual damper force and desired "skyhook" force are of the same sign. Otherwise, the actual force is set to zero (more realistically, an orifice would be modulated to its largest area). The damping coefficient, and therefore the damper force, are controlled by modulation of the damping orifice, independent of the relative velocity across the damper. Only low level electrical power is needed for the necessary signal processing and orifice modulation. Thus, the active damper requires no hydraulic power supply.

Although the hardware implementation of the active damper is significantly simpler and less costly than a complex, fully active system with its large power requirements, the cost and complexity of the active damper using "skyhook" control may still be prohibitive for general industrial utilization. The "skyhook" active damper requires a high bandwidth servovalve and a microprocessor control system capable of implementing a force feedback control loop. In an effort to simplify the hardware implementation and reduce the cost of the active damper to a point where general industrial use is feasible, a simplified "on-off" control scheme is used.

The "on-off" active damper operates as a conventional passive damper during the vibration attenuation portion of the vibration cycle, but assumes a zero damping coefficient when a passive damper would normally accelerate the mass.

In 1975, D. G. Roley[3] analytically studied the use of the "on-off" active damper concept as suspension elements for a farm tractor cab. In his Ph. D. dissertation at the University of California at Davis, Roley determined that good ride quality was achievable with reduced suspension travel

requirements. In 1980, a hardware prototype of a single degree of freedom "on-off" active damper was successfully reduced to practice at Lord Corporation.

The purpose of this paper is to demonstrate the experimental performance of the "on-off" active damper and compare it to analytical simulations, passive isolation systems, and experimental "skyhook" active damper performance. The experimental results of the "on-off" active damper demonstrate its superior performance when compared with conventional passive systems, in spite of its simple control scheme and hardware implementation.

The development work conducted thus far has analytically and experimentally demonstrated the feasibility of an "on-off" active damper through the implementation of an operating hardware prototype.

PASSIVE AND ACTIVE DAMPER SYSTEMS

The analytical performance of the conventional passive vibration control system and the passive "skyhook damper" isolation system, illustrated in Figures 1a and 1b respectively, is discussed quite extensively in References 1 and 2 and therefore will only be summarized here. The differential equation of motion for the suspended mass in the conventional passive, linear system is given by the following expression:

$$m\ddot{x} = -b(\dot{x}-\dot{x}_o) - k(x-x) \qquad (1)$$

This equation reveals that the damper force is opposite in sign but proportional to the relative velocity across the damper. Thus during a portion of the vibration cycle energy is being put into the mass through the damper, resulting in the typical mass spring damper performance.

The "skyhook damper" isolation system, illustrated in Figure 1b, can also be constructed of passive elements. The equation of motion representing this system is given in the following expression:

$$m\ddot{x} = -k(x-x_o)-b\dot{x} \qquad (2)$$

The damper force in this isolation system, $(-b\dot{x})$, is opposite in sign but proportional to the absolute velocity of the mass. In this configuration the "skyhook damper" always removes energy from the mass. Figure 2[2] illustrates the performance of a "skyhook" isolation system utilizing various damping ratios. The performance advantage of the "skyhook" system over a conventional isolation system is evident in two main areas. First is the substantial reduction in the mass motion amplification in the resonance region. Second, the high frequency performance of the "skyhook" damper system has an attenuation rate of 12 db per octave where the conventional system attenuates at a rate of 6 db per octave.

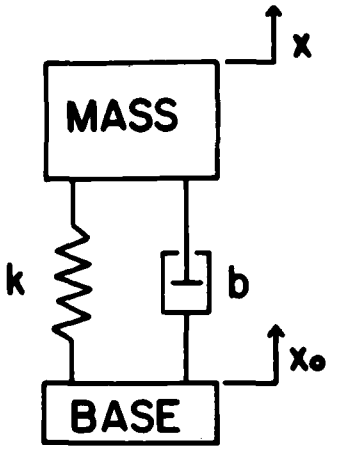

a. Conventional Vibration Isolation System

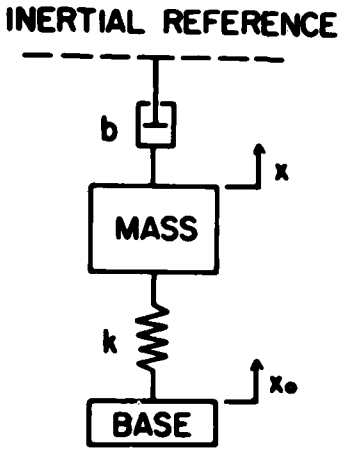

b. The Skyhook Damper Configuration
Figure 1

A detailed explanation of the "skyhook" active damper concept is presented in References 1 and 2. Basically, the "skyhook" active damper is a passive device, but it does have the capability of externally controlling the force generated in the damper independent of the relative velocity across the damper. The varying damper force is generated by modulating the damping coefficient through modification of the damping orifice. The modulating orifice must be capable of adjustments during a single cycle of vibration. Therefore a high bandwidth servovalve must be used.

When the active damper is used in the conventional, base shake, mass-spring-damper

isolation system illustrated in Figure 3, the capability exists to actually generate the "skyhook" damping force, $b\dot{x}$, during part of the cycle of operation. This force developed in the active damper is proportional to the absolute velocity of the mass and is equivalent to the force that would be developed in a viscous damper if it were connected between the mass and an inertial reference frame. Because no external power is supplied to the active damper system, this force can only dissipate energy; therefore the following relationship exists:

$$F=F_d=b\dot{x}, \text{ if } \dot{x}(\dot{x}-\dot{x}_o) > 0 \qquad (3)$$

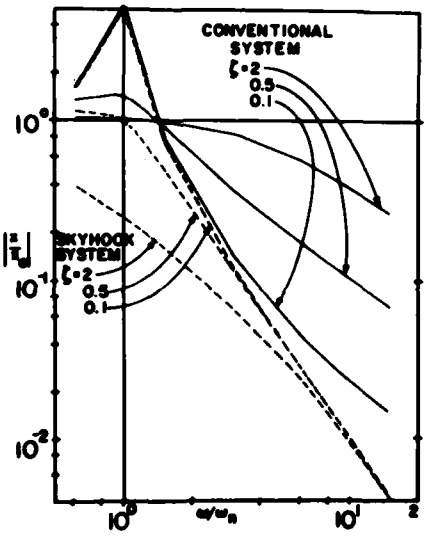

Figure 2
Conventional and Skyhook Passive Systems

In the conventional isolation system configuration, mass deceleration can only be accomplished wherever the sign of the relative velocity (between base and mass) is in proper relation to the absolute velocity of the mass as shown in Equation 3.

As discussed previously, this "skyhook" force is most desirable in isolating base excited vibrations. Whenever the situation exists where the available damper force is opposite in sign to the desired force ("skyhook" force), the best the active damper can do is provide no force, thereby eliminating damper acceleration of the supported mass. This relationship is shown below:

$$F=0, \text{ if } \dot{x}(\dot{x}-\dot{x}_o) < 0 \qquad (4)$$

The condition where the relationship, $\dot{x}(\dot{x}-\dot{x}_o)=0$, exists creates two special cases for

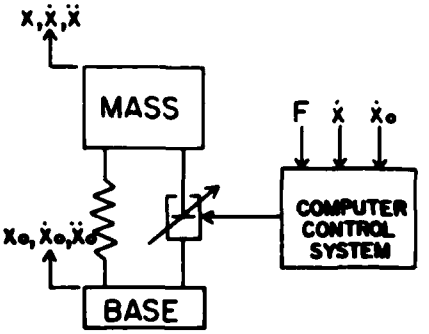

Figure 3
An Active Damper Isolation System

the active damper. The first is that if $\dot{x}=0$, then the desired force $F_d=0$. The second case exists where $(\dot{x}-\dot{x}_o)=0$ and $\dot{x}\neq 0$. Here, the active damper responds by attempting to generate the desired force F_d. If the quantities $\dot{x}$ and $(\dot{x}-\dot{x}_o)$ change so the criteria of Equations 3 or 4 apply, normal control continues. If the desired force $b\dot{x}$ is larger than the maximum available damper force, the active damper will lock up the system resulting in $\dot{x}-\dot{x}_o=0$ for a finite time. During the lock up state the damper force is:

$$F=m\ddot{x}_o + k(x-x_o) \qquad (5)$$

Thus, the two conditions that must exist for the active damper to lock up are that $(\dot{x}-\dot{x}_o)=0$, and that the desired force, F_d, be larger in magnitude than the force determined in Equation 5. Therefore, three possible values of the damper force F exist: (1) the desired force $b\dot{x}$, (2) zero force, or (3) the lock up force. Switching between the three possible force values is determined by the base input and resultant system response. This switching of states makes the active damper, programmed to simulate a skyhook damper, a non-linear element. The performance advantages of the "skyhook" active damper system become quite apparent in Figure 4[2], which is a displacement transmissibility comparing the theoretical responses of a critically damped "skyhook" system, a conventional system, and an active damper system simulating a critically damped "skyhook" damper.

THE ON-OFF ACTIVE DAMPER

As previously described, the damper in a passive isolation system will tend to accelerate or add energy to the supported mass during part of the vibration cycle. The active damper discussed in the previous section utilizes force feedback control to vary the damping coefficient in an

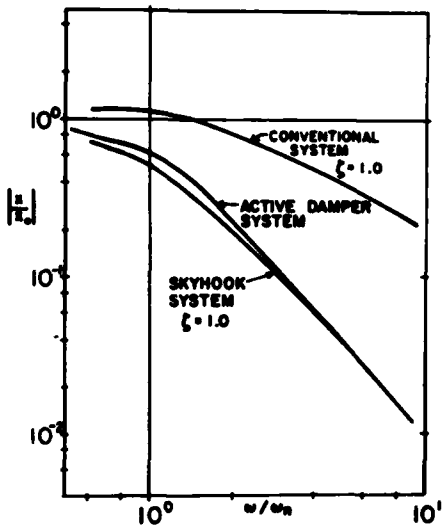

Figure 4
Comparing the Response of Passive and Active Damper Systems

attempt to eliminate damper acceleration of the supported mass. The hardware implementation of this active damper can be significantly simplified if an "on-off" control scheme is used; thus the name "on-off" active damper. In this form the "on-off" active damper operates as a conventional passive damper, with a constant orifice opening, during the part of the vibration cycle when it acts to attenuate vibration, but assumes a zero damping coefficient during the portion of the vibration cycle when a passive damper would normally accelerate the mass.

The "skyhook" active damper logic has already demonstrated that the switching of the damper can be controlled by the term $\dot{x}(\dot{x}-\dot{x}_o)$. If the product of the absolute velocity of the mass and the relative velocity between the mass and the base is positive the damper is switched "on", so a force attenuating mass acceleration is generated. If this term is negative, then the damper is switched "off" so that no force is generated. This switching logic is accomplished through the following damping force equations, using the sign convention of Figure 1a:

$$F_d = b(\dot{x}-\dot{x}_o) \text{ if } \dot{x}(\dot{x}-\dot{x}_o) > 0 \qquad (6)$$

$$F_d = 0 \text{ if } \dot{x}(\dot{x}-\dot{x}_o) < 0 \qquad (7)$$

The equation of motion for a single degree of freedom conventional isolation system utilizing an "on-off" active damper is identical to Equation 1, which is the equation for a conventional passive system except that the damping coefficient is determined by the relative velocity across the damper:

$$m\ddot{x} = -b'(\dot{x}-\dot{x}_o)-k(x-x_o) \qquad (8)$$

where

$$b' = b \text{ if } \dot{x}(\dot{x}-\dot{x}_o) > 0 \qquad (9)$$

$$b' = 0 \text{ if } \dot{x}(\dot{x}-\dot{x}_o) < 0 \qquad (10)$$

Another convenient way to represent the logic relationship between the absolute velocity of the mass and the relative velocity between the mass and the base is shown in Figure 5.

When working with an actual hardware prototype of the active damper, it is impossible to achieve a damping coefficient of zero. Therefore the active damper will actually switch between two damping coefficients, a high value and a low value. Since the objective of the "off" state of the damper is to minimize the acceleration of the mass, the low value of the damping coefficient should be as low as physcially practical. But, because some energy is being transferred to the mass in the "off" state, the performance of the "on-off" active damper prototype will be slightly degraded from the ideal theoretical performance.

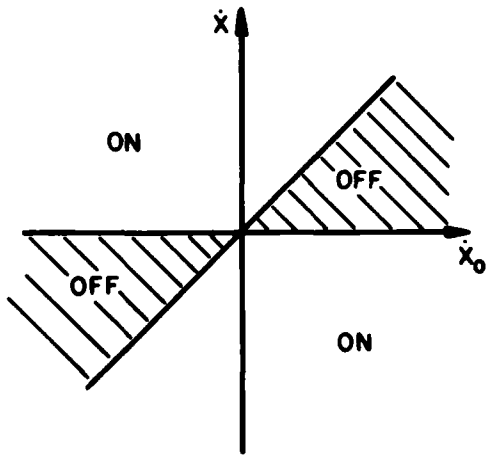

Figure 5
Velocity Relationship for "On-Off" Active Damper Control Logic

THE EXPERIMENTAL PERFORMANCE OF THE "ON-OFF" ACTIVE DAMPER

The active damper prototype utilized in the testing of the "on-off" control policy is the same hardware used to determine the performance of the "skyhook" active damper described in Reference 2. This hardware was developed at Lord Corporation in 1979. The active damper consists

of a hydraulic actuator used in conjunction with an electro-hydraulic servovalve modulating the controlling orifice area. The mass-spring-active damper test system consisted of a 213.6 Kg (471 lb.) mass, resulting in an undamped natural frequency of 1.631 Hz measured at the point of a 90° phase shift between base and mass displacement. The sensor signal processing and control of the servovalve were carried out by digital logic techniques. The performance testing of the active damper using sinusoidal vibration input was conducted using an MTS test machine. Transmissibility and phase information for sinusoidal base excitation were determined using a Hewlett Packard 5420A digital signal analyzer.

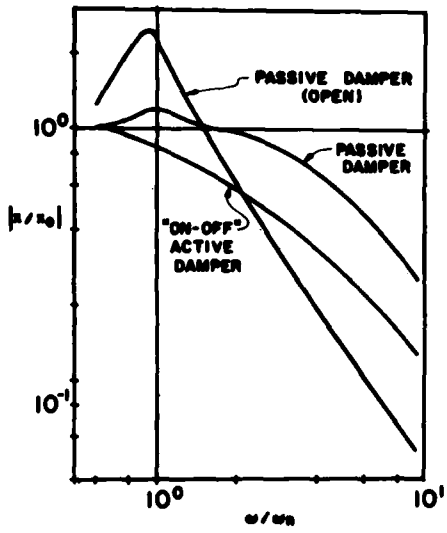

Figure 6
Comparing the Experimental Performance of Passive and "On-Off" Active Damper Systems

Figure 6 illustrates the actual experimental performance of the "on-off" active hardware prototype. This transmissibility curve of the "on-off" active damper is presented with the experimental curves of two constant orifice passive damper systems. This constant orifice damper is actually the varying orifice active damper hardware held at a constant orifice opening with a constant D.C. voltage applied to the valve. The damper open curve represents the most lightly damped system attainable with this test rig. The damper open curve corresponds to the "off" state of the "on-off" active damper. This state is achieved by applying full voltage to a normally closed valve. The third curve represents a highly damped passive system.

In this test the "on-off" active damper was switched between an "off" state in which full command voltage was applied to the valve, and a very heavily damped "on" state in which zero voltage was applied to the valve. In this latter case the valve was almost totally closed off. Leakage flow through the valve in the closed position was not a significant factor.

The performance comparison of Figure 6 reveals the significant performance advantage of the "on-off" active damper over a passive isolation system with a damping value adequate to limit the mass motion amplification at resonance. This advantage is apparent in both the resonance and the high frequency regions. The "on-off" active damper achieves system isolation at the natural frequency of the undamped system while still providing adequate performance improvement in the high frequency region. When compared with the lightly damped (open) passive system, the performance of the "on-off" active damper is obviously superior in the resonance region. At the damped natural frequency the open system has a transmissibility of 2.5 where the active damper provides isolation with a transmissibility of 0.89. In the high frequency region, the performance of the open passive system is better, but for any passive system with good high frequency performance one must also accept significant amplification at resonance.

Theoretically, the high frequency performance of the "on-off" active damper system should be superior to that of an isolation system with a constant damping value equivalent to the "off" setting of an "on-off" active damper. This is possible because the "on", or more highly damped state of the "on-off" active damper, makes it possible to remove more energy from the mass during a given vibration cycle. Thus, the high frequency displacement transmissibility of the "on-off" active damper system should be superior to the passive system.

Figure 7 compares the actual experimental performance of the "on-off" active damper with the transmissibility plots of two moderately damped passive suspension systems. Again, these constant orifice dampers are actually the active damper hardware held at a constant orifice opening with a constant D.C. voltage applied to the servovalve. The performance advantage of the "on-off" active damper is demonstrated quite clearly.

Figure 8 illustrates the experimental performance of the "on-off" active damper compared with the experimental performance of the continuously variable "skyhook" active damper. The displacement transmissibility curve of a passive damping system with minimum damping is also included for comparison. The experimental performance curve for the "skyhook" active damper is taken from Reference 2. As mentioned previously, the same hardware was utilized for both the "skyhook" and "on-off" active damper testing. The base input displacements and frequencies were also identical. This plot clearly illustrates that the performance of the "on-off"

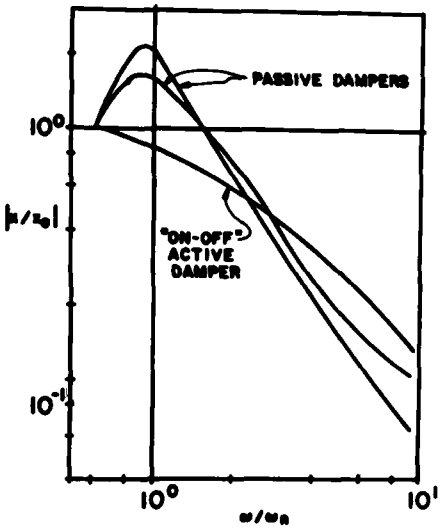

Figure 7
Comparing the Experimental Performance of Passive and "On-Off" Active Damper Systems

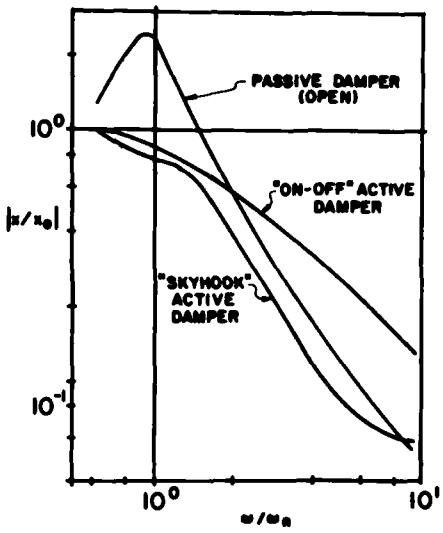

Figure 8
Comparing the Experimental Performance of Passive, "On-Off", and "Skyhook" Active Damping

active damper approaches that of the "skyhook" system in the resonance region. The high frequency performance of the "on-off" active damper prototype is degraded somewhat from the performance of the skyhook active damper system. It is interesting to observe that the "skyhook" active damper prototype outperforms both the lightly damped passive isolation system and the "on-off" active damper throughout the entire frequency range tested.

Figure 9 illustrates the performance of an "on-off" active damper with a heavily damped "on" state, compared with the same damper using a critically damped "on" state. All "on-off" active damper performance data previously discussed in this paper was determined using an active damper isolation system with a heavily damped "on" state. Utilizing the more lightly damped system provides better high frequency performance at the cost of increased mass motion amplification of resonance. As the value of damping used in the "on" state of the active damper is varied, the performance of the system is modified. Typically, as the value of damping used for the "on" state is decreased, the high frequency performance improves and the performance in the resonance region degrades. Therefore, the "on-off" active damper may be tuned to meet the high and low frequency performance requirements of individual systems.

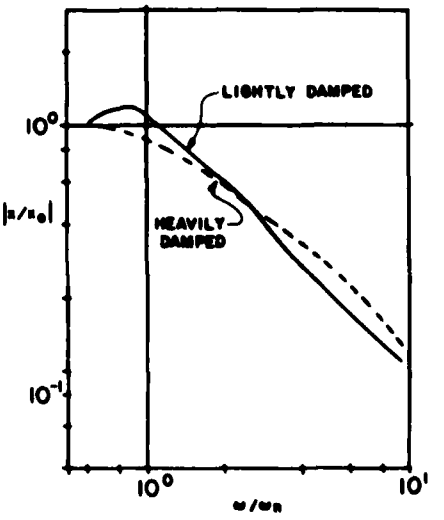

Figure 9
The "On-Off" Active Damper with Modified Damping Values

CONCLUSIONS

The experimental performance of an "on-off" active damper used in a conventional isolation system configuration has been demonstrated. The simplified "on-off" control scheme eases the hardware implementation and reduces the cost of

an active damper by not requiring a high bandwidth servovalve and microprocessor control system, as does the "skyhook" active damper. In this way the "on-off" active damper hardware is approaching the point where general industrial use of the active damper performance advantages is feasible. These performance advantages of the "on-off" active damper appear quite significant when comparisons are made with a passive isolation system with a damping value adequate to limit the mass motion amplification at resonance.

The performance limitations of the "on-off" active damper, particularly in the high frequency region, are apparent when compared with the "skyhook" active damper. But this difference in performance may be justified by the increased simplicity in the "on-off" active damper hardware, control logic, and control implementation, over the "skyhook" active damper. Both the "skyhook" and "on-off" active damper isolation systems are significantly simpler and less costly than a fully active isolation system which is typically complex, expensive, and requires large quantities of power. The justification of the "on-off" active damper's simplicity becomes substantial when the superior performance of the "skyhook" active damper is not a necessity, but when the desired performance cannot be obtained with a conventional passive system.

REFERENCES

1. Karnopp, D.C., Crosby, M.J., Harwood, R.A., "Vibration Control using Semi-Active Force Generators," ASME Paper No. 73-DET-123 (June, 1974).

2. Krasnicki, E.J., "Comparison of Analytical and Experimental Results for a Semi-Active Vibration Isolator," Proceedings of the 50th Shock and Vibration Symposium, Colorado Springs, Colorado (1979).

3. Roley, D. G., "Tractor Cab Suspension Performance Modeling," Ph. D. Thesis, University of California, Davis, California (June, 1975).

5185B/djr

FLUID-STRUCTURE INTERACTION

AN EVALUATION OF: DOUBLY ASYMPTOTIC APPROXIMATION; STAGGERED SOLUTION SCHEMES; USA-STAGS

R. S. Dunham, R. J. James, A. S. Kushner and D. E. Ranta
Pacifica Technology
San Diego, California

This report presents a comprehensive review and evaluation of the doubly asymptotic approximation and the staggered solution scheme implemented in the USA-STAGS computer codes. The equations are derived and discussed in detail. Various solution strategies are examined. A stability analysis of the staggered scheme and a fully implicit integration scheme is done using the Lax-Richtmyer approach. Solutions to several problems are presented and comparisons made to closed form solutions. Detailed conclusions and recommendations are made, and appendices provide a list of errors and recommeded improvements in both the USA and STAGS codes.

1. INTRODUCTION

The calculation of the response of submerged shell structures to acoustic wave loads is a problem of significant interest within the naval community. Among the early directly applicable studies were those of Carrier[1] and of Mindlin and Bleich[2] who studied the two-dimensional elastic response of a cylinder to a step wave loading. No attempt will be made in this report to review all such pertinent works. The significant point is that analytical solutions are restricted to very simple, two-dimensional structural configurations and simple fluid loads within the content of acoustics. The analysis of complex, three-dimensional structures almost always requires the utilization of a numerical discretization procedure such as the finite element or finite difference method.

For realistic structures under conditions of general incident fluid loadings, the solution of the full fluid-structure interaction equations poses a computationally intractable problem. This has lead to the development of a series of techniques referred to as surface interaction approximation techniques. An excellent historical review of applications of these techniques has been given by Geers[3]. The theoretical foundations for such techniques were presented by Carrier[4] and summarized by Huang[5]. The most successful of these techniques has been the doubly asymptotic approximation (DAA)[6]. This report is concerned with evaluating the computational aspects of the numerical implementation of the DAA. The DAA and all other commonly used surface interaction approximations are restricted to the interaction of a structure with an acoustic medium. We shall not address the limitations and restrictions which this assumption implies, although we do feel that the implications of utilizing the DAA at high incident pressure levels (5,000 psi) is a subject which should be studied in greater detail. Another serious restriction associated with the implementation of the DAA is the ignoration of incident wave diffraction by the target structure. While we will not study diffraction effects themselves, we shall discuss how ignoring of diffraction leads to an inconsistency in the incident wave definition.

The next section of this report contains a general discussion of the DAA and of the various techniques proposed for its implementation. Next a numerical evaluation of the stability and damping characteristsics of the displacement extrapolation method of integrating the DAA equations is presented. This analysis follows the classical Lax-Richtmyer approach and provides an alternate evaluation to the approach of Park et al.[7]. Lastly the USA-STAGS code, developed for transient, fluid-structure interaction via the DAA, is used to solve several benchmark cases. The results of these computations are assessed in terms of their implications concerning the DAA and staggered solution procedures, and, a comprehensive set of conclusions and recommendations are given. Detailed evaluations and suggestions for improvement of the STAGS and USA codes are given in appendices.

2. BACKGROUND

In this section the Doubly Asymptotic Approximation (DAA) is described and discussed in conjunction with various solution strategies including the staggered solution scheme. The DAA methodology has been advanced by the pioneering work of Geers and his colleagues at Lockheed. The DAA has been described in many recent publications[3-24] which tend to focus on the mathematical formulations and specialized generic

applications. The most expository discussions are given in references [5 & 24], and general reviews are given in references [9 & 10].

The DAA is a method that combines two basic ideas in a manner that is physically appealing. In addition to the clever combination of the asymptotic solutions, Geers and others were able to express the basic equations in a matrix form that was convenient and suitable for combination with conventional finite element and finite difference codes[24,25].

DAA Equations

Consider an acoustic, plane shock wave impinging on a rigid structure submerged in an infinite fluid. Let* P_i and u_i represent the incident pressure and scalar velocity at a point on the structure; both are functions of time. If the structure is a rigid plane, then the rigid-body scattered pressure (P_s) at that point can be expressed

$$P_s = \rho c \dot{u}_i \qquad (1)$$

where ρ is the fluid density and c is the acoustic wave speed. In actual practice, equation (1) is used for structures that are not plane and for plane, cylindrical, and spherical waves. The utilization of equation (1) for non-planar structures and incident waves is, of course, approximate. The most serious approximation is undoubtly the interference to the incident wave caused by reflections. For typical applications, equation (1) is recast into the form

$$P_s = -\rho c(\underset{\sim}{n} \cdot \dot{\underset{\sim}{u}}_i - \underset{\sim}{n} \cdot \dot{\underset{\sim}{u}}) \qquad (2)$$

where n is the outward normal vector, u_i is the incident velocity vector, and u is the velocity vector for a point on the structure. Equation (2) is applied at all points on the wetted surface of the structure. The two terms on the right-hand side are called the rigid body scattered pressure and non-rigid body scattered, or radiated, pressure, respectively. In the sequel, the combined effects will sometimes be called the scattered pressure, but the meaning should be clear from the context.

Equation (2) is generally accepted to be a good approximation to the true hydrodynamic behavior for short times, provided that the curvature of the incident wave is small compared to that of the structure, and the pressure is in the acoustic regime ($p_i < 5000$ psi). A physical basis for equation (2) is that the fluid is unable to move away from the structure, and is compressed as a result of their relataive motions. There is no suitable general definition of short time, however, times greater than the longest natural period of the fluid-structure system are clearly not short.

At long times, the fluid-structure system is assumed to vibrate in its lowest frequencies and corresponding mode shapes. Because this motion is slow compared to the incident wave velocities, the fluid is assumed to act as an incompressible, inviscid media. This is also generally accepted to be a good approximation, and it has been demonstrated that long wavelength acoustic fluid-structure response asymptotically approaches incompressible, inviscid flow[26]. The physical basis for this assumption is that the fluid around the structure moves in-phase with the structure without being compressed. This assumption is commonly used in analyzing the response of fluid-structure systems such as dams and reservoirs to earthquakes[27]. The theory and solution of incompressible, inviscid flow equations are well known. For present purposes, the most convenient representation is*

$$[A]\{P_s\} = [M_A]\{\underset{\sim}{n} \cdot \ddot{\underset{\sim}{u}}\} \qquad (3)$$

where [A] is a diagonal matrix of tributary areas, $\{P_s\}$ is a vector of pressure acting at the fluid-structure interface as a result of the structural motion, $[M_A]$ is the full, symmetric, so-called added mass matrix of the fluid, and $\{n \cdot u\}$ is the normal component of the acceleration of the fluid-structure interface referred to the same set of points used for the pressure. A more complete presentation of the derivation of equation (3) is given by Roderick, et al.[25], and DeRuntz, et al.[28,29]. The added mass matrix can be computed from a Green's function solution to the acoustic problem or from a condensed finite element mesh. However, the numerical procedures used in references [25] and [28,29] to perform the actual computations differ considerably. The standard matrix ([ ]) and vector ({ }) notation used in equation (3) is intended to refer to a vector of nodal point [25] or element [28] surface pressures. The fluid points are usually chosen to coincide with the centroids of the structural elements of the structural nodal points for convenience, although this is not a requirement[29].

It is important that the acceleration vector in equation (3) is not that of the incident wave, it is the acceleration caused by the motion of the fluid-structure system. The scattered pressure in equation (3) has the same meaning as that in equation (2), except, of course, there is no rigid body scattering component. Equation (3) is fundamentally different from equation (2), reflecting the differences in acoustic theory and incompressible, inviscid theory. Equation (3) would, presumably, be a good approximation of the scattered pressure at late times after the incident wave transient has passed.

The Doubly Asymptotic Approximation

The contribution of the DAA is in combining equations (2) and (3) so that the motion of the fluid-

*Superimposed dots denote time derivatives, e.g., $\dot{u} = \frac{\partial u}{\partial t}$

*The matrix notation '] and { } will generally refer to nodal point quantities, whereas the tensor notation $\underset{\sim}{u}$ will generally refer to Cartesian quantities.

structure system can be approximated continuously from the short time shock response to the long time low frequency response. To accomplish this, equation (2) is written at the same discrete points used for equation (3)

$$\{P_s\} = -\rho c \{\underset{\sim}{n} \cdot \dot{\underset{\sim}{u}}_i - \underset{\sim}{n} \cdot \dot{\underset{\sim}{u}}\} \quad (4)$$

Equations (2) and (3) are then solved for the normal components of the nodal velocities;

$$\{\underset{\sim}{n} \cdot \underset{\sim}{u}\} = \frac{1}{\rho c} \{P_s\} + \{\underset{\sim}{n} \cdot \dot{\underset{\sim}{u}}\} \quad (5)$$

and

$$\{\underset{\sim}{n} \cdot \dot{\underset{\sim}{u}}\} = [M_A^{-1}] [A] \int_0^t \{P_s\} d\tau , \quad (6)$$

respectively. It is necessary to integrate equation (3) with respect to time, and this is done assuming the initial velocity vanishes.

The terms on the left-hand side of equations (5) and (6) are not the same, although the same symbols have been used for them. Roderick, et al [25] refer to the short time motion of equation (5) as the "first kind" of motion and the long time motion of equation (6) as the "second kind" of motion. No such distinction is made here to emphasize the basic methodology of the DAA.

The basic approximation of the DAA in combining these two types of motion into a single equation is that the total motion of the structure is the sum of the short and long time motions. Thus, the DAA equation becomes

$$\{\underset{\sim}{n} \cdot \dot{\underset{\sim}{u}}\} = \frac{1}{\rho c} \{P_s\} + \{\underset{\sim}{n} \cdot \dot{\underset{\sim}{u}}_i\} + [M_A^{-1}] [A] \int_0^t \{P_s\} d\tau \quad (7)$$

or as it is more commonly written

$$\frac{1}{\rho c} \{P_s\} + [M_A^{-1}][A] \int_0^t \{P_s\} d\tau = \{\underset{\sim}{n} \cdot (\dot{\underset{\sim}{u}} - \dot{\underset{\sim}{u}}_i)\} \quad (8)$$

The preceeding development departs from the u_1, u_2 notation [25] to emphasize that the DAA equation cannot be derived from basic principles; the DAA equation itself is an approximation. This is not a criticism of the DAA, rather it is an attempt to give insight into the very fundamental physical approximations of the method. Indeed, the DAA has been successfully used in many applications.

Structural Equation Of Motion

The equation of motion for a linear elastic undamped structure is

$$[M] \{\ddot{u}\} + [K] \{u\} = \{F\} , \quad (9)$$

where [M] is the consistent or lumped structural mass matrix, [K] is the structural stiffness matrix, and {F} is a vector of applied nodal point forces. The nodal points used for the structural discretization include both "wet" and "dry" points as necessary. The wet structural nodes can be the same as the points used to identify the pressure and normal fluid velocity in equations (3) and (4) [25], or the fluid points can be taken at the center of one or more wet structural elements [29]. When the discretization for the fluid and structural surface elements do not coincide, it is necessary to introduce a transformation matrix to combine equations (8) and (9) [7]. This complicates the formulas, and because it does not contribute to an understanding of the fundamental principles, it is omitted from the present development.

Equation (8) and (9) are the standard form of the DAA fluid-structure interaction equations. These equations are strongly coupled because the structural velocity vector appears explicitly in (8) and the force vector on the right-hand side of (9) depends explicitly on the scattered pressure.

Solution Strategies For The DAA Equations

Equations (8) and (9) can be solved in many different ways [12,16-19]. The particular strategy used can have a dramatic effect on the stability of the results [7,30]. Since the majority of finite element structural analysis codes contain implicit conditionally or unconditionally stable time marching algorithms [32], it would be desirable for accuracy and stability to use similar algorithms on the coupled DAA equations. This approach was rejected by Lockheed because the computational effort was deemed excessive. Generally, there is one pressure degree-of-freedom for every wet structural element or node. Since the structure is typically a shell there are 5 or 6 degrees-of-freedom per node. Thus, adding the pressure unknowns to the solution vector would only increase its length by 20 percent. However, the added mass matrix is full[25,28,29], not banded like the structural mass and stiffness matrices. Thus, even if a bandwidth optimizer is used, the bandwidth is likely to increase by 100-200 percent which would increase the computational expense by 300-1000 percent. Of the many strategies proposed to solve the DAA equations, the most successfully and widely used is the staggered solution procedure[7,29].

Although not discussed herein, there would seem to be a use for explicit methods to solve the DAA equations when used in conjunction with an explicit finite difference structural code. Since small (Courant stability) time steps must be used in the structural code, there may be no additional stability penalty to be paid for the solution of the fluid equations. This seems particularly attractive for the early time response.

Staggered Solution Procedures

Park, et al.[7] have described several possibilities for effecting a staggered solution procedure including: Pressure Extrapolation (PE); Pressure-Integral Extrapolation (PIE); Velocity Extrapolation (VE); and Displacement Extrapolation (DE). All methods are named to indicate the variable that is first extrapolated. For example, in the PE procedure the pressure is extrapolated from the present time (using a single or multistep formula) to the end of the current step (e.g., $p_1 = p_o + \dot{p}_o \Delta t$, etc). The extrapolated pressure is then used to define the right-hand-side of (9) which in turn is solved for the structural displacements, velocities and accelerations. The new structural velocities are then used to solve (8) to give the new pressures. The "staggered" procedure can be terminated at this point if, for example, the extrapolated pressure agrees with the computed pressure, or an additional iteration* can be made through (9), or through both (9) and (8). However, the simplest and cheapest approach is the basic 3 steps:

(1) extrapolate $\{p_s\}$;

(2) solve (9) for $\{u\}$, $\{\dot{u}\}$, $\{\ddot{u}\}$; ; and

(3) solve (8) for $\{p_s\}$.

The stability analysis of the PE formulation performed by Park, et al.[7] gave several interesting conclusions: most, but not all, PE iterative methods are conditionally stable; the stability limit imposes restrictions on the time step size similar to explicit methods; and, there is no stability advantage to performing iterations, indeed, there are disadvantages. Obviously, Park, et al.[7] recommended against the use of the PE. The present authors concur with this recommendation.

The VE procedure is essentially the same as the PE except that the structural velocity is extrapolated and used to define the right-hand-side of (8) which is solved for the pressure which is then used to drive the structural equation (9). Park, et al.[7] did not explcitly treat the VE procedure, however, they claim that its stability properties are identical to the PE. Thus, they did not recommend the VE procedure. The present authors also concur with this recommendation. The PE and VE methods are not desirable because the pressure anad velocity are primary variables that in a typical problem change rapidly. Extrapolation is more accurate when applied to the pressure impulse and/or displacement because they change more slowly and often are monotonic.

Pressure Integral Extrapolation (PIE)

The PIE procedure does not solve equations (8) and (9) directly, instead, a modification of the basic equations is made. The force vector on the right-hand-side of (9) is expressed

$$\{F\} = -[GA]\{P_i + P_s\} \tag{10}$$

where the matrix [GA] is a concatenation of the transformation matrix [G] and area matrix [A] used in reference [7]. This represents the consistent force vector applied to the structure as a result of the incident and scattered pressure. The scattered pressure in equation (10) is then replaced from equation (8) by

$$\frac{1}{\rho c}\{P_s\} = \{\underset{\sim}{n} \cdot (\dot{\underset{\sim}{u}} - \dot{\underset{\sim}{u}}_i)\} - [M_A^{-1}][A]\int_o^t \{P_s\}\, d\tau \tag{11}$$

Substituting (11) into (10), and into (9) gives

$$[M]\{\ddot{u}\} + [K]\{u\} = -[GA]\{\{P_i\} + \rho c\, \underset{\sim}{n} \cdot (\dot{\underset{\sim}{u}} - \dot{\underset{\sim}{u}}_i) - \rho c [M_A^{-1}][A]\int_o^t \{P_s\}\, d\tau\} \tag{12}$$

in which only the integral of the scattered pressure appears. The unknown structural velocity $\{\underset{\sim}{u}\}$ is moved to the left-hand-side where it assumes the role of a structural damping

$$[M]\{\ddot{u}\} + [GA_n]\{\dot{u}\} + [K]\{u\} = -[GA]\{\{P_i\} - \rho c\, \underset{\sim}{n} \cdot \dot{\underset{\sim}{u}}_i \rho c [M_A^{-1}][A]\int_o^t \{P_s\}\, d\tau\}\,. \tag{13}$$

The PIE staggered solution procedure is to extrapolate the pressure time integral (impulse), solve equation (13) for the structural variables, and then solve equation (8) for the scattered pressure. Iterations are possible but not recommended. The PIE has good stability characteristics and has been shown to iterate to unconditional stability[7].

Park, et al.[7] do not recommend the PIE procedure because it involves modifying the structural equations with the damping matrix $[GA_n]$. The present authors disagree with this philosophy and strongly recommend a thorough evaluation of the PIE. It offers several very appealing features: the addition of structural damping at early time is desirable for shock loadings; the damping matrix is banded; the extrapolation of the integral of pressure is likely to be quite accurate because the integral is almost monotonic; the damping matrix can be neglected or reduced on an element by element basis after the shock has abated at, say, one-half to one transit times; and the accuracy of the PIE appears better than the DE[7]. The addition of a damping matrix to any well written structural code is straightforward. The philosophy of not modifying the structural code seems unwarranted.

*Iterations of the structural equations should be avoided because of their expense. Smaller time steps are preferable to iterations.

Displacement Extrapolation (DE)

The method selected by Lockheed for implementation of the USA code is the displacement extrapolation procedure[7,33]. The DE procedure likewise requires a modification of the basic DAA equations. Instead of using the integral form of (8) in which the pressure and pressure impulse appear, the equation is differentiated once in time to give

$$\frac{1}{\rho c}\{\dot{P}_s\} + [M_A^{-1}]\,[A]\,\{P_s\} = \{\underset{\sim}{n}\cdot(\ddot{\underset{\sim}{u}} - \ddot{\underset{\sim}{u}}_i)\} \tag{14}$$

However, the structural acceleration now appears on the right-hand-side of (14). To obtain the desired displacement, (9) with (10) substituted for the right-hand-side is solved for acceleration in terms of displacement, i.e.,

$$\{\ddot{u}\} = -[M^{-1}]\,[GA]\,\{P_i + P_s\} - [M^{-1}]\,[K]\,\{u\}\ . \tag{15}$$

This indicates that the mass matrix of the structure is assumed to be lumped or diagonal; an assumption that is undesirable for the cubic elements used in the USA-STAGS code because it reduces the modeling advantages of higher order elements. Equation (15) can now be substituted into (14) to give

$$\frac{1}{\rho c}\{\dot{P}_s\} + [[M_A^{-1}]\,[A] + [M^{-1}]\,[GA]]\,\{P_s\} = -\underset{\sim}{n}\cdot\{[M^{-1}]\,[GA]\,\{P_i\} + [M^{-1}]\,[K]\,\{u\} + \{\ddot{u}_i\}\} \tag{16}$$

It is suprising that this form was chosen because better numerical results are almost always obtained from higher order formulas (i.e., the PIE with P_s & u_i). Also, the DE procedure considerably complicates the equations and requires that the structural mass be diagonal. We do not agree that this complication and limitation are warranted.

The DE solution procedure is to extrapolate the structural velocity vector, solve equation (16) for the pressure, then solve equation (9) and (10) for the structural variables, and finally equation (16) is resolved to obtain a slightly improved pressure. This final step is of unknown value, because it only influences the pressure used in the next step.

Removal Of Shock Wave Singularities

The actual equations implemented by Lockheed in USA-STAGS are further complicated by the procedures used to remove the singularities in the incident acceleration vector in equations (14 & 16).* Since the USA code is primarily a three-dimensional code, only the case of a spherical wave will be considered. Let S be a reference standoff distance. Usually S is the distance from the source of the spherical wave to a pressure transducer that records the pressure time history at that point. (It is convenient but not necessary that S also be the distance from the source to the nearest point on the structure.) Let P(t) be the pressure time history measured at the standoff distance. Then the incident pressure at any point (on the structure) is

$$P_i(R,t) = \frac{S}{R}\,P\left(t - \frac{R-S}{c}\right), \tag{17}$$

where R is the distance from the source to the point on the structure, and c is the wave speed. Equation (17) shows that the incident pressure amplitude decays as 1/R. It is understood by the context that when the corresponding incident velocity is

$$\dot{u}_i(R,t) = \frac{S}{R}\,\frac{P\left(t - \frac{R-S}{c}\right)}{\rho c} + \frac{S}{R^2\rho}\int_0^{t-\frac{R-S}{c}} P(\tau)\,d\tau\ , \tag{18}$$

and the incident acceleration is

$$\ddot{u}_i(R,t) = \frac{1}{\rho c}\dot{P}_i(R,t) + \frac{1}{\rho R}P_i(R,t) \tag{19}$$

The singularity in the incident acceleration occurs from the time derivative of P_i at $t = R-S/c$. There is a discontinuity, but no singularity in the incident velocity.

In order to remove this singularity, a "modified" pressure is defined as

$$P_m = \Gamma\,P_i + P_s \tag{20}$$

where Γ is the direction cosine between the inward normal to the structure and the radius vector from the spherical source. Without reproducing the extensive algebra required, substituting (20) into (12) and (16) gives

$$[M]\,\{\ddot{u}\} + [K]\,\{u\} = [GA_n]\,\{P_m + (1-\Gamma)\,P_i\} \tag{21}$$

and

$$\frac{1}{\rho c}[A]\,\{\dot{P}_m\} + [D]\,\{P_m\} = -[GA_n]^T[M^{-1}][K]\,\{u\} - [H]\,\{P_i\}\ . \tag{22}$$

*These singularities were introduced in the DE implementation by the time differentiation; the incident velocity vector is discontinuous but not singular.

The details of the matrices [D] and [H] are given in reference [29].

Lockheed refers to (21) and (22) as the modified, augmented, interaction (DAA) equations. The differences between the basic DAA equations given in (8) and (9), and the modified, augmented equations are substantial. The motivation for using (21 & 22) is that the structural code, e.g., STAGS used for the solution (21) can be separated, except for the right-hand-side calculation, from the solution of (22), e.g., USA.

Solution Procedure Used In USA-STAGS

The staggered solution procedure implemented in the USA-STAGS code is as follows:

(1) extrapolate the structural displacements $\{u^*\}$;
(2) using the extrapolated displacements, solve (22) for $\{p_m{}^*\}$;
(3) using $\{p_m{}^*\}$, solve (21) for $\{u\}$, $\{\dot{u}\}$, and $\{\ddot{u}\}$ at the next time step; and
(4) using $\{u\}$, solve for $\{p_m\}$ at the next time step.

The extrapolation is actually performed on the structural force $[K]\{u\}$, not the displacement; in a nonlinear problem this is an important difference. There are 3 extrapolation formulas, two for starting up and one for the typical case. Let $\{f\}_n = [K]\{u\}_n$, the structural forces at the n^{th} time step. Then, the start up extrapolation procedure is

$$f_1^* = f_o \tag{23}$$

for the initial step and the first step after a restart (f_o is based on the initial displacements). The next step is extrapolated using

$$f_2^* = 2f_1 - f_o , \tag{24}$$

and the procedure for a typical step is

$$f_{n+1}^* = 2.5f_n - 2f_{n-1} + .5f_{n-2} \tag{25}$$

These formulas are limited to a constant time step, which is a restriction on the USA code.

The solution for the fluid pressure in steps (1) and (4) is done using the Park time marching scheme[34,35]. This is an average of the Gear 2nd and 3rd order methods[36], but with superior accuracy and convergence features. The procedure for a typical step is

$$P_{n+1} = .6\Delta t\, P_{n+1} + 1.5\, P_{n-1} + .1\, P_{n-2} \tag{26}$$

Since the procedure involves the history from 3 previous steps, there is a 2 step start-up procedure

$$P_1 = .6\Delta t\, P_1 + P_o + .4\Delta t\, P_o \tag{27}$$

and

$$P_2 = .6\Delta t\, P_2 + 1.2\, P_1 - .2\, P_o + .2\Delta t\, P_1 \tag{28}$$

Equations (26-28) are also limited to a constant time step size.

The solution of the structural equations can be done several ways. If STAGS is used then there are several integration options: explicit central difference; implicit trapezoidal; implicit 2nd or 3rd order Gear; and the implicit Park method. If the USA code is used with any other structural code, then the structural response is done within USA using the trapezoidal rule and only linear response can be calculated. The trapezoidal rule can be expressed

$$\dot{u}_{n+1} = \dot{u}_n + \frac{1}{2}(\ddot{u}_n + \ddot{u}_{n+1})\,\Delta t \tag{29}$$

and

$$u_{n+1} = u_n + \dot{u}_n \Delta t + \frac{1}{4}(\ddot{u}_n + \ddot{u}_{n+1})\,\Delta t^2 \tag{30}$$

Computation Of Incident Pressure In USA

The procedures used by Lockheed for the evaluation of the right-hand side of equations (21 & 22) are critically important to the overall accuracy of the solution, and since these are not explicitly discussed in any of their reports, a brief description will be given herein.

The USA code is based on an interpolation of the pressure at the centroid of a fluid element which can overlap one or more wet structural (shell) elements. This of course, limits the accuracy of the structural force vector, which is calculated assuming the right-hand-side of (21) is constant over the fluid, and, consequently, the structural elements it contains. The normal vector to the structural element is likewise interpolated at only one point.

The procedure used for the right-hand-side of (22) is much more detailed, presumably to properly account for the moving wave. A total of 17 points are evaluated to compute the incident pressure on a single element. One point is at the center of the fluid element, and there are 2 rings with 8 points each (every 45) located at radii of 0.296 and 0.491 times the square root of the area of the fluid element. This procedure is used for all fluid element without discrimination to element shape. Various approximations are used to account for the orientation of the element and its curvature; these limit accuracy when the element is close to the source.

The present authors suggest that alterante procedures be investigated for the computation of the right-hand-sides of the DAA equations. In particular, the shape of the element should be taken into account and a Gaussian quadrature formula, either a 3x3 or 4x4, used to perform the integration. An improvement in accuracy, at a minimal computational penalty, could be achieved if

the fluid nodes coincided with the structural nodes rather than being positioned at the element centroids.

Summary

This background section has given a very detailed description of the DAA equations, staggered solution schemes to solve these equations, and a description of how these equations were actually implemented and solved in the USA-STAGS computer programs. In the next section, a detailed analysis of the staggered solution scheme used in the USA-STAGS code is given.

3. NUMERICAL ANALYSIS OF THE USA-DAA INTEGRATION OPERATOR

The modal decomposition of the governing equations of motion describing a structure interacting with an acoustic medium results in the following equations for a two-degree of freedom system[7]

$$m_s \ddot{u} + k_s u = -a\dot{q} \tag{31}$$

$$m_f \dot{q} + \rho c a q = \rho c m_f \dot{u} \tag{32}$$

where u represents the structural displacment, u the structural acceleration, $\dot{q}$ the pressure in the fluid, and q its time integral. The constants ρ and c are the fluid density and the speed of sound in the fluid respectively. The quantities m_s, m_f, and k_s are measures of the structural modal mass, fluid modal mass, and structural modal stiffness, respectively, and the parameter a corresponds to the wetted surface area.

Displacement Extrapolated Staggered Operator (D.E. DAA)

At the time of this analysis, the version of the USA-STAGS code under consideration employed the displacment extrapolation method for the staggered solution scheme. As discussed in the previous section, the basic equations of motion are modified by time differentiation of equation (32) and substitution for the resulting u from (31) and division of both by m_s to yield,

$$\ddot{u} + \omega^2 u = -A\dot{q} \tag{33}$$

$$R\ddot{q} + \rho c A (1 + R)\dot{q} = \rho c R \omega^2 u \tag{34}$$

where $\omega^2 = k_s/m_s$, $r = m_f/m^s$, and $A = a/m_s$. The following scheme is then followed to advance the solution in time (the superscript * represents an extrapolated value):

1) Extrapolate the displacement by a two-point predictor in order to find an approximate forcing function for (34),

$$u^*_{n+1} = 2u_n - u_{n-1}; \tag{35}$$

2) Solve for the predicted wettted surface pressure by integrating (34), using Park's stiffly-stable operator[34],

$$\ddot{q}_{n+1} = (10\dot{q}^*_{n+1} - 15\dot{q}_n + 6\dot{q}_{n-1} - \dot{q}_{n-2})/6\Delta t \tag{36}$$

$$R\ddot{q}^*_{n+1} + \rho c A(1 + R)\dot{q}^*_{n+1} = -\rho c R\omega^2 u_{n+1} \tag{37}$$

3) Solve for the structural kinematics by integrating (33) using one of the structural integrators available in STAGS (the trapezoidal rule will be used for all work),

$$u_{n+1} = u_n + \frac{\Delta t}{2}(\dot{u}_n + \dot{u}_{n+1}) \tag{38}$$

$$\dot{u}_{n+1} = \dot{u}_n + \frac{\Delta t}{2}(\ddot{u}_n + \ddot{u}_{n+1}) \tag{39}$$

$$\ddot{u}_{n+1} + \omega^2 u_{n+1} = -A\dot{q}^*_{n+1}; \tag{40}$$

4) Reinsert the corrected value of structural displacement into the fluid pressure (34), and solve for the corrected fluid pressures,

$$\ddot{q}_{n+1} = (10\dot{q}_{n+1} - 15\dot{q}_n + 6\dot{q}_{n-1} - \dot{q}_{n-2})/6\Delta t, \tag{41}$$

and

$$R\ddot{q}_{n+1} + \rho c A(1 + R)\dot{q}_{n+1} = -\rho c R\omega^2 u_{n+1}. \tag{42}$$

Analysis Methodology

The integration operator defined by equations (35) through (42) can be evaluated by using a Lax-Richtmyer amplification matrix approach[32]. Basically, each step in the procedure constitutes a row in the two matrices A_0 and A_1 that will eventually lead to the amplification matrix. In this case,

$$\underset{\sim}{A}_0 \cdot \underset{\sim}{u}^{n+1} = \underset{\sim}{A}_1 \cdot \underset{\sim}{u}^n + \underset{\sim}{B} \tag{43}$$

where B is a forcing vector, and the vector u has entries,

$$\underset{\sim}{u}^T = \langle u^*, u, \dot{u}, \ddot{u}, \dot{q}^*, \ddot{q}^*, \dot{q}, \ddot{q} \rangle . \tag{44}$$

In actual practice, the matrices A_0 and A_1, and the vector u are expanded to account for the trivial steps that update previously known information; for example, the u_n in (35) becomes u_{n-1} when the subsequent solution is sought. After the matrices A_0 and A_1 area developed (see Appendix A), the square matrix A_0 is inverted to obtain,

$$\underset{\sim}{u}^{n+1} = \underset{\sim}{A}_0^{-1} \cdot \underset{\sim}{A}_1 \cdot \underset{\sim}{u}^n + \underset{\sim}{A}_0^{-1} \cdot \underset{\sim}{B} \tag{45}$$

The behavior of the integration operator is thus examined by consideration of the characteristics of

the amplification matrix, $A_0^{-1} A_1$, as functions of the time step size (Δt), the structural natural frequency (ω^2), the fluid to structure mass ratio (R), the wetted surface area to structural mass ratio (A), and the problem constant ($\rho_f c$).

To assure meaningful values when varying the large number of parameters, the numerical evaluation was carried out by consideration of a physical problem and relating the parameters to physical entities. This study is thus concerned with steel shells in water, so that the constants ρ_f, c, and ρ_s are fixed (ρ_f = 9.35 E-5, ρ_s = 7.25 E-4, c = 57111). A plane strain cylinder is then chosen as a representative problem from which the ranges of parameters can be determined.

Range Of Parameters

The parameter A represents the ratio of wetted surface area to structural modal mass. The frequency dependent generalized structural modal mass for a plane strain cylinder has been given by Love[37] as,

$$m_s = \rho_s \pi r h \frac{n^2 + 1}{n} \tag{46}$$

in which r is the cylinder radius, h the thickness, and n is the mode of vibration. An expression for A thus becomes,

$$A = \frac{2\pi r}{\pi r h \rho_s \left(\frac{n^2 + 1}{n}\right)} = \frac{2}{\rho_s h} \frac{n}{n^2 + 1} \tag{47}$$

An expression for the natural frequency of a plane strain cylinder is well known and is given by Love[27] as

$$\omega_n^2 = \frac{k_s}{m_s} = \frac{Dh^2}{r^4} \frac{n^2 (n^2 - 1)^2}{n^2 + 1} \tag{48}$$

where

$$D = \frac{E}{12\rho_s (1 - \nu^2)} \tag{49}$$

with E being Young's modulus and ν Poisson's ratio.

The ratio of fluid mass to structural mass is also clearly a function of the vibrational mode, n. Geers [19] obtains the n^{th} frequency of vibration for a cylindrical shell in water as (n > 0)

$$\Omega_n^2 = \frac{\omega_n^2}{1 + \frac{\rho \pi r}{n m_s^n}} \tag{50}$$

where m_s^n is the generalized mass of the shell for mode n given by equation (46) and ω_n^2 is the structural natural frequency of mode n as given in (48). This combined fluid-structure frequency can also be expressed as,

$$\Omega_n^2 = \frac{k_s^n}{m_s^n + m_f^n} \tag{51}$$

and since $R = m_f/m_s$ and $\omega^2 = k_s/m_s$,

$$\Omega_n^2 = \frac{\omega_n^2}{1 + R} \tag{52}$$

Thus, a measure of the ratio of fluid mass to structural mass is,

$$R = \frac{\rho}{\rho_s} \frac{r}{h} \frac{n}{n^2 + 1} \tag{53}$$

The evaluation of the operator is now carried out by choosing a value of n, computing h from equation 47 using representative values of A, computing r from (53) using representative values of R, and computing a consistent value of ω^2 from (48).

Results

For each set of parameters as discussed above, 20 values of Δt were supplied to the integration operator and the spectral characteristics of the amplification matrix were computed for each Δt. The results are presented by plotting the magnitude of the complex pair which has the largest magnitude for Δt near zero vs. the ratio $\Delta t/T$, where T is the natural period of the structure adjusted for the added mass of the fluid, i.e., $T = 2\Pi/\Omega_n$. These plots are a measure of the artificial damping present in the operator for time step to period ratios. A unit magnitude implies no artificial damping. A magnitude greater than unity indicates instability, where subsequent response would continue to grow without bound as the operator marches forward in time. The other useful result is a measure of the periodicity (or phase) error that is present in the operator. This characteristic is presented by plotting the imaginary plane angle, corresponding to the eigenvalue whose magnitude was plotted in the artificial damping plot, vs. the incremental phase, $\Omega_n \Delta t$. In these plots a striaght line at 45 degrees is the line of zero periodicity error, whereas curves below this line represent an elongation of the response period as the operator advances in time.

As a point of reference, Figures 3.1a and 3.1b show these plots for three common operators and for the degenerate case of D.E. DAA with A=R=0. The labels 1,2,3, and 4 correspond to the trapezoidal, Wilson-θ (θ = 1.4), Houbolt, and the D.E. DAA (A=R=0), respectively. It is obvious that for no fluid the D.E. DAA behaves similarly to the trapezoid rule. It is not the same however since the degenerate DAA has five non-trivial eigenvalues, one real and two pairs of complex conjugates. The real eigenvalue has a constant value of unity, whereas the real root for the trapezoidal operator has a constant value of zero. Again, the complex conjugate root with the largest magnitude for Δt near zero has been plotted as it varies with increasing values of Δt.

In all the rest of the figures, the labels, 1,2,3,4, and 5 refer to shell radius to thickness ratios, r/h, of 10, 20, 50, 100, 500, respectively.

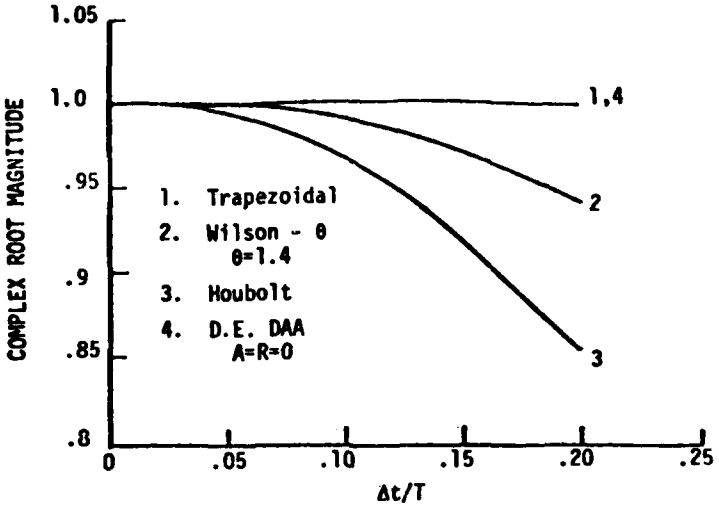

Figure 3.1a. Common Operators, Artificial Damping

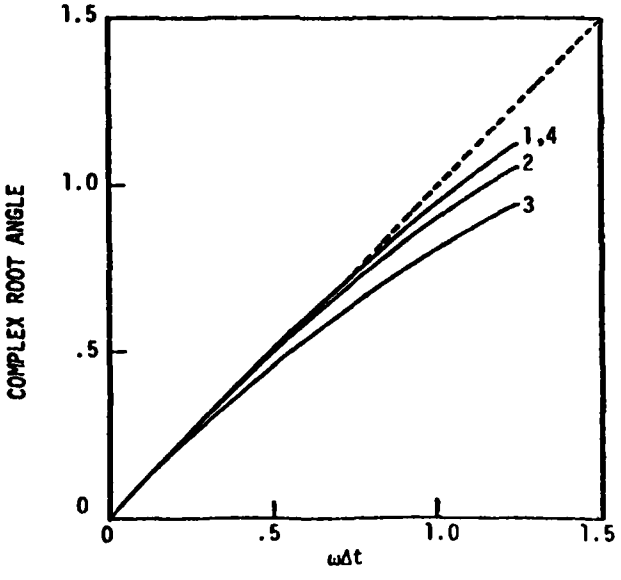

Figure 3.1b. Common Operators, Periodicity Error

Since for a given value of h and n in equation (53), variation of R is equivalent to variation of r/h, the more meaningful values of r/h rather than R were plotted. Also shown on these figures is a value used for the shell thickness, h, since in (47) for a given value of n variation of A is equivalent to variation of h.

Figure 3.2a illustrates the artificial damping present in the D.E. DAA operator when trying to capture the lower frequency (or longer wavelength) components of the solution. In general, for small time step to system periods ($\Delta t/T < .03$), the operator has little artificial damping independent of r/h ratios as would be expected. For larger ratios ($\Delta t/T > .2$) the operator would better capture the amplitudes for larger r/h ratios. In the transition range of $\Delta t/T$ ratios, the added mass of the fluid has a substantial effect on the artificial damping characteristics for varying values of r/h since for larger r/h ratios at low frequency the added mass of the fluid significantly lowers the structural natural frequency.

Figure 3.2b reveals that for a given time step the D.E. DAA operator elongates the true period of response more and more for thinner and thinner shells. For moderately thin shells this elongation for the low frequency component is very substantial unless very small time step to period ratios are chosen. For this mode 2 response analysis using a value of A ~1100) which produces a thickness of 1 in., the D.E. DAA amplification matrix has 7 non-trivial eigenvalues, 1 real and 3 pairs of complex conjugates.

Figures 3.3a and 3.3b show the operator characteristics when capturing the high frequency response of a mode 10 vibration shape. Curves 4 and 5 (large r/h) behave similarly to those of mode 2 response in that substantial damping and period elongation are present unless small time steps are used. Curves 1, 2, and 3 indicate that the operator changes characteristics when considering these thicker shells vibrating in a high frequency mode. The discontinuities in Figures 3.3 occur when the eigenvalues change from only 5 non-trivial roots (1 real and 2 pairs of complex conjugates) at the smaller time steps to the 7 non-zero roots as seen in the mode 2 curves. Thus for a given value of ω^2 in the amplification matrix, there are values of R (or r/h) such that for certain values of Δt, the matrix looses two non-trival roots.

The next two pairs of figures, 3.4 and 3.5, illustrate the effect of variation of A in the amplification matrix. Figures 3.4a and b show the operator characteristics for the mode 2 response using a value of A that corresponds to a shell thickness of .1 inch. Here it is seen that an r/h value of 10 produces this same anomoly of root degeneration for $\Delta t/T$ below .06. Otherwise the operator behaves similarly to that for much smaller ranges of A. Figures 3.5a and b illustrate the operator characteristics for a mode 10 response using a value of A which is an order of magnitude larger than that used in Figures 3.3a and b. The root degeneration has occurred for a larger range of $\Delta t/T$ for r/h of 50 (than in Figures 3.3) and has also shown up in the r/h = 100 curve. Note that curvs 1 and 2 have 1 real and 2 pairs of complex conjugates for the entire range of $\Delta t/T$ plotted.

Figures 3.6 and 3.7 show the results when using a fully implicit method in solving the DAA equations. Basically, the operator evaluates equations (31) and (32) at time $t + \Delta t$ and uses the trapezoidal rule in expressing u, u, and q at $t + \Delta t$ as functions of the other unknowns. (See Appendix B for derivation of this amplification matrix). Figure 3.6b shows that very little artificial damping occurs for the mode 2 response for even large $\Delta t/T$ ratios. More importantly, Figure 3.6b illustrates the independence of problem size for the periodicity error present in the fully implicit operator. The elongation of the response period for the fully implicit operator is very much smaller than that for the D.E. staggered integration scheme.

Figures 3.7a and b show the aritifical damping and periodicity error for the fully implicit operator for high frequency response. Again, the amplificaton matrix has lost roots for certain combinations of ω^2, R, A, and Wt values. Notice also (as was the case with the D.E. staggered operator) that substantial damping seems to occur at high frequency even for very small time steps.

Figure 3.8a is a plot of the magnitude of the real root corresponding to Figure 3.2a and is included to illustrate the extraneous root behavior. Figure 3.8b is the real root corresponding to the D.E. DAA operator, mode 10 (Figure 3.3). The real roots of the fully implicit operator also behave similar to this with discontinuities occurring when the amplification matrix changes characteristics.

Conclusions

Care must be used in choosing time steps for the staggered solution scheme for solving the D.E. DAA equations to insure a minimum of period elongation, especially for low frequency response and relatively thin shells. When a sufficiently small time step is used to prevent period elongation for relatively thin shells, the artificial damping of the response amplitude by the operator is minimal. However, for only moderately thin shells, the time step must be chosen by considering the amplitude damping as the critical factor. In general more artificial damping but less period elongation is present in the operator when capturing high frequency response. The added mass of the fluid as a function of the radius to thickness ratio is an important consideration in choosing time step size because of the non-linear effect on damping of the structural natural freuqency.

The phenomena of changes in spectral characteristics of the operator for critical values of structural natural frequency, ω, mass ratio, R, wetted surface to mass ratio, A, and time steps, Δt needs additional study to formulate this in physical terms. The question of whether contradictory values of the parameters havae been fed to the operator, or indeed, if small enough time steps

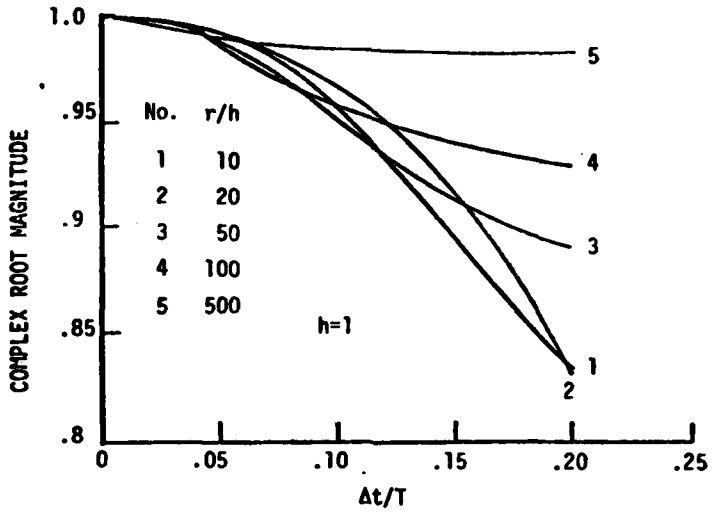

Figure 3.2a. D.E. Staggered DAA, Mode 2 Artificial Damping

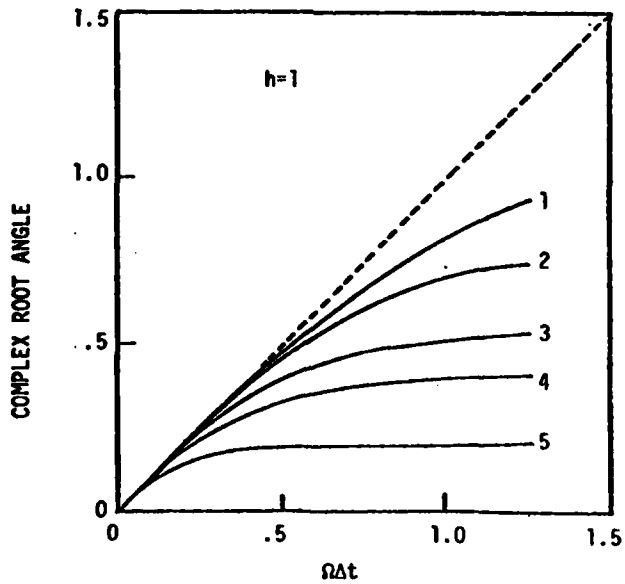

Figure 3.2b. D.E. Staggered DAA, Mode 2 Periodicity Error

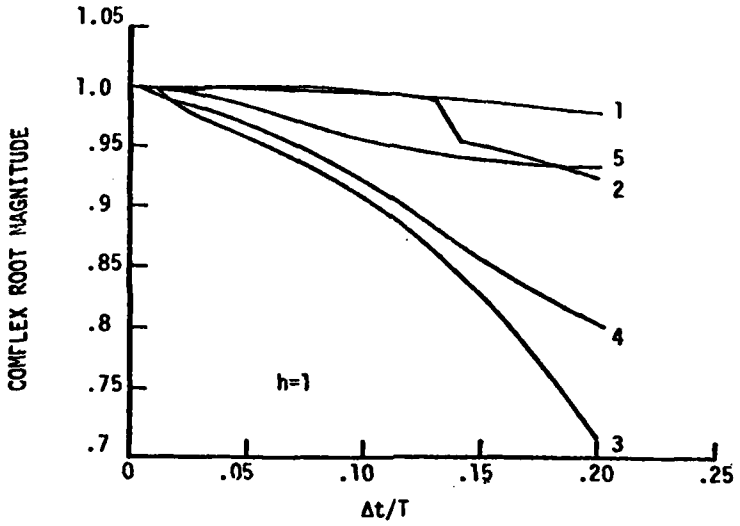

Figure 3.3a. D.E. Staggered DAA, Mode 10 Artificial Damping

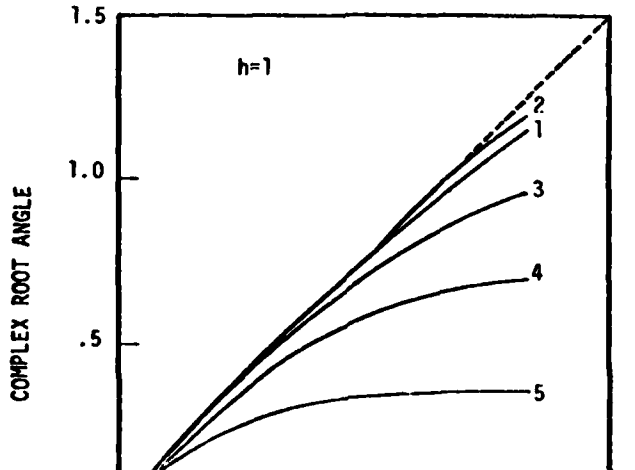

Figure 3.3b. D.E. Staggered DAA, Mode 10 Periodicity Error

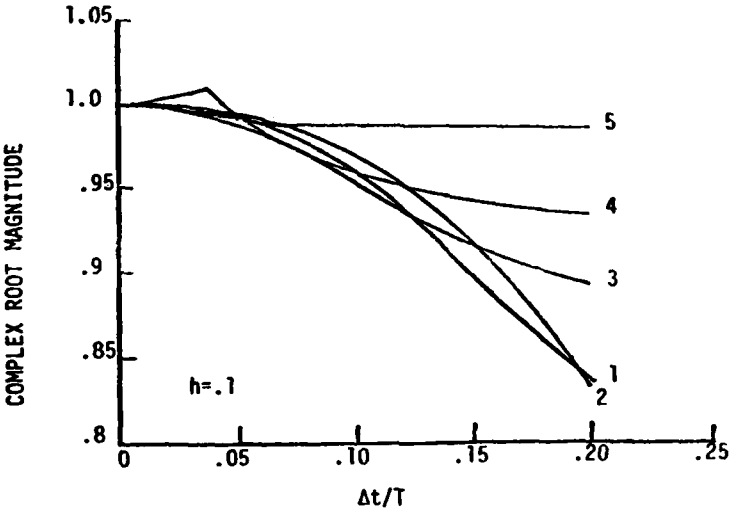

Figure 3.4a. D.E. Staggered DAA, Mode 2 Artificial Damping

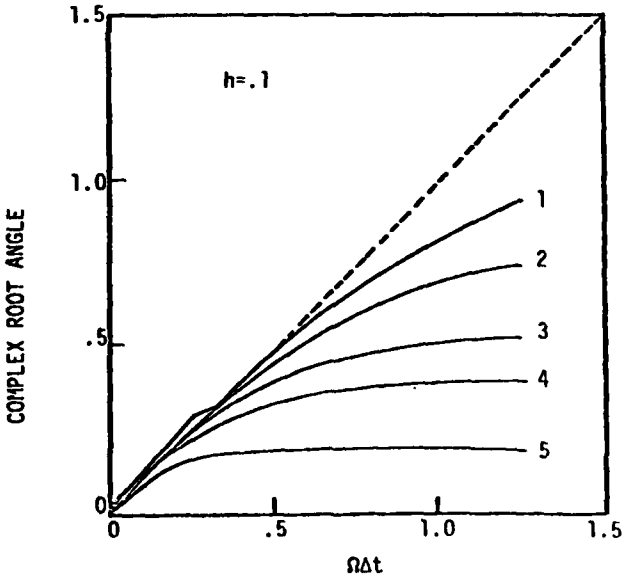

Figure 3.4b. D.E. Staggered DAA, Mode 2 Periodicity Error

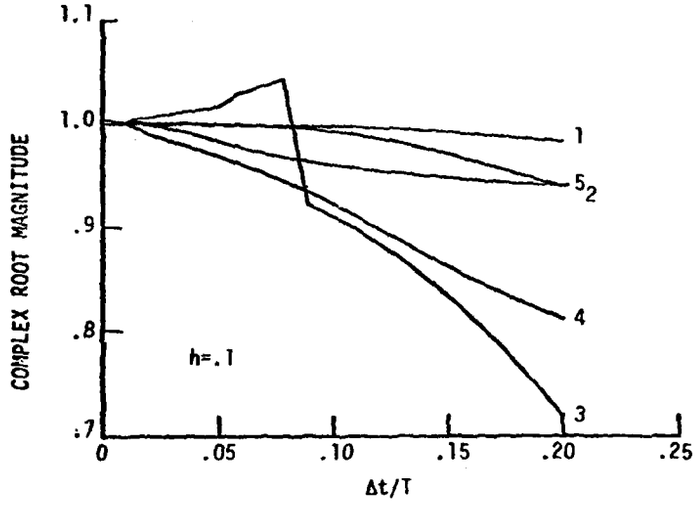

Figure 3.5a. D.E. Staggered DAA, Mode 10 Artificial Damping

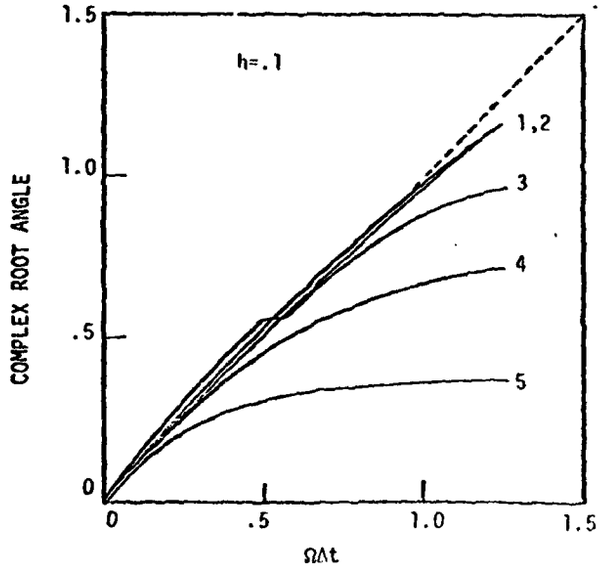

Figure 3.5b. D.E. Staggered DAA, Mode 10 Periodicity Error

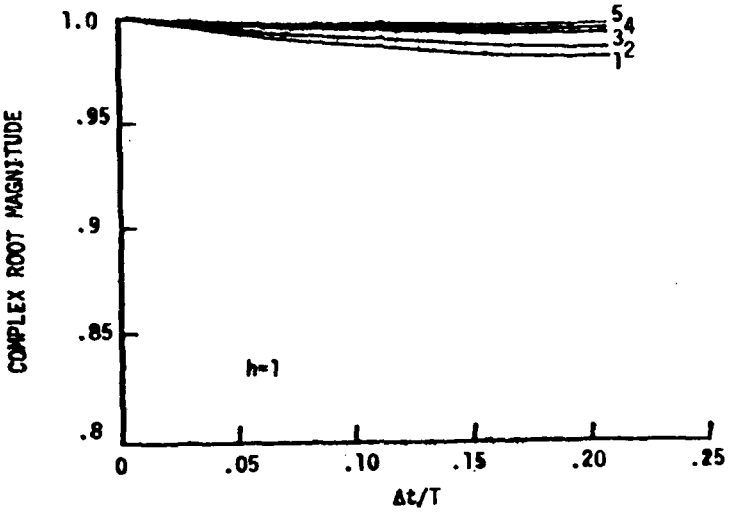

Figure 3.6a. Fully Implicity, Mode 2 Artificial Damping

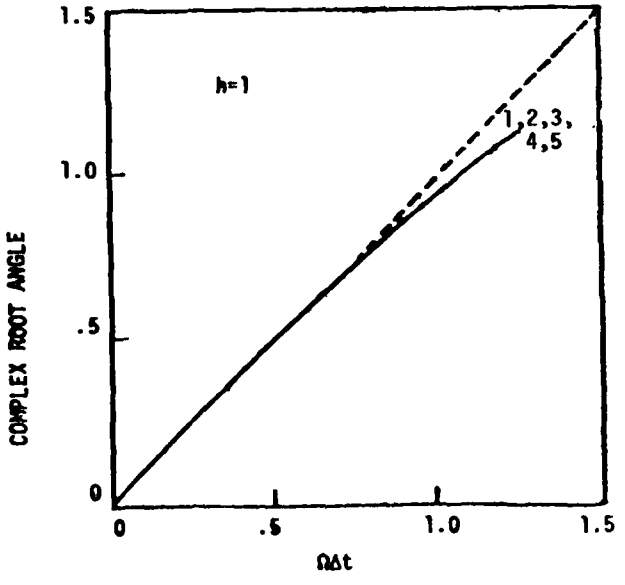

Figure 3.6b. Fully Implicit, Mode 2 Periodicity Error

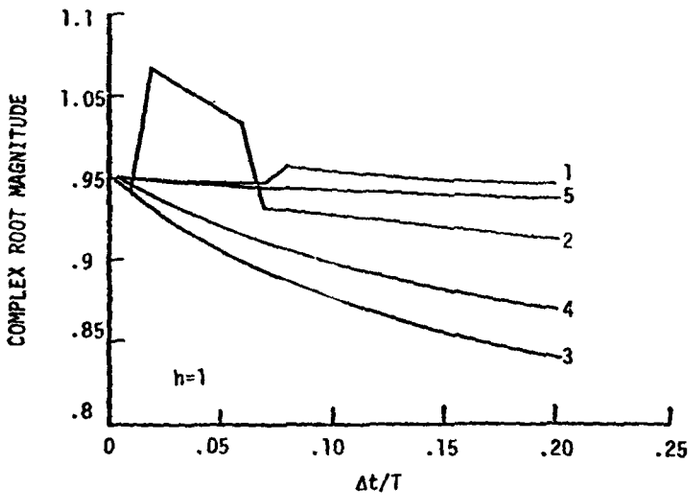

Figure 3.7a. Fully Implicit, Mode 10 Artificial Damping

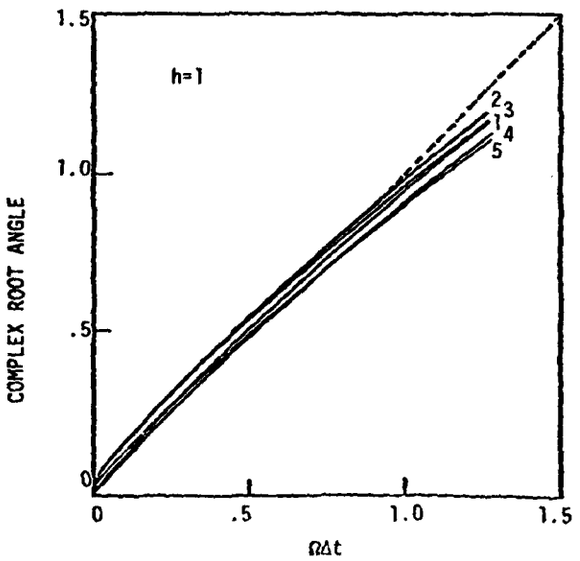

Figure 3.7b. Fully Implicit, Mode 10 Periodicity Error

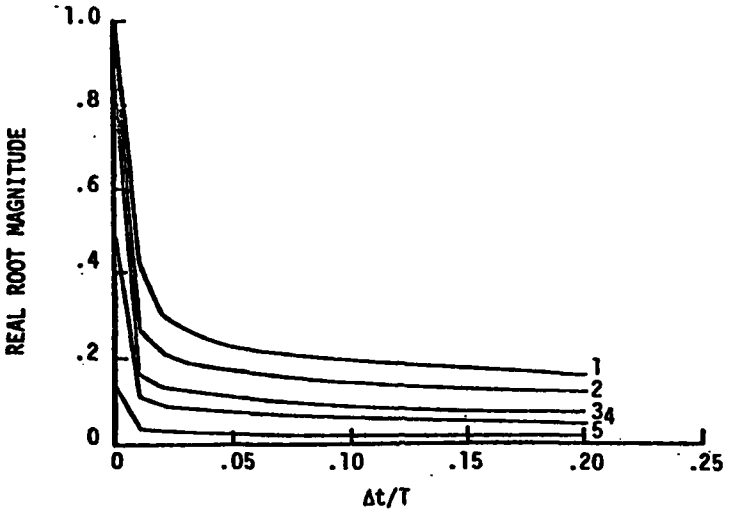

Figure 3.8a. D.E. Staggered DAA, Mode 2 Extraneous Root Damping

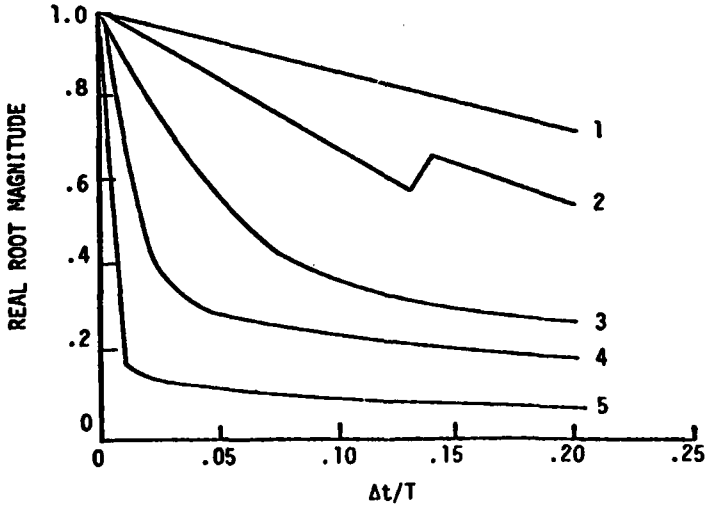

Figure 3.8b. D.E. Staggered DAA, Mode 10 Extraneous Root Damping

produce a numerical instability for certain characteristics in the DAA equations have not been fully addressed.

4. EVALUATION OF DAA CALCULATIONS

General

A large number of DAA calculations, with and without the staggered solution, have been compared to exact, linear acoustic-structural solutions and exact solutions of the linear DAA equations, [3,5,6,16-24,29,38] and recently comparisons have been made on "exact" solutions of the DAA equations versus the staggered solution procedure for inelastic structural response calculations[39]. In all the above cited references, except reference [39], the exact solutions of the DAA equations and the staggered solution procedure have been found to give accurate solutions. Indeed, the DAA has been used for the prediction of the response of many submerged structures subjected to acoustic wave loads[8,10-13], and in most cases DAA results correlate well with the measured response. The evaluation given in this chapter does not take exception to these past studies, rather, the present work is directed to the specific task of evaluation of the USA-STAGS DAA implementation.

The DAA has been shown to asymptotically converge to the highest and lowest frequency in the model[24]. Thus, it is a suitable approach for studying the "long" time response of submerged structures subjected to wave loadings. In the present work, a study was undertaken to evaluate the accuracy of the DAA in the "intermediate" frequency regime. For this reason, only linear elastic structural behavior was studied. The problems selected for study were submerged thin, elastic, spherical and cylindrical shells subjected to a plane step wave[16,38]. Closed form ("exact") solutions to the coupled acoustic-structural equations have been given by Huang in references [16,17 & 38] and were available for comparison with the USA-STAGS DAA solutions. Dr. Hanson Huang of the Naval Research Laboratory, Washington, D.C., gratiously made his computer code available for direct recomputation of the closed form solutions. His cooperation is gratefully acknowledged.

Concern over the accuracy of the DAA implemented in USA-STAGS was manifested because of the results of Huang's DAA computations for the sphere[5]. This excellent study was done on the basic DAA equations (8 and 9) and not the staggered procedure implemented in USA-STAGS, equations (21 and 22). In particular, Figures 5 and 6 of reference [5] show heavy damping in the DAA calculations by a time equal to 10 transits of an acoustic wave across the spherical radius. This is late time, and the results at earlier times were accurate, but the heavy damping is a cause of concern.

The DAA solutions given by Huang[5] and in many of the references cited in the first paragraph of this section were developed using Fourier series expansions for the shell displacements and fluid pressure, not from a full three-dimensional model such as is used in USA. The displacements and pressure are expressed as

$$w(\theta,t) = \sum_{n=0}^{N} w_n(t) \cos n\theta \qquad (54)$$

and

$$p(\theta,t) = \sum_{n=0}^{N} p_n(t) \cos n\theta \qquad (55)$$

This leads to two coupled ordinary differential equations for $w_n(t)$ and $p_n(t)$. Note, these are not eignefunction solutions (which are used in Section 3), these are modal DAA equations. The solution for each DAA mode (n = 0,1,2....,N) should achieve asymptotic convergence to the highest and lowest frequencies in that model following the same arguments of Geers[24]. This implies that if a full three-dimensional model is used (USA-STAGS models), there ae 2 asymptotes; but if a Fourier series is used, there are 2N asymptotes. This implication is contradicted by the results given in the USA reference manual[29], which were performed with a full three-dimensional model, and the results presented herein. The USA-STAGS full three-dimensional models gives the same general frequency accuracy as the modal results.

Plane Step Wave On a Submerged Sphere

The first problem selected for study is a submerged thin spherical shell subjected to a plane step wave. A closed form Fourier-Legendre polynomial solution to the coupled acoustic-structural equations (not the DAA equations) has been given by Huang[11,12]. The geometry and loading are illustrated in Figure 4.1. The following physical properties and dimensions were used in the USA-STAGS model:

E = 20×10^6 psi - Shell Modulus;

ν = 0.3 - Poisson's Ratio;

ρ_s = 7.28×10^{-4} lb-sec^2/in^4 - Shell density;

a = 60 in - Shell Radius;

2h = 1.2 in - Shell Thickness

c = 6×10^4 in/sec - Fluid Wave Speed*;

ρ = 9.35×10^{-5} lb-sec^2/in^4 - Fluid Density.

All of the results given by Huang are in dimensionless form, using the following normalizing parameters:

Z = z/a - Dimensionless coordinate;

*Huang used a wave sp = 5.75×10^4 in/sec (C=3.70), approximately ver than the prsent value. Since the results a given as a function of dimensionless time, this discrepancy is negligible.

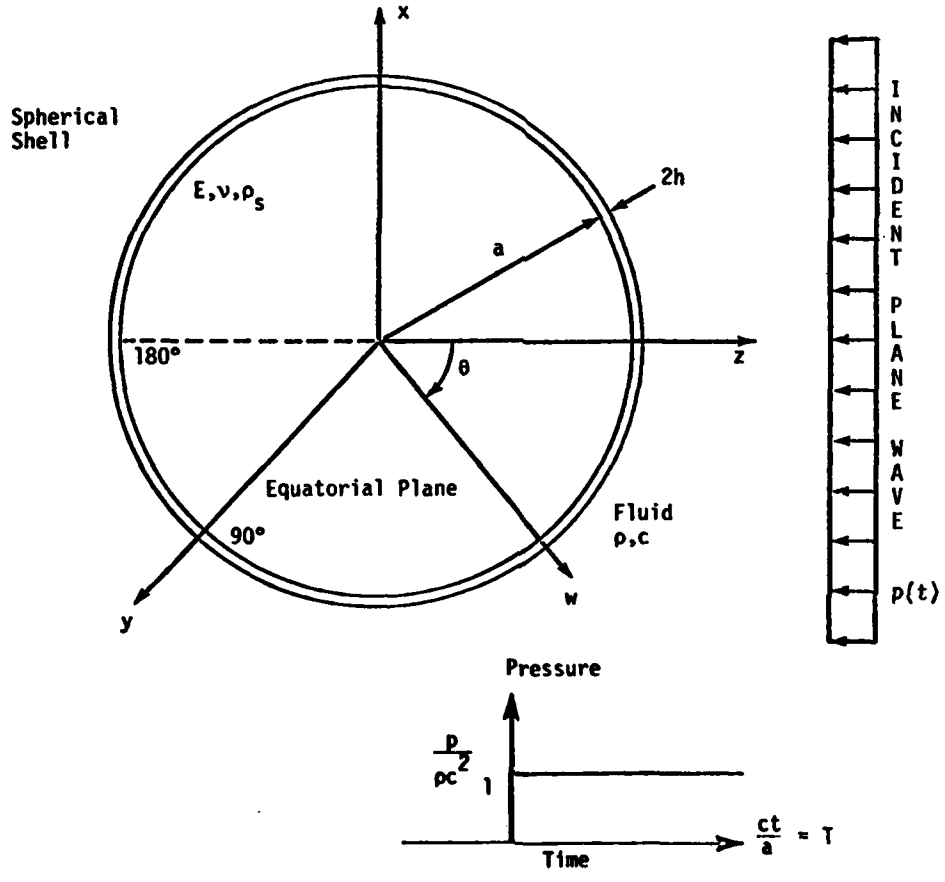

Figure 4.1. Submerged Spherical Geometry and Step Wave Loading

ζ = h/a - Dimensionless thickness;

W = w/a - Dimensionless displacement;

T = ct/a - Dimensionless time;

π = $p/\rho c^2$ - Dimensionless pressure;

M = $a/2hp_s$ - Buoyancy parameter;

C = $\sqrt{E/\rho_s(1-\nu^2)}$ - Relative wave speed.*

For the given parameters ζ = .01, M = 6.42, and since M > 3 the shell is positively buoyant.

The STAGS finite element model used a one-quarter model of the sphere with 15 equally spaced nodal lines around the equatorial plane (x = 0), thus, $\Delta\theta$= 180°/14 = 12.9°, and 7 equally spaced nodal lines between the equator and pole (x = a, y = z = 0), thus $\Delta\phi$ = 90°/6 = 15°. Only four node flat quadrilateral plate elements were available in the pre-release version of STAGS-C1 that was used, so the model did not extend to the exact pole, rather a small 4° hole was left in the model. Inspection of the results and subsequent comparison with a model using triangles extending to the pole revealed that this approximation had a negligible effect on the results at the equator. The planes x = 0 and y = 0 were modeled as symmetry planes. This problem is axisymmetric about the z-axis, but this symmetry was not modeled because USA-STAGS does not have an axisymmetric modeling capability. A constant time step Δt = .25 ms (Δt = .25) was used for the USA-solution.

The results of the USA-STAGS computations are shown against Huang's closed form solution[16,16] in Figures 4.2-4.6. The solid line is the USA-STAGS solution and the dashed line is the closed form solution. The plots are for the dimensionless outward normal displacement (Figures 4.2 and 4.3) and velocity (Figures 4.4-4.6) versus dimensionless time to T = 16 (a time equal to 16 radius transits). Because the solution for the velocity asymptotically approaches a steady translational velocity W_z = W(θ = 180°) = -W(θ = 0°) = 3M/(6 + M) = 1.55, the rigid body motion obscures the structural response at θ = 0° & 180°. For this reason, Figure 4.2 shows the average of the outward normal displacements at θ = 0° & 180°, i.e., the radial 'stretch'.

These results clearly demonstrate the excess damping in the DAA. Qualitatively these results are quite similar to Huang's for the exact solutions of the DAA equations[5]. However, there are important quantitative differences:

(1) Huang's results showed the exact DAA and the closed form solution to be virtually the same for $0 \leq T \leq 1.2$, whereas the USA-STAGS results lag the closed form solution;

(2) Curiously, the USA-STAGS results for the outward normal displacement at θ = 90° (Figure 4.3) and the velocity at θ = 180° (Figure 4.5) are very accurate to T = 4;

(3) The USA-STAGS results for the outward normal velocity at θ = 0° (Figure 4.4) indicate the initial acceleration is approximately 6 times less than the closed form solution; and

(4) At late times (T > 10), the USA-STAGS results appear to be less damped than the exact DAA results.

Single Pulse Wave On A Submerged Sphere

The second problem selected for study is the same submerged sphere, however, the loading is now a plane pulse wave of duration T = 2 (2 radial transits = engulfment time). The pressure time history is shown in Figure 4.7. All the parameters and the USA-STAGS model are otherwise the same as the previous problem (including the 4 percent slower wave speed for the closed form solution). The closed form solution for this loading has not been published, but Dr. Hanson Huang of the Naval Research Laboratory kindly agreed to compute the closed form solution to this new loading. The duration, T = 2, was chosen in an attempt to excite significant response amplitudes in frequencies higher than those observed with the previous loading. The USA-STAGS solution was again calculated using a constant time step Δt = .25.

The comparisons between the USA-STAGS calculations are shown in Figures 4.8-4.11 for the normal displacement and velocity at 0° and 90° in the equatorial plane. The USA-STAGS solution is again the solid line. Qualitatively the comparisons are similar to the results for the step wave. The major difference is at late time where the USA-STAGS results seriously underestimate the amplitudes which for the pulse loading are greater than the early time amplitudes. For example, the velocity (W) at 0° reaches a minimum of -1.4 at T = .5, but attains a maximum of 1.8 at T = 15. The USA-STAGS results are accurate at early time, but are less than 10 percent of the closed form solution of T = 15. The frequency content of the USA-STAGS solution is quite close to the closed form solution, and, again, the tendency of USA-STAGS to lag at early times and lead at late times is observed. The asymptotic values for displacement and velocity are quite close.

Step Wave On A Submerged Cylinder

The third problem selected for study is a submerged cylinder. The cylinder has the same geometric and material properties as the previously analyzed sphere. The problem is one of plane strain and the loading is again a plane step wave. The closed form solution to this problem has also been given by Huang[38]. The USA-STAGS model consisted of 2 rows of 36 equally spaced elements around the circumference ($\Delta\theta$ = 10°). A full wave model was used and symmetry about θ = 0° was not enforced. A full three-dimensional model was used, with an axial spacing of Δz = 10°. Symmetry

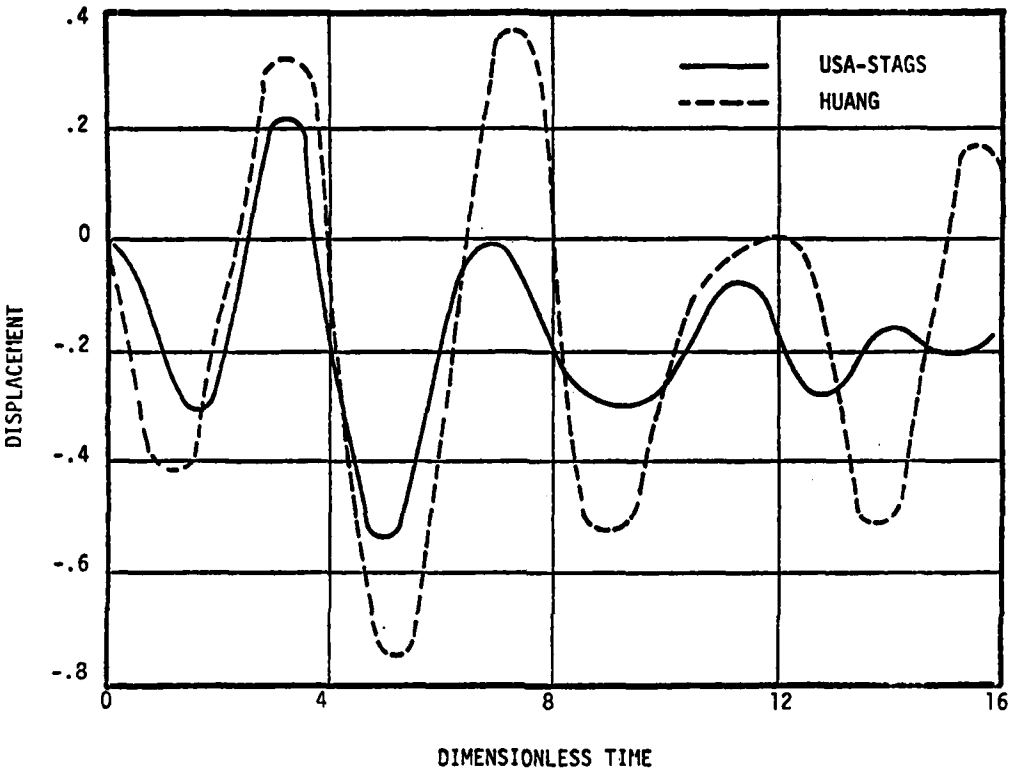

Figure 4.2. Radial Stretch Displacement 0.5* [(W/0)+W(180)], Sphere, Step Wave

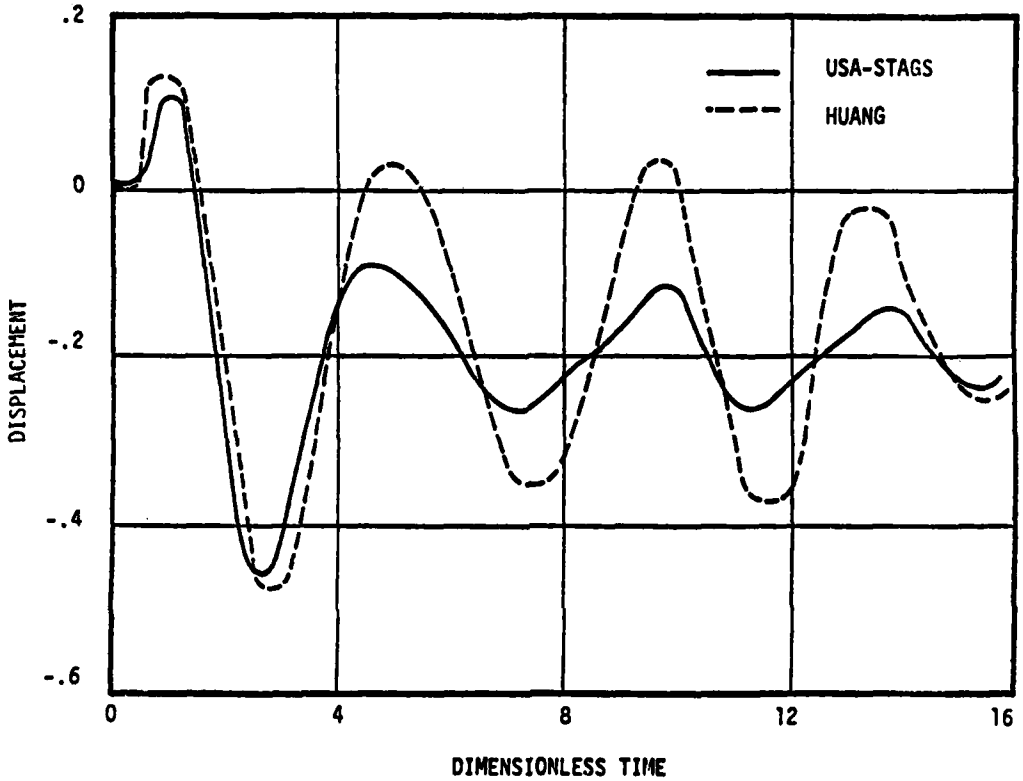

Figure 4.3. Outward Normal Displacement at 90°, Sphere, Step Wave

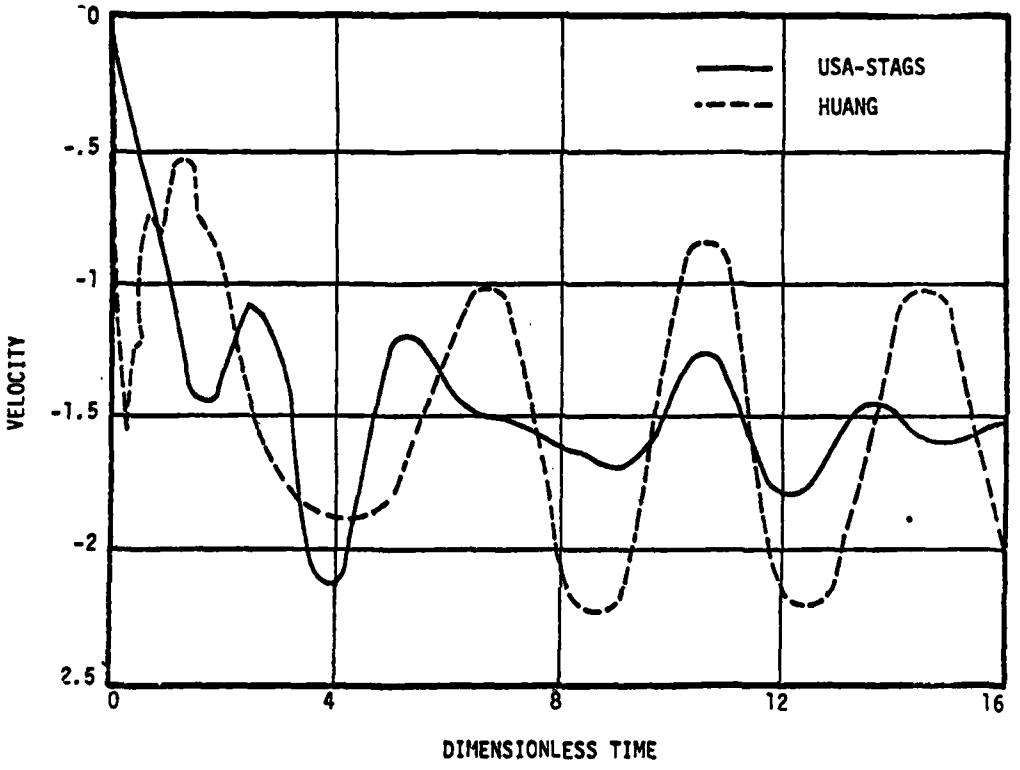

Figure 4.4. Outward Normal Velocity at 0°, Sphere, Step Wave

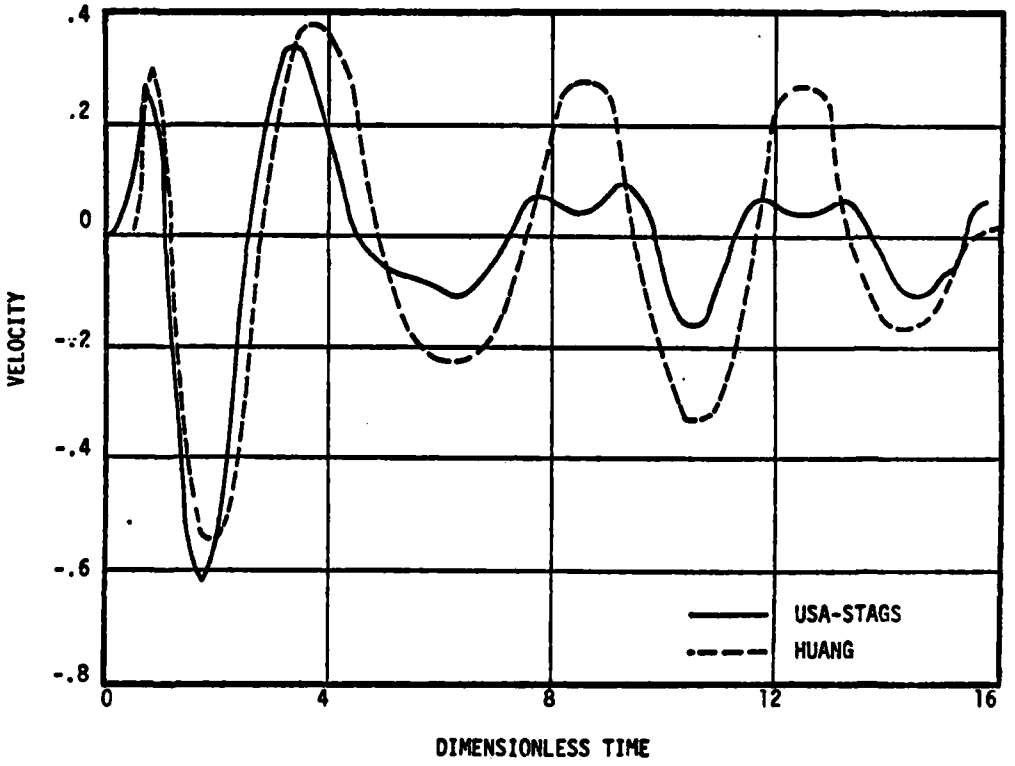

Figure 4.5. Outward Normal Velocity at 90°, Sphere, Step Wave

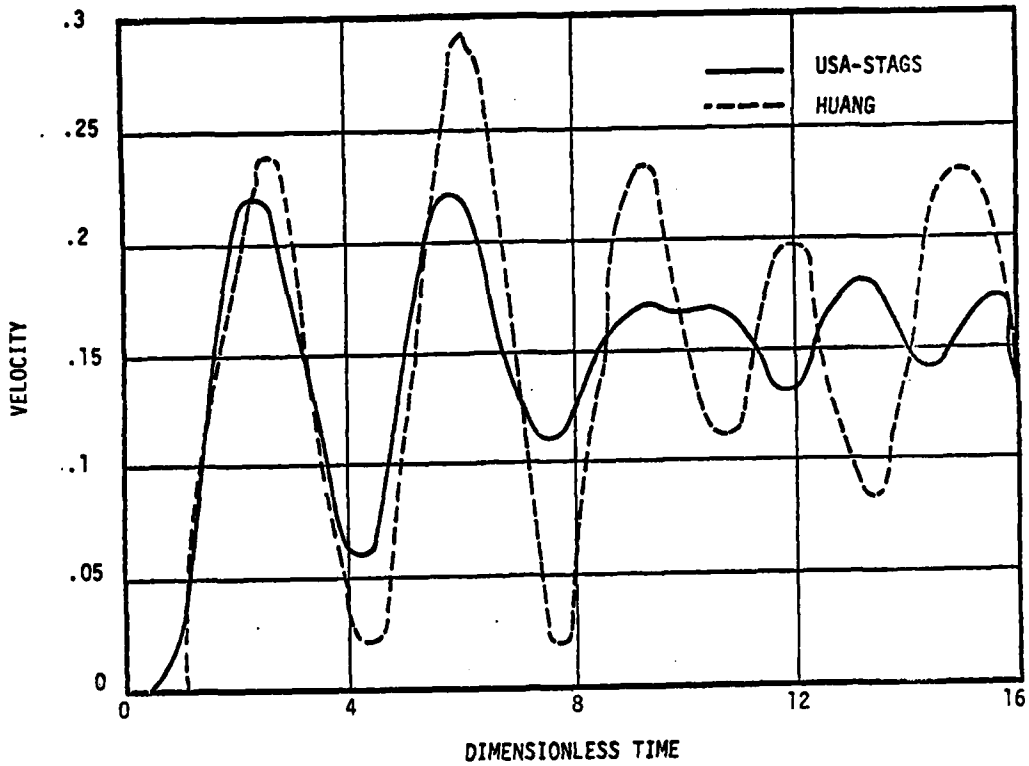

Figure 4.6. Outward Normal Velocity at 180°, Sphere, Step Wave

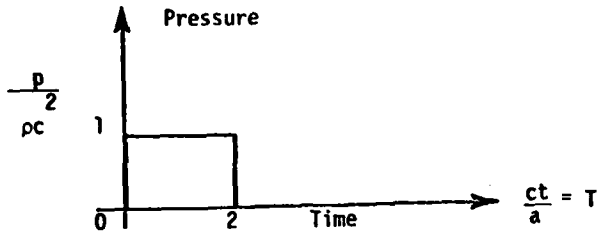

Figure 4.7. Single Pulse Wave Loading

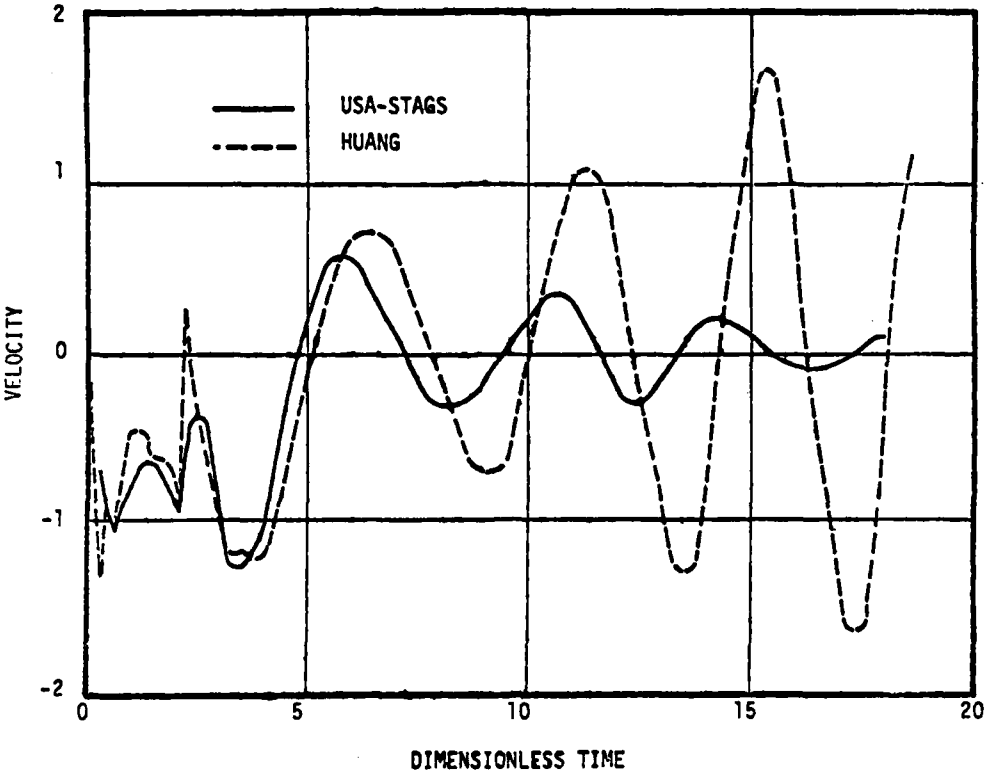

Figure 4.8. Outward Normal Velocity at 0°, Sphere, Pulse Wave

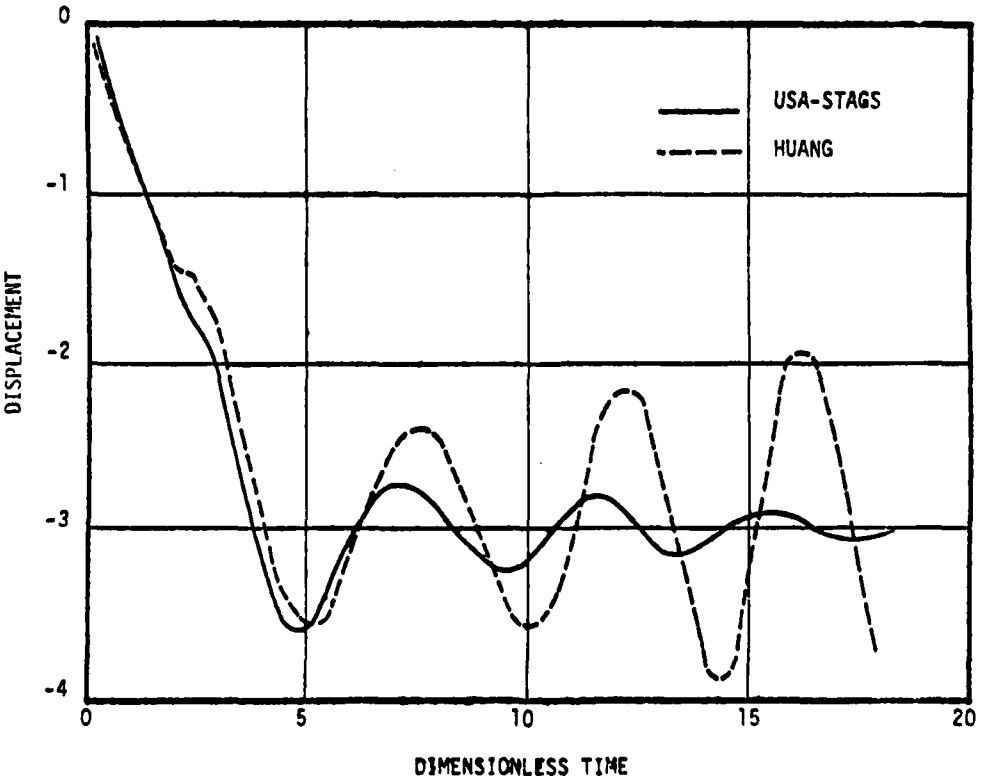

Figure 4.9. Outward Normal Displacement at 0°, Sphere, Wave Pulse

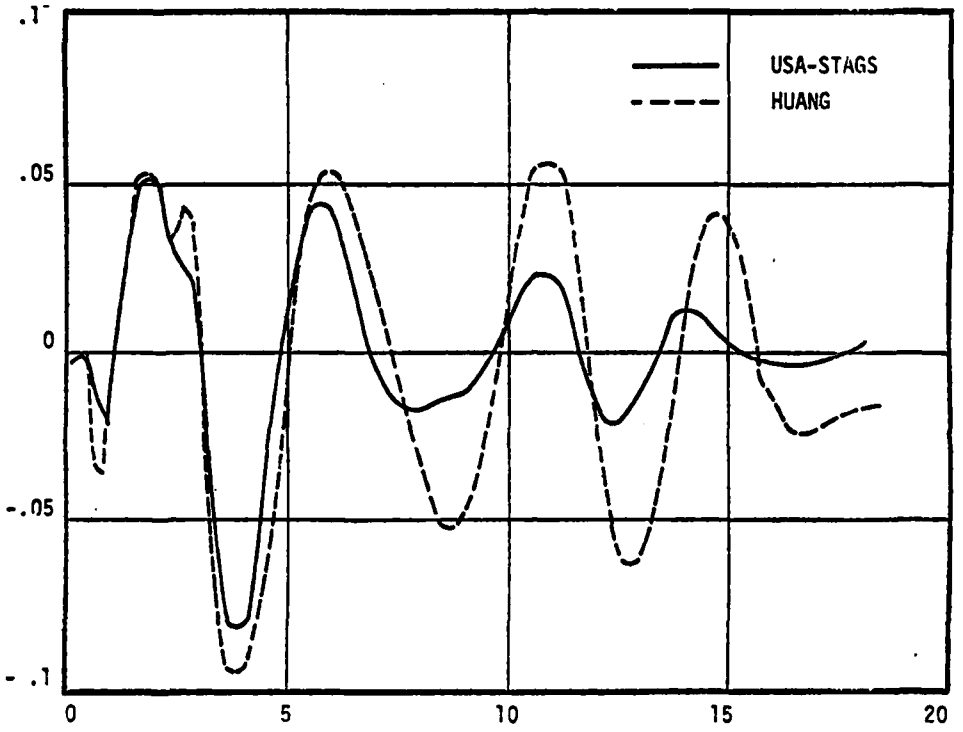

Figure 4.10. Outward Normal Velocity at 90°, Sphere, Wave Pulse

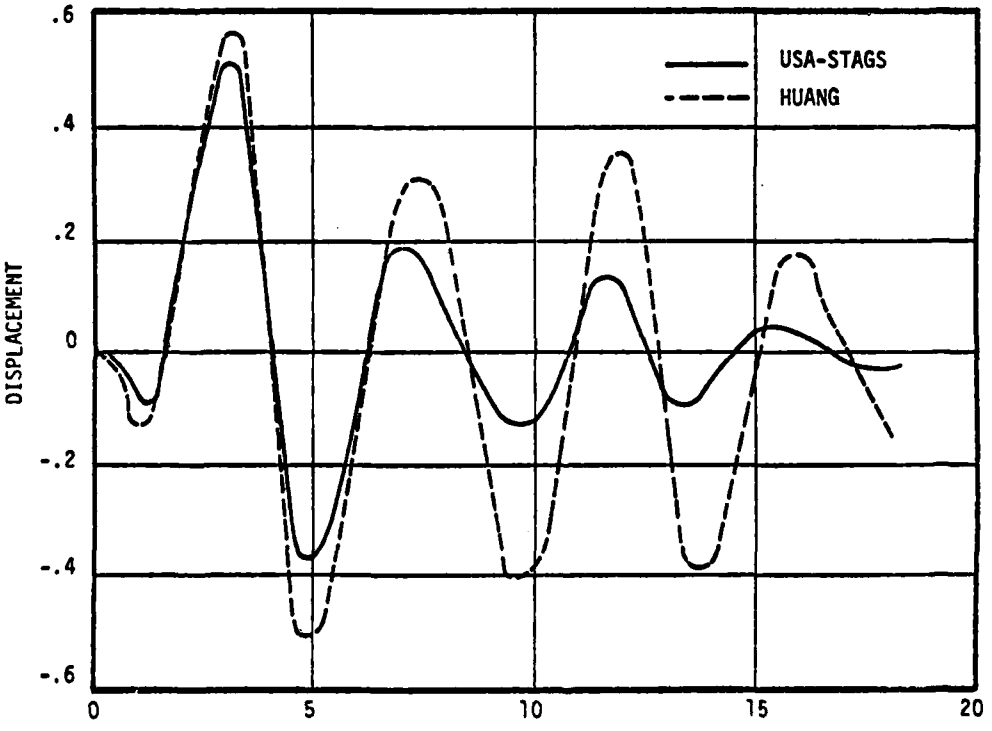

Figure 4.11. Outward Normal Displacement at 90°, Sphere, Pulse Wave

boundary conditions in the axial direction were imposed to effect the plane strain solution. In USA it is necessary to artifically extend the cylinder to accurately compute the plane strain added mass matrix. This was done using NUMZ = 500 and ZLEN = 10, see page 8-6 of the USA manual[29]. A constant time step Δt = .125 ms (Δt = .125) was used. Thus, both the grid size and time step for the cylinder are finer than for the sphere. To remove the rigid body translation in the direction normal to the incident wave propagation direction, the circumferential displacement was constrained at both 0° and 180°. In a trail run that was made without these boundary conditions, the computed solution was noticably inferior. This is surprising because there is inertia in this direction, and, thus, the effective stiffness matrix is not singular.

The USA-STAGS results are compared to Huang's closed form solution which were not taken from reference [38] but were reproduced using the computer code that Huang was kind enough to provide us. For the cylinder problem, the closed form results were computed using the same fluid wave speed as used in the USA-STAGS solution (c = 60 x 10^3 in/s). Figures 4.12, 4.13, and 4.15 show the outward normal displacement at 90°. Figures 4.16-18 show the hoop strain at 0°, 90°, and 180°, respectively.

The solution to this problem exhibits little harmonic behavior, and as expected, the USA-STAGS solution agrees very well with the closed form solution.

5. CONCLUSIONS

As described in Appendices C and D, there are many errors and needed improvements in both STAGS and USA. Considerable time and effort will be required before they will evolve into fully operational, verified codes. The personnel at Lockheed are capable of accomplishing this, but they are subjected to conflicting pressures that make the eventual outcome questionable. It is difficult to maintain sufficient interest and funding in this type of code development activity.

The modified, augmented, interaction equations and the displacaement extapolation staggered solution scheme for the DAA were chosen because they permit separation of the fluid (USA) and structural (STAGS) codes, not because this is the best procedure for solving the DAA equations. We do not agree with this philosophy which has lead to needless complications and redundant and confusing data requirements without improving the overall quality of the solution.

The present configuration of the combined USA-STAGS codes for the solution of submerged shells subjected to transient excitations is cumbersome, requires redundant data and too many control cards, and is a source of many potentially serious errors. For the typical user, this inhibits effective utilization of the codes. For this highly specialized application, the typical user would be better served by a single code.

We believe the selection of fluid pressure degrees-of-freedom at the centroid of the fluid elements is inferior to using nodal point fluid degrees-of-freedom. Nodal point pressures would make the USA code more like a finite element code and would undoubtly improve the accuracy of the consistent nodal point forces.

The staggered solution scheme implemented by Lockheed in the USA code appears to work reasonaby well and has given reliable solutions to many problems. However, the Lax-Richtmyer stability analysis revealed significant phasing errors and discontinuties in the behavior of the operator that may give rise to improper behavior for some problems. The analysis revealed a need for small time steps for low frequencies and/or very thin shells, but most applications of interest do not appear to be in this regime. The analysis also indicated that a fully implicit implementation of the DAA equations would have superior phasing characteristics, avoid the behavioral discontinuities, and be unconditionally stable.

The calculations performed on the various test cases reported in Section 4 and on many other unreported problems show the same qualitataive and quantitative behavior reported by Huang in 1975[5]. The present authors fully support and agree with Huang's conclusions and recommendations. The DAA solutions are indeed overdampled compared to the true hydrodynamic-structural dynamic response. However, the USA-STAGS calculations generally agree well with the exact DAA calculations reported by Huang and others. It is not possible to fully access the implications of the approximations required to solve and implement the DAA equations. We believe that there will be many situations in which USA-STAGS will work well and others where it will not.

We have found both USA and STAGS to be highly effective, useful, and efficient codes for the computaitons of the response of submerged shells to shock loadings. There is much that needs to be done to improve and correct these codes, and to that extent it is not possible to make a final judgement, but we believe these are excellent codes. We have no hesitation in recommending their usage.

6. RECOMMENDATIONS

Both USA and STAGS area valuable tools with which to access damage to submerged structures subjected to shock loads. They should continue to be supported until they evolve into more fail-safe, easy-to-use codes. These codes should provide effective and efficient service to both Navy laboratories and contractors for many years to come.

However, there is a strong need for further work in this area directed both at improving currently used techniques and developing new, more accurate and efficient techniques. The following is a list of four such recommendations:

(1) Develop and evaluate various methods

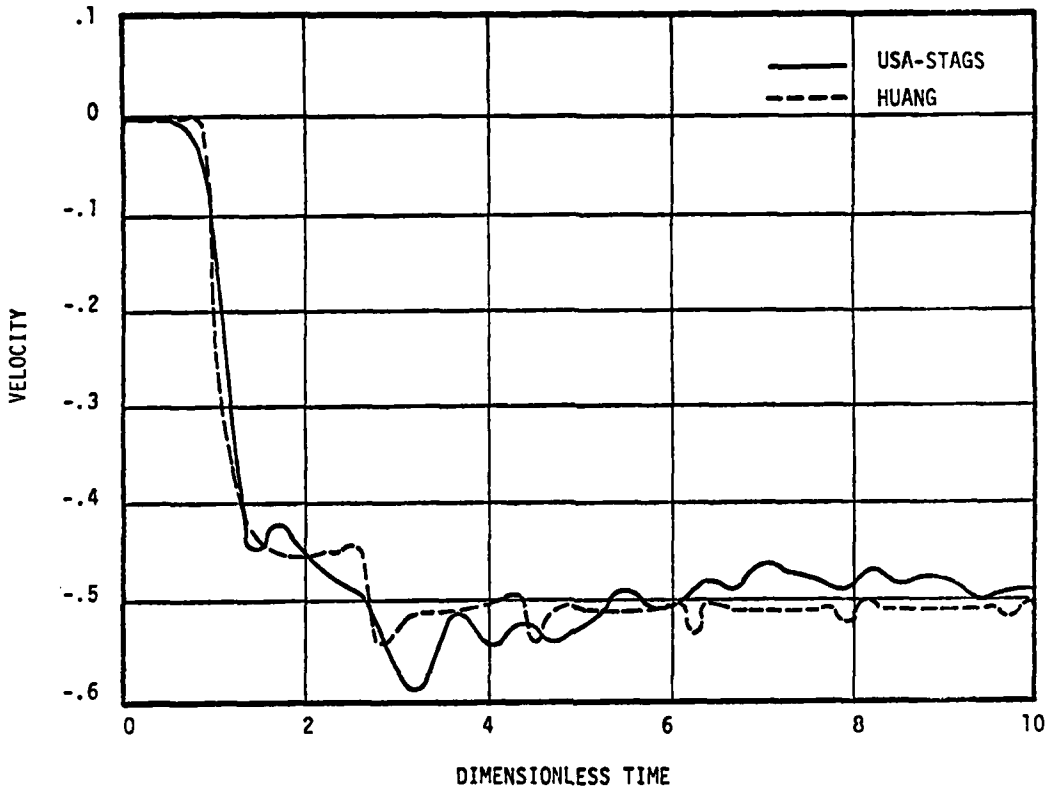

Figure 4.12. Outward Normal Velocity at 0°, Cylinder, Step Wave

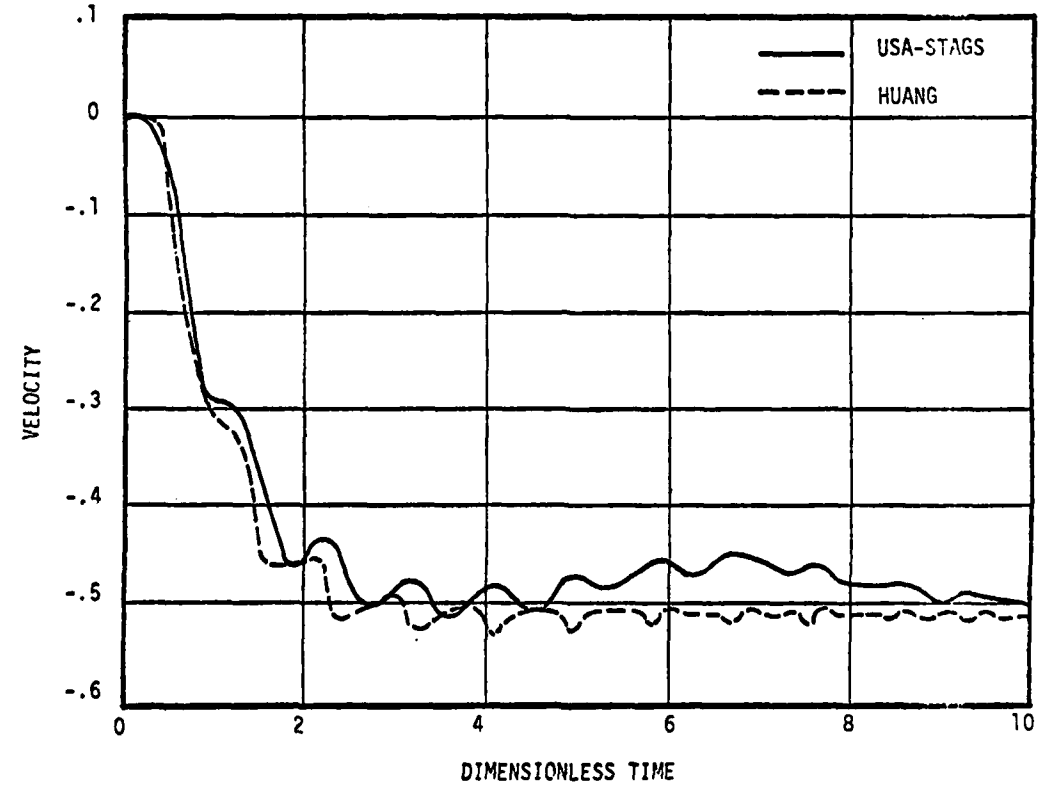

Figure 4.13. Outward Normal Velocity at 90°, Cylinder, Step Wave

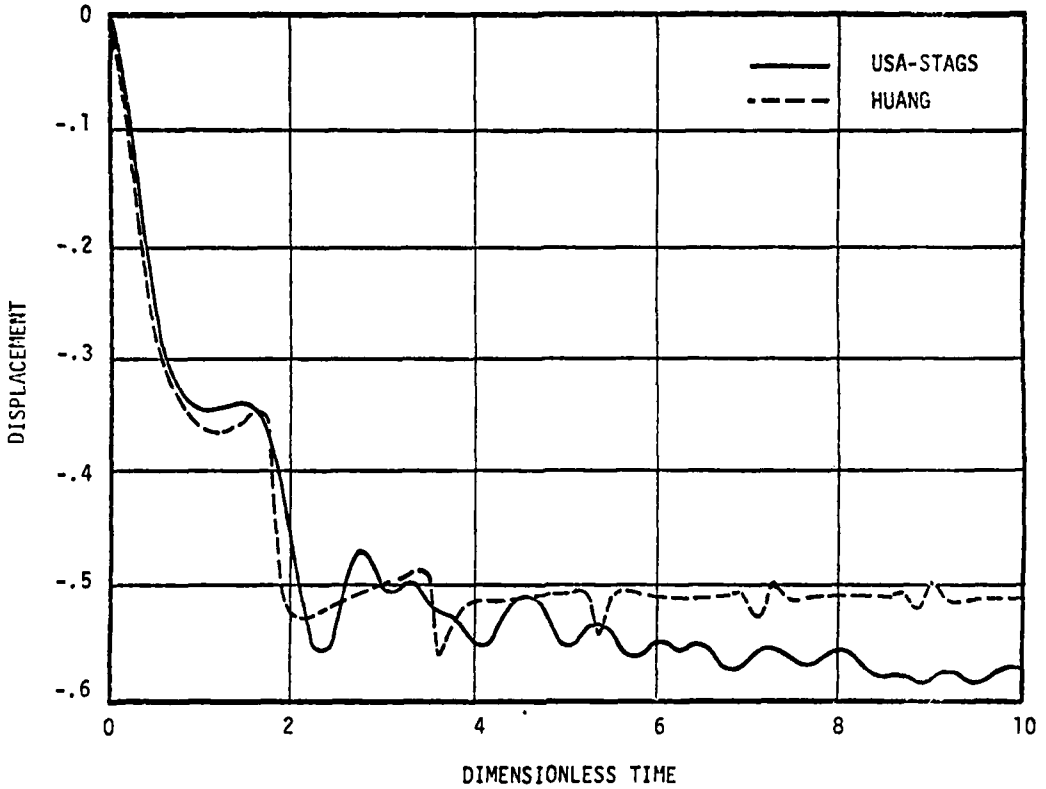

Figure 4.14. Outward Normal Displacement at 90°, Cylinder, Step Wave

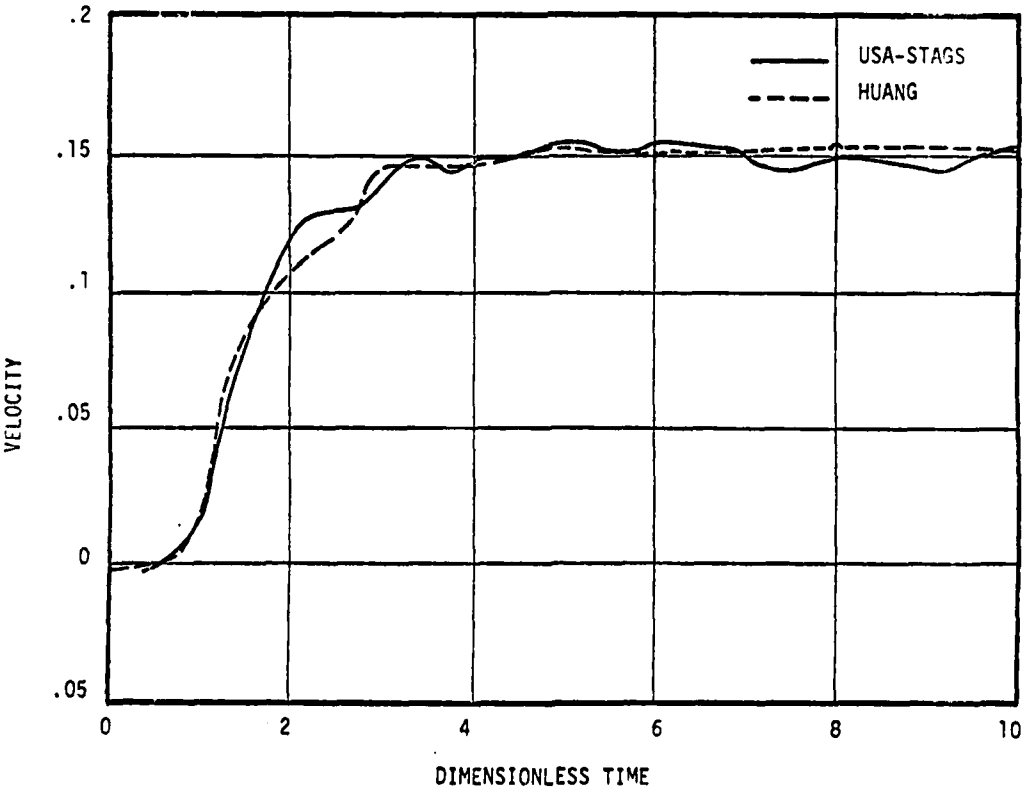

Figure 4.15. Outward Normal Velocity at 180°, Cylinder, Step Wave

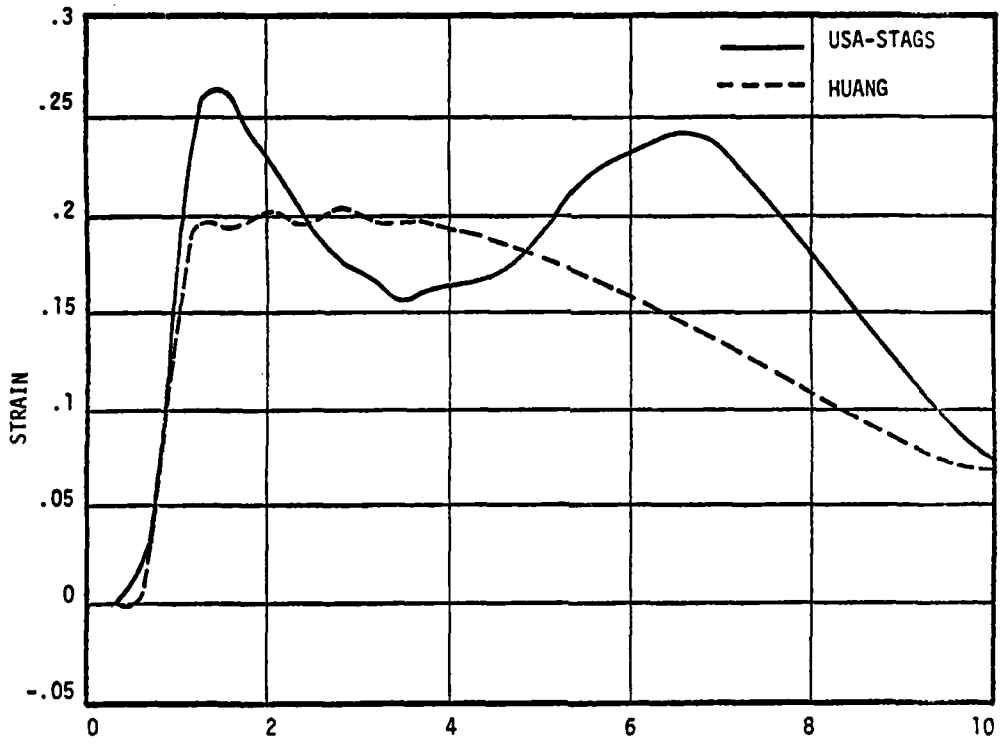

Figure 4.16. Hoop Strain at 0°, Cylinder, Step Wave

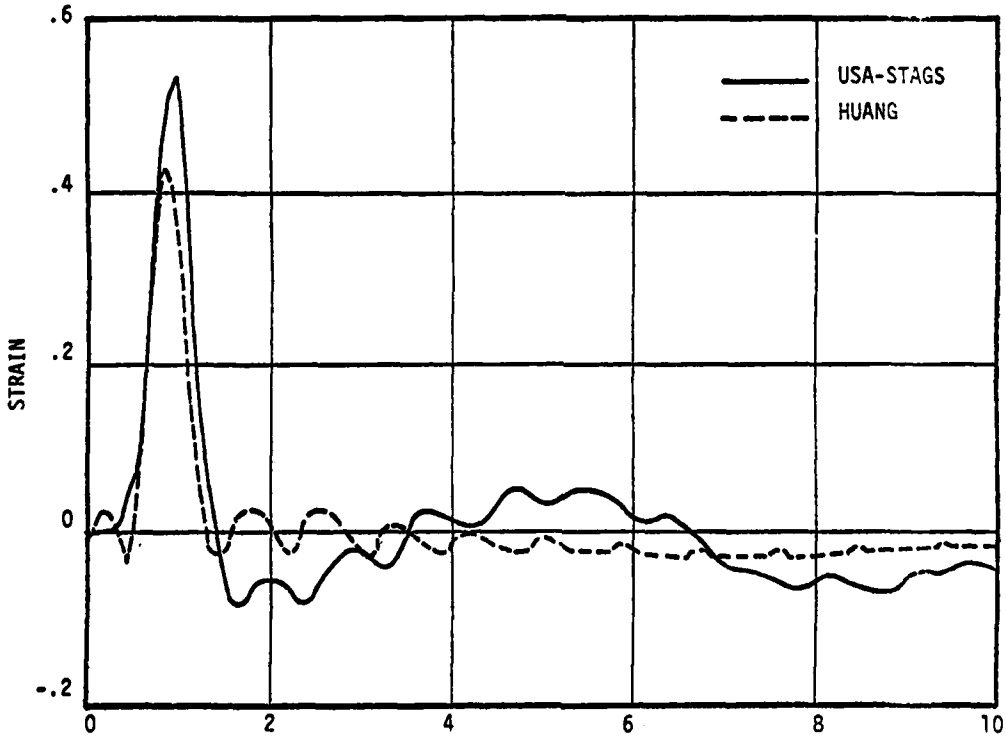

Figure 4.17. Hoop Strain at 90°, Cylinder, Step Wave

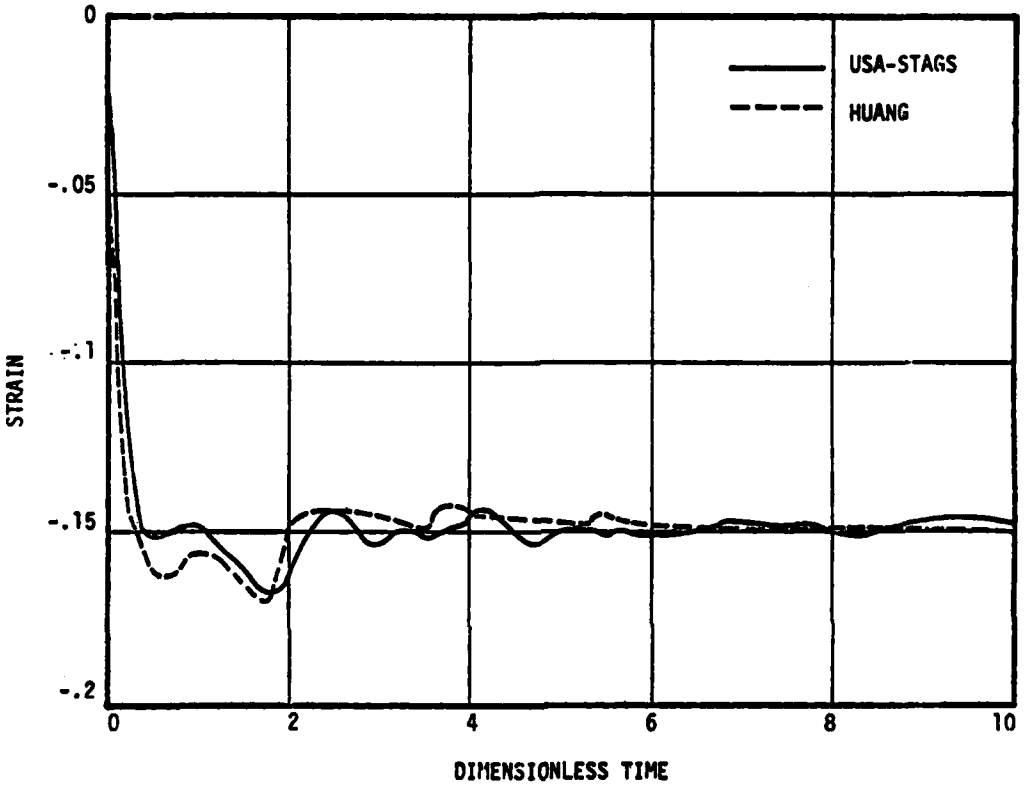

Figure 4.18. Hoop Strain at 180°, Cylinder, Step Wave

for banding the fluid mass matrix. There are several promising approaches, and banding the matrix will permit the consideration of many options that are presently computationally expensive;

(2) Develop and evaluate an unconditionally stable, fully coupled (implicit) solution algorithm for the fundamaental DAA equations. A banded added mass matrix would make this approach viable. This would eliminate the staggering of the solution scheme and would encourage the elimination of the USA code;

(3) Implement and evaluate the Pressure Integral Extrapolation (PIE) solution scheme. By Lockheed's own analysis, the PIE is as good or better than the Displacmeent Extrapoliation scheme; and

(4) Continue the evaluation of the DAA when implemented with Fourier series representations, particularly the DAA-DYNAPLAS implementation.

REFERENCES

[1] Carrier, G. F., "The Interaction of an Acoustic Wave with an Elastic Cylindrical Shell," Brown University Technical Report #4, 1951.

[2] Mindlin, R. D., and Bleich, H. H., "Response of an Elastic Cylindrical Shell to a Transverse Shock Wave," J. App. Mech, Vol. 20, 1953, pp 189-195.

[3] Geers, T. L., "Transient Response Analysis of Submerged Structures," Finite Element Analysis of Transient Nonlinear Behavior, Belytschko, T., Osias, J. R., and Marcal, P. V., eds., AMD-Vol. 14, ASME, NY, 1975, pp 59-84.

[4] Carrier, G. F., "Analytic Approximation Techniques in Applied Matahematics," J. Soc. of Ind. App. Math., Vol. 13, No. 1, Mar. 1969, pp 68-95.

[5] Huang, H., "A Qualitative Appraisal of the Doubly Asymptotic Approximation for Transient Analysis of Submerged Structures," N.R.L. Memo. Report 3135, Naval Research Lab., Sep. 1975.

[6] Geers, T.L., "Residual Potential and Approximate Methods for Three-Dimensional Fluid-Structure Interaction Problems," J. Acoust. Soc. Am., Vol. 49, No. 5, May 1971, pp 1505-1510.

[7] Park, K.C., Felippa, C.A., and DeRuntz, J.A., "Staggered Solution Procedures for Doubly Asymptotic Fluid-Structure Interaction Analysis," DNA Report 4525F and LMSC Report D624324, Feb 1978.

[8] Wang, Y.F., Everstine, G.C., Huang, H., Neilson, H.C., and Lu, Y.P., "Response of Main Pressure Hull to Underwater Shock Waves," DTNSRDC Report 4533, Apr. 1975.

[9] Klosner, J.M., "Response of Shells to Acoustic Shocks," Proc. Cong. Theo. & App. Mech; 1975.

[10] DiMaggio, F.L., and Baron, M.L., "A Review of Methods for Including the Effect of Indirect Fluid Loading on the Dynamic Response of Submerged Structures," Tech. Report No. 23, Weidlinger Assoc. NY, July 1978.

[11] Ranlet, D., and McCormick, J.M., "Transient Response of Submerged Shells of Finite Length to Full Envelopment Type Shock Waves, Part II: Comparison of Predictions and Measured Test Results for Side-On Loading," Tech Report No. 14, Weidlinger Assoc., NY, April 1974.

[12] Ranlet, D., Bleich, H.H., DiMaggio, F.L., and Baron, M.L., "Transient Response of Submerged Shells of Finite Length to Full Envelopment Type Shock Waves, Part IV: Comparison of Predicted and Measured Results for Side-On Loading of a Shell Containing Internal Structure-Configuration 1," Tech Report No. 17, Weidlinger Assoc., NY, 1974.

[13] Felippa, C.A., Geers, T.L., and DeRuntz, J.A., "Response of a Ring Stiffened Cylindrical Shell to a Transient Acoustic Wave," LMSC Report D403671, Lockheed Palo Alto, June 1974.

[14] Geers, T.L., and DeRuntz, J.A., "Transient Response Analysis Methods for Submerged Structures," LMSC Report D313297, Dec. 1972.

[15] Yen, C-L, Geers, T.L., and DeRuntz, J.A., "Response of Long and Short Cylindrical Shell Structures to Transient Acoustic Waves," LMSC Report 633352, Jan 1979.

[16] Huang, H. and Strandell, P., "Transient Response of a Spherical Shell to Plane Underwater Shock Waves," DTNSRDC Report MACHLAB 88, Jan 1979.

[17] Huang, H., "Transient Interaction of Plane Acoustic Waves with Spherical Shell," J. Acoust. Soc. Am., Vol. 45, No. 3, 1969, pp 661-670.

[18] Geers, T.L., "Excitation of an Elastic Cylindrical Shell by a Transient Acoustic Wave," J. Appl. Mech., Vol. 36, 1969, pp 459-465.

[19] Geers, T.L., "Response of an Elastic Cylindrical Shell to a Transverse Acoustic Shock Wave in a Light Fluid Medium," J. Acoust. Soc. Am., Vol. 48, No. 3(Part 2), 1970, pp 692-701.

[20] Geers, T. L., "Scattering of a Transient Acoustic Wavae by an Elastic Cylindrical Shell," J. Acoust. Soc. Am., Vol. 51, No. 5 (Part 2), 1972, pp 1640-1651.

[21] Geers, T.L., "Shock Response Analysis of Submerged Structures," Shock and Vibration Bulletin, Vol. 44, Supp. 3, Aug 1974, pp 17-32.

[22] Huang, H., Everstine, G.C., and Wang, Y.F., "Retarded Potential Techniques for the Analysis of Submerged Structures Impinged by Weak Shock Waves," Computational Methods for Fluid-Structure Interaction Problems, AMD-Vol. 26, ASME, NY, 1977, pp 83-93.

[23] Everstine, G.C., and Wang, Y.F., "The Response of a Cylindrical Hull with Internal Structure to Underwater Nuclear Shock Waves," DTNSRDC Report 77-0037, Apr. 1977.

[24] Geers, T.L., "Doubly Asymptotic Approximations for Transient Motion of Submerged Structures," J. Acoust. Soc. Am., Vol. 64, No. 5, Nov 1978, pp 1500-1508.

[25] Roderick, J.E., Jones, R.F., and Costello, M.G., "TRAINS-A Finite Element Computer Program for the Transient Large Deflection Analysis of Inelastic Structures," DTNSRDC Report M-17, Vol. 1, Basic Equations, Feb. 1978.

[26] Nickell, R.E., and Dunham, R.S., "Numerical Methods for Fluid-Structure Interaction," Part 1, Pacifica Technology Report PT-U79-0324, June 1979.

[27] Chopra, A.K.,, "Earthquake Behavior of Reservior-Dam Systems," ASCE J. Eng. Mech. Div., Vol. 94, No. EM6, Dec 1968, pp 1475-1500.

[28] DeRuntz, J.A., and Geers, T.L., "Added Mass Computation by the Boundary Integral Method," Int. J. Num. Meth. Eng., Vol. 12, 1978, pp 531-550.

[29] DeRunts, J.A., Geers, T.L., and Felippa, C.A., "The Underwater Shock Analysis (USA) Code, A Reference Manual," DNA Report 4524F and LMSC Report D624328, Feb. 1978.

[30] Zilliacus, S., Toridis, T., and Giacofci, T., "Analysis of Wave Excited Submerged Structures," Proc. ADINA User's Conference, Aug. 1979.

[31] Everstine, G.C., and Wallace, D.R., " A Guide to the Interfacing of NASTRAN with a Lockheed Integrator," DTNSDRC-TM-184-77-07, Oct. 1977, see also, NASTRAN: User's Experiences, NASA TM X-3428, Oct 1976, pp 207-228.

[32] Nickell, R.E., "Direct Integration Methods in Structural Dynamics," ASCE J. Eng. Mech. Div., Vol. 99, No. EM2, Apr 1973, pp 303-317.

[33] Park, K.C., Felippa, C.A., and DeRuntz, J.A., "Stabilization of Staggered Solution Procedures for Fluid-Structure Interaction Analysis," Computational Methods for Fluid-Structure Interaction Problems, AMD-Vol. 26, ASME, NY, 1977, pp 95-124.

[34] Park, K.C., "An Improved Stiffly Stable Method for Direct Integration of Nonlinear Structural Dynamic Equations," J. Appl Mech., Vol. 42, No. 2, 1975, pp 464, 470.

[35] Felippa, C.A., and Park, K.C., "Computational Aspects of Time Integration Procedures in Structural Dynamics," LMSC Report 556147, Lockheed Palo Alto, Jan. 1977; to appear in J. Appl. Mech.

[36] Gear, C.W., "Numerical Integration of Stiff Ordinary Differential Equations," Report No. 221, Department of Computer Science, University of Illinois, 1967.

[37] Love, A.E.H., A Treatise on the Mathematical Theory of Elasticsity, Dover, NY, 1927, 4th Ed.

[38] Huang, H., "An Exact Analysis of the Transient Interaction of Acoustic Plane Waves with a Cylindrical Elastic Shell," J. App. Mech., Vol. 37, No.12, 1970, pp 1091-1099.

[39] Geers, T. L., and Yen, C.-L., "Inelastic Response of an Infinite Cylindrical Shell to a Transient Acoustic Wave," LMSC Report D-676214, Lockheed Palo Alto, Mar. 1979.

[40] Felippa, C.A., and Geers, T.L., "Axisymmetric Free Vibration of a Submerged Spherical Shell," Lockheed, Palo Alto, to appear.

[41] Park, K.C., and Felippa, C.A., "Partitioned Transient Analysis Procedures for Coupled-Field Problems:Accuracy Analysis," LMSC Report D678072, Lockheed Palo Alto, July, 1979.

[42] Almroth, B.O., Brogan, F.A., and Stanley, G.M., "Structural Analysis of General Shells. Volume II: User Instructioins for STAGS C," LMSC Report D633873, Lockheed Palo Alto, Apr. 1979.

APPENDIX A

DEVELOPMENT OF LAX-RICHTMYER MATRICES FOR D.E. STAGGERED SOLUTION

In addition to equations (35 thru 42) described in Section 3, the following three identity equations for updating unknowns are used in the development of the amplification matrix;

$$u_n = u_n$$

$$\dot{q}_n = \dot{q}_n$$

$$\dot{q}_{n-1} = \dot{q}_{n-1}$$

The amplification matrix is $A_o^{-1} \cdot A_1$ where

$$\underset{\sim}{A}_o \underset{\sim}{u}^t + \Delta t = \underset{\sim}{A}_1 \underset{\sim}{u}^t + \underset{\sim}{B}$$

expresses unknowns at time $t + \Delta t$ as functions of unknowns at time t. The vector of unknowns at $t + \Delta t$ is

$$\langle u \rangle^{t+\Delta t} = \langle u^*_{n+1}, u_{n+1}, u_n, \dot{u}_{n+1}, \ddot{u}_{n+1}, \dot{q}^*_{n+1}, \dot{q}_{n+1}, \dot{q}_n, \dot{q}_{n-1}, \ddot{q}^*_{n+1}, \ddot{q}_{n+1} \rangle$$

The 11 x 11 matrix A_o is thus

$$\begin{bmatrix}
1 & 0 & 0 & 0 & 0 & 0 \\
0 & 1 & 0 & -\Delta t/2 & 0 & 0 \\
0 & 0 & 1 & 0 & 0 & 0 \\
0 & 0 & 0 & 1 & -\Delta t/2 & 0 \\
0 & \omega^2 & 0 & 0 & 1 & A \\
\rho cR\omega^2 & 0 & 0 & 0 & 0 & \rho cA(1+R) \\
0 & \rho cR\omega^2 & 0 & 0 & 0 & 0 \\
0 & 0 & 0 & 0 & 0 & 0 \\
0 & 0 & 0 & 0 & 0 & 0 \\
0 & 0 & 0 & 0 & 0 & -10/6\Delta t \\
0 & 0 & 0 & 0 & 0 & 0
\end{bmatrix}$$

$$\begin{bmatrix}
0 & 0 & 0 & 0 & 0 \\
0 & 0 & 0 & 0 & 0 \\
0 & 0 & 0 & 0 & 0 \\
0 & 0 & 0 & 0 & 0 \\
0 & 0 & 0 & 0 & 0 \\
0 & 0 & 0 & R & 0 \\
\rho cA(1+R) & 0 & 0 & 0 & R \\
0 & 1 & 0 & 0 & 0 \\
0 & 0 & 1 & 0 & 0 \\
0 & 0 & 0 & 1 & 0 \\
-10/6\Delta t & 0 & 0 & 0 & 1
\end{bmatrix}$$

and the 11 x 11 matrix A_1 becomes

$$\begin{bmatrix}
0 & 2 & -1 & 0 & 0 & 0 \\
0 & 1 & 0 & \Delta t/2 & 0 & 0 \\
0 & 1 & 0 & 0 & 0 & 0 \\
0 & 0 & 0 & 1 & \Delta t/2 & 0 \\
0 & 0 & 0 & 0 & 0 & 0 \\
0 & 0 & 0 & 0 & 0 & 0 \\
0 & 0 & 0 & 0 & 0 & 0 \\
0 & 0 & 0 & 0 & 0 & 0 \\
0 & 0 & 0 & 0 & 0 & 0 \\
0 & 0 & 0 & 0 & 0 & 0 \\
0 & 0 & 0 & 0 & 0 & 0
\end{bmatrix}$$

$$\begin{bmatrix}
0 & 0 & 0 & 0 & 0 \\
0 & 0 & 0 & 0 & 0 \\
0 & 0 & 0 & 0 & 0 \\
0 & 0 & 0 & 0 & 0 \\
0 & 0 & 0 & 0 & 0 \\
0 & 0 & 0 & 0 & 0 \\
0 & 0 & 0 & 0 & 0 \\
1 & 0 & 0 & 0 & 0 \\
0 & 1 & 0 & 0 & 0 \\
-15/6\Delta t & 1/\Delta t & -1/6\Delta t & 0 & 0 \\
-15/6\Delta t & 1/\Delta t & -1/6\Delta t & 0 & 0
\end{bmatrix}$$

APPENDIX B

DEVELOPMENT OF LAX-RICHTMYER MATRICES FOR FULLY IMPLICIT INTEGRATION

To develop the fully implicit integration operator, equations (31) and (32) area divided by m_s and evaluated at $t + \Delta t$,

$$\ddot{u}_{n+1} + \omega^2 u_{n+1} = A \dot{q}_{n+1}$$

$$R q_{n+1} + \rho cA \dot{q}_{n+1} = \rho cR u_{n+1}$$

To complete the system of 5 equations and 5 unknowns, the following trapezoidal expressions are postulated,

$$u_{n+1} = u_n + \frac{\Delta t}{2}(u_n + u_{n+1})$$

$$u_{n+1} = u_n + \frac{\Delta t}{2}(u_n + u_{n+1})$$

$$q_{n+1} = u_n + \frac{\Delta t}{2}(q_n + q_{n+1})$$

The vector of unknowns in equation (43) now becomes

$$\langle u \rangle_{n+1} = \langle u_{n+1}, u_{n+1}, u_{n+1}, q_{n+1}, q_{n+1} \rangle,$$

and the 5 x 5 matrices A_o and A_1 are,

$$\begin{bmatrix}
\omega^2 & 0 & 1 & 0 & A \\
0 & -\rho cR & 0 & \rho cA & R \\
1 & -\Delta t/2 & 0 & 0 & 0 \\
0 & 1 & -\Delta t/2 & 0 & 0 \\
0 & 0 & 0 & 1 & -\Delta t/2
\end{bmatrix} \{u\}_{n+1} =$$

$$\begin{bmatrix}
0 & 0 & 0 & 0 & 0 \\
0 & 0 & 0 & 0 & 0 \\
1 & \Delta t/2 & 0 & 0 & 0 \\
0 & 1 & \Delta t/2 & 0 & 0 \\
0 & 0 & 0 & 1 & \Delta t/2
\end{bmatrix} \{u\}_n$$

APPENDIX C

EVALUATION OF STAGS COMPUTER PROGRAM

Pacifica Technology has been using both the "C" and "C1" versions of the STAGS code for several years. The "C" version was an intermediate version (a finite element version of a finite difference code) that was released exclusively to the Naval Surface Weapons Center in White Oak, Maryland. The contents of STAGS-C were, and still are, largely unknown. Our C1 version was obtained from Lockheed in April, 1979. PacTech has been using STAGS-C1 since then. We have found it to be a very excellent computational tool for the general analysis of shell structures. STAGS has been developed exclusively for the analysis of shells; its name comes from Structural Analysis of General Shells.

Perhaps the most important virtue of STAGS is that it has been developed exclusively for the analysis of general shell structures; it is not a general purpose code, but it is a very robust special purpose code. It can solve any type of shell problem: static; dynamic; elastic; inelastic; large deformation; buckling and static collapse; modal analysis; and it has both explicit and implicit transient integration operators. These capabilities are nicely augmented by an extensive library of input options for the specialized description of shell problems, for example, shell coordinate systems, stiffener eccentricities to the mid-surface, and imperfections. These are essential features for any shell code, and too often they are not available in general purpose codes. STAGS is also a computationally efficient code, especially for central processor time, compared to general purpose codes, but are discussed below the I/O efficiency could be improved.

Although STAGS is an excellent code, the C1 version is in effect an entirely new code and, as such, it is undergoing extensive review and correction. It will take at least one and probably two more years to evolve into a properly functioning analysis tool. This will occur only if Lockheed places emphasis on the debugging and correction of the present version, and avoids the temptation to embellish the code.

At present the most significant problem with STAGS-C1 is a lack of documentation. Although a great deal has been written about STAGS and its use, the only documentation that exists for the C1 version is a users manual[42]. This manual, in spite of its size, does little but define the data cards that are required. There is virtually no discussion or guidance, and few recommendations are given. Even skilled and experienced finite element code users have difficulty learning to use STAGS-C1 because of the lack of adequate documentation. There seems to be a great deal of emphasis in the manual on identifying the FORTRAN variable names and little concern on identifying the physical meaning of the variables, or the consequences of their use or omission. The users manual should be entirely rewritten to include much more guidance for the average user.

While there are many very useful options described in the manual, our experience is that many of these options have not been implemented and often one option will not work when other options are used, for example, user loads do not work when a user grid is employed. Also, there appears to be a number of options that are in the code but that are not documented in the manual.

The lack of a theoretical manual is surprising. In one application a serious modeling error was made because we incorrectly assumed that STAGS formed a full tangent stiffness matrix. STAGS does form a partial tangent stiffness matrix for the large deflection terms, however, the nonlinearities due to plasticity are handled entirely by a pseudo force vector. Other features that need further description in a theoretical manual include: nonlinear solution strategy; convergence tolerances; the 5 point integration rule for the 410 element; the mechanical sublayer plasticity and how it is handled computationally; constraints; and integration through the thickness. (The Volume I theory manual was released by Lockheed after this report was prepared.)

Lockheed needs to develop a more organized method of interfacing with the STAGS user community. Although they use the CDC UPDATE processor for making corrections, they do not keep track of the correction IDENTS and hence loose valuable archival information. Lockheed only infrequently makes updates available to the user community. Also, the versions of STAGS that Lockheed has released to us and the Naval Surface Weapons Center at White Oak, and Lockheed's own version of the Air Force Weapons Lab computer system appear to be unknown quantities, i.e., no one remembers what is in them.

The following is a list of errors and suggested improvements:

(1) The users manual should be rewritten with greater emphasis being given to examples and recommended practices;
(2) A theory manual should be written;
(3) A full tangent matrix appraoch should be available as an option;
(4) The element I/O should be dramatically reduced. The 420 element currently reads and/or writes about 2500 words per iteration. This is excessive. Tradeoffs between disk, ECS or LCM, and recomputation should be made. Possibly an option to recompute or read can be included. The I/O structure of the code is excessively complex, it needs to be simplified.
(5) The constraints (full and partial) available in STAGS work only in certain restrictive situations and are subject to serious numerical difficulties. Erroneous solutions are frequently obtained when using constraints. Currently, constraints are available only in local coordinates. Options

should be added for global coordinate constraints. The Lagrange multiplier constraint leads to spurious eigenvalues that are undsirable. Penalty function constraints should be available in their place. When constraints are used, each DOF retains a column number in the assembled marix. This inefficiency should be eliminated;

(6) The equation solver used in STAGS has too fine a tolerance for the detection of rigid body motion and roundoff error. Also, the skipping of blank or empty columns is a dangerous practice that permits modeling errors to go undetected;

(7) The TAPE21 geometry data for the postprocessor appears to be overwritten by the constraints;

(8) The IGLOBE=3 option did not work correctly, this has subsequently been corrected. The IGLOBE=4 and 5 options should be documented;

(9) The restart file used by STAGS is much too large. Virtually everything is saved every time step to permit postprocessing. What is needed is a separation between restart data and time history data. Restart and solution contour data should be put on one file, and selective time history data should go on another file. The user should have the options of having data saved every "n" steps or every Δt seconds. At program exit, restart data should always be written for the last successful step;

(10) The program printout needs improvement. The selected output options do not work correctly and frequently generate more printed lines than a normal output. The "overwriting" formats with + signs in column one should be eliminated.

(11) The memory allocation algorithm is not foolproof (especially true for USA-STAGS);

(12) The solution strategy, while generally working well, could use options to permit further user control;

(13) The EIGA,EIGB frequency bounds sometimes give undesired results;

(14) In addition to CP time checking, automatic I/O time checking should be done each iteration as well as every time step;

(15) The user load option does not work with a user grid. Many other user defined options appear not to work in conjunction with one another;

(16) The overrelaxation factor tends rapidly to 2.0 and then remains fixed. This is not optimal. Some user control is desirable for this factor;

(17) The output from linear and nonlinear branches is quite different. This is undesirable. Computing stresses and strains with different logic for linear and nonlinear branches is a needless source of error;

(18) For inelastic analyses, Poisson's ratio must be set to 0.5 for beam and truss elements, the code does not automatically do this;

(19) Time varying loads do not appear to work properly with some nonlinear shell units;

(20) The load step control for nonlinear static analyses does not function properly. The zero step is always linear and the subsequent first nonlinear step is always to the same load factor. The rapid convergence causes the load step to be doubled, something that is not always desirable. The repat of step zero is an inefficiency;

(21) Substantially different iterative convergence is observed with the A and B load systems. Load system B seems to work as a preload with iterations being best done with load system A. This should be corrected;

(22) Despite the many load systems available in STAGS, we have experienced difficulty in conveniently defining general load systems. Also, many load options do not function properly. It is curious that USA has very convenient logic for handling moving, decaying lods, but that STAGS has no efficient option for this type of loading;

(23) A compatible curved shell element should be included;

(24) The version of STAGS that is distributed to the user community should contain the comment cards included in the Lockheed version;

(25) There is a major error in the handling of the area damping that causes several serious errors including the generation of negative damping. The diagonal damping matrix is input and treated as a vector. In the case of orthogonal local-global transformations at angles other than 90, both the magnitudes and signs may be incorrect;

(26) The transformatioans performed at the pole of the spherical coordinate systems causes fatal execution errors;

(27) Distributed loads are not treated consistently and work only for regular grids and shell units;

(28) Temporal and spatial loading (UPRESS) cannot be accessed with linear shell units;

(29) Area damping cannot be used with element units;

(30) Stiffness damping can cause the solution to diverge;

(31) Nodal damping values cannot be input;

(32) Loads referred to an undefined load systems are applied without an error message being written;

(33) Setting the initial velocity flag (IVELO) without specifying initial velocities gives erroneous results;

(34) The manual is not clear for initial velocity input (the load type is not irrelevant as the manual claims, it must be one of the possible load types); and

(35) The code goes into an infinite loop when a bad element Jacobian is found;

(36) There is no output for beam (stiffener) elements that are not plastic; and

(37) There is no method to control the bandwidth numbering; this generates a very large bandwidth and subsequent I/O charges for a full cylinder.

The programming philosophy used in developing STAGS is not easy to understand, and,

consequently, it will be difficult for even skilled finite element code developers to modify STAGS for their individual needs. Even after a year of intensive study and general use, we are reluctant to make changes in STAGS. A *programmers manual* would be very useful in this regard.

In summary, the extent of the above list is evidence that the C1 version of STAGS is in a primitive form and in need of extensive corretion and improvement. Our review has been daetailed and critical because we believe that STAGS can be a very efficient and effective code for the solution of all types of shell problems. It needs much additional work, but the STAGS support personnel at Lockheed are highly skilled and capable of performing the needed improvements. We encourage them to do so, and receommend that shell analysts acquire and use STAGS.

APPENDIX D

EVALUATION OF THE USA CODE

Pacifica Technology has also been using the USA code in conjunction with STAGS for several years. We have found it to be an efficient and effective code for the solution of the modified, augmentd, interaction equations via the displacement extrapolation staggered solution method described in Section 2. This is an important, but limited application. In particular, the USA code is highly effective in tandum with STAGS for the solution of submerged stiffened shells subjected to shock loads which produce significant plasticity and/or large deformations. Ths class of problems is a significant interest to the Navy. The use of the USA code in a stand-alone capacity, or with other structural codes for the solution of linear problems seems of more academic than practical value.

One of our main criticisms of the USA code is the philosophy that spawned its creation. Lockheed believed that the DAA needed to be implemented in a code that was entirely separate and independent from the structural code. This lead them to the derivation of the modified, augmented, interaction equations, and the displacement extrapolation staggered integration method. We believe that neither of these are desirable, and certainly disagree with the basic philosophy that lead to their selection. The USA-STAGS codes are not separate stand-alone codes, they are coupled and strongly dependent. Also, attempts to use other structural integrators have required substantial programming efforts to implement. It is our opinion that any well written structural code can be readily modified to accomodate the DAA as in the case of TRAINS[25], ADINA[30], and EPSA[15], and having a single special purpose code would lead to many added benefits. Besides, USA is a special purpose code that is limited to this one class of problems. Since the DAA and the staggered solution method have been discussed and evaluated elsewhere, the remainder of this appendix will be directed to the evaluation of the USA code.

Like STAGS, the documentation for USA is inadequate. Again, only a users manual is available[29], and the manual seems to concentrate on the identification of the FORTRAN variable names without defining the physical nature of the data. Since the DAA is not well understood, this problem is much more serious with USA than with STAGS (there are many knowledgeable finite element code users). Although there are several examples of typical data for USA, all of these are for stand-alone USA runs. There are no examples of the USA-STAGS data, indeed, the manual[29] discusses only USA. This is again a product of the separate-and-equal philosophy. Lockheed has written two reports to the Defense Nuclear Agency whose purpose is to serve as USA-STAGS manuals. These have never been distributed and are said to be out-of-date.

Because of the separate-and-equal philosophy, the data structure that is required for a USA-STAGS run is extremely complex, redundant, confusing, and a source of needless error. A typical USA-STAGS run requires a STAGS1 preprocessor data deck and execution, a FLUMAS data deck and execution, an AUGMAT data deck and execution, and a combined USAS(STAGS2) data deck and execution. Also, both USA and STAGS have postprocessors that require data and execution. These difficulties are further compounded when user supplied subroutines must be compiled in the run stream, or when special coding is used to generate required data (a procedure we find useful and frequently use). Also, USA-STAGS makes extensive use of dynamically assigned permanent files which require manipulation in the run stream. To make matters even more overwhelming, the execution modules (STAGS1, FLUMAS, AUGMAT, USAS(STAGS2), and the postprocessors require a special loading sequence; and because there is a high degreee of fraternization between the modules (use of common subroutine and/or routines with the same name but different instructions), it is necssary to form "libraries" from the various groupings of the relocatable binary records before the absolute elements can be formed. This is an extremely complex process, the results of which depend on the order of libraries specified, thus, creating another source of error. It is not uncommmon for a typical USA-STAGS run to require 100 control cards to obtain a complete solution with postprocessing. In order to reduce the possibility of error, it is necessary to use control cards macros to effect the complex process of multiple executions and file manipulations. This procedure is extremely complex and beyond the scope of all but the most expert user. Also, there is no documentation on how to perform these intricate steps. These are serious deficiencies and should be remedied.

The final step in the staggered solution sequence for the displacement extrapolation method is a correction of the pressure. The only use for this correction is to change the history terms that will be used for the fluid equation in the next time step. The effect of this final correction has never been evaluated, it was included because it could be done inexpensively. There is one bad feature of this

final step, it permits the "pressure" for which history is retained and printed to be different than the pressure used to drive the structure. This is undesirable. Our experience has shown that differences between these values can be significant at early times. We suggest that either this step be eliminated or the pressure applied to the structure be printed. In any case, logic should be added to insure that the two values agree to a reasonable tolerance.

The selection of the fluid degrees-of-freedom at the fluid element centroids we believe is inferior to the fluid element nodes (for example, as used by Roderick, et al.[26]). While a high order (17 point) formula is used to evaluate the incident pressure term for the fluid equation, because of the selection of the centroidal pressures only one integration point per overlain structural element is used for the structural equation. This is much too crude for the structure and too fine for the fluid. This should be corrected. Another related problem is that USA computes the consistent force vector rather than sending a vector of pressures back to STAGS. This is a source of error and has caused a great deal of trouble in developing a "live load" capability (one that accounts for the large rotations). We recommend that pressures, not forces, be passed to the structural code.

The USA modules receive a great deal of data both from STAGS and via input. However, in many of the important computational routines only sparse subsets of this data are available. This appears to have led to a number of unusual approximations. For example, the incident pressure is evaluated on two circles drawn about the fluid element centroid without regard to the actual element shape, and although data is available on the actual doubly curved geometry, a single radius of curvature is used. The errors associated with this model are generally small, but the approximations are needless and inaccurate for stand-off distances that are small compared to the shell diameter. We recommend that the basic data from the structural code be retained and used in USA (nodal point coordinates, curvatures, etc.).

Lockheed chooses to have the user identify the fluid elements by defining the structural nodes to which each fluid element is "attached". This is dangerous since it is possible to inadvertently omit structural nodes. These omitted structural nodes are treated as dry and thus receive no direct fluid loading. Since the only proper modeling is to have a fluid element overlay one or more structural elements, a more fail-safe input scheme would be to define for each element the overlain structural elements and have USA construct the correct "fluid nodes" from the structural connectivities.

The line-of-sight algorithm used to compute the incident velocity used, say, in equation (22) causes an undesirable unloading of the ends and backsides of most structures. When the vector dot product of the normal to the structure and the line-of-sight vector is positive the initial value computed for the scattered pressure is negative. This is incorrect because reflections and diffractions will generally give a positive value initially. This inaccuracy has never been evaluated, and it may be the cause of the low axial strain computations frequently observed.

The following is a list of suggested improvements and errors (other than those previously discussed):

(1) the time step sepcified to USA can be different than that used by STAGS, thus producing an erroneous run;

(2) The QUAMOD symmetry flag is redundant, this information should come from the structural code;

(3) a half symmetry option should be coded and the restrictions on the symmetry planes removed;

(4) the NUMZ and ZLEN parameters should be eliminated and the actual 2D influence functions used for a plane strain analysis;

(5) the symmetry options do not work with a 2D run;

(6) the AUGMAT processor should be integrated with the FLUMAS processor.

DISCUSSION

Mr. Orne (Westinghouse): How meaningful would a first order approximation of the rigid shell analysis be on this kind of a problem? Is there some way to check the solutions against a limiting case of a non deformable structure, either for cylindrical shells or spherical shells? The USA-STAGS code is a combined code and STAGS takes into account the elastic properties of the structure itself. In the limiting case where the structure is rigid, a rigid sphere or a rigid cylindrical shell, what would that code project and how would that compare to other kinds of simple models of that situation?

Mr. Dunham: It would probably do better, the elastic case is the more severe case.

Mr. Orne: How much difference would there be in terms of the pressure that would impinge on the peak pressures that you are talking about from a structural engineer's point of view? What load would you apply to a given structure to analyze it? How much different would the pressure loading be on either sperical or cylindrical structures in the two cases where you take the elasticity of the structure into account and other cases where you don't to get the rigid body motion?

Mr. Dunham: First of all there would be less damping.

Mr. Orne: Are we talking about factors of two or three difference in pressure?

Mr. Dunham: No, I don't think so. I think there would be a lot of similarity. I would not recommend this is a procedure to solve rigid structure problems because you are wasting a great deal of the computational capabilities. You would be better off with a code that just treated the fluid.

Mr. Orne: I realize that. I am just asking about this as a check case.

Mr. Kushner: As I understand it you want to know how close would you be to the total load on the structure if you just used the load scatter pressure on the rigid cylinder instead of calculating it with a DAA. In most of these problems you would be pretty far off, perhaps by a factor of two or three.

Mr. Meller (Lockheed Missiles & Space Co): I would like to make two comments. First the STAGS code is really not restricted to shells. You can use all kinds of finite elements in conjuction with shells. The other comment is in regard to the damping. Do you know where the damping comes from? Does it come from the USA part or from the STAGS part of the code? The time integration procedure is used and I'm not sure which one is used; but if you use the Park implicit method in the STAGS code then it has mathematical damping which depends on the time steps and it is available in literature. The type of damping you use depends on the type of damping you are talking about, time integration or the USA method.

Mr. Dunham: The point is well taken. We did not use the Park method, we used the trapezoidal rule which has no damping in it. The damping in the figures that you saw are intrinsic to the method itself. The DAA has its damping so the answer is that it indeed does come from the USA part, it does not come from the STAGS part. You do not control the integration operator in the USA-STAGS combination through STAGS. The USA modules, or the USA-STAGS modules do that. Your point about the finite elements in STAGS is undoubtably true for the people who use STAGS at Lockheed and it is not true for anybody else. We have the distributed version of STAGS and our version does not have that capability.

MEDIA-STRUCTURE INTERACTION COMPUTATIONS EMPLOYING FREQUENCY DEPENDENT MESH SIZES WITH THE FINITE ELEMENT METHOD

A. J. Kalinowski and C. W. Nebelung

Naval Underwater Systems Center
New London, Connecticut

The general problem of treating the numerical linear dynamic response of structures imbedded in a medium (fluid or solid) while subject to either radiation conditions or incident traveling wave inputs is considered. The formulation models both the imbedded structure and surrounding medium with finite elements and treats the absorption of waves radiated outward from the structure by means of appropriately sized dampers. Transient solutions are obtained by first computing the steady state transfer function for the response quantity of interest, and later post-processing this function with an FFT algorithm in conjunction with the specific input wave form. Segments of the transfer function are computed with the finite element method in the frequency domain by employing a set of frequency dependent mesh size finite element models, carefully designed to operate over a limited frequency band. The entire transfer function is obtained by piecing together the individual segments.

INTRODUCTION

This paper addresses the general problem of numerically computing the linear dynamic response of structures imbedded in a medium (fluid or solid) while subject to an incident traveling wave or radiation condition type of loading. The class of problems we address is broad and encompasses fields such as fluid-structure interaction problems encountered in underwater acoustics (both harmonic and shock wave type loadings) and solid-structure interaction problems encountered in seismic response computations. Specifically, the model configuration consists of a general elastic structure surrounded by an infinite medium (which may be fluid or solid). The loading conditions are either radiation or scattering time dependent conditions and result in either outward or inward propagating pressure (or stress) waves within the surrounding infinite medium. The temporal nature of the loading will be both time harmonic (i.e., all response quantities vary as $e^{i\omega t}$, ω and t being frequency and time respectively) and transient. The basis for the solution procedure for both temporal problem types focuses on the determination of the transfer function of the system (i.e., the time harmonic response of certain response quantities of interest vs. loading frequency ω). For problems where only the time harmonic response is desired, the transfer function for response quantities of interest is viewed as the final product; for transient inputs, the transient response is obtained by simple processing of the input wave form with Fast Fourier Transforms (FFT's).

The finite element method of solution is employed as the technique for determining the structure-infinite media transfer function. Modeling the structure with finite elements is straightforward, however, modeling the infinite domain involves two basic problems: (1) placing the proper radiation boundary condition at the media mesh truncation cut, (2) insuring that the mesh is fine enough to accurately represent wave propagation through the media, yet not be so fine that it results in an impractically large system of equations to solve. The high frequency end of the transfer function demands that a fine mesh be used, and the low frequency end of the transfer function demands that the radiation boundary be placed far from the structure (say 1-1/2 acoustic wavelengths). Employing a single fine mesh that satisfies the high frequency sampling requirements and is far enough from the boundary to meet the low frequency radiation requirements is theoretically correct but not feasible from a practical point of view, due to the fact that this approach results in a set of simultaneous linear equations that is too large to treat numerically. Instead, a variable mesh approach is employed wherein the complete transfer function is generated from a sequence of individual meshes, which are designed to work over a specific frequency range and only contain elements of a sufficiently small size and an infinite domain truncation boundary sufficiently far to accurately treat the specified frequency range of interest. The complete transfer function over the whole frequency range of interest is formed by patching together the individual transfer functions obtained from each of the optimized meshes.

A simple example problem of the methodology is presented which includes all of the important features of the solution technique. An elastic cylinder is submerged in an infinite fluid and subject to an incident cylindrical wave. The pressure field surrounding the cylinder is computed for an exponential input pulse shock wave. The transfer function results as determined by the exact solution and variable mesh finite element solution are compared; further, the transient response obtained by processing both of these transfer functions through an FFT processor are also compared.

STATEMENT OF THE PROBLEM

To develop a numerical technique (we refer to as the "frequency dependent mesh" procedure) for solving linear media-structure interaction problems that employ a finite element type representation for both the structure and surrounding media, yet avoids excessive undesirable fine mesh requirements dictated by high frequency response requirements. The primary application is for treatment of submerged structures subject to transient incident shock waves; secondary, applications are for submerged structures subject to radiation loads (i.e., transient loadings originate from the structure and radiate energy into the media).

OUTLINE OF THE FREQUENCY DEPENDENT MESH PROCEDURE

Step 1 -

Solve for the steady state response (i.e., the system transfer function for all response quantities of interest where inputs vary harmonically as $e^{i\omega t}$) in the frequency domain with the finite element method

- accomplished by employing a sequence of N finite element meshes.
- a typical n^{th} mesh, n=1, 2, . . . N, is optimized for a minimum degree-of-freedom model size which adequately provides the transfer function over a specific frequency range $(f_\ell)_n \le f \le (f_h)_n$, where $(f_\ell)_n$, $(f_h)_n$ are the low and high frequency limits respectively of the n^{th} mesh.
- the full transfer function is obtained by piecing together the N individual transfer function in segments; some blending is done at the frequency interface between neighboring segments.

Step 2 -

The Transient Solution is obtained by post-processing the transfer function in conjunction with the input wave form with a standard Fast Fourier Transfer (FFT) algorithmn.

FEATURES OF FREQUENCY DEPENDENT MESH PROCEDURE

- Potential errors introduced when approximate media-structure interaction laws are employed (e.g., such as the "doubly asymptotic approximation, DAA" reference [1]) are avoided by explicitly modeling the media.
- Total finite element model size requirements are more favorable (less degrees-of-freedom) with the frequency dependent mesh procedure than with a straight direct time integration method of the full structure-media finite element mesh.
- Obtaining responses for a parametric set of transient input wave forms requires no new finite element computer runs, wherein all new cases are computed with FFT post-processing.

CRITERIA FOR MESH SIZE OPTIMIZATION

Consider the optimization problem of determining a single mesh that will adequately represent the solution response quantity transfer function over the n^{th} frequency range defined by the frequency limits $(f_\ell)_n \le f \le (f_h)_n$. The quantity (or "objective function") we wish to minimize is the total degrees-of-freedom for the mesh. More important, the optimization is made subject to two key counteracting constraints, namely

- Element Size Constraint

The biggest element length, $(\Delta L_{max})_n$ in the medium surrounding the structure should be equal or smaller than a fraction, β, of a medium wave length, $(\lambda_h)_n$, where $(\lambda_h)_n = c/(f_h)_n$ and c corresponds to the medium wave speed (c corresponds to the acoustic wave speed for fluid media; or, c corresponds to the shear wave speed for solid media); thus

$$(\Delta L_{max})_n \le \frac{\beta c}{(f_h)_n} \qquad (1)$$

wherein the value of β, discussed later, is related to the type of finite element employed.

- Boundary Placement Constraint

The placement of the outer boundary should be such that the distance, $(\tilde{D}_{min})_n$, between a point on the boundary of the media truncation and the closest point on the structure should be equal or greater than α times a medium wave length, $(\lambda_\ell)_n$, where $(\lambda_\ell)_n = c/(f_\ell)_n$; thus

$$(\tilde{D}_{min})_n \ge \frac{\alpha c}{(f_\ell)_n} \qquad (2)$$

wherein the size of α, discussed later, is directly related to the energy absorbing boundary condition.

The degrees-of-freedom for the n^{th} frequency range model are implicitly kept to a minimum by employing the largest size element permitted by constraint (1) and the closest boundary permitted by constraint (2) (i.e., employ the equality sign in the constraining equations (1) and (2)). In approaching the problem in this manner, we are not employing the phrase "minimum" in the strict sense of mathematical optimization theory, although it would be possible to formulate the problem statement in this fashion. Instead, creating a mesh that meets the equalities of both constraints will result in a "nearly optimum" mesh that is fine enough to handle the highest frequency in the n^{th} range of interest, $(f_h)_n$, and yet have a boundary placed just far enough to make the radiation boundary absorbers work

at the lowest frequency in the frequency range, $(f_\ell)_n$.

Determination of β Multiplier

The value of β depends on the type of element employed to represent the fluid medium. Experience with finite elements with nodes only at the element corners (either 2-D or 3-D elements) has shown that β should be no bigger than 1/8, which is equivalent to modeling 8 elements per medium wave length, see references [2], [3]. Higher order elements with nodes on the sides and element corners should allow one to increase the β factor larger than 1/8.

Determination of the α Multiplier

The value of the α multiplier is directly related to the treatment of the absorbing boundary. In the case of fluid media, a simple, yet effective procedure for treating the waves radiating from the structure is to invoke a plane wave boundary condition of the form

$$P_r = \rho c (V_n)_r \qquad (3)$$

where P_r is the radiated component of the total pressure, $(V_n)_r$ is the radiated component of the media particle velocity normal to the wave front, ρ is the media density and c is the media compressional wave speed. The application of this boundary condition involves applying radiation "dampers" normal to the outer fluid mesh boundary, wherein the magnitude of the dampers is equal to ρcΔA, where ΔA is an appropriate area factor relating distributed surface pressure to lumped nodal force. For pure radiation problems (forcing functions originating within the structure), only radiation dampers are applied around the outer boundary of the model; however, for incident wave type problems, applied forces corresponding to the incident loading, also enter at the same boundary nodal points. References [6], [7] gives additional details on loading the outer boundaries for fluid-structure interaction problems. Reference [5] discusses a similar radiation boundary condition for solid-structure interaction problems where both normal and tangential dashpots are applied at the boundary.

The boundary condition, equation (3), is strictly valid when the radiating wave is plane and normal to the surface. If the radiating wave is plane, but not normal, most of the radiating energy is still absorbed, references [5], [7]. Employing the equations in reference [5] for the case of fluids, it can be shown that the dampers still absorb 90% of the energy even when the angle of incidence is 30° (90° being normal incidence).

Another condition, which must be met in order to strictly apply equation (2), is the fact that the radiating wave should be planar. This planar condition can, however, be relaxed by observing that the structure radiation in the fluid can be approximated by removing the radiating structure and then replacing it with a distributed set of point sources (line sources for 2-D problems) around the inner surface of the fluid media that is normally in contact with the structure (i.e., the wet surface). This equivalent problem is explained in reference [4]. At this point in the development, we need not concern ourselves with the magnitude of these sources, for it has no bearing on the following. Next, consider the relation between the radiated pressure and normal velocity for one of these sources. It is convenient to consider the ratio of pressure divided by velocity, (i.e., the point impedance, Z), and compare the source impedance value to the ideal planewave impedance, Z_{pw}, where from equation (3) it follows $Z_{pw}=\rho c$. Upon employing known relations for the pressure and velocity field of 2-D and 3-D sources, reference [8], the following relationships follow

3-D point source impedance (spherical wave spreading) $Z_{sw}=\rho c\frac{[(kr)^2+ikr]}{[1+(kr)^2]}$ (4)

2-D line source impedance (cylindrical wave spreading) $Z_{cw}=\frac{[-H_0^{(2)}(kr)]}{[H_1^{(2)}(kr)]}\rho c$ (5)

where $k=\omega/c$, r=radial distance from the source, and $H_0^{(2)}$, $H_1^{(2)}$ are zeroth and first order Hankel functions of the second kind.

It is noted that in the limit as $kr\to\infty$, both point source impedance and line source impedance $\to\rho c[1.0+0.0i]$; that is both Z_{sw} and Z_{cw} approach the desired plane wave impedance, ρc. Moreover, we need not go an infinite distance from the source to reach the plane wave impedance; instead, this situation is very closely approached at just 1.5 wave lengths (i.e., α = 1.5 in equation (2)) away from either the point source location for 3-D problems or the line source location for 2-D problems. For example, evaluating both equations (4) and (5) at a 1.5 wave length distance from the source (i.e., $kr=1.5x2\pi$), it follows that $|Z_{sw}|=.994\rho c$ with a 6° phase angle and $|Z_{cw}|=.997\rho c$ with a 2.5° phase angle. Thus, the simple ρc boundary dashpots will also absorb spherical waves with a 0.6% error in boundary impedance for 3-D problems and absorb cylindrical waves with a 0.3% error in boundary impedance for 2-D cases.

Often it is desirable to trade off some boundary absorber accuracy to reduce the distance from the structure surface to the outer boundary of the mesh (equivalently makes the finite element model smaller). Thus letting α=1.0, it follows that the simple ρc boundary dashpots will absorb spherical waves with a 1.4% error in boundary impedance for 3-D problems and absorb cylindrical waves with a 0.8% error in boundary impedance. The curves given in Fig. 1 provide a plot of the complex impedance for both the spherical wave and cylindrical wave vs. the α parameter, wherein it is demonstrated that severe errors in the boundary impedance start occurring for values of α<0.3.

The absorption argument has focused on a single source. The total problem response can be viewed as superimposing the responses to each of the sources individually, wherein the radiation from each source will be automatically absorbed by the fixed dashpot placed along the outer mesh boundary.

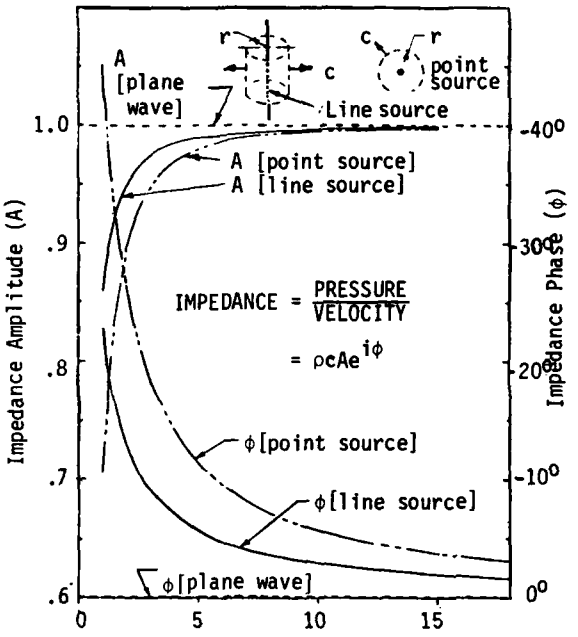

FIG. 1 - Impedance vs. Distance for Plane, Line and Point Sources

Estimate of Minimum Number of Medium Elements Between Structure and Boundary

By employing inequalities (1) and (2) it is possible to estimate minimum number of equal size elements that are needed along a ray extending between the structure surface and outer boundary of the mesh. If equal size elements are employed, the distance $(\tilde{D}_{min})_n$ in relation (2) is given by

$$(\tilde{D}_{min})_n = m(\Delta L_{max})_n \qquad (6)$$

where m is the number of elements along the ray and $(\Delta L_{max})_n$ is the element thickness along the ray. Upon substituting relations (1) and (2) (employing the equal sign in the inequality) into equation (6) and solving for m, we arrive at

$$m = \left(\frac{\alpha}{\beta}\right) \cdot \frac{(f_h)_n}{(f_\ell)_n} \qquad (7)$$

For example, substituting typical values for α=1.0, β=1/8 and subdividing the frequency range into 1.0 octave bands (i.e., $(f_h)_n/(f_\ell)_n$=2.0), we arrive at m=16 elements along a typical ray in the mesh.

Equation (7) indicates that there is a trade off between the large modeling effort required to make many meshes (N large) with a small $(f_h)_n/(f_\ell)_n$ ratio (and consequently a small m for each mesh)--as compared to--a small modeling effort required to make a few meshes (N small) with a large $(f_h)_n/(f_\ell)_n$ ratio (and consequently large m for each mesh.

GUIDELINES FOR MESH CONSTRUCTION

This section considers the practical problem of constructing a mesh that meets the criteria governed by inequalities (1) and (2). In particular, emphasis is placed on the situation where a finite sized structure is imbedded in the infinite medium. Two approaches to forming the set of N meshes for each frequency range, $(f_\ell)_n \leq f \leq (f_h)_n$, are considered. The first method involves generating a brand new mesh for each of the n=1, 2, . . . N frequency ranges. The second method employs a single master mesh for all N frequency ranges, wherein each individual transfer function segment is obtained by appropriately "peeling" off the larger outer elements for each higher frequency range considered.

Mesh Regeneration Approach

The approach simply involves creating a brand new mesh for each of the n=1, 2,. . . N frequency ranges for each segment of the desired transfer function. This method is best suited for situations where the mesh can be automatically generated. For a specific frequency range, say $(f_\ell)_n \leq f \leq (f_h)_n$, envision laying out a constant element size mesh meeting the equality limits of the optimum mesh criteria, equations (1) and (2). Next superimpose on this field the structure and appropriately blend in the media elements to the structure surface node distribution and at the same time remove media elements previously occupied by the media volume now occupied by the structure. The nodal distribution of the structure should be dictated by the expected modal response excited for the n^{th} frequency range under consideration. In some cases, the distribution of the structure surface nodes may be different than the mesh size dictated by inequalities (1) and (2). In particular, at the lowest frequency range, n=1, the media elements are usually large compared to the structure elements; consequently, an intermediate zone of finer elements could be used to blend the structure nodes into the media nodes. Another approach is to employ some sort of averaging procedure between those surface nodes on the structure which have no corresponding node in the media and the nearest nodes in interfacing media.

Mesh "Peeling" Approach

This approach is particularly useful when the structure model is complex and thus is inconvenient to create brand new meshes for each of the N frequency ranges. This approach is perhaps more convenient to employ than the previous mesh regeneration approach, however, it would generally result in overall finite element models whose total degree-of-freedom size is larger than the previous mesh regeneration approach, but still smaller than a mesh designed to work directly with the transient approach. The mesh peeling approach begins by first observing that the low frequency models, say, n=1, 2, usually need some sort of blending to match the coarser size media elements to the finer distributed structure nodes. Therefore, a single variable sized mesh is envisioned which starts out fine at the structure-media interface (say fine

enough to meet both the geometrical shape definition requirements and/or the highest modal response requirements of the structure) and becomes increasingly coarse as one moves radially away from the structure interface approaching the outer boundary of the media mesh. The largest element in the medium (farthest away from structure) meets the inequality (1) for n=N, and the outer boundary distance for n=1 meets inequality (2). Further, the distribution of element size in the radial direction (starting at the surface of the structure and moving radially away from the structure towards the outer boundary) should be such that N distinct radial zones of elements are identifiable (corresponding to the N frequency segments of the desired transfer function). The largest element in the n^{th} zone meets inequality (1) and the radial distance between the outer boundary of the zone and the surface structure meets inequality (2). Once having the master mesh as defined above, the full transfer function is generated in steps, starting with frequency segment n=N first (i.e., exercising the finite element model with the full mesh with all N media mesh zones included). Once the model is exercised with the finite element method and $T_N(\omega)$ is obtained and recorded for $(f_\ell)_N \leq f \leq (f_h)_N$, the appropriate outer zone of coarse elements is "peeled away" and the boundary loading moved inward to the new media outer boundary for the n=N-1 case. The new peeled model is executed, and $T_{N-1}(\omega)$ is obtained for $(f_\ell)_{N-1} < f < (f_h)_{N-1}$. The process is repeated for n=N-2, N-3, . . . 2, 1, thusly obtaining the full transfer function over the desired frequency range.

A demonstration problem employing the mesh peeling method is given later and will clearly illustrate the steps involved in the peeling procedure.

FORMATION OF THE TRANSIENT SOLUTION

Time History from Fourier Convolution

The desired transient response, $P_r(t)$ due to an input wave form, $P_i(t)$, can be routinely obtained by processing the system transfer function, $T(\omega)$, for the response quantity of interest with the input wave form by employing the standard convolution relation, reference [11], relation

$$P_r(t) = \frac{1}{2\pi} \int_{-\infty}^{\infty} T(\omega)\ F(\omega)\ e^{i\omega t}\ d\omega \qquad (8)$$

where

$$F(\omega) = \int_{-\infty}^{\infty} P_i(\tau)\ e^{-i\omega\tau}\ d\tau \qquad (9)$$

The evaluation of equation (8) is performed with Fast Fourier Transforms processing wherein the integral limits in equation (8) are truncated at $\pm\omega = 2\pi f_{max}$, where f_{max} is the largest frequency processed in equation (8) (e.g., see references [10], [12] for details on signal processing which are beyond the scope of interest of this paper).

Transfer Function Alterations

There are certain problems associated with the conversion of the steady state solution into the transient solution that needs further elaboration. In particular, the problems associated with joining neighboring segments of the numerically obtained transfer function and obtaining the very low frequency portion and very high frequency parts of the transfer function need further clarification.

- joining transfer functions of the n^{th} and $n+1^{th}$ segment

Theoretically, the value of the transfer function, $T(2\pi f)$ should be exactly the same when evaluated at the end of the n^{th} frequency range, $f=(f_h)_n$, and again evaluated at the start of the n+1 frequency range, $f=(f_\ell)_{n+1}$. The transfer functions would be equal if an exact analytical solution is evaluated; however, because of the manner in which the element size errors and absorbing boundary errors enter into the finite element solution procedure, it follows that the numerical values of $T(2\pi f)$ computed by the n^{th} and $n+1^{th}$ meshes are not exactly equal at the junction. Consequently, the average value is taken at the junction, i.e.,

$$T(2\pi f)_{av} = \frac{T(2\pi \cdot (f_h)_n) + T(2\pi \cdot (f_\ell)_{n+1})}{2} \qquad (10)$$

where

$$f = (f_h)_n = (f_\ell)_{n+1}$$

- low frequency alteration

The static (or D.C.) solution often has to be treated as a special case, even when analytical solutions are employed. For example, analytical solutions for wave propagation type problems involving structures submerged in a fluid usually have analytical solutions wherein the response quantity of interest requires the evaluation of a 0/0 in determinant form in the limit as $\omega \to 0.0$. In the case of finite element models, the zero frequency limit often results in a free-free structure which will behave like a mechanism in the sense that a singular stiffness matrix, [K], will remain at $\omega \to 0$, as can be seen by observing the governing finite element equations

$$[-\omega^2[M] + i\omega[C] + [K]]\{U\} = \{F\} \qquad (11)$$

where [M], [C], and [K] are the finite element mass, damping and stiffness matrices respectively. The quantities {U}, and {F} are the displacement and applied force vectors respectively. In the instance where part of [K] is made up from a fluid finite element displacement approach, [K] will also have many kinematic mechanisms in addition to the rigid body modes, (e.g., reference [9]).

The static solution can usually be easily obtained by separate considerations depending on the response quantity being sought and the type of input loading encountered in the problems at hand. For example, suppose the response quantity of interest is the stress in the structure at some point, and the loading is a traveling harmonic wave of the form $P_i = 1.0\ e^{i(\omega t + kx)}$. As

$\omega \to 0$, the loading reduces to exposing the free-free structure to a constant hydrostatic unit load, P=1.0psi, which can be obtained as a separate finite element solution with the statics portion of the particular finite element program being employed. Similarly, if the total pressure on the surface of the structure was the response quantity desired, then P_T=1.0.psi at ω=0 would be corresponding static transfer function value.

If the solution to equation (11) cannot be directly obtained at ω=0 for the singularity reasons just mentioned, then it follows that the solution of equation (11) will also have trouble in the immediate neighborhood of ω=0. The problem is overcome by establishing some safe low frequency cut off, $\omega = 2\pi f_{\ell c}$, below which the finite element solution is not exercised. The missing portion of the transfer function between $0 < \omega < 2\pi f_{\ell c}$ is generated by employing linear interpolation on the separate real and imaginary parts of the transfer function response quantity of interest. Most modern finite element programs will trigger warning flags when the user operates at ω values too close to the ω=0 singularity, in which case the $f_{\ell c}$ cut value can be adjusted accordingly.

• high frequency alteration

The time sampling of the output of the FFT processor, Δt, is directly related to f_{max}, namely $\Delta t = 1/f_{max}$. Thusly, if one requires a fine sampling of the transient output, the upper integral truncation limit of equation (8) must be large. The impact of this statement on the finite element method is that the transfer function response for range of the last segment of the transfer function, $(f_\ell)_N \le f \le (f_h)_N$, may be too high to obtain from a practical point of view. Theoretically the transfer function could be obtained for the high frequency range, however, its contribution to the integral in equation (8) may be minimal when the multiplying wave form transform, $F(\omega)$, is very small. Therefore, a high frequency cut off, $\omega = 2\pi f_{hc}$, is employed, wherein the transfer function, $T(\omega)$, is thusly only actually computed with the finite element method for frequency in the range $2\pi f_{\ell c} \le \omega \le 2\pi f_{hc}$. There are several choices open with regard to the value of $T(\omega)$ within the finite element computed frequency range of

$$f_{hc} < f < (f_h)_N \qquad (12)$$

The simplest case is when $F(\omega) \approx 0$ over the above range (12), wherein $T(\omega)$ is simply set =(0.0+i 0.0) for the range (12). Another option available, is for situations where the response quantity of interest has a predictable high frequency limit, $T(\infty)$, and at the same time, $F(\omega)$, may not be small enough to neglect over the range (12). In such cases, $T(\infty)$, rather than (0.0+i 0.0) can be employed over the range (12). For example, in situations where the reflected fluid pressure is the response quantity of interest, the $T(\infty)$ value can be determined from a separate finite element run wherein the surface of the elastic structure is replaced by a zero normal displacement boundary condition, thus simulating the reflection from a rigid structure.

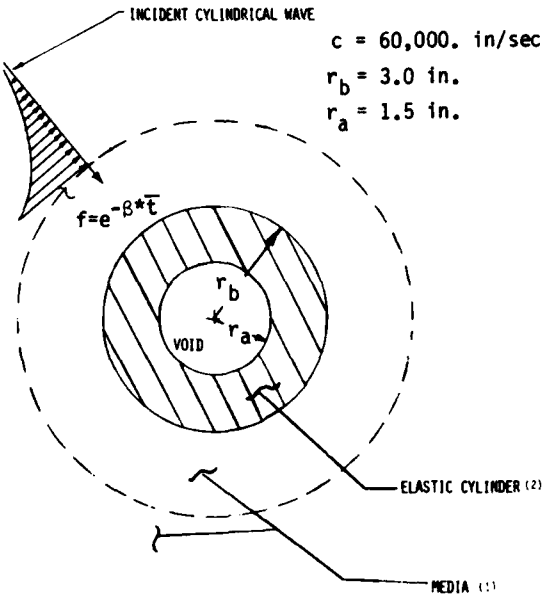

FIG. 2 - Submerged Infinitely Long Elastic Cylinder

DEMONSTRATION PROBLEM - 1

A sample demonstration problem is needed to illustrate the application and solution accuracy of the proposed frequency dependent mesh procedure. The example selected is an infinitely long thick-walled cylindrical shell subject to an incident converging cylindrical pressure wave (see Fig. 2). The origin of the input wave can be thought of as converging in on a sink located at the center of the cylinder, wherein the free field representation of the input wave, far away from the sink can be expressed in the form

$$p^i(r,t) = \frac{A^* f(\bar{t}) H(\bar{t})}{\sqrt{r}} \qquad (13)$$

with

$$\bar{t} = t + \frac{r}{c} - \frac{r_b}{c}$$

where A^* is the strength of the sink (adjusted in magnitude to provide a unit incident pressure at $r=r_b$, $t=0$); $f(\bar{t})$ is the wave form (e.g., $f=e^{-\beta * \bar{t}}$), $H(\bar{t})$ is the Heaviside step function, r_b is the cylinder outer radius. Solution (13) satisfies the acoustic pressure field equations

$$\frac{1}{r}\left(\frac{\partial}{\partial r}(rp)\right) = \frac{1}{c^2}\frac{\partial^2 p}{\partial t^2} \qquad (14)$$

provided

$$\frac{f(\bar{t})}{\frac{r^2}{c^2}\frac{\partial^2 f(\bar{t})}{\partial \bar{t}^2}} \ll 1 \qquad (15)$$

For example, in the demonstration problem an exponential decay waveform, $f(\bar{t}) = e^{-\beta * \bar{t}}$, is employed. Consequently inequality (15) becomes

$$\left(\frac{c}{r\beta^*}\right)^2 \ll 1 \qquad (16)$$

The approach to solving the transient demonstration problem is to solve the complete problem in the frequency domain, and then convert the result into the corresponding desired transient solution. This process is done twice, first employing the exact transfer function in conjunction with equation (8), and secondly, with the numerically obtained transfer function employing the finite element method.

The demonstration problem selected, although simple in appearance, has many important features we wish to exhibit that are representative of a more complex problem; namely, curved wave inputs, exponential shape pressure waveform, elasticity of the submerged structure and a sequence of submerged resonant modes. The resonant modes of the problem are the breathing mode and wall thickness resonances that occur whenever the frequency of the incident harmonic wave results in an elastic material 1/2 wave length that is a multiple of the cylinder thickness. These wall thickness resonant modes are present because of the elasticity theory representation for the cylinder; in contrast, shell theory would assume the thickness of the shell to be rigid, consequently only the breathing mode would be the only symmetrical mode excited by the symmetrical nature of the incident wave loading.

Exact Solution Transfer Function

The exact solution to the demonstration problem in the frequency domain is given in the appendix, and is specifically provided by equation (12-A), for an $e^{-i\omega t}$ type of loading. The processing of the transfer function and input waveform into the exact solution requires a solution for $e^{+i\omega t}$ if the format of equation (8) is employed. Consequently, the exact transfer function, $T_{EX}(\omega)$, for use in equation (8) is obtained by simply taking the conjugate of the equation (12-A) result, i.e.,

$$T_{EX}(\omega) = \overline{P(r)} \qquad (17)$$

Finite Element Transfer Function

Next consider generating the finite element transfer function, $T_{FE}(\omega)_n$, by employing the frequency dependent mesh procedure outlined earlier. In particular, the mesh peeling approach is used to generate the segmented transfer function. The cylindrical symmetric structure is subject to a cylindrically symmetric input wave, consequently only a typical wedge of the full media need only be modeled as illustrated in Fig. 3. The nodal loading at the outer boundary is computed by employing the normal incident wave pressure, i.e., equation (4-A) sutstituted into equation (3-A) and appropriately converted into complex radial nodal forces at the outer boundary cut. Since each of the N meshes in the peeled mesh approach continues to move the mesh boundary inward with increasing n, the values of the outer boundary forces are recomputed for each of the N separate transfer function finite element models.

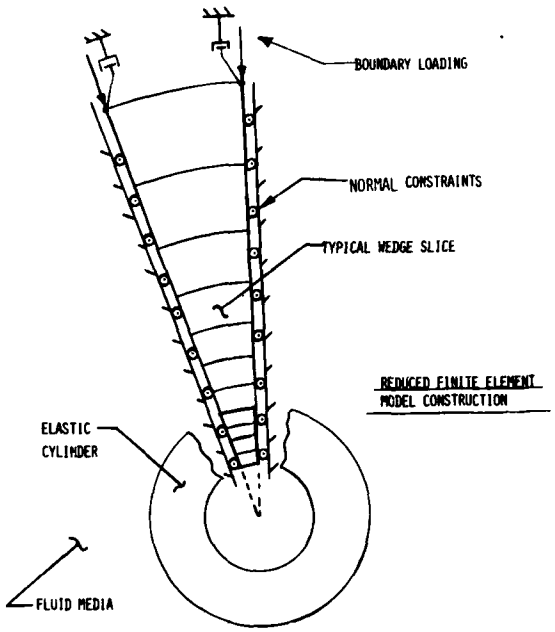

FIG. 3 - Plane of Symmetry Cuts

Six separate models, N=6, are employed, and are designed to work in the frequency range given in the following table.

TABLE 1 - FREQUENCY RANGES

n	$(f_\ell)_n$;kHz	$(f_h)_n$;kHz
1	0.30	0.70
2	0.70	1.60
3	1.60	3.50
4	3.50	7.10
5	7.10	12.50
6	12.50	18.40

Since we are allowing elasticity through the thickness of the cylinder, 16 elastic elements are used to model through the wall thickness. The six finite element meshes are illustrated in Fig. 4. The element sizes appear to be slightly different in the Fig. 4 plot, but this is due to the fact that the plotting scale is changed for each of the six mesh plots so that the total plotted length of the model takes up the same amount of space on the figure. The finite element models employ CQDMEM quadralateral elements in conjunction with the NASTRAN finite element computer program. The program is operated in a cylindrical coordinate system, consequently enforcement of the constraints normal to the plane of symmetry cuts is straightforward. The material constants are modified to automatically convert the NASTRAN plain stress elements into plain strain elements. The following table provides the material constants employed in both

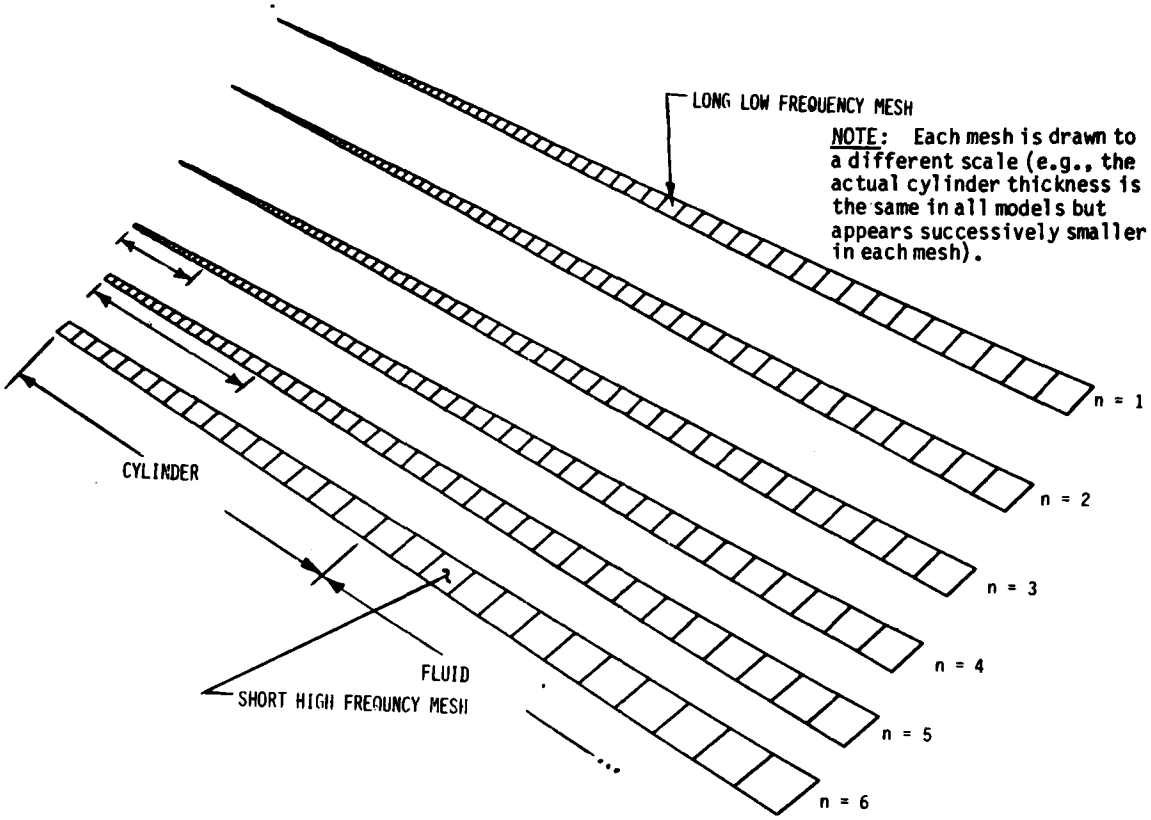

FIG. 4 - Sequence of Finite Element Meshes

the finite element and exact solution formulation.

TABLE 2 - EXAMPLE MODEL MATERIAL CONSTANTS

MATERIAL / PROPERTY	CYLINDER (silver)	MEDIUM (water)
λ(psi)	11,737,000.	345600.
μ(psi)	4,124,000.	0.0
$\rho\left(\frac{\text{lb-in}^4}{\text{sec}^2}\right)$	.000982	.000096

The first, n=1, mesh in Fig. 4 is designed to work in the n=1 frequency range of Table 1, and all media elements in the media meet the inequality constraints of inequalities (1) and (2). The second mesh, n=2, is obtained by simply peeling off the outer 20 elements of the n=1 mesh and assigning new loads and dampers to the new outer boundary, wherein, all elements in the n=2 mesh again meet the inequality constraints (1) and (2). Similarly, mesh n=3, is obtained by peeling 19 elements from mesh 2; mesh n=4 peels 19 elements from mesh n=3; mesh n=5 peels 16 elements from mesh n=4 and finally, mesh n=6 peels 13 elements from mesh n=5.

The angle of the wedge in all 6 meshes was held constant; this is in keeping with the mesh peeling approach which maintains the same media-structure interaction model for all N meshes. However, had the mesh regeneration approach been taken, the angle of the wedge could have been appropriately changed for each n value, thus allowing a larger segment of the cylinder to be covered for the lower frequency model, and consequently, the number of radial elements would be substantially smaller for the n=1, 2, 3 lower frequency models.

The finite element transfer function, for the total pressure (reflected plus incident) over the six frequency ranges given in Table 1 is plotted in the lower half of Fig. 5; for comparative purposes, the corresponding exact solution is plotted in the upper half. The finite element transfer function is altered employing the junction averaging, low frequency interpolation and high frequency extrapolation notions discussed earlier in the Transfer Function Alteration section. The low frequency limit is taken as 0.0+i0.0 and is a result of the fact that when the acoustic wave lengths are long relative to the shell thickness, the incident wave, in effect acts like it is reflecting off of the inner void, wherein the incident and reflected waves are such that they cancel each other. The high frequency

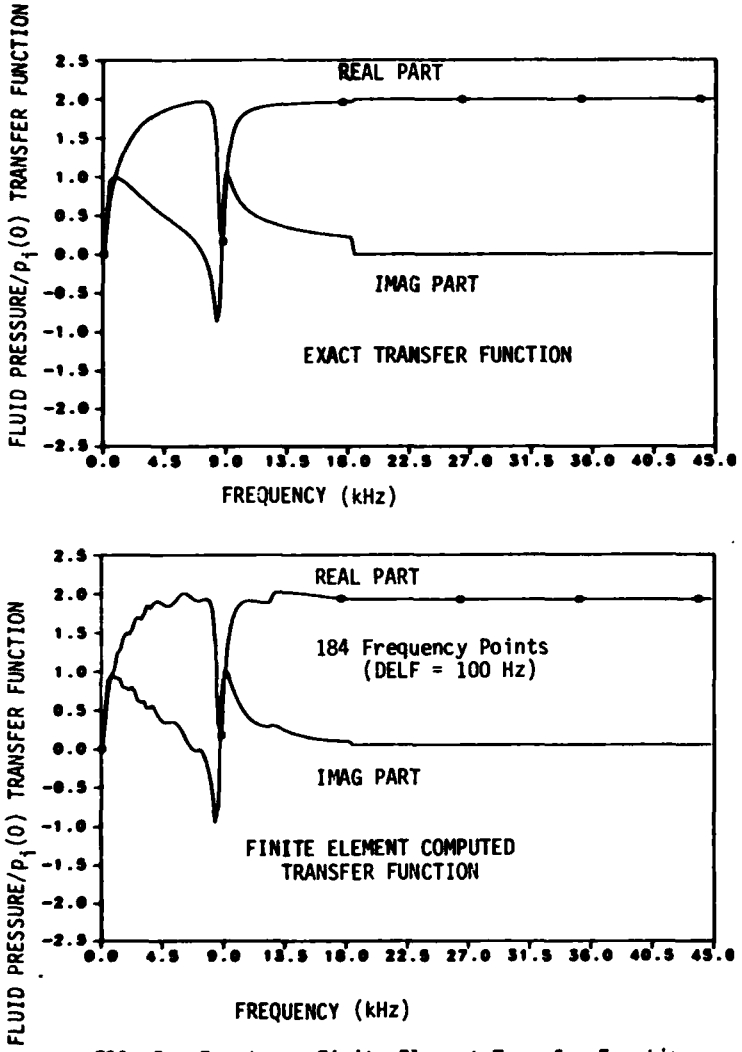

FIG. 5 - Exact vs. Finite Element Transfer Function

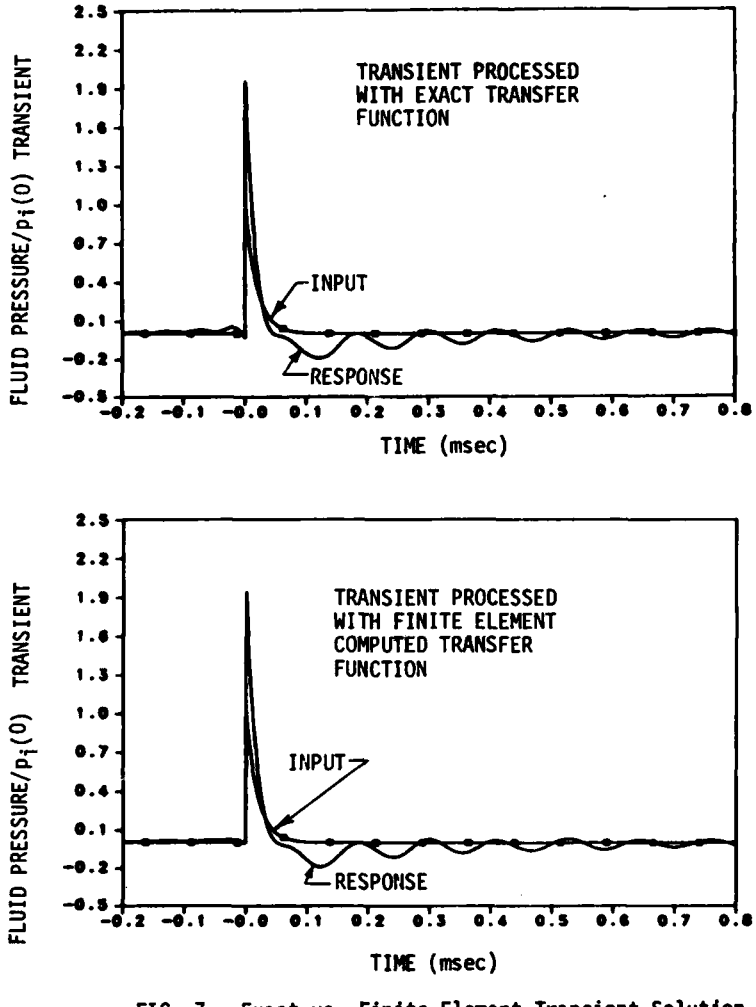

FIG. 7 - Exact vs. Finite Element Transient Solution

limit is obtained analytically by allowing the cylinder properties to be extremely stiff. The finite element high frequency limit was obtained as a separate run with the n=6 mesh, by setting the normal displacement of the cylinder=0.0 as an imposed boundary condition. The exact solution transfer function is evaluated slightly off of the cylinder fluid-solid interface, at a distance corresponding to 1/2 the thickness of the interfacing fluid element. This offset is imposed because the fluid pressure is computed with the finite element displacement method; consequently, pressure is evaluated as a post-processing step within the finite element program wherein the pressure value is valid at the center, rather than the surface of the element.

The comparison between the exact and finite element transfer functions, illustrated in Fig. 5, is good. It is felt that the dip in the transfer function occurs at the breathing mode of the thick wall shell. For example, employing the appropriate in vacuum thin wall shell formula

$$f_b = \frac{1}{(r_b+r_a)\pi}\sqrt{\frac{E}{\rho(1-\nu^2)}}$$

results in a breathing mode frequency of f_b=8168 Hz (the values of λ, μ, from Table 2 are equivalent to E=11,300,000 psi and ν=.37), which is very close to the sharp dip in the transfer function. The finite element method was able to properly pick up this dip.

Exact Transient Solution

The transient input waveform is that of an exponential input, $f(t)=e^{-\beta^* t}$, in conjunction with equation (13). The β^* decay constant is selected, β^*=53000., so that a large portion of the frequency content of the input waveform is in the neighborhood of the breathing mode frequency; consequently, it is expected that some sort of shell ringing mode might be activated. The Fourier transform of equation (13) evaluates at $r=r_b$, is plotted (amplitude only) in Fig. 6.

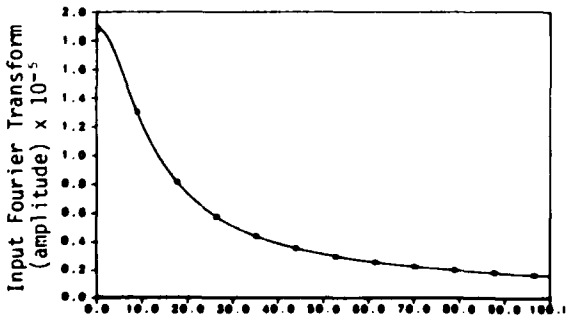

FIG. 6 - Frequency Content of Exponential Step Wave

Upon substituting the exact transfer function (upper Fig. 5 result) and the exponential decay input wave into the FFT counterpart of equations (8) and (9), the desired total pressure response is obtained and is plotted in the upper half of Fig. 7. For reference, the corresponding input waveform is superimposed on the same plot. It is noted that a near doubling of the incident pressure is experienced, as is very common in shock problems of this type. It is also noted that the reciprocal of the period of the shell ringing occurs at a frequency corresponding to the sharp dip in the transfer function of Fig.5.

Finite Element Transient Solution

The transient solution, employing the finite element method data is obtained in exactly the same manner as that of the exact solution, the only difference being that the FFT algorithm operates on the finite element generated transfer function (lower Fig. 5 plot) rather than the exact transfer function (upper Fig. 5 plot). The resulting transient solution is plotted in the lower half of Fig. 7. Comparison of the Fig. 7 response curves shows excellent agreement between the exact and finite element generated solutions.

TRANSIENT SOLUTION SENSITIVITIES

In this section, sensitivities of the transient response to certain operations in the frequency domain-to-transient domain are investigated. The previous demonstration problem again is employed to examine problem formulation sensitivities.

Sampling Rate of Finite Element Transfer Function

The Figs. 5, 7 base case run employed 184 finite element calculations at a sampling interval of .1 kHz. Next we consider the consequence of running a sequence of numerical solutions, wherein the only thing changed from the base case is the fact that fewer finite element generated transfer function points (cruder frequency sampling rates are employed) are used. It is emphasized, however, that the Δf rate at which the FFT sampling is performed (i.e., in the evaluation of equation (8)) is still held the same as the base case. In other words, linear interpolation of the finite element generated transfer function is employed over longer frequency spans, the coarser the finite element generated frequency sweep. The base case results, for the finite element transfer function and corresponding transient solution, are shown in the lower half of Figs. 5, 7, respectively. The results shown in Figs. 8-11 illustrate the consequence of defining the transfer function with fewer and fewer data points starting with 184 frequency points for the base case (.1 kHz sampling rate); 39 frequency points for Fig. 8 results (.5 kHz sampling rate); 21 frequency points for Fig. 9 (1.0 kHz sampling rate); 12 frequency points for Fig. 10 (2.0 kHz sampling rate) and finally the ultra coarse 7 frequency points (4.0 kHz sampling rate) for Fig. 11. The Fig. 8, 39 point case and Fig. 9, 21 point case are practically as good as the base case, wherein the shell after shock ringing and peak response are still well defined. The Fig. 10, 12 point case starts to lose the shell ringing and the upstream pressure response

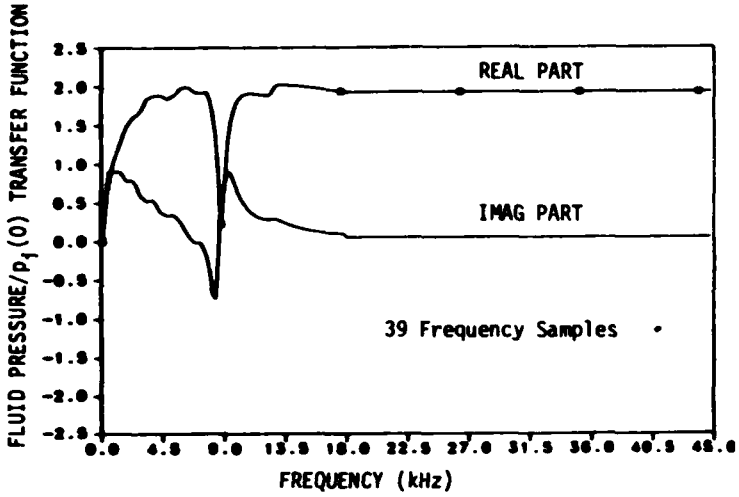

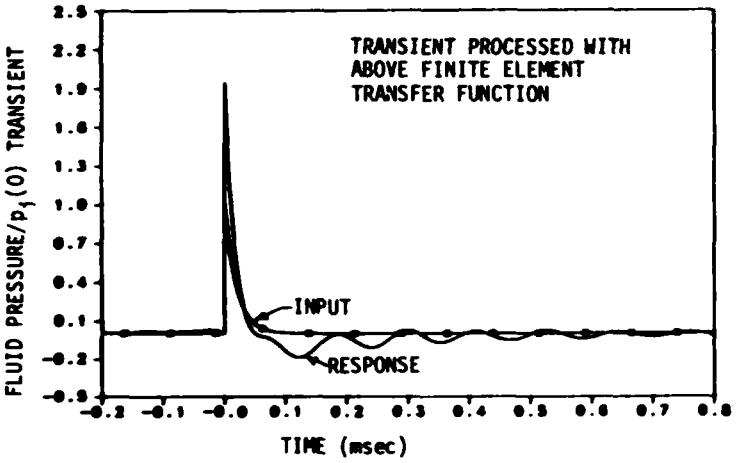

FIG. 8 - Finite Element Solution (39 Frequency Samples, DELF = 500 Hz)

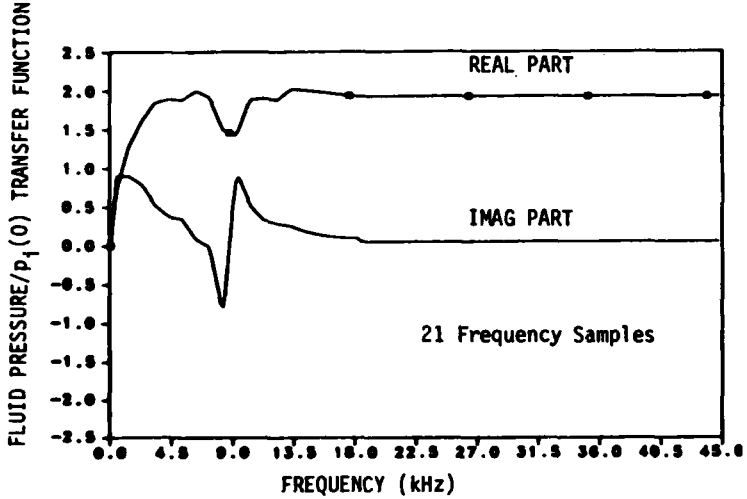

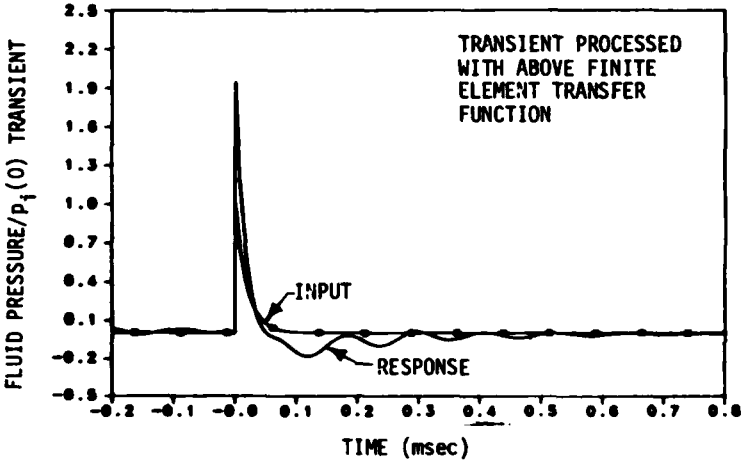

FIG. 9 - Finite Element Solution (21 Frequency Samples, DELF = 1000 Hz)

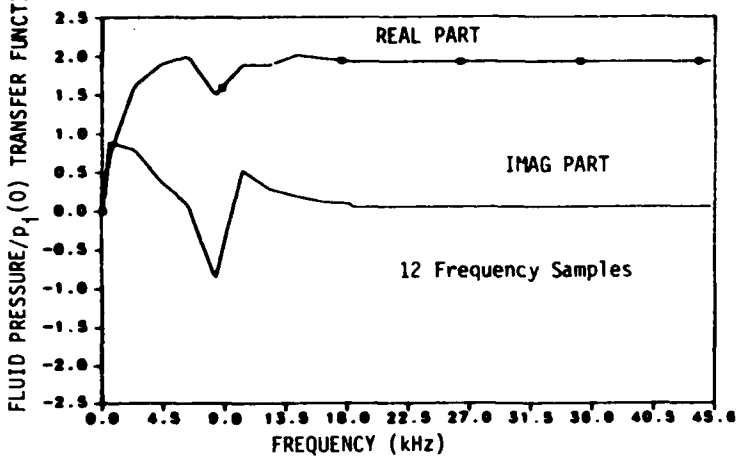

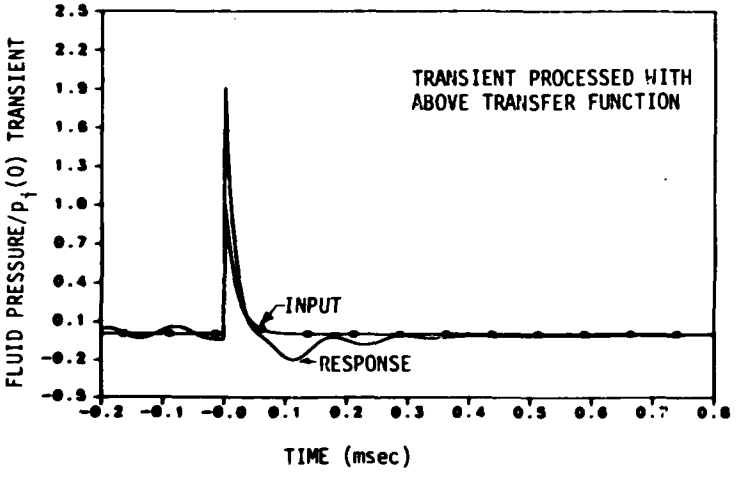

FIG. 10 - Finite Element Solution (12 Frequency Samples, DELF = 2000 Hz)

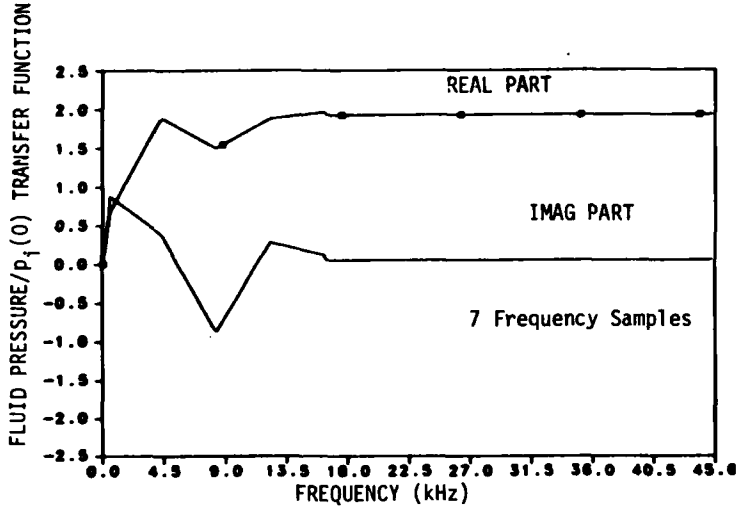

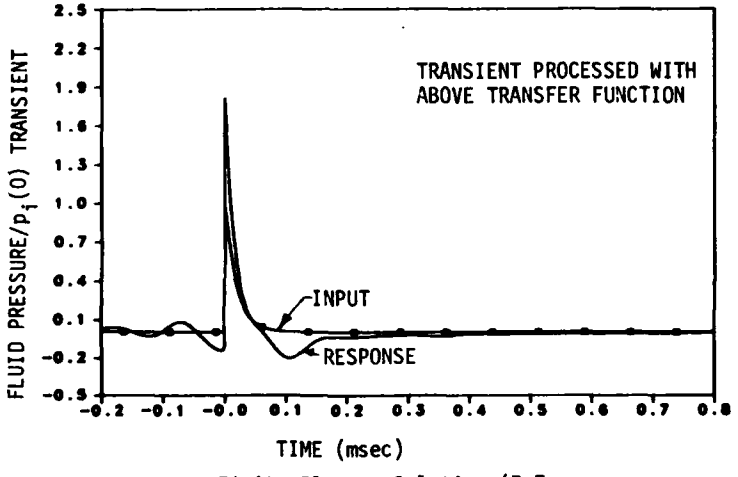

FIG. 11 - Finite Element Solution (7 Frequency Samples, DELF = 4000 Hz)

errors (prior to shock arrival) are starting to build up. Finally, in the ultra coarse 7 point case, 15% upstream pressure errors are experienced, the after shock shell ringing is completely lost, and the peak response has degraded.

Mesh Coarseness Sensitivity

In this example, the consequence of employing a mesh that does not fully meet inequality (1) is examined. In particular, the n=1 mesh (of Fig. 4) is employed for the full frequency sweep. Of course, the results for the n=1 frequency range in Table 1, will still be the same as the base case; however, exercising the model beyond f=.3 kHz will result in increasingly more serious errors, the larger the frequency. The resulting transfer function (drawn to a different scale than the base case Fig. 5) is shown in the upper half of Fig. 12, wherein it is seen to be quite different than the peeled mesh model. In fact, beyond f=2.7 kHz, the transfer function response dies off giving an erroneous zero response (including the erroneous high frequency response limit, also obtained with the n=1 model with zero radial constraints at the cylinder surface). Upon processing the upper Fig. 12 transfer function, the corresponding lower Fig. 12 transient response is obtained. As seen, the response is totally wrong in comparison to the Fig. 7 base case response. This example clearly illustrates the danger of having coarse elements in the mesh (i.e., violating inequality (1)).

Omission of High Frequency Elastic Response Modes

In this example, the consequence of omitting higher elastic response modes in the transfer function is considered. The base case transfer function has only one elastic response resonance, namely the breathing mode as explained earlier. In this next example, we consider the effect of including the next two higher elastic response modes (namely due to the elastic compressibility of the thick cylinder wall). The wall resonances are predictable (i.e., when wall thickness is a 1/2 wave length multiple); thus

$$f_{wm} = \frac{m}{2(r_b - r_a)} \sqrt{\frac{\lambda_2 + 2\mu_2}{\rho_2}} \qquad (19)$$

$$m = 1, 2, \ldots$$

Upon substituting the silver properties from Table 2 into equation (19), we arrive at f_{wm}=47.5 kHz for the first resonant wall mode and f_{wm}=95.1 kHz for the second. These frequencies line up very well with the second and third dips indicated in the Fig. 13 evaluation of the exact solution. Beyond 108 kHz, the transfer function is truncated with the high frequency limit. No corresponding finite element runs are made, since our goal is to investigate the effect on the signal processing, if higher modes are omitted, regardless of how we obtain the transfer function. Upon processing the upper Fig. 13 transfer function with the FFT algorithm, we arrive at the lower Fig. 13 transient solution. The effect of adding in the two additional resonances introduced some minor pertubations about the breathing mode ringing. Upon careful examination, it can be seen that the period of these minor fluxuations occur at frequencies corresponding to the 47.5 kHz and 95.1 kHz wall resonances.

The consequence of truncating the transfer function with a zero contribution instead of the high frequency limit is considered in the example presented in Fig. 14. The resulting transient solution is still basically the same as the previous Fig. 13 result, except that a small portion of the peak shock response is missing. The shell ringing portion appears to be essentially the same.

MULTIPLE SHOCK EXAMPLE

In the next example, the notion of processing new response results, for new inputs, without having to make any new finite element runs is demonstrated. The example treated is the same as the base case except that a double shock input wave is considered. The spacing of the second shock is selected so that it nearly corresponds to the period of the breathing mode. The corresponding response (in addition to the double shock unit input) is plotted in Fig. 15. Note that the timing of the second shock superimposes a second wave that tends to nullify the periodic nature of the base case shell ringing experienced for a single shock.

DEMONSTRATION - 2

In this example, our goal is to demonstrate a problem set up for a three-dimensional model, short of actually obtaining numerical results. The intent is simply to illustrate the difference between a problem employing a "mesh regeneration approach" as compared to one employing the "mesh peeling approach". Consider a finite length axisymmetric rib stiffened cylindrical shell subject to a non-axisymmetric point load which is applied at the mid-length and points in the radial direction. The cylindrical shell has a plane of symmetry located at the mid-length and is perpendicular to the z axis of revolution. Since the radial point load, $F_r(t)$, is also acting at the mid-length, it follows that only one half of the cylindrical shell need be modeled, wherein appropriate axial constraints are applied at the plane of symmetry cut. The problem, as defined, constitutes an axis of revolution generated body subject to a non-axisymmetric loading, consequently a conventional Fourier harmonic representation of the radial loading can be employed along with the corresponding harmonic stiffness, mass and damping matrices for each harmonic, n, in the load expansion. Thus one only need model a r-z cylindrical coordinate slice of the model (e.g., Fig. 16) and resolve the resulting two-dimensional problem for each Fourier harmonic term in the radial load harmonic expansion. This is a standard feature in several general purpose finite element computer programs such as NASTRAN, for example. The final three-dimensional response is thus obtained by superimposing the results of a sequence of smaller two-dimensional solutions. This demonstration problem - 2 differs from problem - 1 in the respect that the previous example was one of

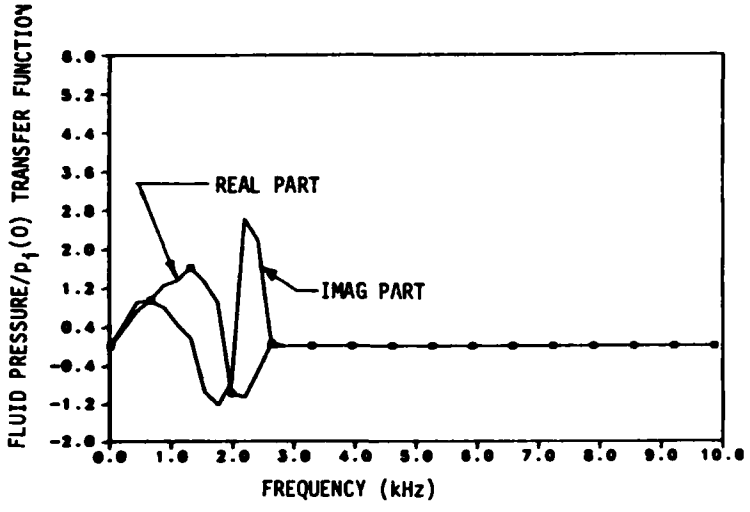

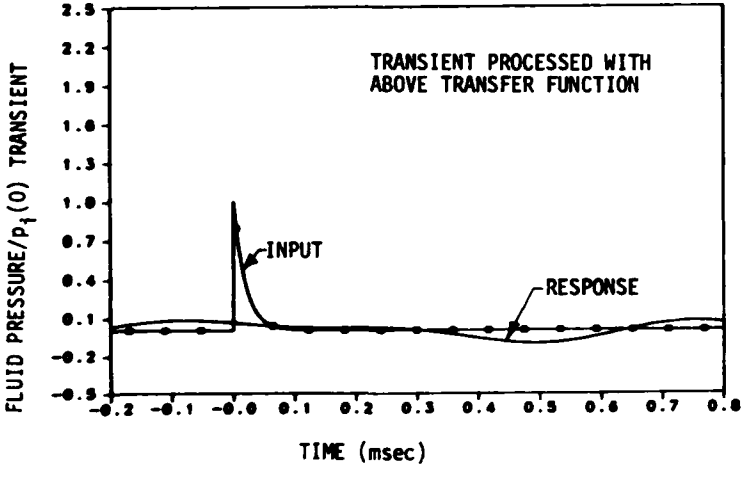

FIG. 12 - Improper Coarse Mesh Response Demonstration

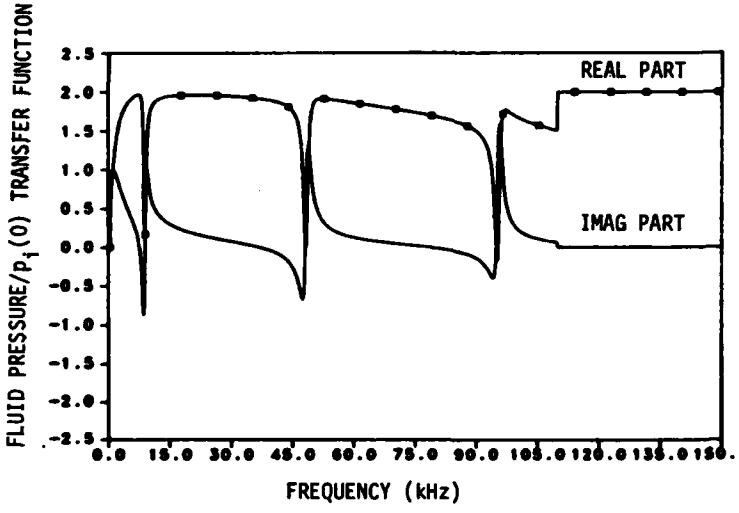

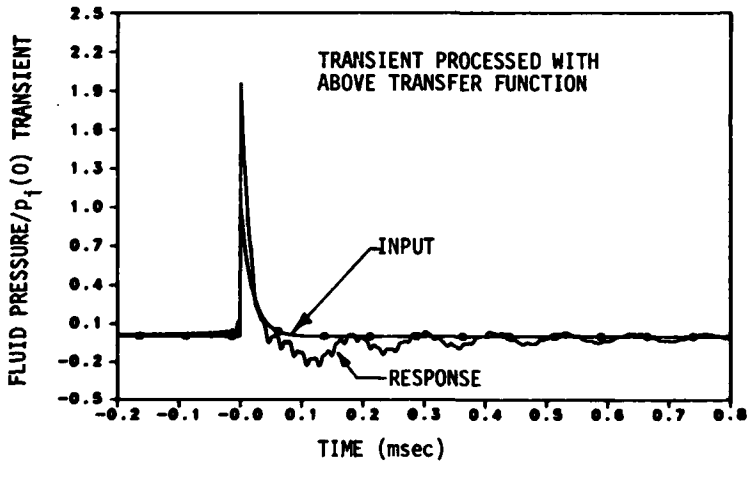

FIG. 13 - Transient Processed From Exact Transfer Function With Three Resonances Included and With High Frequency Limit

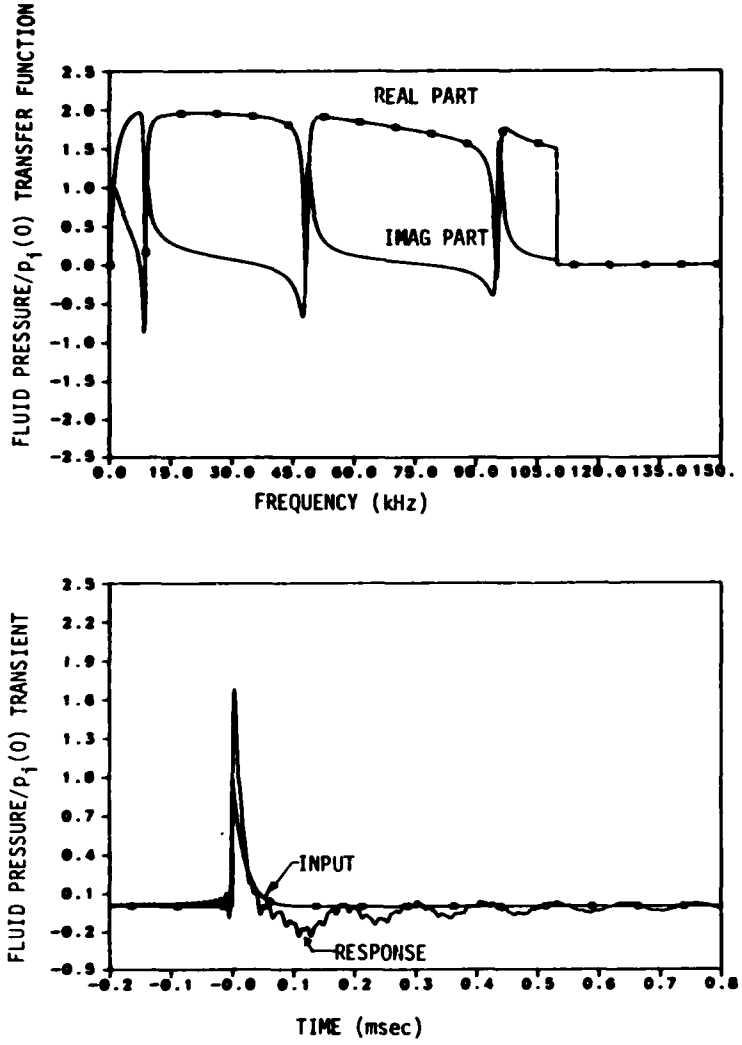

FIG. 14 - Transient Processed from Eact Transfer Function with Three Resonances Included and Without a High Frequency Limit

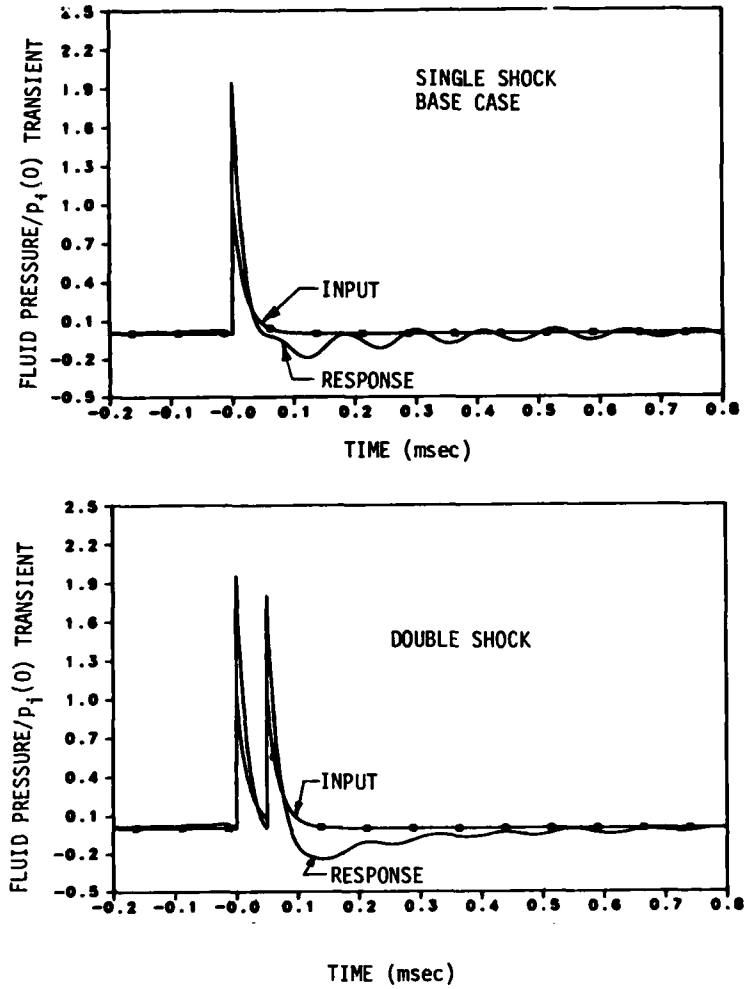

FIG. 15 - Multiple Shock Input Comparison Example

applying the methodology to a scattering type situation in contrast to the current problem which constitutes a radiation condition (induced by the internal point load).

The finite element model shown in Fig. 16 is an example of the "mesh regeneration approach" discussed earlier. A high frequency model (fine mesh) and intermediate frequency mesh (coarser mesh) as shown in respectively in Fig. 16. The structure model surface node spacing Δs and the fluid finite element spacing Δs^1 will not be compatible for both models if the structural model is held fixed each time the fluid media surface mesh is changed. Thus some sort of multi-point media-to-structure node compatibility condition as discussed earlier would have to be imposed when $\Delta s \neq \Delta s^1$. This is a disadvantage of the "mesh regeneration approach", however as shall be seen, it has the advantage that the elements are more efficiently and uniformly distributed than in the "mesh peeling approach". The "mesh peeling approach" as applied to the same cylinder problem utilized one basic mesh. Upon constructing the low frequency master mesh (e.g., the large upper model of Fig. 17), the high frequency mesh is immediately constructed by peeling away the unwanted coarser elements (above and to the right of the two dashed lines marked A-A) and simply moving in the radiation dashpots along the new outer surface. Note with this mesh, the problem of connecting unequal spaced structure and fluid media nodes is not encountered wherein the structure and interfacing fluid nodes are the same for both models. The disadvantage of this approach is that care must be taken to be sure the geometrical progression increase of the radial growth of the elements meets the maximum element size requirements for the particular frequency range of interest. A further disadvantage is that more elements are employed for the larger radial dimension, low frequency models. Finally, again it is pointed out the Fig. 16 and Fig. 17 meshes are only included here for discussion purposes and it is indeed not meant to imply that one can necessarily generate the full transfer function of interest with only two mesh for all problems.

CONCLUDING REMARKS

A procedure is given for solving transient linear media-structure interaction problems by explicitly modeling both the structure and media with finite elements. All finite element results are obtained in the frequency domain, wherein transient responses are subsequently post-processed with FFT algorithms. Running parametric studies of response, due to different input waveforms, consequently do not require any new finite element reruns.

Substantial savings on the finite element model size (total degrees-of-freedom) should be possible by building a segmented transfer function with a set of small meshes rather than with a single large fine mesh value over all frequencies of interest. Comparison of results, between the exact solution and finite element solution, is good for a simple, but conceptually representative sample problem. As yet, the presented frequency dependent mesh procedure has not applied to real large problems, however, in theory, this should be possible. The mesh peeling method for constructing the sequence of finite element models is more convenient to use then the mesh regeneration approach; however, the latter approach leads to smaller size models which is in the spirit of the frequency dependent mesh procedure.

REFERENCES

1. R. S. Dunham, A. S. Kushner, D. E. Ranta, "An Evaluation of: Doubly Asymptotic Approximation; Staggered Solution Schemes; USA-STAGS", The Shock and Vibration Bulletin, Vol. 51, 1981.
2. A. J. Kalinowski, "Modeling Structural Damping for Solids Having Distinct Shear and Dilatational Loss Factors", Seventh NASTRAN USER's COLLOQUIUM, Oct. 1978, (NASA CP-2072).
3. A. J. Kalinowski, "Solution Sensitivity and Accuracy Study of NASTRAN for Large Dynamic Problems Involving Structural Damping", Ninth NASTRAN USER's COLLOQUIUM, Oct. 1980, NASA CP-2151.
4. L. H. Chen, D. G. Schweckert, "Sound Radiation from an Arbitrary Body", Journal of the Acoust. Society of America, Vol. 35, No. 10, 1963.
5. J. Lysmer, R. L. Kuhlemeyer, "Finite Dynamic Model for Infinite Media", ASCE J. Engr. Mech. Div., 95 (EM4), Proc. Paper 6719 (Aug. 1969).
6. A. J. Kalinowski, "Fluid-Structure Interaction", Shock and Vibration Computer Programs, Review and Summaries, Pilkey and Pilkey, eds., SVM-10, Shock and Vibration Information Center (1975).
7. A. J. Kalinowski, "An Approximate Absorbing Boundary Condition for Fluid-Structure Interaction Problems", Computational Methods for Infinite Domain Media-Structure Interaction A. Kalinowski, Editor, to be published ASME Publication, Nov., 1981.
8. R. Courant, D. Hilbert, "Methods of Mathematical Physics, Vol. 2, Partial Differential Equations, Interscience, New York, 1962.
9. A. J. Kalinowski, "Transmission of Shock Waves Into Submerged Fluid Filled Vessels", Fluid Structure Interaction Phenomena in Pressure Vessel and Piping Systems, M. Wang and S. J. Brown Rds., ASME 19, Nov. 1977.
10. A. J. Kalinowski, "Stress Wave Measurement Techniques", The Shock and Vibration Bulletin, Vol. 43, June 1972.
11. A. Papoulis, The Fourier Integral and it's Applications, McGraw-Hill, N.Y., 1962.

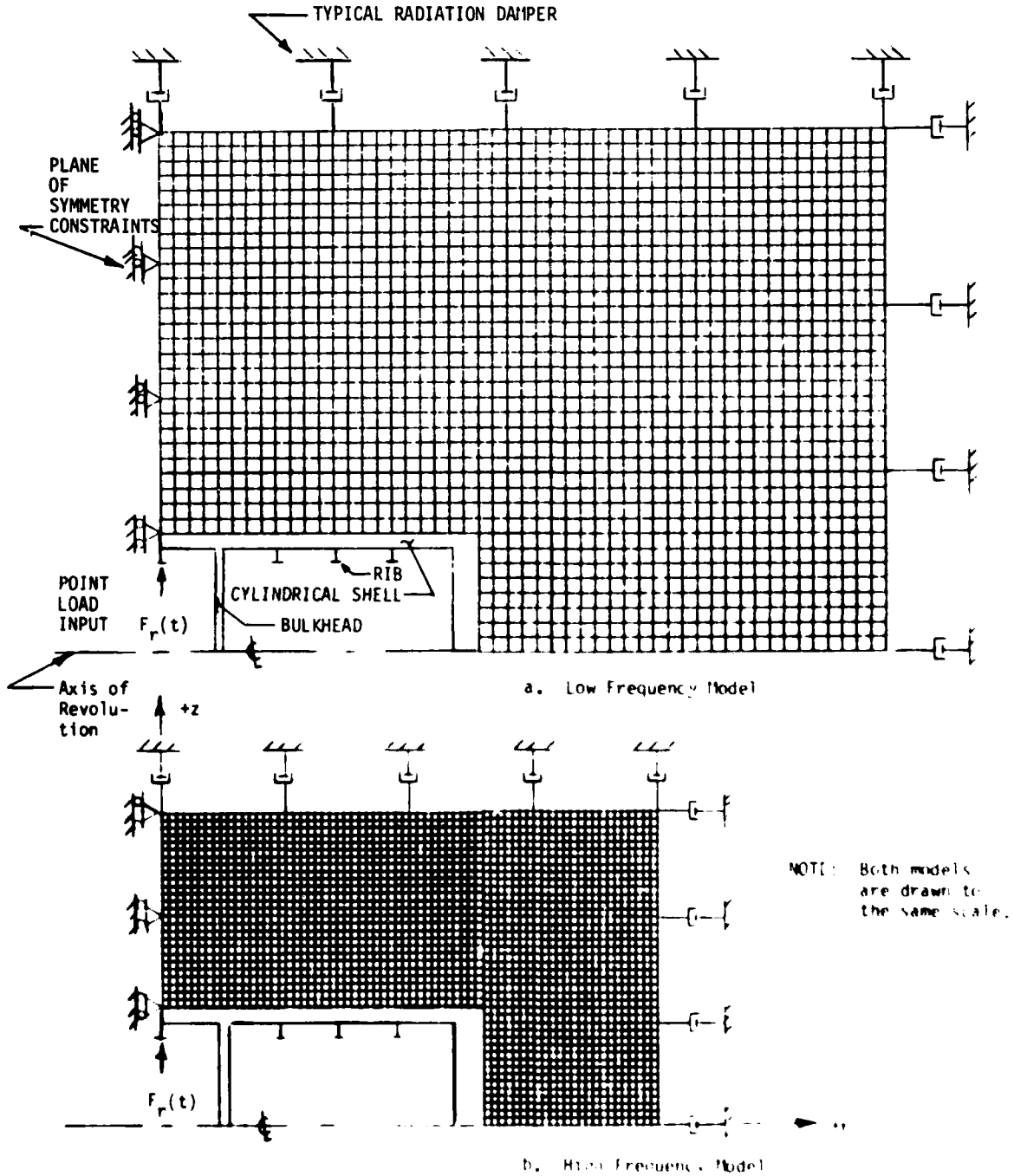

FIG. 16 - "Mesh Regeneration Approach" Example Model

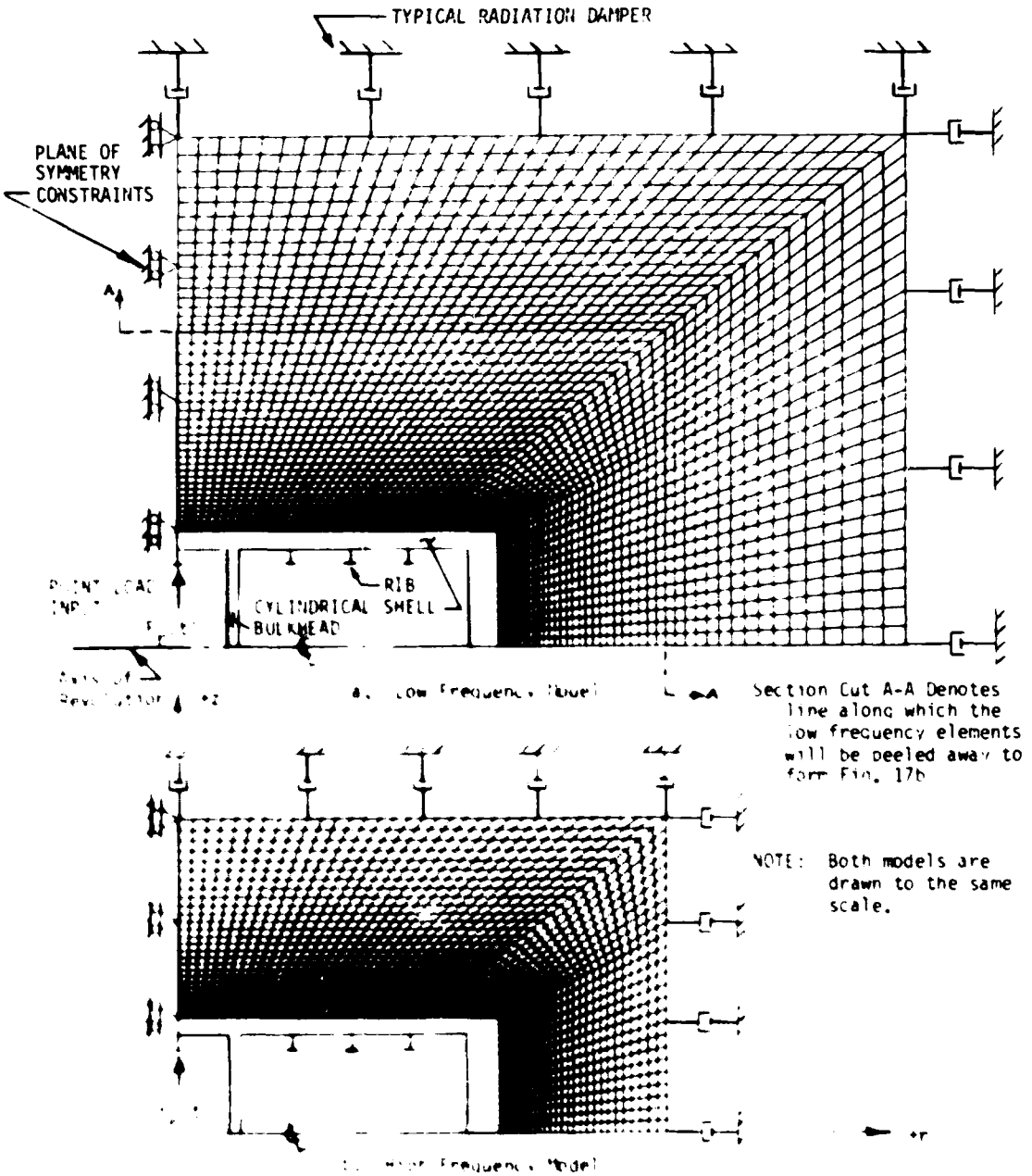
TYPICAL RADIATION DAMPER
PLANE OF SYMMETRY CONSTRAINTS
A
RIB
CYLINDRICAL SHELL
BULKHEAD
Section Cut A-A Denotes line along which the low frequency elements will be peeled away to form Fig. 17b
NOTE: Both models are drawn to the same scale.

12. W. J. Cooley, D. A. Lewis, D. D. Welch, "Applications of the Fast Fourier Transform to Computation of Fourier Integrals, Fourier Series, and Convolution Integrals", IEEE Transaction on Audio and Electroacoustics, AO-IS(2), June 1967.

13. Y. H. Pao, C. C. Mow, Diffraction of Elastic Waves and Dynamic Stress Concentrations, Crane, Russah and Comp., Inc., NY, NY, 1971.

APPENDIX A

EXACT SOLUTION FOR DEMONSTRATION PROBLEM

Consider an infinitely long, elastic, cylindrical thick-walled cylinder, imbedded in an infinite elastic medium, subject to a converging incident cylindrical wave (Fig. 2). The fluid media solution is easily recovered from the solid medium solution by simply letting the shear modulus, μ_1 is in the surrounding media=0.0, and the λ_1 Lame' constant of the elastic media equal the bulk modulus of the fluid.

Since the cylinder is thick-walled, the exact theory of elasticity is used in place of thin-wall shell theory. Both the response of the cylinder and of the medium are represented by the dynamic equations of elasticity, namely

$$(\lambda_i+\mu_i)\nabla(\nabla\cdot\overline{U})+\mu_i\nabla^2\overline{U} = \rho_i \frac{\partial^2\overline{U}}{\partial t^2} \qquad (1\text{-A})$$

where λ_i, μ_i are the Lame' constants, ρ_i is the material density, t is time and $\overline{U}$ is the displacement vector and subscript i=2 is for the cylinder and i=1 is for the media. The nature of the symmetric structure and symmetric loading in cylindrical coordinates, will result in a displacement field with no shear distortion. Consequently, employing the methods of reference [13], it can be shown that the solution to equation (1-A) can equivalently be represented by solutions of the potential wave equation

$$c_i^2\nabla^2\phi_i = \frac{\partial^2\phi_i}{\partial t^2} \qquad (2\text{-A})$$

where

$$c_i^2 = (\lambda_i+2\mu_i)/\rho_i$$

The radial displacement component of $\overline{U}$, i.e. U_r, and the radial stress, σ_{rr}, are related to the potential values by

$$(U_r)_i = \frac{\partial\phi_i}{\partial r}$$

$$(\sigma_{rr})_i = \lambda_i \nabla^2\phi_i+2\mu_i \frac{\partial^2\phi_i}{\partial r^2} \qquad (3\text{-A})$$

In keeping with the notation of reference [13], $e^{-i\omega t}$ type input loading is employed. The response to the desired $e^{+i\omega t}$ input is obtained by taking the complex conjugate of the final result. The incoming incident wave in potential form is given by

$$\phi_1^i(r,t) = \hat{A}\, H_0^{(2)}(\alpha_1 r)e^{-i\omega t} \qquad (4\text{-A})$$

where

$$\alpha_1 = \omega/c_1 \text{ and } H_0^{(2)}$$

is a zero order Hankel function of the 2nd kind.

An incident compressional wave of strength σ_{rr}=-1.0 psi at r=r_b is desired; consequently, substituting equation (4-A) into the right side second of equation (3-A) while the left side of equation (3-A) is set=-1.0, enables one to solve for the strength of the input wave, $\hat{A}$.

In medium-1, the total potential consists of the incident potential, ϕ_1^i plus the reflected wave potential, ϕ_1^r, thus

$$\phi_1 = \phi_1^i+\phi_1^r \qquad (5\text{-A})$$

where the reflected potential is an outgoing wave given by the expression

$$\phi_1^r = B\, H_0^{(1)}(\alpha_1 r)e^{-i\omega t} \quad \text{outgoing wave}$$

where B is the yet to be determined amplitude, and $H_0^{(1)}$ is a zero order Hankel function of the first kind.

Similarly, in the cylinder (medium 2), the total potential, ϕ_2, is made up of a reflected potential, ϕ_2^r, (off of inner surface void) and a transmitted potential, ϕ_2^t; thus

$$\phi_2 = \phi_2^r+\phi_2^t \qquad (6\text{-A})$$

where

$$\phi_2^r = C\, H_0^{(1)}(\alpha_2 r)e^{-i\omega t} \quad \text{outgoing wave}$$

$$\phi_2^t = D\, H_0^{(2)}(\alpha_2 r)e^{-i\omega t} \quad \text{incoming wave}$$

with $\alpha_2=\omega/c_2$, and C and D are yet to be determined constants.

The three constants B, C, D are determined by the three boundary conditions:

$(U_r)_1 = (U_r)_2$ at $r = r_b$ — continuity of normal displacement across media-cylinder interface (7-A)

$(\sigma_{rr})_1 = (\sigma_{rr})_2$ at $r = r_b$ — continuity of radial stress across media-cylinder interface (8-A)

$(\sigma_{rr})_2 = 0$ at $r = r_a$ — zero surface traction on inner surface of cylinder (9-A)

Upon substituting equations (5-A) and (6-A) into equation (3-A), and then equation (3-A) into the boundary conditions (7-A) through (9-A), we arrive at three linear equations with three unknowns for the unknown amplitudes B, C, D. Setting up the linear equations we obtain

$$[a_{ij}]\{b_j\} = \{c_i\} \quad ; \quad i, j = 1, 2, 3 \qquad (10\text{-A})$$

where

$$[a_{ij}] = \begin{bmatrix} -c_1^{(1)}(r=r_b) & c_2^{(1)}(r=r_b) & c_3^{(1)}(r=r_b) \\ -\frac{1}{r}\frac{d}{dr}H_0^{(1)}(a_1 r)\Big|_{r=r_b} & \frac{1}{r}\frac{d}{dr}H_0^{(1)}(a_2 r)\Big|_{r=r_b} & \frac{1}{r}\frac{d}{dr}H_0^{(2)}(a_2 r)\Big|_{r=r_b} \\ 0 & c_2^{(1)}(r=r_a) & c_3^{(2)}(r=r_a) \end{bmatrix};$$

$$[b_j] = \begin{Bmatrix} B \\ C \\ D \end{Bmatrix}; c_m^{(n)} = (\lambda_m + 2\mu_m)\frac{d^2}{dr^2}\left(H_0^{(n)}(a_m r)\right) + \frac{\lambda_m}{r}\left(H_0^{(n)}(b_m r)\right); \quad m,n = 1,2$$

$$[c_i] = \begin{bmatrix} \hat{A}\, c_1^{(1)}(r=r_b) \\ \frac{\hat{A}}{r}\frac{d}{dr}H_0^{(1)}(a_1 r)\Big|_{r=r_b} \\ 0 \end{bmatrix}$$

Solving equation (10-A) by Cramer's Rule, we obtain

$$B = \begin{vmatrix} c_1 & a_{12} & a_{13} \\ c_2 & a_{22} & a_{23} \\ c_3 & a_{32} & a_{33} \end{vmatrix} \div |a_{ij}|$$

$$C = \begin{vmatrix} a_{11} & c_1 & a_{13} \\ a_{21} & c_2 & a_{23} \\ a_{31} & c_3 & a_{33} \end{vmatrix} \div |a_{ij}| \qquad (11\text{-A})$$

$$D = \begin{vmatrix} a_{11} & a_{12} & c_1 \\ a_{21} & a_{22} & c_2 \\ a_{31} & a_{32} & c_3 \end{vmatrix} \div |a_{ij}|$$

Back substituting equations (11-A) into equations (5-A) and (6-A) and then into equation (3-A), all response quantities of interest can be computed in both the cylinder and media. Upon setting $\mu_1 = 0$, the special case of obtaining the total fluid pressure, P(r), due to an incident pressure wave is obtained where the fluid pressure, P(r), is simply

$$P(r) = -\sigma_{rr}(r) \qquad (12\text{-A})$$

DISCUSSION

Mr. Wu (U. S. Army): Have you heard of moving finite elements, so called?

Mr. Kalinowski: What was the phrase again?

Mr. Wu: Moving finite elements.

Mr. Kalinowski: Moving finite elements for using these in the time domain?

Voice: Moving coordinates?

Mr. Wu: Right. Actually the mesh of the finite elements will move towards where it is needed most. I think that is the basic concept.

Mr. Kalinowski: You are essentially reseaning. I am not too familiar with that. I know that in the finite difference approach as opposed to the finite element approach they do continually change the shape of the elements as they process in the time domain, but I am not sure if they can do it with finite elements.

Mr. Wu: I think the basic idea there is to use the location of node points as well as the field function itself as generalized coordinates in the variational procedure.

Mr. Kalinowski: That would be an example of changing the mesh even in he time domain as you go along.

Mr. Wu: Right. I would like to see you comment on that.

Mr. Kalinowski: I'm not that familiar with it to really make a good comment on it.

SIMILITUDE ANALYSIS AND TESTING OF PROTOTYPE AND 1:13.8 SCALE MODEL OF AN OFFSHORE PLATFORM

C. S. Li*, C. S. Yang†, Nicholas G. Dagalakis‡, and William Messick
Mechanical Engineering Department
University of Maryland
College Park, MD 20742

The purpose of this investigation was to determine the dynamic similitude laws between a prototype offshore platform and its scale model and to investigate the accuracy of these laws and the effects of practical modeling assumptions with the use of finite element dynamic models of the platform and model. Dynamic similarity in a model experiment requires that model and prototype be geometrically and kinematically similar and that the loading be homologous in location and scaled appropriately in magnitude. In order to derive the scaling parameters for the modeling of the offshore platform, deep cantilever beam equations with hydrodynamic loading similar to the one acting on a circular cylindrical pile were used. Eleven scaling parameters were obtained for the dimensional analysis and from these parameters eight dimensionless groups and corresponding scaling equations were derived. The results of this analysis was applied to the design of an 1:13.8 scale model of an existing four legged oil platform. The accuracy of the dynamic similitude analysis was investigated with finite element computer models of both the prototype and the 1:13.8 scale model. Dynamic characteristics of the prototype like eigenvalues, mode shapes and transient response were compared with those of the model, and the influence of the degree of detail of the finite element model on these characteristic responses was determined. A study of the effect of approximations in the model designs to exact scaling requirements indicated that if cost considerations in model fabrication dictate the use of stock piping and materials, then all of the response parameters of the model cannot be directly scaled to obtain prototype response. One needs to combine scaling laws, model response measurements, and finite element modeling in order to obtain a reliable and relatively inexpensive method for designing better offshore platforms.

INTRODUCTION

The high cost and sophistication of today's offshore oil platforms increases the necessity for accurate modeling techniques. The objective of our work was to utilize finite element modeling to identify the effects of some commonly made approximations in the construction and testing of models of offshore platform designs.

In Section I of this paper, the appropriate laws for the scaling of an offshore platform are derived and it is shown that for exact scaling the designer must satisfy one very difficult scaling law relating the moduli of elasticity and densities of the model and prototype platforms. If the modulus of elasticity of the model material is the same as the prototype material, then the model material density must be λ times the prototype material density, where λ is the scaling ratio ℓ_p/ℓ_m. For any reasonable value of λ, the model density requirement is impossible to satisfy because of material unavailability.

Another difficulty in the construction of scaled structures is the availability of structural members which are exact replicas of the corresponding prototype members. For the particular model that was being investigated, stock steel tubes with the proper external diameter and cross sectional areas required by the scaling laws were not available. Since the order of special size steel tubes for the application was prohibitively expensive, a modeling compromise was made. Since the main objective of the work was to study the dynamic

*Professor, National Taiwan University

†Professor, Mechanical Engineering Department, University of Maryland

‡Assistant Professor, Mechanical Engineering Department, University of Maryland

characteristics of the offshore platform, it was decided to select the dimensions of the steel tubes such that the total moment of inertia about a horizontal axis for the model and prototype satisfy the corresponding scaling law. This scaling causes a discrepancy in stress scaling.

To compare the dynamic response characteristics of the model and prototype structures, finite element models were developed. The prototype and model under investigation and the model test results are described in Section II.

A simple NASTRAN beam model was developed and is described in Section III of the paper. After the first experimental data showed that this finite model was not accurate enough, a NASTRAN space frame model was developed and it is discussed in Section IV. In order to investigate the errors introduced by modeling approximations four different finite element models were used to obtain predicted dynamic response characteristics.

I. SIMILITUDE ANALYSIS

For dynamic similarity in a model experiment, the requirements are that the model and prototype be geometrically and kinematically similar and that the loading be homologous in location and scaled appropriately in magnitude. Geometric similarity requires that the model have the same shape as the prototype and that all linear dimensions of the model be related to the corresponding dimensions of the prototype by a constant scale factor. Kinematic similarity of two elastic bodies requires that the rate of change of generalized displacement at corresponding points in the two bodies are in the same direction and related in magnitude by a constant scale factor. Dynamic forces on the two bodies at corresponding points must be parallel and related in magnitude by a factor at similar times. The similar times are related by a scale factor. The test conditions must be estimated so that all important forces are related by the same scale factor between two elastic bodies. When dynamical similarity exists, data measured in a model test may be related quantitatively to conditions in the prototype.

In order to insure dynamic similarity or similitude, the dimensionless groups relating the variables must be the same for both the model and the prototype. One way of obtaining the relevant dimensionless groups is to use The Buckingham Pi Theorem. This method is particularly useful if the differential equations governing the phenomenon are unknown. Success with this method depends upon the insight of the investigator in selecting the variables affecting the problem. If one of the important variables is left out, correlation of the data will be impossible. A more reliable method of obtaining the dimensionless groups utilizes the differential equations describing the phenomena, if they are known. These may be non-dimensionalized and the resulting non-dimensional coefficients of the terms will be the non-dimensional groups.

If the differential equations of a structural dynamics problem are not known one may start by considering an equation of the form

$$\sigma = F(R, t, \rho, \nu, E, a, g, \ell, P) \qquad (1)$$

relating all physical quantities of the problem [1, 2, 3]. Forming the proper dimensionless groups between the physical quantities one has

$$\frac{\sigma}{E} = f\left[\frac{R}{\ell}, \frac{t}{\ell}\sqrt{\frac{E}{\rho}}\frac{a}{g}, \frac{g\ell\rho}{E}, \frac{P}{E\ell^2}, \nu\right] \qquad (2)$$

To assure dynamic similitude one must ensure that the dimensionless groups of equation (2) have the same value for both the model and the prototype, but this is difficult if not impossible, because of practical considerations. The main difficulty comes from $\frac{g\ell\rho}{E}$ dimensionless group term, which contains the gravitational constant g. Assuming g is constant then the following requirement must be satisfied:

$$\frac{(E/\rho)_{prototype}}{(E/\rho)_{model}} = \frac{\ell_{prototype}}{\ell_{model}} \text{ or } \left(\frac{E}{\rho}\right)_r = \ell_r \qquad (3)$$

where the subscript r refers to the ratio of the the prototype to model quantities.

Relationship (3) means that the use of prototype material for the construction of a true replica model is impossible. If for example steel tubes are used for the construction of the model platform and the same modulus of elasticity E is maintained then the density of the model material must be:

$$\rho_{model} = \rho_{prototype}\frac{\ell_{prototype}}{\ell_{model}} \qquad (4)$$

Since the maximum size of the model structure is dictated by the size of available testing facilities and ℓ_r cannot be less than 15 to 10 we see that ρ must be 10 to 15 times the density of the steel prototype material. Materials which have a lower modulus do not have the required density.

From the rest of the dimensionless products in equation (2), assuming the same modulus of elasticity for model and prototype the following scaling laws [4, 5, 6, 7] must be satisfied along with the density law (eq (4)):

$$t_p = \sqrt{\lambda}\, t_m, \text{ (Time Scaling Law)} \qquad (5)$$

$$P_p = \lambda^2 P_m, \text{ (Force Sacling Law)} \qquad (6)$$

$$\sigma_p = \sigma_m, \text{ (Stress Scaling Law)} \qquad (7)$$

$$\bar{R}_p = \lambda \bar{R}_m, \text{ (Displacement Scaling Law)} \quad (8)$$

$$a_p = a_m, \text{ (Acceleration Scaling Law)} \quad (9)$$

$$\text{From (5): } f_p = \frac{1}{\sqrt{\lambda}} f_m \text{ (Frequency Scaling Law)} \quad (10)$$

The motion of an offshore platform structure involves bending of pipe elements which are loaded by waves. A deep beam bending model can then be used to derive the differential equation which approximates the motion of the structure.

A deep beam is defined as one in which the depth of the cross section is not considered small compared with the length of the beam so that both shear and rotary inertia effects must be included. The forces and moments on a beam element are shown in Figure 1. The dynamic equation of motion of the beam is derived using the force and moment equations. For small deflections and rotations, the deep beam equation is:

$$\frac{\partial^4 V}{\partial x^4} + \frac{m}{EI}\frac{\partial^2 V}{\partial t^2} - \left(\frac{m}{k'AG} + \frac{mr^2}{EI}\right)\frac{\partial^4 V}{\partial x^2 \partial t^2} +$$

$$\frac{m^2 r^2}{EIK'AG}\frac{\partial^4 V}{\partial t^4} = \frac{\bar{p}}{EI} - \frac{1}{k'AG}\frac{\partial^2 \bar{p}}{\partial x^2} + \frac{mr^2}{EIK'AG}\frac{\partial^2 \bar{p}}{\partial t^2} \quad (11)$$

The deformation of the beam (V) is affected by the following physical quantities:

Mass of beam per unit length m
Modulus of elasticity E
Moment of inertia of cross sectional area I
Time t
Beam cross sectional area A
Shear area coefficient k'
Shear rigidity G
Radius of gyration of beam cross section r
Load per unit length p

All these quantities can be expressed in terms of the basic quantities of force F, length L and time T. The corresponding dimensional matrix will then be:

	V	x	m	E	I	t	A	K'	G	r	$\bar{p}$
F	0	0	1	1	0	0	0	0	1	0	1
L	1	1	-2	-2	4	0	2	0	-2	1	-1
T	0	0	2	0	0	1	0	0	0	0	0

The rank of the matrix is 3, so we must have 11 - 3 = 8 independent dimensionless groups.

$$\Pi_1' = \frac{I}{x^4} \quad (13) \qquad \Pi_2' = \frac{1}{t}\sqrt{\frac{m}{E}} \quad (14) \qquad \Pi_3' = \frac{G}{E} \quad (15)$$

$$\Pi_4' = K' \quad (16) \qquad \Pi_5' = \frac{A}{x^2} \qquad \Pi_6' = \frac{r}{x} \quad (18)$$

$$\Pi_7' = \frac{V}{X} \quad (19) \qquad \Pi_8' = \frac{\bar{P}}{XE} \quad (20)$$

From the above dimensionless parameters and assuming that the model and the prototype materials are the same, so that $E_p = E_m$ and $\rho_p = \rho_m$ we have the following scaling laws:

$$\text{From (14) } t_p = \lambda t_m, \text{ (Time Scaling Law)} \quad (21)$$

$$\text{From (20) } P_p = \lambda^2 p_m, \text{ (Force Scaling Law)} \quad (22)$$

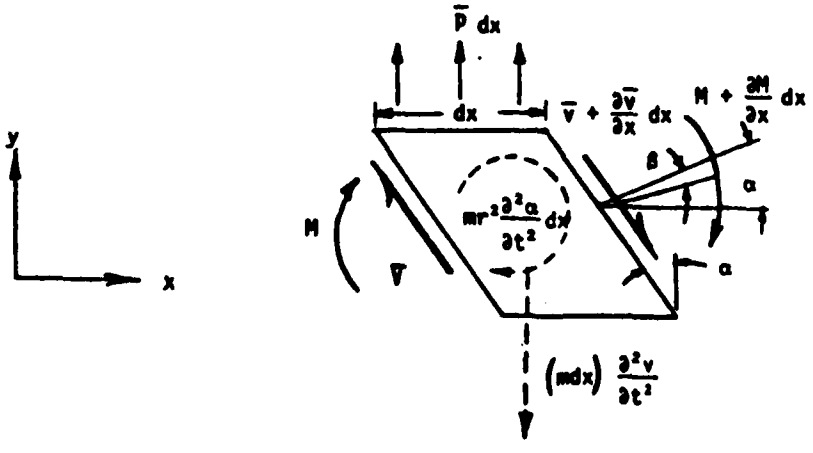

FIGURE 1 - FORCES AND MOMENTS ON A DEEP BEAM ELEMENT

From (20) $\sigma_p = \sigma_m$, (Stress Scaling Law) (23)

From (19) $V_p = \lambda V_m$, (Displacement Scaling Law) (24)

From (14) $a_p = \frac{1}{\lambda} a_m$, (Acceleration Scaling Law) (25)

From (21) $f_p = \frac{1}{\lambda} f_m$, (Frequency Scaling Law) (26)

The differences in the true replica model scaling laws (equations (4) through (10)) and the scaling laws for a real model (equations (21) through (26)) are easily identified. For both laws, the dynamic stresses in the model and prototype are equal. If the model is to have the same static stress as the prototype then the following relationship must be satisfied:

$$\rho_m = \lambda \rho_p \quad (27)$$

Thus to ensure equal total stress in the model and prototype, the model density must be scaled and the resulting relations for the dynamic response will be equations (5) through (10).

II. MODEL DESIGN AND TEST RESULTS

A. Prototype Structure Description

The offshore platform under consideration in this study is shown in Figure 2. It consists of five sublevels and is topped off with an assumed total loading of 234 tons uniformly distributed on the structure supported by four $34^{"\phi}$ x $\frac{3}{4}"$ main legs. Each level has $16^{"\phi}$ and $14^{"\phi}$ square and diagonal bracing respectively. A catwalk is located on the periphery of the fifth level. A $12.75^{"\phi}$ central pipe is located between the first and second, and the second and third level. Additional stiffening is obtained from two pipes running from the center of the second level to diagonally opposite corners of the third level. Detailed structure and pipe dimensions are given in Figure 3.

B. Model Structure Description

A scaling factor of 13.8 was selected based on the model basin geometric and wave-making constraints as well as stocktubing availability (see Appendix I). The details of the model platform that has been constructed are given in Figure 4 and Appendix I. The main support columns are $2^{"\phi}$ - 20 $\overline{BW}$.Ga., electric resistance welding, 1020 carbon steel tubes, the central tube is $\frac{9}{16}^{"\phi}$ - 20 $\overline{BW}$.Ga. and the cross tubes are $\frac{3}{4}^{"\phi}$ - 18 $\overline{BW}$.Ga., drawn over mandrel, 1020 carbon steel tubes. All tube materials are ASTM-A513-70 standard, with minimum tensile strength 80,000 psi., and the top plate is 35" x 35" x $\frac{1}{8}$ steel plate.

C. Model Testing

The 1/14 offshore platform model has undergone several dynamic analysis tests. A 25 lbs shaker was placed on a supporting structure so that it can be attached to different points of the model. A random input excitation as well as a sine sweep test were conducted.

Several accelerometers were mounted at different points of the model. The response acceleration was then recorded and analyzed.

The power spectrum of the random input excitation response and the sine sweep have indicated the presence of a large number of resonant frequency models. This is expected for such a complex structure. The resonant frequencies of the first five of these models are listed on Table 1.

TABLE 1

Resonant Frequencies of Real Model (Hz)

8
20-23
40
47
57
65-66

III. NASTRAN BEAM MODEL RESULTS

A. Finite Element Model

NASTRAN beam finite element models were developed for the prototype and model structures. Fourteen NASTRAN CBAR cards were connected between fifteen GRID points to generate a homogenized cantilever beam model. The grid point locations for each model are given in Figure 5, the total degrees of freedom is 84. The mass elements that were used for the model were CONM1 elements to simulate the distributed mass moment of inertia for the vertical legs of the platform, and CONM2 elements at each sublevel of the platform to simulate the distributed mass moment of inertia of the horizontal member array shown in Figure 6. The stiffness and consistent mass properties associated with the vertical leg cross sectional properties were generated from PBAR card data. The stiffness calculations for moments of inertia and cross sectional area did not include the vertical diagonal bracing contributions, but the mass of the vertical diagonal bracing between levels is included as non-structural mass on the PBAR card.

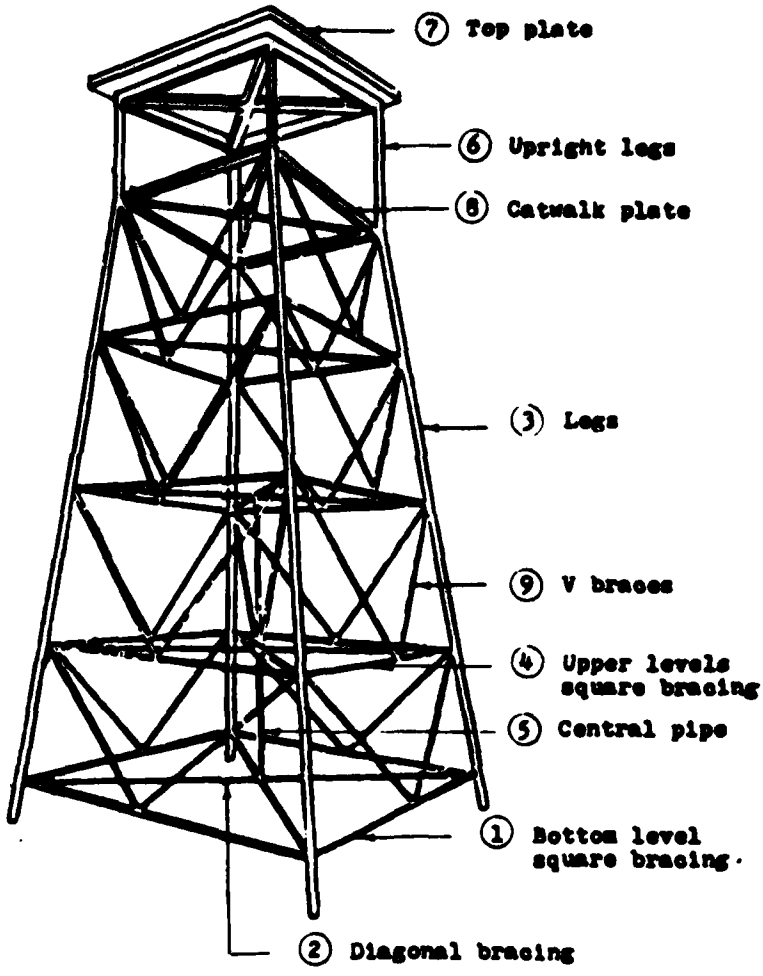

FIGURE 2 - SCALE MODEL OF OFFSHORE PLATFORM

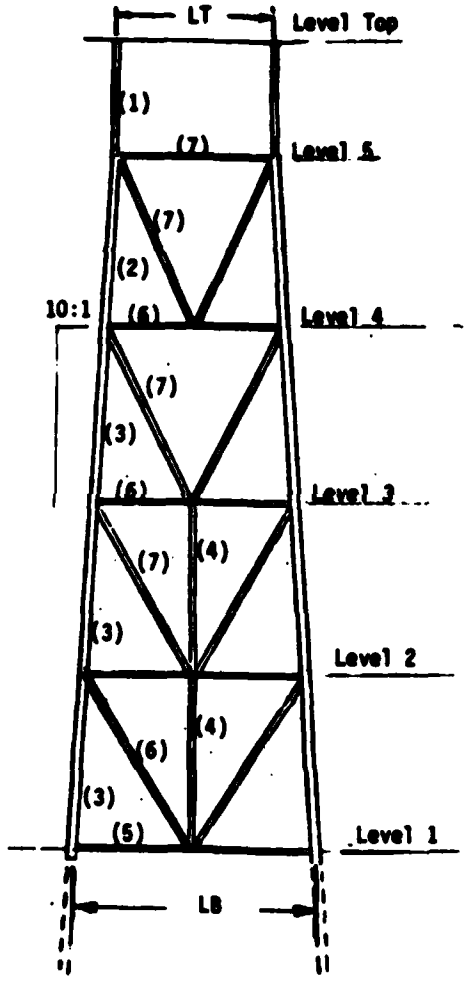

Dimension of Segments:

(1) $30"^{\phi}$ x 3/4" pL.

(2) $34\ 1/2"^{\phi}$ x 3/4" pL.

(3) $34"^{\phi}$ x 3/4" pL.

(4) $12\ 3/4"^{\phi}$ x 49.6 lbf/ft.

(5) $18"^{\phi}$ x 82 lbf/ft.

(6) $16"^{\phi}$ x 73 lbf/ft.

(7) $14"^{\phi}$ x 63 lbf/ft.

Materials:

A-36 Gas-pipe Steel

Height of Levels: H_1

H_1	0.00'
H_2	33.00'
H_3	62.02'
H_4	90.04'
H_5	116.04'
H_{Top}	155.02'

Top and Bottom Widths:

LT	40.0'
LB	65.6'

FIGURE 3 - PROTOTYPE DETAILS

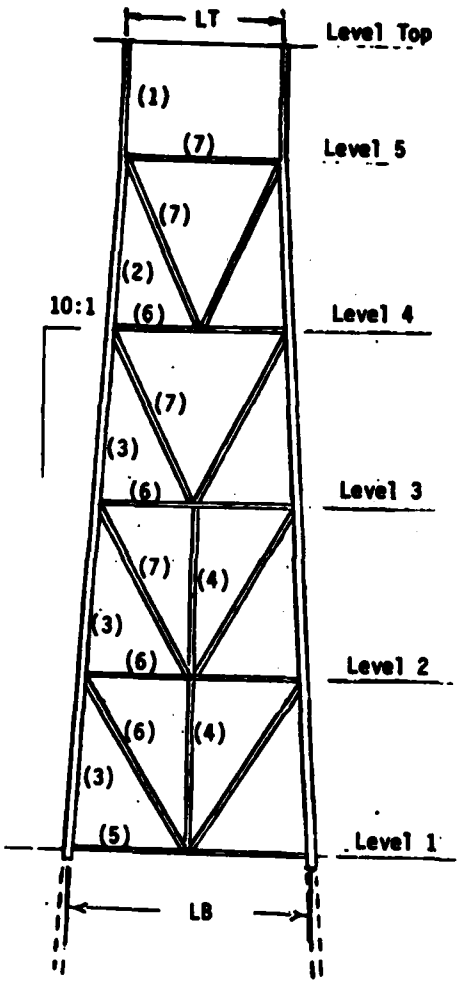

Dimensions of Segments:

1. $2^{"\phi}$ - B.W. Ga. 20
2. $2^{"\phi}$ - B.W. Ga. 20
3. $2^{"\phi}$ - B.W. Ga. 20
4. $9/16^{"\phi}$ - B.W. Ga. 20
5. $3/4^{"\phi}$ - B.W. Ga. 17
6. $3/4^{"\phi}$ - B.W. Ga. 18
7. $3/4^{"\phi}$ - B.W. Ga. 18

Materials:

ASTM A513-70 and QQT-7-830A
By RYERSON

Heights of Levels:

H_1	0.00'
H_2	2.39'
H_3	4.57'
H_4	6.53'
H_5	8.41'
H_{Top}	11.23'

Top and Bottom Widths:

LT	2.899'
LB	4.750'

FIGURE 4 - MODEL PLATFORM DETAILS FOR 13.8 SCALE FACTOR

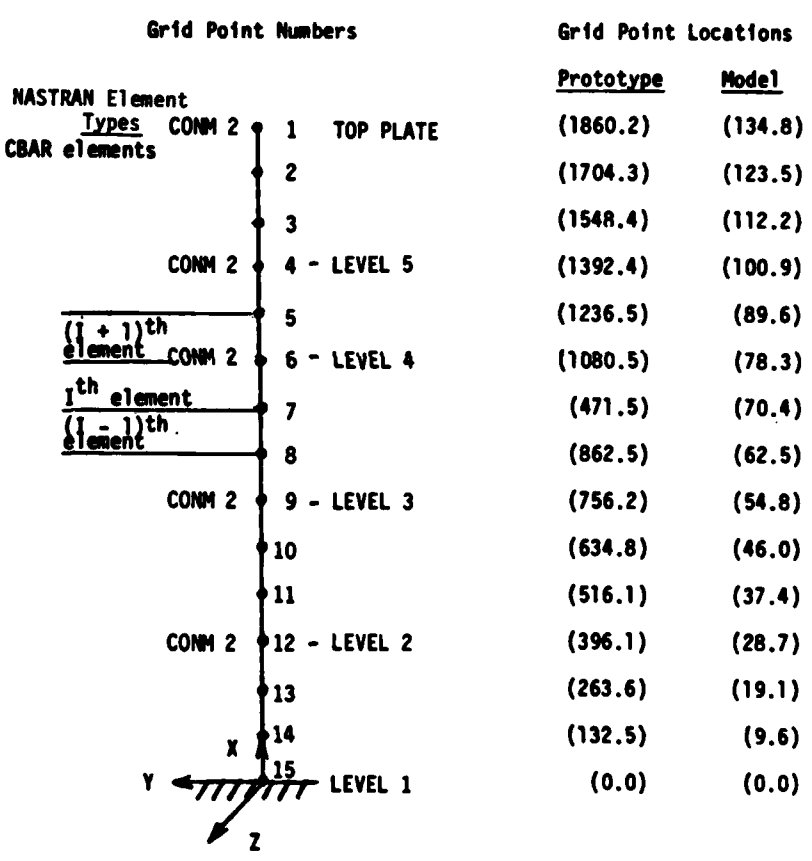

FIGURE 5 - FINITE ELEMENT MODELS

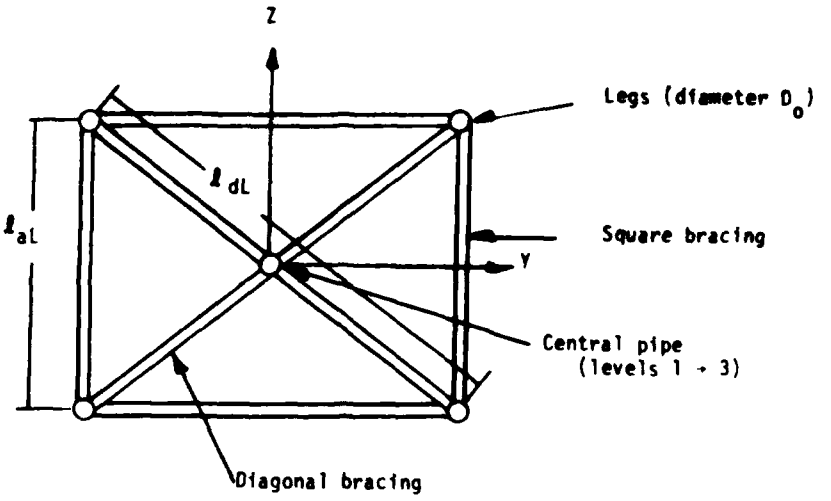

FIGURE 6 - HORIZONTAL MEMBER ARRAY AT THE L^{TH} LEVEL

B. Natural Frequency Results

The model described in the previous subsection of this report was put into NASTRAN Rigid Format 3 for a normal mode analysis using the Givens method of solution.

Table 2 summarizes some of the results of the NASTRAN beam model investigation. The first 10 natural frequencies of the finite element models of the prototype are compared with the corresponding natural frequencies of the real model.

According to the scaling laws derived in Section I for the case where $E_p = E_m$ and $\rho_p = \rho_m$, f_m/f_p must be λ. As seen in Table 2, the finite element modeling of the prototype and fabricated (real) model indicate that there is considerable modeling errors for some frequencies. However, the absolute values of the errors obtained from the NASTRAN results are not in agreement with the measured model fundamental frequency.

TABLE 2

NASTRAN Beam Model Results

Nat. Frequency - (Hz)

Prototype	Real Model	f_m/f_p	Error
2.08	25.25	12.13	-12.1%
2.43	28.93	11.90	-13.7%
7.98	96.40	12.08	-12.4%
9.93	124.21	12.50	- 9.4%
12.37	154.95	12.52	- 9.2%
20.80	270.84	13.02	- 5.6%
26.25	337.68	12.86	- 6.8%
31.23	339.44	12.93	- 6.3%
34.20	412.87	12.07	-12.5%
34.71	533.45	15.36	+11.3%

IV. NASTRAN SPACE FRAME MODEL

The NASTRAN beam model was the first attempt to get an estimate of the error in satisfying the scaling laws between the prototype and the model platform. The computer model was simple and relatively inexpensive to run even for long dynamic response simulations.

As soon as the model platform was completed though it became apparent that this approximate model was giving results, which were off by as much as 100% to 300% of the actual measured data. For example the fundamental flexural mode frequency was measured to be 8 Hz, while the NASTRAN beam model predicted it to be 25 Hz. Furthermore the beam model was very crude and did not allow evaluation of the stresses of individual beam members.

For these reasons, NASTRAN space frame models were developed for the prototype and the real model platform (see Figure 7). Also, to investigate the error introduced by taking $E_p = E_m$ and $\rho_p = \rho_m$ a NASTRAN space frame model of the real model with scaled density $\rho_m = \rho_p$ was developed. To investigate the error resulting from not scaling the exact cross sectional geometry of the prototype beams in the real model, a NASTRAN space frame model of a prototype scaled up from the real model was developed.

Because there were a number of different model and prototype designs to be analyzed all with the similar configuration of four legs and vertical and horizontal diagonal bracing, a pre-processor program (GENER) was written to generate NASTRAN coordinate and connection cards (GRID and CBAR). The pre-processor program will automatically generate all the connectivity cards associated with all the piping of the platform except for the central pipe which is added by hand, with the option of connecting juncture points of the structure with one or two CBAR elements. Two CBAR elements were connected by platform juncture points for this study. Individual piping cross sectional area, mass, and moment of inertia properties are included in the model through the NASTRAN PBAR card. The grid point numbering sequence produced by the generator program is not banded, so after the central piping and plate elements are added to the finite element model, BANDIT is used to obtain sequenced grid point connectivity.

The results of the NASTRAN Rigid Format 3 (Normal Mode Analysis) computer runs are summarized in Tables 3, 4, and 5. Table 3 compares the natural frequencies of the prototype scaled up from the real model, with the model that has density properly scaled. Since these two hypothetical models satisfy all the scaling laws (equations (4) to (10)), the frequency ratio relationship $f_m/f_p = \sqrt{\rho_p/\rho_m} = \sqrt{13.8} = 3.71$ should be satisfied with great accuracy, and as shown in Table 3, there is excellent agreement between the results from the two finite element models.

Table 4 compares the natural frequencies of the prototype scaled up from the real model to those obtained from the finite element model of the real platform. Since these models assume equal moduli and material densities as well as all other scaling laws, that is, satisfying the equation (26), the frequency ratio $f_m/f_p = \sqrt{\rho_p/\rho_m} = \sqrt{13.8} = 3.71$ should be satisfied. The error in the first four modes are less than two per cent. Also from Table 4, it can be seen that the agreement of the finite element model fundamental frequency of 8.5 Hz and the measured frequency of 8 Hz for the constructed real model is good.

Table 5 compares the NASTRAN natural frequencies of the real prototype with the real model. The frequency ratio relationship $f_m/f_p = \sqrt{\rho_p/\rho_m} = \sqrt{13.8}$ is not well satisfied. This error is a direct result of the modeling criterion that was used in the model design and construction, that is, since stock tubing was not available in sizes which directly scale from the real prototype pipe sizes, then available piping would be used to scale the total cross sectional area of the vertical members and the bending moment of inertia produced by the vertical legs.

To investigate the scaling accuracy of the dynamic response variables, the NASTRAN finite element models were loaded with a square pulse force applied at node A in the Y direction as shown in Figure 7 to simulate a ship impact on an offshore platform. The amplitude of the pulse is F_o and its duration is T_o. Each of the above mentioned finite element models was run in NASTRAN Rigid Format 9 (Transient Response) to obtain the displacement, acceleration and stress at critical points as a function of time. For the offshore platform finite element model, F_o and T_o were selected to be 10^6 lbs and 1.15 seconds, respectively. Using the appropriate scaling law, equations (5), (6), (21), or (22), the following loadings in Table 6 were obtained.

Typical dynamic responses at point A of the space frame model in Figure 7 are shown in Figure 8 through 13. The acceleration in the Y direction at point A in Figure 7 for the real model, the model with scaled density, and the prototype scaled up from the real model are shown in Figures 8, 9, and 10, respectively. The time scales in these figures are scaled according to the appropriate scaling law, and as can be seen both the timing and scaled magnitude of the response agrees excellently. The real model acceleration should be 1 times the scaled-up prototype. The displacements, as would be expected, also show excellent agreement. The implication of these results are that the finite element models demonstrate that the scaling laws are correct.

Natural Frequencies of NASTRAN Space Frame Models (in Hz)

TABLE 3

Prototype Scaled Up From Real Model	Model with Scaled Density	f_m/f_p (Should be $\sqrt{\lambda}$ = 3.71)	Error
6.	2.29	3.75	+1.0%
6.	2.29	3.75	+1.0%
89	3.32	3.73	+0.5%	
[illegible]	8.70	3.71	+0.0%
[illegible]76	10.28	3.72	+0.2%
[illegible]76	10.28	3.72	+0.2%

TABLE 4

Prototype Scaled Up From Real Model	Real Model	f_m/f_p (Should be λ = 13.8)	Error
.61	8.52	13.96	+1.2%
.61	8.52	13.96	+1.2%
.89	12.33	13.85	+0.3%
2.34	32.81	14.02	+1.6%

TABLE 5

Prototype	Real Model	f_m/f_p (Should be λ = 13.8)	Error
.77	8.52	11.06	-19.8%
.77	8.52	11.06	-19.8%
1.08	12.33	13.07	-17.2%
2.51	32.81		- 5.2%

TABLE 6

Dynamic Loading Parameters

Real Prototype	Real Model	Model With Scaled Density
F_o (lbs) 10^6	5,251	5,251
T_o (See) 1.38	0.1	0.371

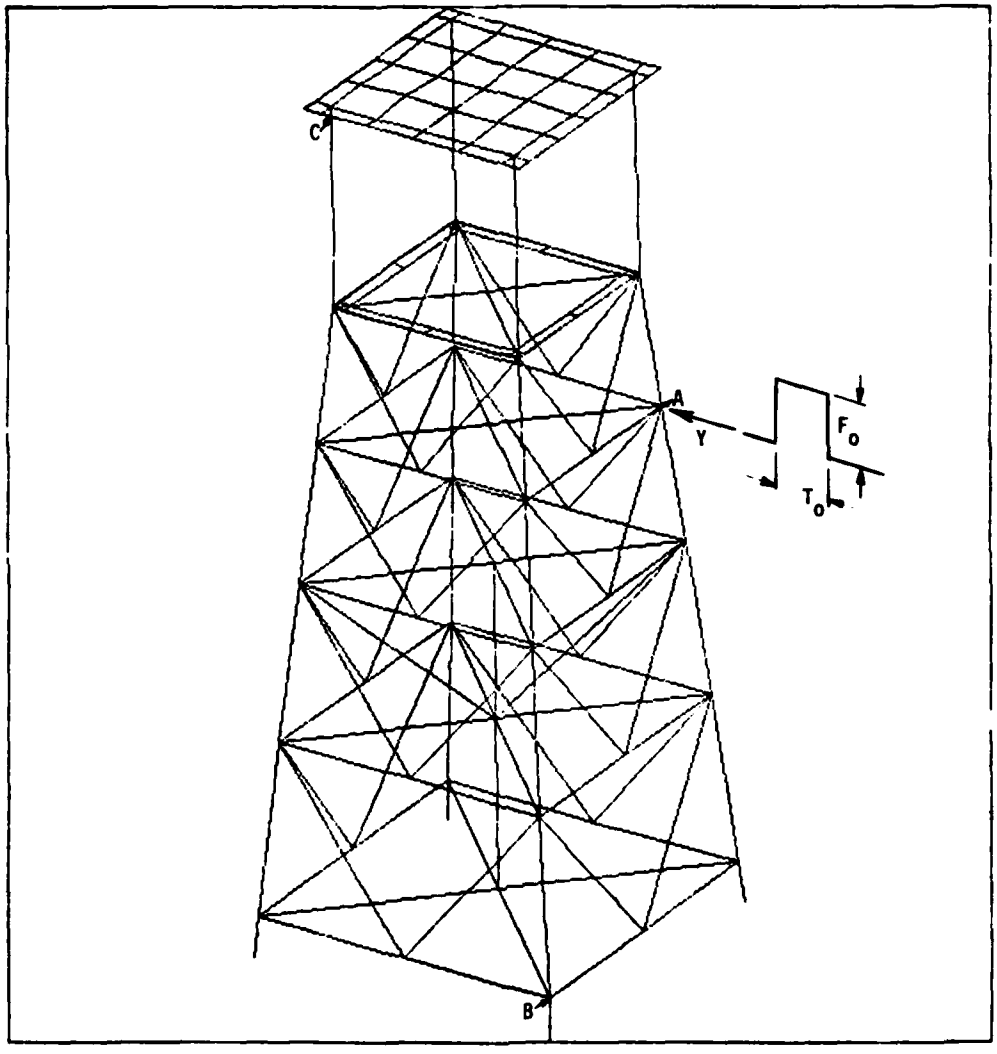

FIGURE 7 - COMPUTER GENERATED PLOT OF NASTRAN FINITE ELEMENT SPACE FRAME MODEL

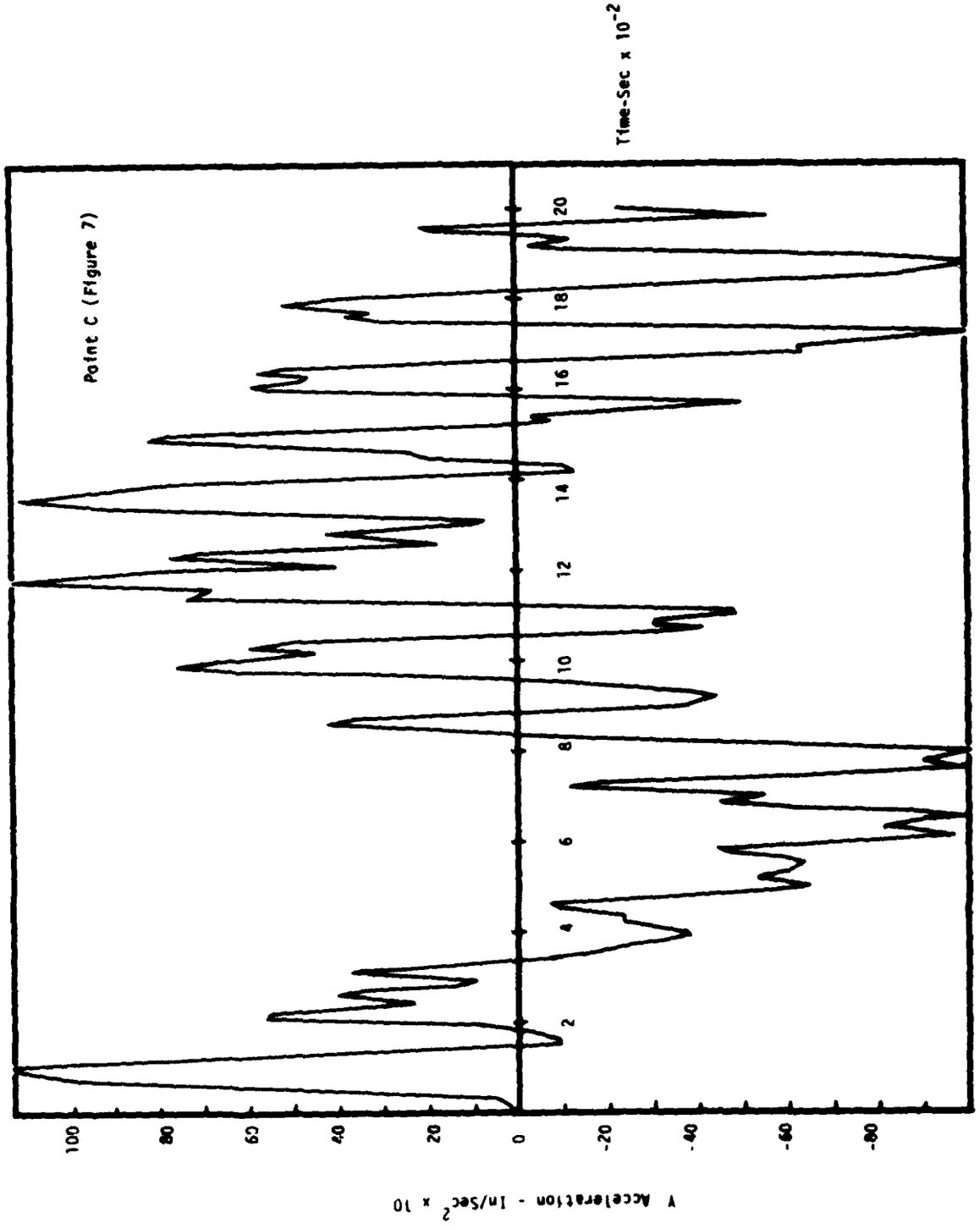

FIGURE 8 - REAL MODEL

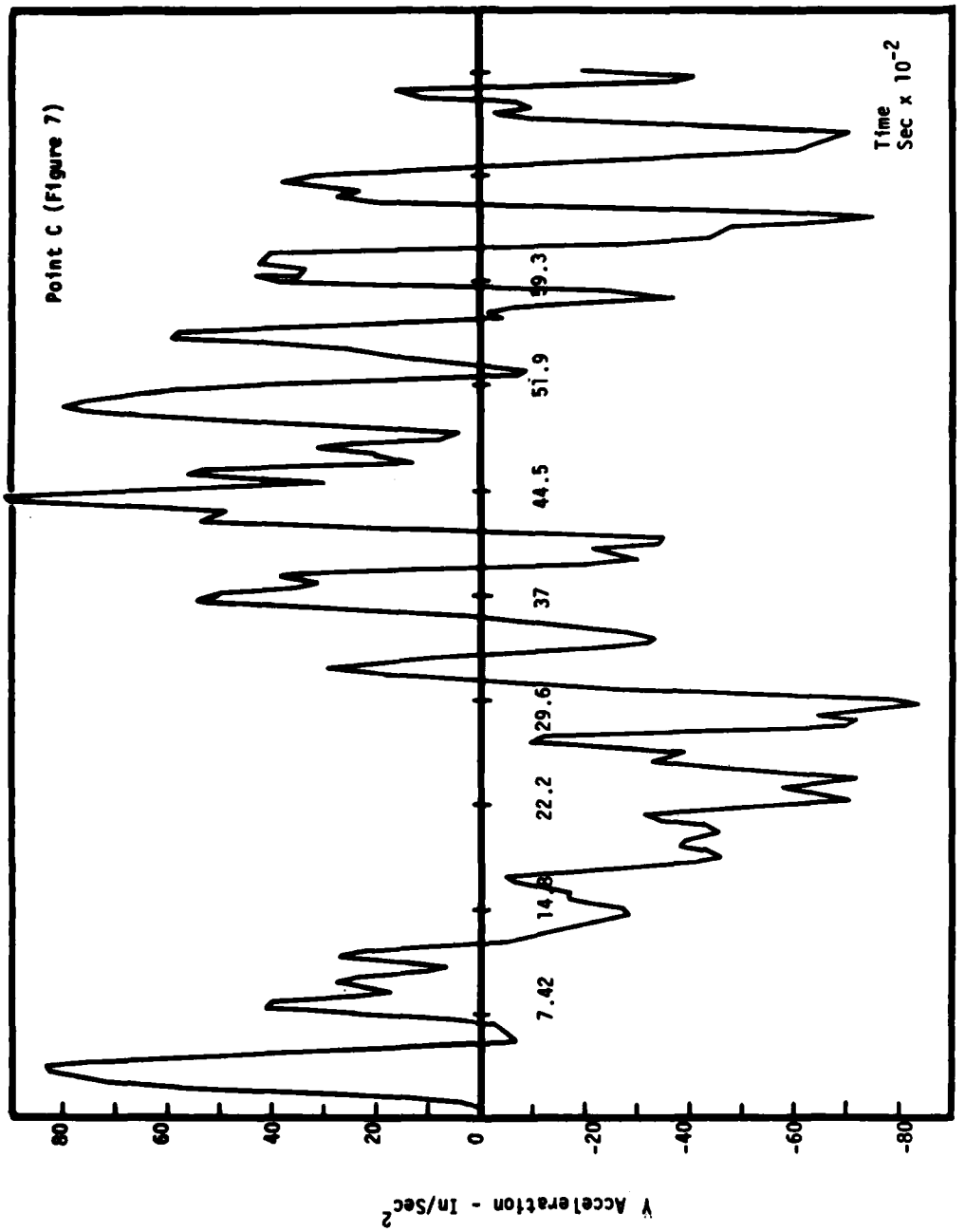

FIGURE 9 - MODEL WITH SCALED DENSITY

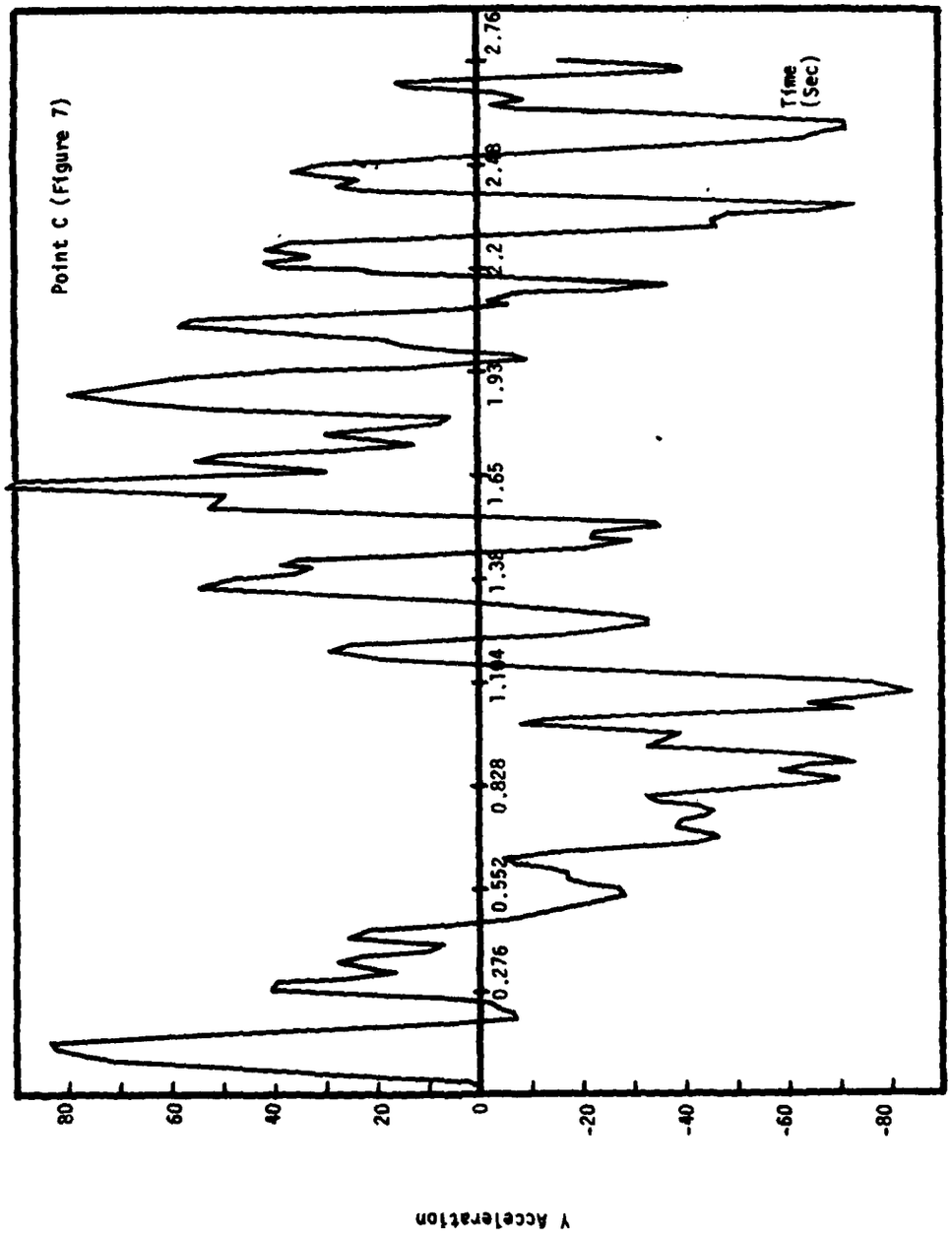

FIGURE 10 - PROTOTYPE SCALED UP FROM REAL MODEL

In contrast to the excellent agreement of these three previously mentioned models, the acceleration response of the prototype is shown in Figure 11. As compared to Figure 10, the phasing of the acceleration is much in error and this is a direct result of the difference in natural frequency response of these two structures. Although the phasing of the real and scaled-up from model prototypes is different, the absolute magnitude of the acceleration is close.

According to equation (7) and (23), stress should scale equally whether density is appropriately scaled or not. The results were obtained on the prototype scaled up from the real model, the real model, and the model with scaled density demonstrated equal stresses at equal scaled time. A big discrepancy was obtained again in the response of the real prototype. Shown in Figures 12 and 13 are the bending stresses at the outside surface of the piping at location B in Figure 7 for the prototype scaled up from the real model and the real prototype. The phasing of the response is not the same because of the previously mentioned natural frequency discrepancies, but instead of equal maximum stresses in both structures the real prototype stress level is one half that of the prototype scaled up from the real model. This error is a direct result of the properties of the piping on each structure. Shown in Table 7 are the properties of the tubing at location B for each structure.

Since the bending stress is

$$\sigma = \frac{M\left(\frac{D_o}{2}\right)}{I} \tag{28}$$

$$\text{then } \frac{\sigma_p\big|_{\text{real}}}{\sigma_p\big|_{\text{scaled up}}} = \frac{\sigma_R}{\sigma_S} = \frac{M_R}{M_S}\,\frac{\left(D_o\right)_R I_S}{\left(D_o\right)_S I_R} \tag{29}$$

Using the properties of Table 7 in equation (29) yields

$$\frac{\sigma_R}{\sigma_S} = .43\,\frac{M_R}{M_S} \tag{30}$$

Even though the static moments are equal for the two structures, the dynamic moments, M_R and M_S won't necessarily be the same because of the different dynamic response of the structures. However they should be close in magnitude and thus, from the difference in tubing properties of the two structures, the stress in the real prototype would be expected to be approximately 43 percent of that in the prototype scaled up from the real model at point B, and this is in close agreement with the NASTRAN results.

V. CONCLUSIONS

Space frame finite element models have been used to substantiate two sets of derived scaling laws for dynamic response of offshore platforms. One set of scaling laws would be satisfied if every member of the model structure were exactly scaled down in dimensions from the prototype structure and the model material modulus was maintained while the density was appropriately scaled up. The other set was derived with the exact same assumptions except that the prototype and model densities are equal. The effects of the modeling differences are that the phasing of the dynamic response of the two different models differ by a $\sqrt{\lambda}$ factor and that acceleration magnitudes of prototype and model are the same when densities are scaled, whereas, the acceleration magnitude differ by a factor of λ when prototype and model densities are the same. With either set of scaling laws, dynamic stresses in both model and prototype are equal and to ensure equal total stresses, the static stresses must be equal which is satisfied by scaling model density.

Two difficulties are encountered in exactly satisfying the scaling laws for offshore platforms: one is obtaining the correct model material density and the other is obtaining model tubing which is an exact scaled-down size of the prototype piping. For practical scaling ratios, the required model material density is very high. For scaled down tubing, it is very unlikely that the correct inside and outside diameters can be obtained in stock sizes. Manufacturing the correct scaled down replica would be prohibitively costly if not impossible

TABLE 7

Tubing Properties in Structures at Location B (Figure 7)

Property	Prototype Scaled Up From Model	Real Prototype
Distance to outside surface $\left(\frac{D_o}{2}\right)\left(\text{in}\right)$	13.8	17.0
Cross sectional area (in^2)	41.1	78.3
Moment of inertia (in^4)	3,783	10,832

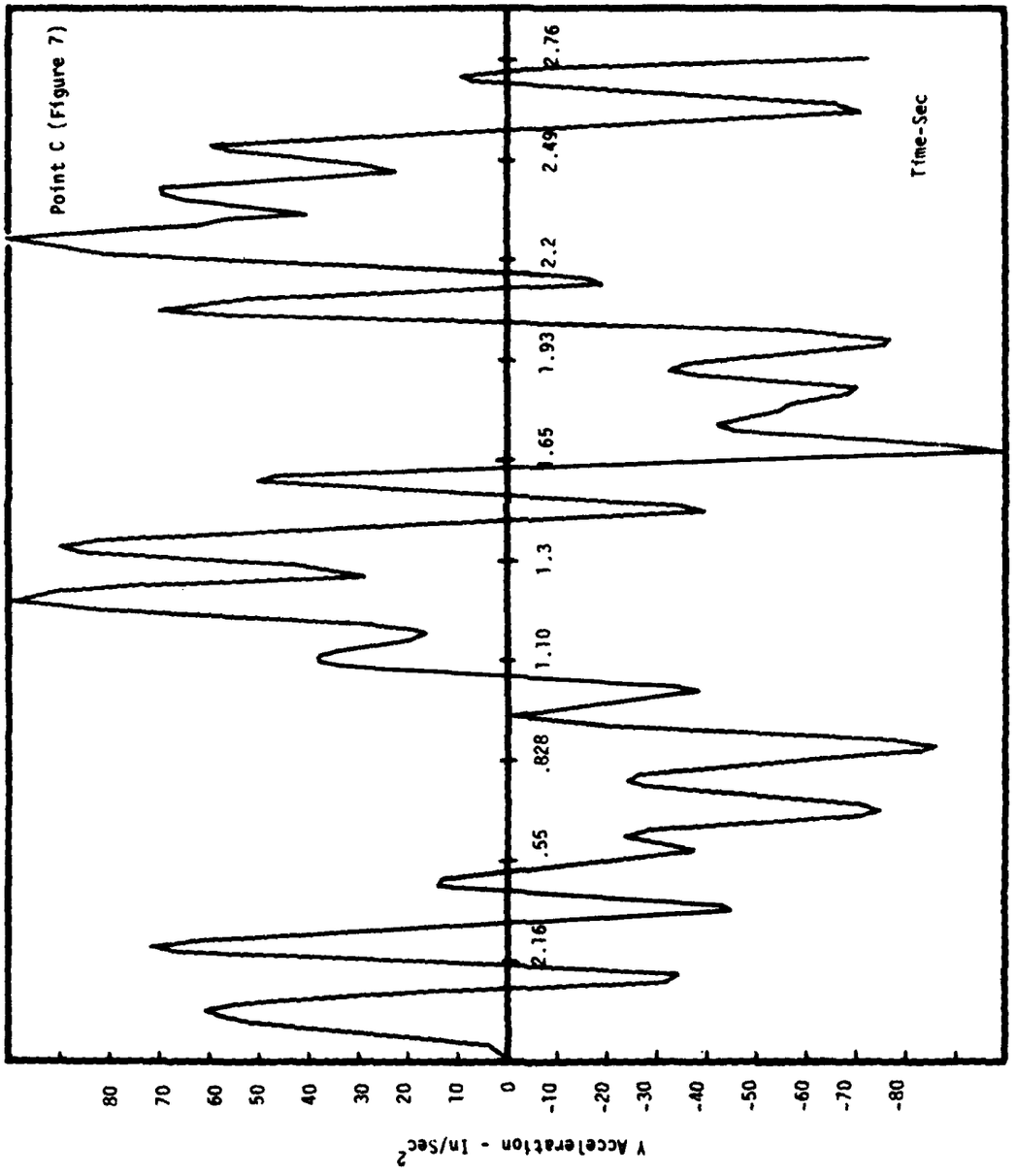

FIGURE 11 - PROTOTYPE

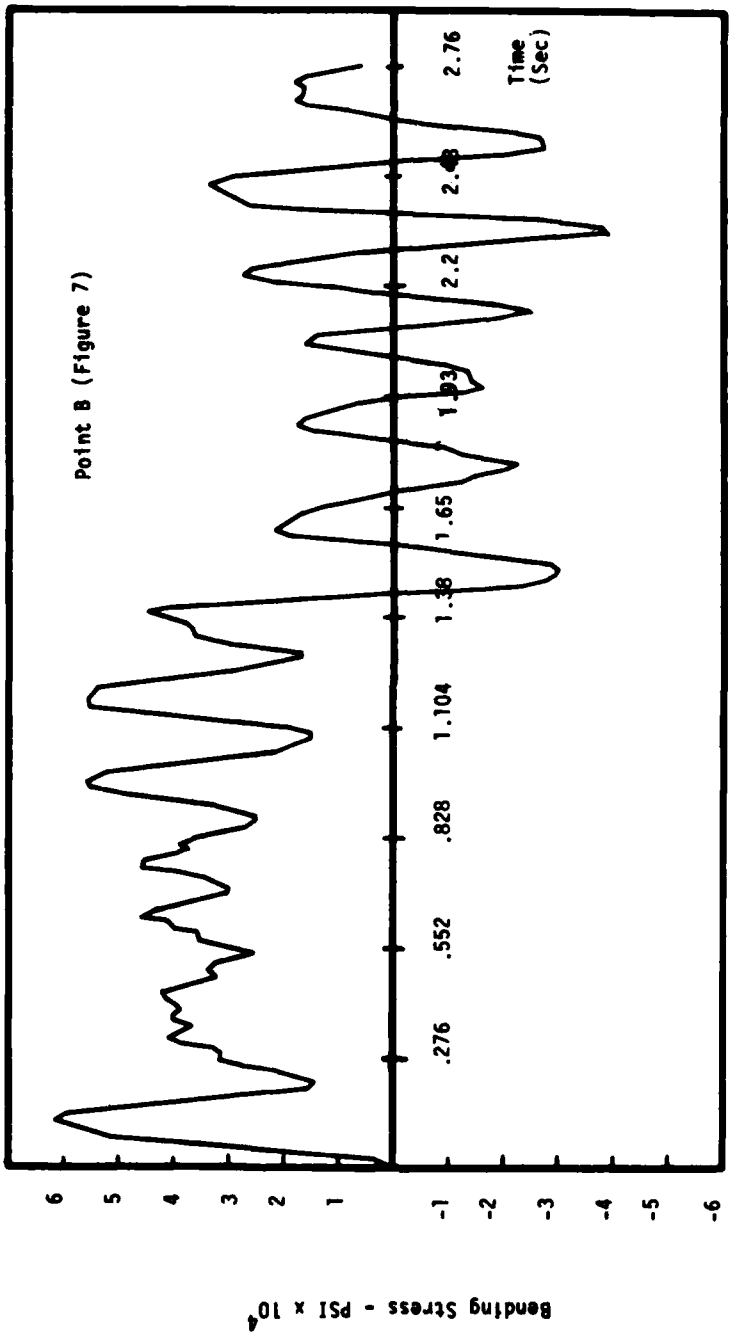

FIGURE 12 - PROTOTYPE SCALED UP FROM REAL MODEL

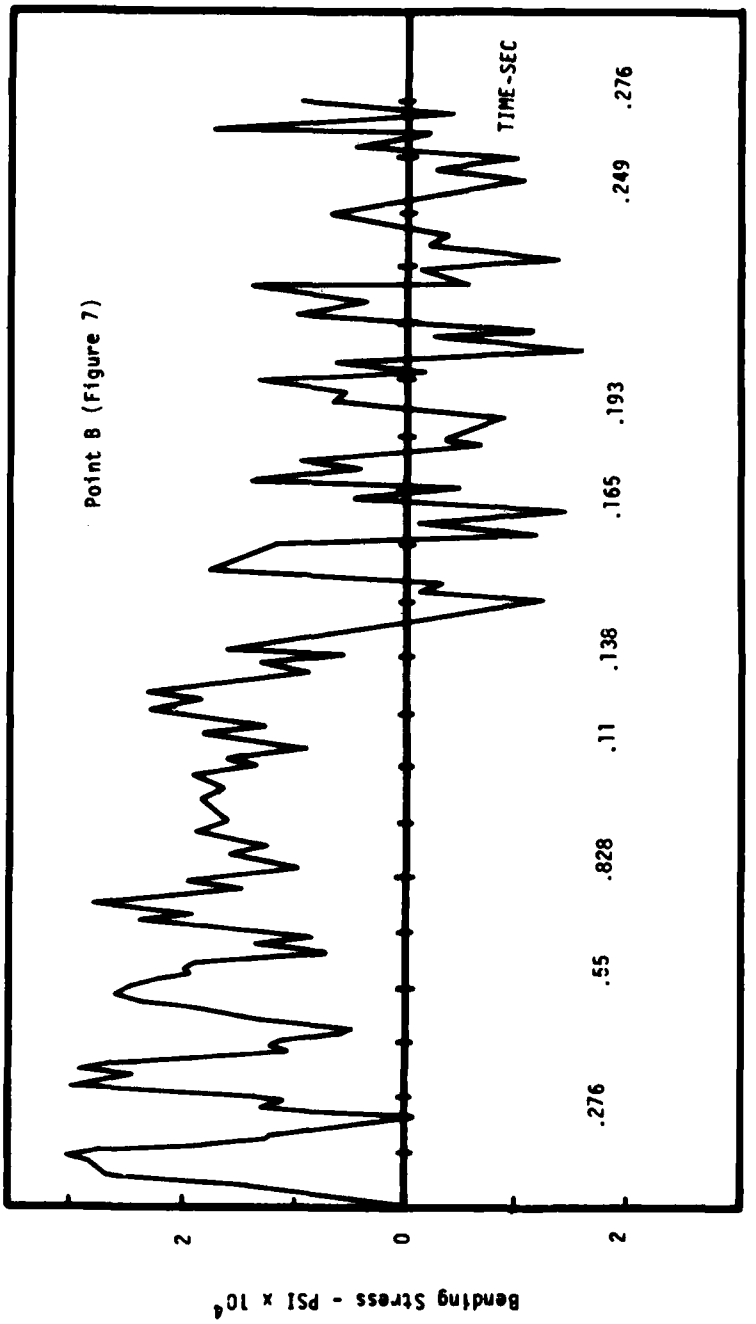

FIGURE 13 - PROTOTYPE

because of minimum gauge requirements or buckling problems.

The best model design for an offshore structure can only be obtained by selecting stock tubing to satisfy scaling laws as nearly as possible and then using finite element modeling of the proposed model and prototype to determine if the dynamic response of the two satisfy scaling laws. If the proposed model doesn't scale accurately enough then other tubing should be selected and modeling done until sufficiently scaling accuracy is obtained.

ACKNOWLEDGEMENTS

This work was supported by the Office of Naval Research and the U. S. Office of Geological Survey under contract N00014-78-C-0675 P00002. We would also like to acknowledgement the help of Mr. Kam Chan for his help with the NASTRAN computer program runs.

REFERENCES

1. H. Krawinkler, R.S. Mills, P.D. Moncarz, "Scale Modeling and Testing of Structures for Reproducing Response to Earthquake Excitation", John A. Blume Earthquake Engineering Center, Stanford University, 1978.

2. P. Le Corbeiller, A.V. Lukas, "Dimensional Analysis", Appleton-Century-Crofts Publishing Co.

3. W.J. Duncan, "Physical Similarity and Dimensional Analysis", Edward Arnold and Co., Publ.

4. H.A. Becker, "Dimensionless Parameters Theory and Methodology", Applied Science Publishers Ltd.

5. A.A. Gukhman, "Introduction to the Theory of Similarity", Academic Press Publ.

6. P.W. Bridgman, "Dimensional Analysis", Yale Univ. Press.

7. C.M. Focken", Dimensional Methods and Their Applications", Edward Arnol- and Co. Publ.

NOMENCLATURE

A	cross sectional area
A_L, A_C	cross sectional area of a leg and central pipe, respectively
a	acceleration
D_o	outside diameter of the leg
E	modulus of elasticity
f	frequency
G	shear rigidity
g	gravitational constant
I	moment of inertia
I_L, I_C	mass moment of inertia about a leg and a central pipe, respectively
K'	shear area coefficient
ℓ	length
ℓ_{aI}	center to center distance between legs of I^{th} BAR element
ℓ_{dL}	center to center diagonal distance between legs at level L
ℓ_I	length of I^{th} BAR element
M	bending moment in beam
m	mass of beam per unit length
P	applied load
p	load pressure
$\bar{p}$	lateral load per unit length of beam
r	radius of gyration of beam cross section
t	time
$\bar{V}$	end shearing force
x	distance along length of beam

Greek Letter Symbols

α	angle of rotation of the beam cross section from its original vertical position (without shear distortion)
β	angle of shear distortion of the beam cross section, β will reduce the slope of the elastic curve of beam axis
λ	ratio of prototype to model length
Π_i	dimensionless group i
ρ	density
σ	stress

Subscripts

m	denotes model
p	denotes prototype
r	indicates ratio of prototype to model quantities

APPENDIX I

Model Design

The offshore platform structure under consideration for this study is shown in Figure 2 with details in Figure 3. It is a 4 pile jacket design with a deck 155 feet above the ocean bottom 105 feet of water. The model scaling was obtained by consideration of commercially available structural members for the model platform construction.

The four legs of the prototype are made

of 34 $\frac{1}{2}$" O. D. x $\frac{3}{4}$" plate pipe spaced 65' 7 $\frac{3}{16}$" apart and the central pipe is 12 $\frac{3}{4}$" O. D. x $\frac{3}{8}$" plate. The total cross sectional areas of these members is thus

$$A_p = 4(A_L)_p + (A_c)_p = 175.39 \text{ in}^2 \quad (A.1)$$

Where A_L, A_c is the cross sectional area of the leg and central pipe respectively.

The moment of inertia of these members about the Z axis in Figure 6 is

$$I_p = (I_c)_p + 4(I_L + A_L k_L^2)_p = 25.064(10^6) \text{ in}^4 \quad (A.2)$$

The model bending moment of inertia is

$$I_m = (I_c)_m + 4(I_L + A_L k_L^2)_m \quad (A.3)$$

The contribution of the moment of inertia of the central pipe, $(I_c)_m$, to the total moment of inertia of the model at the bottom, I_m, is small so it may be neglected. Substituting the scaling relationships $\frac{I_p}{I_m} = \lambda^4$, $\frac{A_p}{A_m} = \lambda^2$ from (13) and (17) into equation (A.2) yields

$$\lambda^4 + \left(\frac{A_L}{I_L}\right)_m \left(k_L\right)_p^2 \lambda^2 - \frac{I_p}{4\left(I_L\right)_m} = 0 \quad (A.4)$$

But

$$\frac{\left(A_L\right)_m}{\left(I_L\right)_m} = \frac{\left(A_L\right)_m}{\left(A_L\right)_m \cdot \frac{1}{16}\left(d_o^2 + d_i^2\right)_m} = \frac{16}{\left(d_o^2 + d_i^2\right)_m} \quad (A.5)$$

Therefore

$$\lambda^2 = \sqrt{\left(\frac{1245799.55}{\left(d_o^2 + d_i^2\right)_m}\right)^2 + \left(\frac{6266065.29}{\left(I_L\right)_m}\right)} - \frac{12945799.55}{\left(d_o^2 + d_i^2\right)_m} \quad (A.6)$$

Equation (A.6) is used to size the model columns and then the central pipe may be sized to satisfy the exact scaling equation. Using Ryerson carbon steel round mechanical tubing 2" O. D. by B. W. Ga. 20, the properties are

$$d_o = 2.0" \quad (A.7)$$

$$d_i = 1.93"$$

$$\left(A_L\right)_m = 0.216 \text{ in}^2$$

$$\left(I_L\right)_m = .1043 \text{ in}^4$$

Substituting into equation (A.6) yields $\lambda = 13.64$. for the central pipe, the properties of Ryerson Carbon steel round mechanical tubing $\frac{9}{16}$" O. D. by B. W. Ga. 20 are:

$$d_o = \frac{9"}{16} \quad (A.8)$$

$$d_i = .493"$$

$$\left(A_c\right)_m = 0.057 \text{ in}^2$$

$$\left(I_c\right)_m = 0.00199 \text{ in}^4$$

Then from (A.1) the scaling factor is:

$$\lambda = \sqrt{\frac{A_p}{A_m}} = \sqrt{\frac{175.39}{4(.216) + .057}} = 13.8 \quad (A.9)$$

Checking the moment of inertia scaling:

$$\sqrt[4]{\frac{I_p}{I_m}} = \sqrt[4]{\frac{25.064(10^6)}{.002 + 4\left(.1043 + .216\left(\frac{393.6}{13.8}\right)^2\right)}} = 13.75 \quad (A.10)$$

Thus a scaling factor of $\lambda = 13.8$ is chosen for the model.

The top deck of the platform was modeled as a uniform thickness plate which was sized in length according to the structural scaling factor λ and in thickness so that the weight is scaled according to the cube of λ. Similar scaling was done on the catwalk at level 5 of the platform. The resulting platform model is shown in detail in Figure 4.

DISCUSSION

Mr. Galef (TRW): I would think that the loads you were mostly concerned about would be the ones from starboard. If we ever had that model in the water the violation of the Froude law scaling that you had would seem to be completely unusable.

Mr. Dagalakis: The loadings that we have is wrong from the waves, is that the question?

Mr. Galef: Yes, that is correct.

Mr. Dagalakis:: And also from collisions. Sometimes the supply ship will collide with the offshore platform. The study that we did here was for that kind of load and occasionally we have collisions.

SOUND PROPAGATION THROUGH LIQUIDS IN VISCOELASTIC CIRCULAR CYLINDERS

Richard A. Skop

Naval Research Laboratory
Washington, D.C. 20375 USA

The propagation of low frequency sound waves through liquids contained in thin walled, viscoelastic circular cylinders is studied. The analysis is based on two suppositions: (i) the sound wave propagates along the cylinder axis and has constant properties over a cross-section transverse to this axis; and, (ii) the dynamic response of the cylinder wall can be calculated adequately from membrane hoop theory. The wall material is described by a general viscoelastic constitutive relation. The results predicted from this analysis are shown to be in good agreement with experiments conducted in viscoelastic cylinders.

1. INTRODUCTION

The propagation of sound waves through fluids in flexible circular cylinders has been studied by many investigators. Jacoby [1], Fay [2], Morgan and Kiely [3], and Lin and Morgan [4] examined wave propagation through fluids in elastic cylinders. Their analyses considered only axial-radial modes of vibration and neglected the presence of fluids external to the cylinder. The presence of external fluids was incorporated in the work of Junger [5]. Ho [6] undertook the resolution of the further complexity added to the problem by allowing angular modes of vibration. More recently, Ellison and Junger [7] have extended the general normal mode solution to cylinders with viscoelastic walls or linings.

In this paper, we present a simplified analysis of low frequency sound wave propagation through liquids contained in thin walled, viscoelastic circular cylinders. We neglect throughout the analysis any effects of fluids external to the cylinder. This implies that the acoustic impedance of the external fluid is much less than the acoustic impedance of the contained liquid.

The analysis is based on two suppositions: (i) the sound wave propagates along the cylinder axis and has constant properties over a cross-section transverse to this axis; and, (ii) the dynamic response of the cylinder wall can be calculated adequately from membrane hoop theory. The wall material is described by a general viscoelastic constitutive relation. The results predicted from this analysis are shown to be in good agreement with experiments conducted in viscoelastic cylinders.

2. FORMULATION OF THE PROBLEM

We wish to develop the equations governing low frequency sound wave propagation through liquids contained in thin walled, viscoelastic circular cylinders. The liquid is characterized by its unperturbed density ρ_l, unperturbed pressure p_l, unperturbed axial velocity $u_l = 0$, and adiabatic sound speed c_l. The unperturbed radius of the cylinder is given by R.

Let us now suppose that at some location along the cylinder a low frequency perturbation is introduced into the liquid. By low frequency, we mean that the wavelength of the perturbation is large compared to the circumference of the cylinder; or, equivalently, that

$$\omega < c_l/R \tag{1}$$

where ω is the radial frequency of the perturbation. Under this condition, it can be assumed that the perturbations about the unperturbed liquid state, which are indicated by a prime ($'$), are essentially constant over a transverse cross-section of the cylinder and propagate primarily along the cylinder axis. The equations describing this propagation are obtained, in the sound wave limit, as [8]

$$\frac{\partial p_i'}{\partial t} + \frac{2\rho_l}{R}\frac{\partial w_d}{\partial t} + \rho_l \frac{\partial u_l'}{\partial x} = 0 \text{ (continuity)} \quad (2a)$$

$$\rho_l \frac{\partial u_l'}{\partial t} = -\frac{\partial p_i'}{\partial x} \text{ (momentum)} \quad (2b)$$

$$p_i' = c_l^2 \rho_l' \text{ (state)}. \quad (2c)$$

Here, t denotes time, x denotes distance along the cylinder axis, and w_d denotes the radial displacement of the cylinder wall in response to the perturbation pressure p_i'.

To calculate w_d, we assume that the cylinder can be treated as "locally reacting" [7]. This assumption, which is equivalent to neglecting longitudinal Poisson stresses in the development of thin shell theory, yields as the governing equation for w_d the membrane hoop equation [9]

$$\rho_d h \frac{\partial^2 w_d}{\partial t^2} = p_i' - \frac{h}{R}\sigma. \quad (3)$$

In this equation, ρ_d is the density of the wall material, h is the wall thickness, and σ is the membrane hoop stress in the wall. This stress is related to the membrane hoop strain ϵ, defined by

$$\epsilon = w_d/R \quad (4)$$

in a manner to be specified later. The validity of the "locally reacting" assumption requires the perturbation frequency to be below the ring frequency of the cylinder or, in quantitative terms,

$$\omega < c_d/R. \quad (5)$$

Here, c_d is the speed of wave propagation in the wall and is given by

$$c_d = \sqrt{E/\rho_d} \quad (6)$$

where E is the Young's modulus of the wall material.

In writing equation (3), we have ignored any effects of fluids external to the cylinder. This implies that the acoustic impedance of the external fluid is significantly less than the acoustic impedance of the contained liquid.

3. HARMONIC SOLUTIONS

On taking $\partial/\partial t$ of equation (2a) and substituting for $\partial u_l'/\partial t$ from equation (2b) and for ρ_l' from equation (2c), an equation relating p_i' and w_d is found as

$$\frac{1}{c_l^2}\frac{\partial^2 p_i'}{\partial t^2} + \frac{2\rho_l}{R}\frac{\partial^2 w_d}{\partial t^2} - \frac{\partial^2 p_i'}{\partial x^2} = 0. \quad (7)$$

Let us seek solutions to the above equation and to equations (3) and (4) of the nature

$$p_i' = P_i(x)\, e^{j\omega t} \quad (8a)$$

$$w_d = W_d(x)\, e^{j\omega t} \quad (8b)$$

$$\sigma = S(x)\, e^{j\omega t} \quad (8c)$$

$$\epsilon = \mathscr{E}(x)\, e^{j\omega t} \quad (8d)$$

where $j = \sqrt{-1}$. From equation (7), W_d is determined as

$$W_d = -\frac{R}{2\omega^2\rho_l}\left[\frac{d^2 P_i}{dx^2} + \frac{\omega^2}{c_l^2} P_i\right] \quad (9)$$

while equations (3) and (4) become

$$P_i = -\omega^2 \rho_d h W_d + \frac{h}{R} S \quad (10a)$$

$$\mathscr{E} = W_d/R. \quad (10b)$$

To proceed further, we must specify the relationship between the hoop stress S and the hoop strain $\mathscr{E}$. For a general viscoelastic material undergoing harmonic oscillations, this relationship is [10]

$$S = [E'(\omega) + j\,E''(\omega)]\,\mathscr{E} \quad (11)$$

where E' and E'' are, respectively, the storage modulus and the loss modulus of the material. For our purposes, it is convenient to rewrite equation (11) as

$$S = E\theta(\omega)[1 + j\Delta(\omega)]\,\mathscr{E}. \quad (12)$$

Here, $\Delta = E''/E'$ is known as the dissipation factor or loss tangent. The quantity θ is termed the storage factor and gives the ratio between $E'(\omega)$ and $E'(0) = E$, the Young's modulus.

On replacing S in equation (10a) by its value from equation (12), we find, after substituting for $\mathscr{E}$ from equation (10b) and for E from equation (6),

$$P_i = \rho_d h\left[-\omega^2 + \frac{c_d^2}{R^2}\theta(1 + j\Delta)\right] W_d. \quad (13)$$

This latter expression becomes, upon substituting for W_d from equation (9) and some algebraic manipulation,

$$\left(\theta - \frac{\omega^2 R^2}{c_d^2} + j\theta\Delta\right)\frac{d^2 P_i}{dx^2} + \frac{\omega^2}{c_l^2}\left(\theta - \frac{\omega^2 R^2}{c_d^2} + j\theta\Delta + \frac{2R\rho_l c_l^2}{h\rho_d c_d^2}\right) P_i = 0. \quad (14)$$

The solutions to this equation can be obtained by looking for $P_i(x)$ in the form

$$P_i \sim e^{j(\omega t \pm k^* x)} \tag{15}$$

where k^* is a dimensionless wave number. We find

$$k^{*2} = 1 + \frac{2\beta\gamma}{\theta - \omega^{*2} + j\theta\Delta} \tag{16}$$

when the dimensionless parameters

$$\omega^* = \frac{\omega R}{c_d}, \beta = \frac{R\rho_i c_i}{h\rho_d c_d}, \gamma = \frac{c_i}{c_d} \tag{17}$$

are introduced. We note that, in terms of these parameters, the upper limit imposed on the frequency by equations (1) and (5) is

$$\omega^* < \min(\gamma, 1). \tag{18}$$

The two roots of equation (16) can be shown, by back substitution, to be

$$k^* = \pm (k_R^* - j k_I^*) \tag{19a}$$

where the real and imaginary parts, k_R^* and k_I^*, of the wave number are

$$k_R^* = \frac{1}{\sqrt{2}} \left\{ 1 + (\theta - \omega^{*2}) Q + \sqrt{[1 + (\theta - \omega^{*2}) Q]^2 + (\theta\Delta Q)^2} \right\}^{1/2} \tag{19b}$$

$$k_I^* = \frac{1}{\sqrt{2}} \left\{ -[1 + (\theta - \omega^{*2}) Q] + \sqrt{[1 + (\theta - \omega^{*2}) Q]^2 + (\theta\Delta Q)^2} \right\}^{1/2} \tag{19c}$$

and where

$$Q = \frac{2\beta\gamma}{(\theta - \omega^{*2})^2 + (\theta\Delta)^2}. \tag{19d}$$

These two roots, + and −, for k^* represent damped sound waves traveling, respectively, in the negative and positive x directions. The dimensionless phase speed $c^* = c/c_i$ of the wave, where c is the actual phase speed, is given by

$$c^* = 1/k_R^* \tag{20a}$$

and the amplitude decrement δ^* of the wave per unit (x/R) is ascertained as

$$\delta^* = \omega^* k_I^*/\gamma. \tag{20b}$$

For a perfectly elastic wall material, the dissipation factor $\Delta = 0$ and the storage factor $\theta = 1$. We find

$$c^* = \left\{ 1 + \frac{2\beta\gamma}{(1 - \omega^{*2})} \right\}^{1/2} \tag{21a}$$

$$\delta^* = 0 \tag{21b}$$

which are the same as the results previously obtained by Lin and Morgan [4].

4. COMPARISON WITH EXPERIMENT

Horne, Hansen, and Ni [11] recently have conducted a series of experiments concerning sound propagation through water contained in an acrylic pipe. The sound waves were generated by a transducer mounted at one end of the pipe while the other end of the filled pipe was open to air.

To model these experiments, we take the perturbation pressure p_i' at $x = 0$ in the form

$$p_i'(0,t) = P_{i0} e^{j\omega t}. \tag{22}$$

Then, from equations (8), (15), and (19), the pressure distribution $P_i(x)$ along the cylinder of length L can be written as

$$\frac{P_i(x)}{P_{i0}} = P_i^*(x^*) = \cos K^* x^* + B \sin K^* x^*. \tag{23}$$

Here, B is a dimensionless constant and we have introduced the dimensionless quantities

$$K^* = K_R^* - jK_I^*, \tag{24}$$

$$K_R^* = \frac{\omega^* l}{\gamma} k_R^*, K_I^* = \frac{\omega^* l}{\gamma} k_I^*,$$

$$l = L/R, x^* = x/L.$$

On making use of the boundary condition that, for an open cylinder, the perturbation pressure must vanish at $x = L$ $(x^* = 1)$, B is readily evaluated and we obtain

$$P_i^*(x^*) = \cos K^* x^* - \frac{\cos K^*}{\sin K^*} \sin K^* x^*. \tag{25}$$

After replacing K^* by its complex form and going through some algebraic and trigonometric manipulations, the modulus (or absolute value) of P_i^* is found as

$$|P_i^*(x^*)|^2 = \frac{1}{2} (\cos 2K_R^* x^* + \cosh 2K_I^* x^*) - \frac{1}{C_3} (C_1 \sin 2K_R^* x^* + C_2 \sinh 2K_I^* x^*) \tag{26a}$$

$$- \frac{C_1^2 + C_2^2}{2C_3^2} (\cos 2K_R^* x^* - \cosh 2K_I^* x^*)$$

where

$$C_1 = \frac{1}{2} \sin 2K_R^* \tag{26b}$$

$$C_2 = \frac{1}{2} \sinh 2K_I^* \tag{26c}$$

$$C_3 = -\frac{1}{2} (\cos 2K_R^* - \cosh 2K_I^*). \tag{26d}$$

In Figure 1, the pressure levels predicted by equation (26a) are compared with some of the experimental results from reference [11]. The experimental setup was characterized by the quantities

$L = 182.9$ cm $\quad R = 9.525$ cm $\quad h = 0.635$ cm

$\rho_l = 1.0$ gm/cm^3 $\quad \rho_d = 1.18$ gm/cm^3

$c_l = 1485.9$ m/s $\quad c_d = 1905.0$ m/s

which yield our dimensionless parameters as

$$\gamma = 0.78 \quad \beta = 9.915 \quad l = 19.20.$$

The dimensionless frequency ω^* is related to the excitation frequency f through

$$\omega^* = 3.142 \times 10^{-4} f.$$

The viscoelastic properties of the acrylic wall material were determined by Hunston [12] who found that, over the frequency range of interest (30 to 1000 Hz), both the storage and dissipation factors are essentially constant and given by

$$\theta(\omega^*) = 1.0 \quad \Delta(\omega^*) = 0.05.$$

As is evidenced from Figure 1, there is substantially good agreement between the predicted and measured sound pressure levels.

5. CONCLUSIONS

A simplified analysis of low frequency sound wave propagation through liquids contained in thin walled, viscoelastic circular cylinders has been presented. The results predicted from this analysis have been shown to be in good agreement with results predicted from more exact theories for infinitely long elastic cylinders and with experiments conducted in acrylic cylinders.

The analysis provides a generally applicable and tractable approach to studing the generic problem for any type of wall material.

ACKNOWLEDGMENTS

The author wishes to acknowledge the support of the Naval Research Laboratory (NRL) for the work reported in this paper. The many helpful discussions with Dr. Robert J. Hansen of the above laboratory are acknowledged. Special thanks go to Dr. George A. Keramidas, also of NRL, for painstakingly checking the mathematical developments.

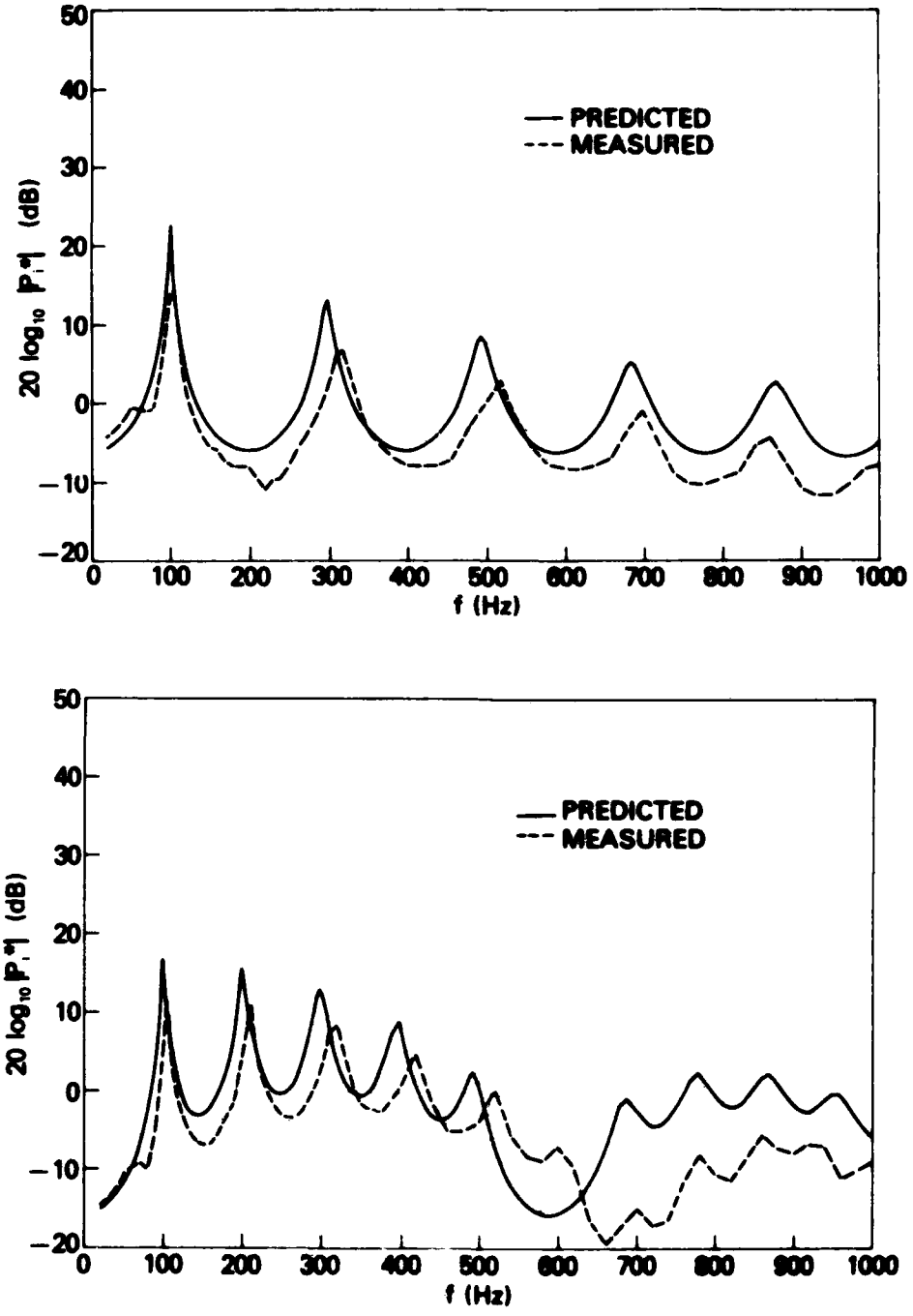

Figure 1. Comparison between the sound pressure levels predicted by equation (26a) and the experimental results of reference [11] for water contained in an open acrylic pipe. (a) $x^* = 1/2$, (b) $x^* = 5/6$.

REFERENCES

1. W.J. Jacobi 1949 Journal of the Acoustical Society of America 21, 120-127. Propagation of sound waves along liquid cylinders.

2. R.D. Fay 1952 Journal of the Acoustical Society of America 24, 459-462. Waves in liquid-filled cylinders.

3. G.W. Morgan and J.P. Kiely 1954 Journal of the Acoustical Society of America 26, 323-328. Wave propagation in a viscous liquid contained in a flexible tube.

4. T.C. Lin and G.W. Morgan 1956 Journal of the Acoustical Society of America 28, 1165-1176. Wave propagation through fluid contained in a cylindrical, elastic shell.

5. M.C. Junger 1955 Transactions of American Society of Mechanical Engineers Journal of Applied Mechanics 77, 227-231. The effect of a surrounding fluid on pressure waves in a fluid-filled elastic tube.

6. L.T. Ho 1968 U.S. Naval Ship Research and Development Center Report 2676. Wave propagation and radiation in the acoustic media within and without a vibrating cylinder.

7. W.T. Ellison and M.C. Junger 1979 Cambridge Acoustical Associates Report U-612-268. Sound propagation in lined pipes — computation schemes and results.

8. L.D. Landau and E.M. Lifshitz 1959 Fluid Mechanics. Reading, Massachusetts: Addison-Wesley. See Chapter VIII.

9. A.W. Leissa 1973 National Aeronautics and Space Administration Report SP-288. Vibration of shells.

10. L.E. Nielsen 1962 Mechanical Properties of Polymers. New York: Reinhold Publishing Corporation. See Chaper 7.

11. M.P. Horne, R.J. Hansen, and C.C. Ni 1980 in preparation. Sound propagation in a liquid contained by a pipe of comparable acoustic impedance.

12. D.L. Hunston 1980 Chemistry Division, Naval Research Laboratory. Private communication.

DISCUSSION

Mr. Seville (Structural Dynamics Research Corporation): Can you go into a little bit of depth on the model itself? Is it a finite element approach?

Mr. Skop: No, you can't get an analytic solution out of it.

Mr. Seville: Oh, it's just a closed situation.

Mr. Skop: It is a closed form solution.

Mr. Seville: The impression I got from the continuity equation is that you are pulling in the boundary condition for the wall into the calculation for the pressure.

Mr. Skop: The wall was moving, breathing in and out, so you have an area change in the pipe. If you take a look at the horn equations for a tuba or a bugle it is a standard approximation. The flow in and the flow out, which is your standard continuity derivation then it becomes affected by the area change in the pipe wall and that is where that term appears.

Mr. Seville: So the wall is moving? It is a flexible wall and the wall is moving as the wave goes by.

Mr. Skop: Yes. They are coupled together.

Mr. Getline (General Dynamics-Convair): What was the relative hardness between the rubber and the acrylic tubes?

Mr. Skop: The outer rubber material was rather hard. I think the effective speed of sound propagation was about 10 percent to 15 percent higher than the acrylic material, and that determines its hardness effect. It has an effective elastic modulus of about 10 to 15 percent higher than the acrylic wall material.

*U.S. GOVERNMENT PRINTING OFFICE: 1981-0-341-334/118